University of Stavanger

Faculty of Science and Technology

MASTER THESIS

Study program/Specialization: MSc Petroleum Geosciences Engineering	Spring semester, 2016 Open access
Writer: Erik Johan Helland	…… (Writer's signature)
Faculty supervisor: Rodmar Ravnås, University of Stavanger, A/S Norske Shell External supervisor(s): Thomas Sandison, A/S Norske Shell	
Thesis title: Middle Jurassic Brent Group fault seal prediction for the Oseberg area. *A locally calibrated method to increase exploration success*	
Credits (ECTS): 30	
Key words: Oseberg, Viking Graben North Sea Fault Seal evaluation	Pages: …… + enclosure: …… Stavanger, 15th June 2016

Middle Jurassic Brent Group Fault Seal Prediction for the Oseberg Area.

A locally calibrated method to increase exploration success.

By

Erik Johan Helland

MSc. Thesis

University of Stavanger
June 2016

Copyright

Erik Johan Helland

Acknowledgements

First and foremost I want to express my sincerest gratitude towards supervisors Rodmar Ravnås and Thomas Sandison for their continuous support and guidance throughout this thesis. They have done their best to tailor an engaging and challenging project which has allowed me to build on and further develop my skills in reservoir modelling and fault seal analysis. Trough weekly meetings and corrections, they have provided thorough and thought-provoking feedback, for this I am truly grateful. Their commitment and encouragement, have been instrumental to the success of this thesis.

This thesis was carried out at Norske Shell AS and the University of Stavanger in the period from January to June 2016. I want to express my gratitude towards Norske Shell for providing access to their database and assets. I also want to express my deepest gratitude towards the talented people working in data management and exploration at Norske Shell for their support and guidance throughout the thesis. Additionally, I want to thank the University of Stavanger for providing state of the art workstations and licenses.

I wish to thank my fellow students and friends at the University of Stavanger for sharing hour long discussions, lunches and laughs. You are the most unique, gifted and cheerful group of people I have ever met and I thank you for making these last two years truly remarkable. I wish you all the best!

Finally, I want to thank my friends, family and my girlfriend for their unending support and encouragement in all my pursuit.

Abstract

This thesis provide a case-study of fault-seal characteristics and consequently the retained hydrocarbon column heights in the Oseberg area. The interpretation of the Oseberg structure utilized seismic and well data to map and characterize the main structural elements and key lithostratigraphic intervals. Along with fault-seal calculations, an evaluation of the Shell developed proprietary Stochastic Trap Analysis and Risking tool (STAR) and its applicability to the Brent Group was carried out. Additionally, this case study provides an assessment of the methodology applied to the construction of a coherent structural and property model with facies distribution by highlighting weaknesses and strengths of each singular process and its ultimate impact on the quality of the end product.

Fristad et al. (1997) previously conducted a similar case study of the fault-sealing potential in the Oseberg area calibrated to well data, and concluded that for Brent level reservoirs in the Oseberg field, sealing faults exhibit typical ranges of SGR (Shale Gauge Ratio). Fristad et al. (1997) found that SGR values of <15 % do not hydraulically isolate structures, SGR in the range 15 % - 18 % support minor pressure differences (<1-2 bar) and that SGR values of >18 % corresponds to significant fault sealing (> 8 bar). This thesis provides comparison to Fristad et al. (1997) and ultimately addresses whether the analogue dataset used to determine limiting SGR values in the STAR tool is applicable. The STAR tool operates with a global database based on analogues from the Niger Delta, Oman, Brunel, GOM, DW Brazil, and the Central and Southern North Sea. Based on this dataset, STAR has predetermined probabilistic column heights associated with specific SGR values. After correlating the SGR calculations in this thesis with cross-fault formation pressure surveys, it was found that faults classified as sealing indicate that higher SGR values (>30 %) can support hydrostatic pressure differences of >8 bar. It was also found that faults displaying SGR values between 24 % and 30 % can be linked with minor cross fault pressure differences of around <1-4 bars. SGR zones displaying values < 24 % are found to be acting as conduits for cross-fault fluid communication between some structural segments. Finally, by applying these SGR calculations, even the P(10) case from STAR underestimate the retained column heights in the defined structural elements in the Oseberg area. As a result, is can be argued that STAR needs to be recalibrated to the specific components and parameters that we see in the Brent Group to be better suited in predictive analysis and fault seal evaluation in the northern North Sea if future opportunities are not to be missed.

Table of Contents

List of Figures

List of Tables

List of Equations

1. Introduction

The northernmost North Sea rift basin known as the Viking Graben and adjacent platform areas were formed during multiple rifting episodes in the Permian – Early Triassic and Middle-Late Jurassic (Ravnås et al., 2000). As a result the area is characterized by large normal faults with N- NE- and NW- orientations. The Oseberg fault block located on the eastern flank of the northern Viking Graben represents a pre-Tertiary structural high formed during the Permo-Triassic and Jurassic extensional episodes (Ravnas et al., 1997). The Oseberg fault block is today categorized by segments of rotated fault block terraces stretching from the Troll field in the east to the Viking Graben in the west (Figure 1).

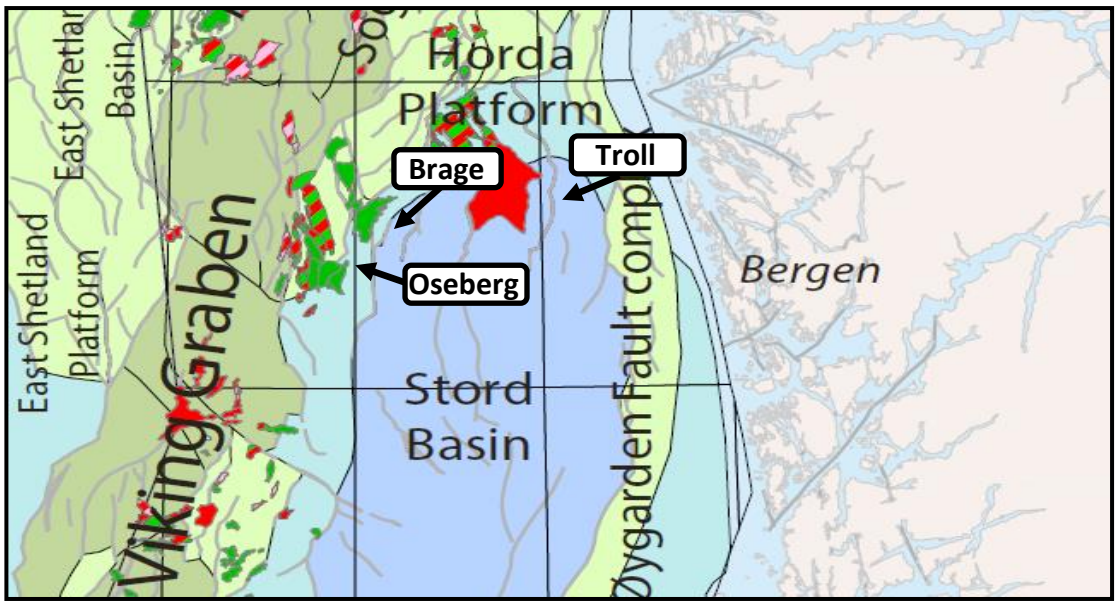

Figure 1: Map over the Northern North Sea displaying the present day structural elements and fields. Modified from Fraser et al. (2003).

Today, the Oseberg and Troll fields are giant oil and gas accumulations containing 69% of the oil and 97% of the gas discovered at the Horda Platform (Johnsen et al., 1995). The size of hydrocarbon accumulations in this part of the Northern North Sea commonly depends on the sealing potential of the bounding faults of the rotated fault blocks. As classic example of this, the Oseberg Syd area is defined by a series of fault-seal dependent hydrocarbon accumulations and compromises 15-20 elongated fault blocks with a general N-S striking pattern running sub-parallel to the Viking Graben (Fristad et al., 1997). A conceptual sketch displaying the faulted half-graben elements of the Oseberg area can be seen in Figure 2.

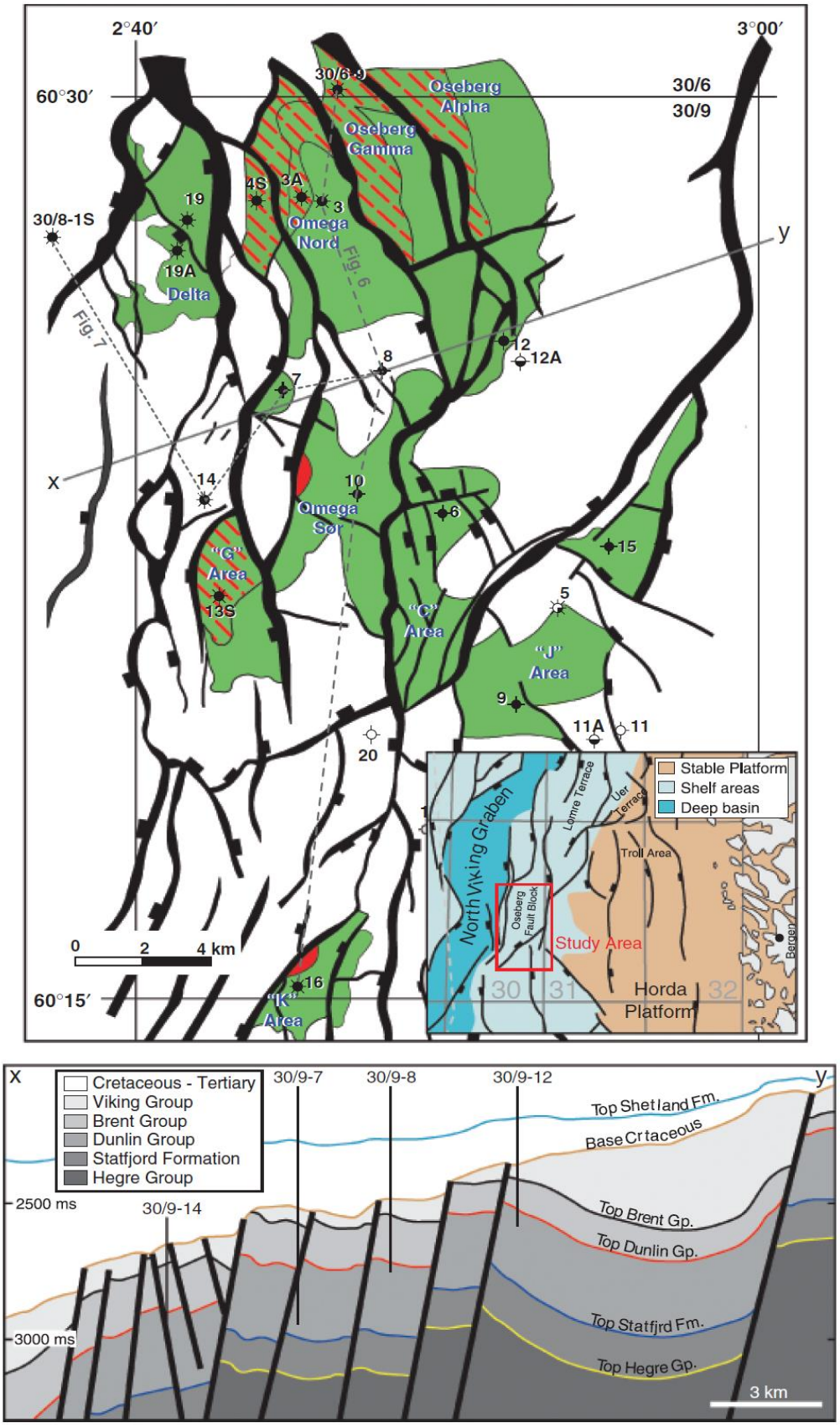

Figure 2: Map of the study area with an E-W cross section illustrating the general stratigraphy and structuration (Løseth et al., 2009).

The main focus of this thesis is to provide and analyze key structural and petrophysical parameters important for the understanding of local fault seal capacity by interpreting seismic surveys, well data and previous publications in the Oseberg area. Fristad et al. (1997) provide a case study of the Oseberg Syd, where fault seal behavior is predicted from the analysis of detailed depth models with lithological control. When comparing the results from this thesis with Fristad et al. (1997)'s paper, special emphasis will be put on the impact of the methodologies used to gather fault seal parameters and how these are subject to variations and uncertainties. The comparison will address the differences between these studies based on interpretation of subsurface properties such as lithology and fault displacement along with petrophysical properties such as Vsh (Volume of shale particles in a fault plane %) and SGR.

Due to the relatively small fault blocks and separate fluid contacts found in the different compartments of the Oseberg Syd area (Fristad et al., 1997), understanding the likelihood of both lateral sealing and individual fault sealing capacity is crucial in order to be able to predict the fault seal retained columns within the Brent Group. The impact fault characteristics and reservoir lithology have on fault sealing capacity; will be investigated in detail by comparing petrophysical well data and fluid contacts across interpreted fault-zones in a constructed structural 3D model. This will serve as a calibration dataset when assessing the predictive potential of Shell Petrel module; Stochastic Trap Analysis and Risking tool (S.T.A.R).

1.1 Objectives

The aim of this study is to investigate controlling fault seal parameters in the Oseberg Field and validate the current methodology used for determining parameters such as probability of fault sealing and maximum potential hydrocarbon column heights. This will be done by carrying out a complete fault seal analysis from scratch and then comparing the results with published field-data. In order to successfully meet the main objective of the study, some cornerstone objectives will have to be carried out:

- Identify and study fault-structures and key lithostratigraphic intervals in the Oseberg area.
- Investigate the fault seal capacity in the Oseberg structures with resulting retained hydrocarbon column heights.
- Examine the applicability of Shell developed proprietary Stochastic Trap Analysis and Risking (STAR) -module as a reliable tool for predicting fault seal-dependent hanging-wall traps in the Brent Group and discuss possible recommendations for local calibration.

2. Previous studies

The lithology of sedimentary sequences displaced along and juxtaposed against the fault-plane have significant impact on the shale gauge ratio of that fault zone, giving a direct indication of the amount of shale minerals smeared along the fault zone (Fristad et al., 1997). Understanding the structural history, depositional environment, facies trends, and controlling parameters of the litho-stratigraphic sequences, is crucial for being able to construct a model which represent the spatial distributions and trends observed in the Oseberg area. The Brent Group is the main target for this thesis, but it was decided to also include the lowermost intervals of the Viking Group and the uppermost section of the Dunlin Group due to the introduced petrophysical parameters of these formations.

2.1 Structural Development

The Northern Viking Graben experienced crustal extension during multiple rifting episodes in the Permian – Early Triassic and Middle-Late Jurassic separated by episodes of relative hiatus in the Middle Triassic and Middle Jurassic (Ravnås et al., 2000). Goldsmith et al. (2003) argue that only minor amounts of crustal extension took place during Bathonian times, and that the rifting in the Arctic spread into the North Sea during the Callovian to Early Kimmeridgian. This rifting is responsible for developing the north to north-easterly trending faults and subsequent transfer faults in the Viking Graben. In the Latest Jurassic to Earliest Cretaceous, the southern part of the Viking Graben experienced an easterly rotation of the established fault blocks, causing local compressional inversion on the basin margins.

The Oseberg area is located just east of the main section of northen Viking Graben, and is comprised of easterly tilted half graben structures bounded by Mid-Late Jurassic faults. According to Fristad et al. (1997), most of the faults in the Oseberg/Oseberg South region strike N-S to NNW-SSE in an anastomosing pattern, subparallel to the Viking Graben. Differential subsidence was present across faults during the Late Jurassic, as evidenced by significant expansion of the Viking Group (R. Færseth & Ravnås, 1998). This Late Jurassic extension and block rotation culminated with the collapse along the crest of already established Lower and Middle Jurassic fault blocks. Fristad et al. (1997) states that the Late Jurassic event culminated in the establishment of a series of small fault blocks in the Oseberg Syd region, where the areal extent of the fault blocks varies from that of 250km^2 to less than 10km^2.

R. Færseth and Ravnås (1998) states that the development of the large Jurassic fault blocks in the Northern North Sea generally can be summarized in three distinct stages, where an evolutionary pattern has been recognized.

1. An early rift stage which is represented by a diffuse transition from pre-rift to syn-rift conditions, controlled by initial block tilting and deposition of gently expanding wedges.
2. A main rift stage, characterized by the maximum extension and accelerated growth fault-block rotation which formed the major fault blocks.
3. A transition from an active rift stage to a post-rift stage ceased the active block-rotation related to the crustal stretching. After rifting ceased, crustal cooling and isostatic subsidence dominated the post-rift subsidence causing rotation towards rift axis of the basin.

From previous seismic studies Fristad et al. (1997) identified a near 100% thickness increase in Middle Jurassic intervals across the major fault between the structures in the Oseberg area. The interval-thickness within each fault block remains more or less the same however. Based on this information, Fristad et al. (1997) concluded that most of the main faults were subject to substantial differential subsidence even prior to the main rifting events of the Late Jurassic, hinting at the existence of an early Viking Graben in the Middle or even Early Jurassic times. The idea of the existence of such an early Viking Graben is further supported by I. B. B. Ramberg, Inge et al. (2008), stating that there was already established noteworthy submergence of the Northern North Sea during the Middle Jurassic, consistent with the creation and uplift of the North Sea Dome across the Southern North Sea (Figure 3).

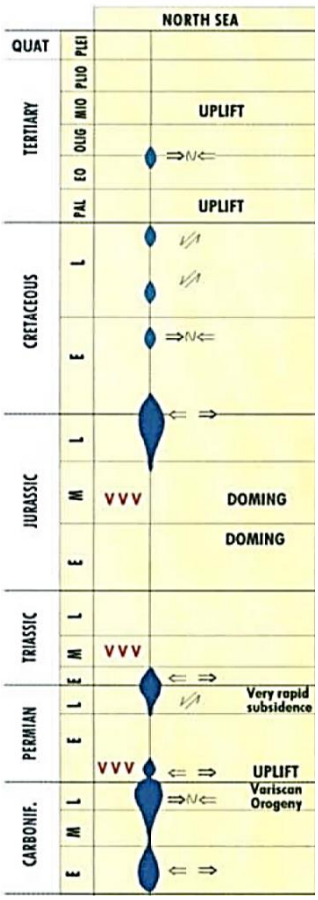

Figure 3: Summary of tectonic activity, North Sea. Modified from Brekke et al. (2001).

2.2 Stratigraphy

The Jurassic section of the Oseberg area can be divided into the Viking, Brent, and Dunlin groups. These groups mark significant changes in depositional environments and can further subdivided into formations. From the Mid-Upper Jurassic Dunlin Group, only the Toarcian to Bajocian Drake Formation has been included in this model as the base of the area of interest. From the Bajocian to Early Bathonian Brent Group, the Oseberg, Etive, Ness, and Tarbert formations were included in this model. The Bathonian to Ryazanian Viking Group is only represented by the Heather and Draupne formations in the areas covered by well data in the Oseberg region (Figure 4).

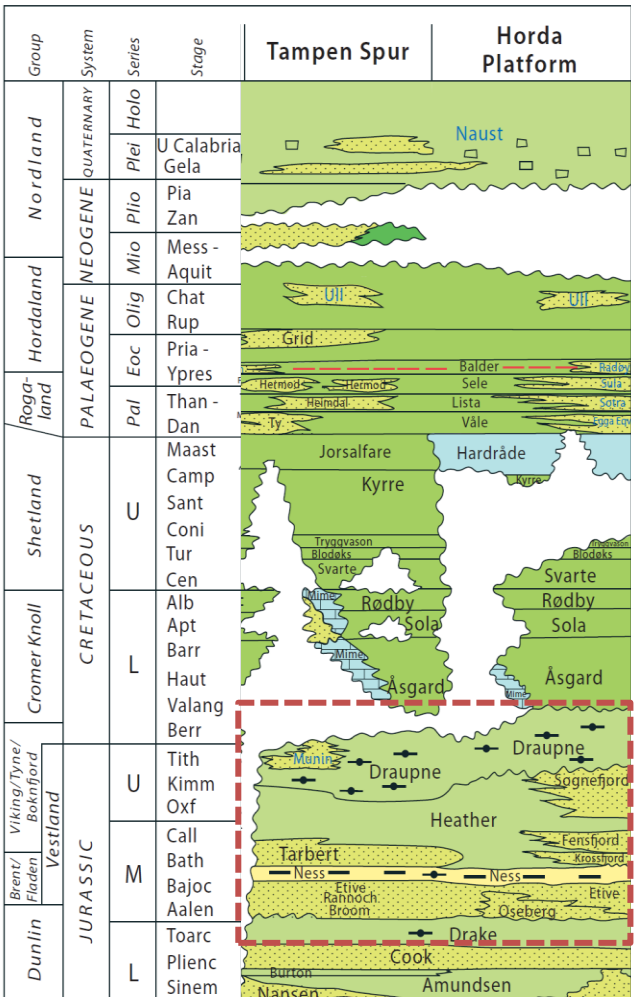

Figure 4: Lithostratigraphic chart of the North Sea and its main sub-sections. Modified from the lithostratigraphic chart «The North Sea 2014» (NPD, 2014).Red box outlines the key lithostratigraphic intervals that have been studied in this thesis.

2.3 Tectonostratigraphic Evolution

2.3.1 Dunlin Group

The Toarcian - Bajocian Drake Formation comprise the uppermost section of the Dunlin Group and is characterized by mudrocks in the Oseberg region (Ryseth, 2000). Figure 5 display a conceptual depositional system representative of the Drake Formation, where the offshore mudstones/shelf siltstones depict what can be observed in the Oseberg area. In the context of the tectonostratigraphic evolution of the Oseberg area, the Drake Formation is classified as a pre-rift deposit displaying some early syn-characteristics in the upper sections.

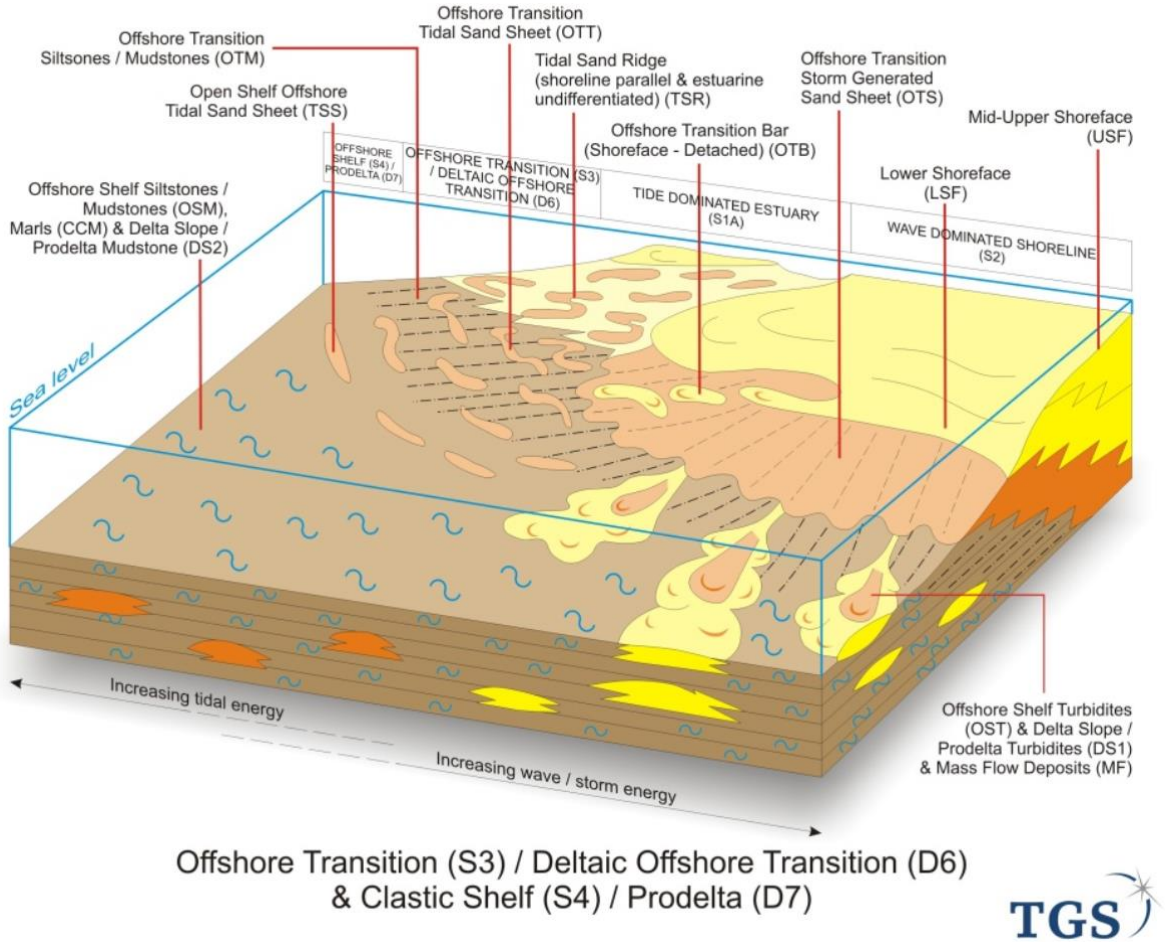

Figure 5: Conceptual depositional model of an offshore transition zone, in this case depicting the offshore shelfal mudstones of the Drake Formation (TGS, FMB)

2.3.2 Brent Group

The formation of the North Sea Dome and subsequent erosion of this new uplifted Early Jurassic and Triassic strata led to the transportation of large volumes of sand and mud towards the Northern North Sea (I. B. B. Ramberg, Inge et al., 2008). The Early Bajocian Oseberg Formation marks the earliest stages of a developing Brent Delta, and can be recognized by the transition from the mudrocks of the Drake Formation to the Bajocian marine sandstones (Helland-Hansen et al., 1992). Although the Oseberg Formation primarily consists of marine sandstones, there are according to Helland-Hansen et al. (1992), some cases where there has be observed fluvial deposits introducing a more coarse grained texture in the otherwise marine-dominated Oseberg Formation.

The transition from the marine sands of the Oseberg Formation into the lower to upper shoreface deposits of Rannoch-Etive formations signify the early progradation of the Brent delta shoreline. In the Oseberg area, the Rannoch Formation represent lower shoreface deposits whereas the Etive Formation is reflected by deposition in an upper shoreface/foreshore setting (Helland-Hansen et al., 1992). The joint thickness of Rannoch and Etive have been observed to range from that of greater than a 100m to a thin layer of 5-15m blanketing the Oseberg formation. These observations further support the notion that the shoreline progradation of the Brent delta took place in relatively shallow water (Ryseth, 2000).

The Lower Bajocian Ness Formation consist of a thick heterolithic interval of delta-plain deposits, making up the terrestrial equivalents of the Rannoch-Etive delta-front deposits (Helland-Hansen et al., 1992). According to Ryseth (2000), the Ness Formation is primarily made up of sandstones, mudrocks and coal beds that can be divided into a lower and upper section due to the differences in coal content and channel distribution (Figure 6). The lower part is characterized by a basal fluvial channel complex with local incisions into the underlying Rannoch, Etive and Oseberg Formations. These basal fluvial channel complexes are often overlain by fine-grained, coal-bearing deposits. In

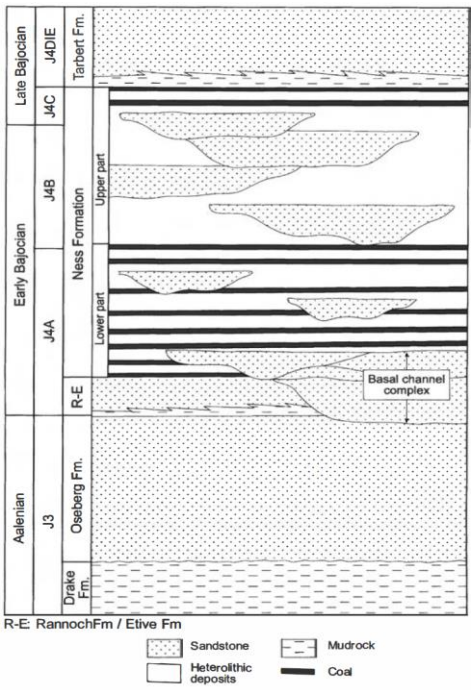

Figure 6: Stratigraphy and main facies of the Brent group in the Oseberg field (Ryseth, 2000)

the upper section of the Ness Formation who also has sandy channel fills, but less coal-bearing, fine-grained deposits (although not absent). Previous studies conclude that observed thickness variation in the Ness Formation can be attributed to syndepositional differential subsidence (Ryseth, 2000). A conceptual model of how the Ness part of the great Brent Delta might have looked at the time of deposition can be seen in Figure 7.

Figure 7: Conceptual model showing how the great delta front of the Brent Delta might have looked like with its north-south meandering distributary channels and vast floodplains(I. B. B. Ramberg, Inge et al., 2008).

The Late Bajocian Tarbert Formation primarily consists of shoreline sandstones and lower delta plain heterolithics, formed during the retreat of the great Brent Delta (Ravnas et al., 1997). The Tarbert Formation mark an important stage in the development of the Brent Delta and display the overall trend of a retreating and submerging Brent Delta which can be seen continued into the Viking Group. Ravnas et al. (1997) state that the Tarbert Formation in the Oseberg Brage area is comprised of backstepping shoreline facies developed predominantly in half-grabens. As a result, the Tarbert Formation display incomplete or absent deposition on structural highs due to rift syn and post depositional erosion. The prograding depositional shoreface to delta-front system observed in the Brent Group can be seen depicted in the conceptual model in Figure 8. Marine sands of the lower shoreface section represent the Oseberg Formation while the rest of the lower and upper shoreface represent the Etive and Rannoch formations. The lower delta plain with tidal channels, distributary channels and overbank tidal flats exemplify a conceptual depositional environment of the Ness Formation.

The Brent Group is displaying a complete range from pre- to syn-rift depositions, with the Oseberg Formation displaying pre-rift characteristics and the Ness and Tarbert formations displaying syn-rift characteristics.

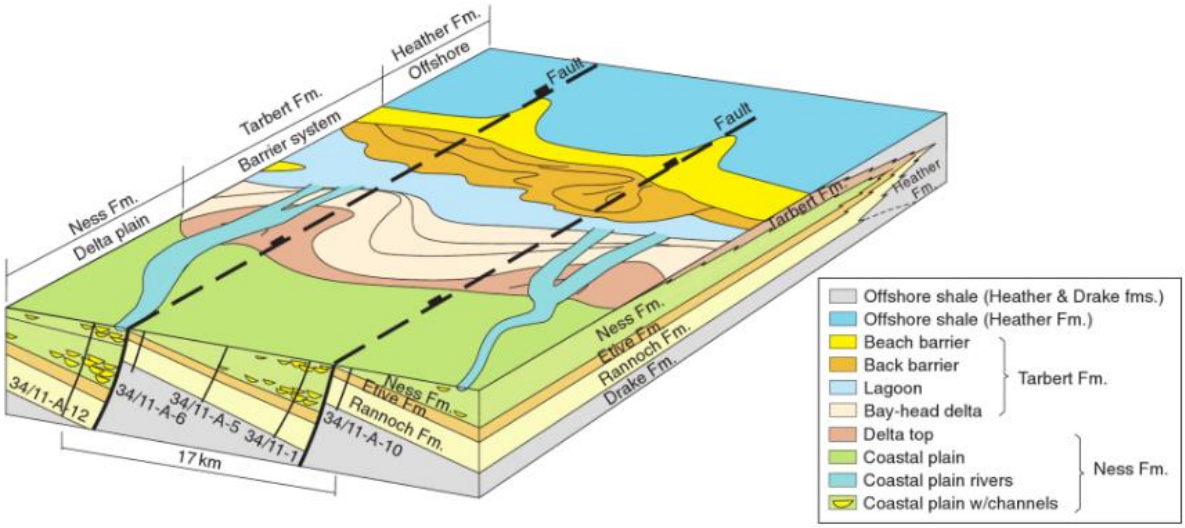

Figure 8: Schematic 3d illustartion of the Brent Group (Martinius et al., 2014).

2.3.3 Viking Group

The Heather Formation consists of Bathonian to Kimmeridgian marine mudstones. While most of the mudstones from the Heather Formation are oxygenated, some of the marine mudstones of the Lower Heather Formation show anaerobic tendencies. It is therefore suggested that these anaerobic mudstones have been deposited in an open marine environment with paleowater depths of more than 60 m (Ravnas et al., 1997). This holds equally true for the overlaying Draupne Formation displaying even more anaerobic mudstones, signifying a change from the oxygenated mudstones of the Heather Formation. This information points towards a mid- to outer shelf depositional environment of the Draupne Formation (R. Færseth & Ravnås, 1998). The proposed depositional environment indicate that significant subsidence of the Oseberg area was ongoing throughout the Middle Jurassic continued into the Late Jurassic, making it possible to classify the Heather and Draupne formations syn to post rift deposits.

2.4 Fault Seal Mechanics

Reservoirs in the western flank of the Horda Platform are found in major eastward-rotated fault blocks, where reservoir sandstones are present at several levels within the deltaic Brent Group. The main reservoir units in these intervals comprise the channel sands within the Upper and Lower Ness Formation and the transgressive marine sands in the Rannoch, Etive and Tarbert formations (Fristad et al., 1997). These reservoir units are sealed between the marine shales of the underlying Drake Formation and the overlaying Heather and Draupne formations. Since most seals in clastic sequences can be attributed to membrane seals (Watts, 1987), the dominant factor for fault sealing in the Brent Group of the Oseberg area is the capillary entry pressure of the seal rock (Fristad et al., 1997). In regards to the nature of the reservoirs in the Brent sequence, it is natural to mention some recognized sealing mechanisms defined by Yielding et al. (1997), where fault planes can provide membrane seals:

1) *Juxtaposition*; Reservoir sands are juxtaposed against a low permeable zone.
2) *Shale-Smear*; Shale minerals exist in the fault causing high entry pressure.
3) *Cataclasis*; Crushing coarser material to fine material increases fault entry pressure.
4) *Diagenesis*; Cementation along previously permeable fault plane.

A schematic illustration depicting some of these sealing mechanisms can be seen in Figure 9.

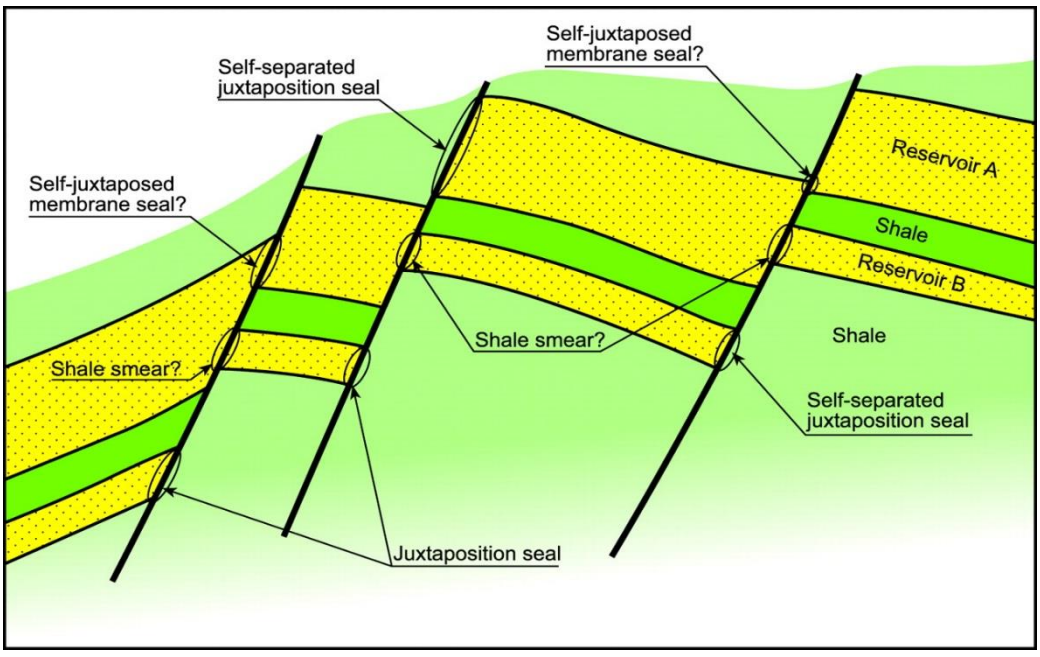

Figure 9: Schematic illustration showing potential sealing mechanisms and potential hydrocarbon traps in a normal fault environment that offsets sand-shale sequences (R. B. Færseth, 2006).

It is possible to observe both reservoir/claystone and reservoir/reservoir juxtaposition in the Oseberg area (Fristad et al., 1997). Reservoir/claystone juxtapositions are well known to be able to support significant pressure differences, while reservoir/reservoir juxtaposition are dependent on specific attributes in the fault plane. Yielding et al. (1997) define shale gauge ration and shale smear potential as two types of attributes that can support reservoir/reservoir juxtaposed pressure differences. The shale gouge ration (SGR) is an estimate of the proportion of fine-grained material entrained in to the fault gauge from the wall rocks, while shale smear potential estimates profile thickness of a shale drawn along the fault plane. Both of these attributes are affected by the mineral composition of intervals dragged along the fault plane (Figure 10). The parameters are therefore varying over the fault plane, meaning that by using these methods, a fault cannot simply be classified as sealing or nonsealing but will rather provide a distribution of sealing potential across the fault plane.

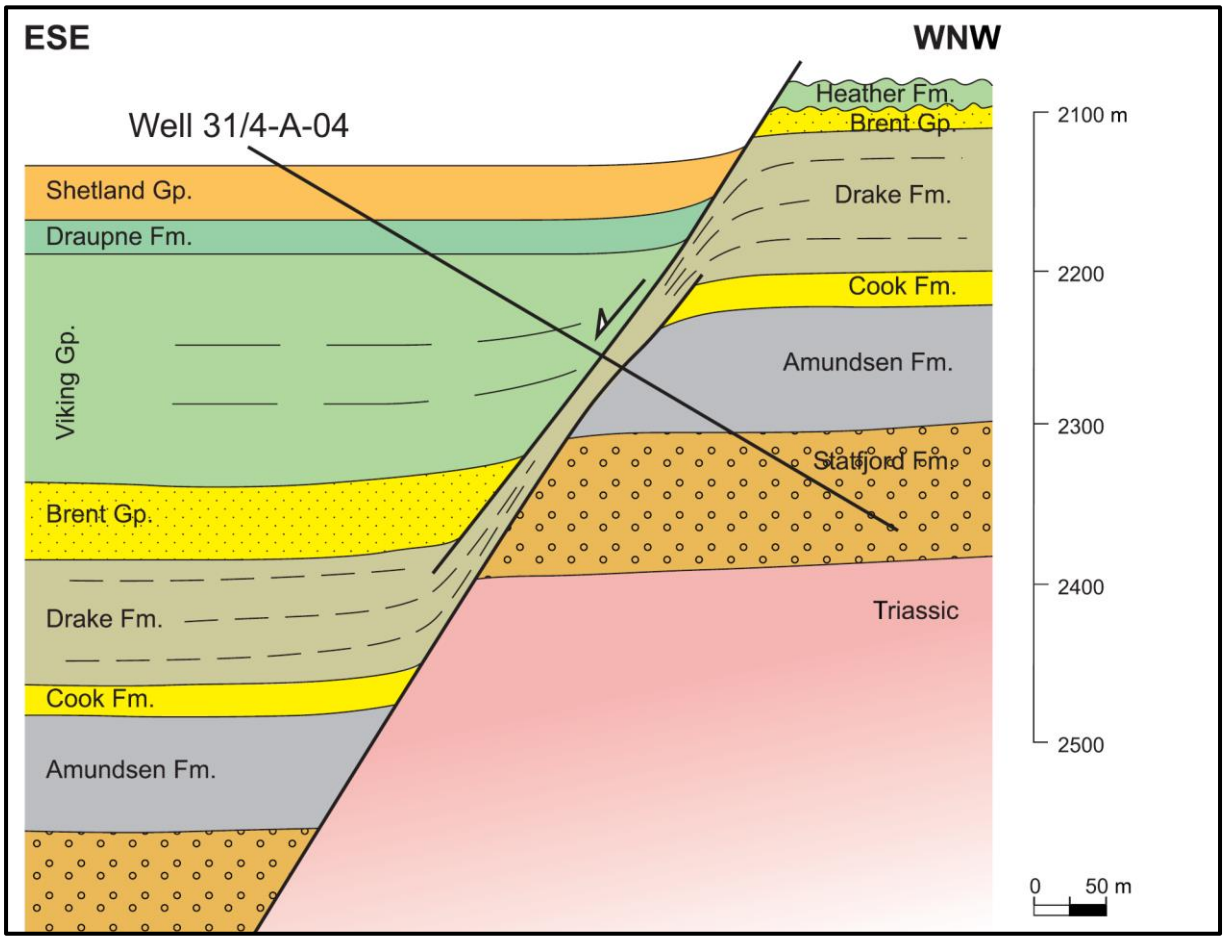

Figure 10: Cross section of a large fault with smear derived from a thick source layer. (Farseth et al., 2007).

There are a number of studies that analyze the effects shale gouge ratio and shale smear potential have on the probability of fault-sealing and supported pressure differences. Fristad et al. (1997) examines the impact the Vsh dependent Shale Gouge Ratio (SGR) have on probabilistic determination of fault sealing in the Brent sequence in the Oseberg South area. Fristad et al. (1997)'s paper emphasizes the observations that has been made regarding the apparent connection between SGR in the fault plane and the probability of static fault sealing occurring between fault-blocks in the Oseberg area. By calculating SGR across fault planes and comparing with published well data, it was observed that the range of the SGR from seal to non-seal is tight but consistent with pressure data and established fluid contacts. Based on this, Fristad et al. (1997) was able to determine specific ranges of SGR that are linked with fault seal behavior in the Oseberg area. Faults with local SGR values of less than 15 %, consistently show that no static fault sealing should be expected, and therefore allow cross-fault fluid communication and no pressure differences. Fristad et al. (1997) also documented that if SGR values is in the range of 15 % to 18 %, it can be expected to encounter some static sealing supporting pressure differences up to 1 to 2 bars. SGR values of 18 % and more are able to support significant cross-fault pressure differences (8 bars and up) and are often linked with significant sealing potential.

Fristad et al. (1997) further states that the eastern area of the central Oseberg area has more heterogeneous reservoir units in the form of channels. This causes the fault seal evaluation to be more uncertain. The reservoir is thinner and sandier in the eastern part, meaning that diagenesis or cataclasis has a more important role in determining fault sealing in this part of the block.

Disclaimer

To be able to manufacture a structural model allowing for detailed operations such as petrophysical property modeling and fault seal analysis, various data from different sources was implemented. In this study, data open to the public as well as proprietary data kindly provided by A/S Norske Shell has been utilized. Some data such as litho-stratigraphic and chrono-stratigraphic well tops have been acquired from publicly open domains such as NPD, while seismic surveys, petrophysical data and company owned methodologies and/or specific algorithms have been provided by A/S Norske Shell or through affiliated providers (Open Works, TGS, Discos, etc.). Some of these specific methodologies and/or algorithms (Like the STAR plugin discussed in the methodology) are owned and/or copyrighted by Norske Shell, and will therefore not be discussed in detail in this thesis.

3. Data

All data used in this thesis is located in the Oseberg Field, with the exception of analogue models or previous studies which will be addressed in detail. The area of interest encompasses all of the data used in this thesis, including seismic data, petrophysical data, time-depth relationships, lithostratigraphic and chronostratigraphic data. The Oseberg field (outlined) with its relative location to the Norwegian coast and Troll and Brage fields can be seen in Figure 11, along with the location of the wells and main seismic survey (NH0402) used in this thesis.

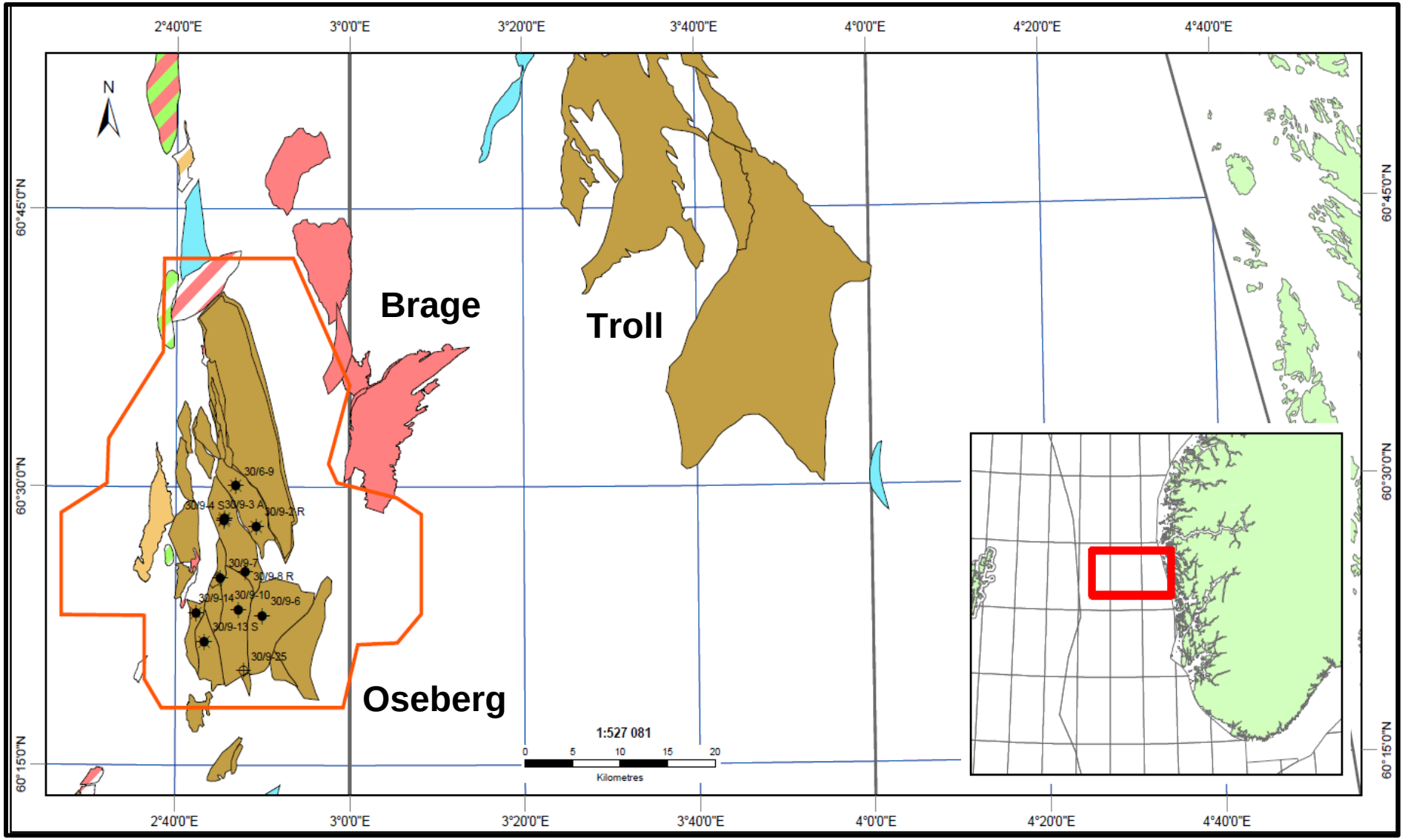

Figure 11: Map displaying the locaiton of the Oseberg field and the seismic survey NH0402 compared to the norwegian coast. Oseberg is outlined by the extent of siesmic survey NH0402, to the west of Brage and Troll fields.

3.1 Well Data

Oseberg South can be sorted into segments with a varying degree of well coverage. For the analysis of these segments, a number of wells with petrophysical data, well tops and reports were provided by Norske Shell (Table 1).

Segment:	B-north	B-south	C	G-Central	G-East	Gamma	Omega North	Omega South
Well:	30/9-4S	30/9-7	30/9-6	30/9-14	30/9-13S	30/9-2R 30/6-9	30/9-3A 30/9-8 R	30/9-10 30/9-25

Table 1: Table displaying the structural element segments and the wells of each segment.

A total of eleven wells have been used in the studies of the Oseberg area. The information about the available data in each well and specific details can be seen in Table 2.

Well data information

Well	Year	Total depth (MD) [m]	Oldest penetrated
30/6-9 R	1990	3476.0	Late Triassic
30/9-2 R	1986	2830.0	Early Jurassic
30/9-3A	1984	4300.0	Middle Jurassic
30/9-4 S	1985	4303.0	Middle Jurassic
30/9-6	1987	3034.0	Early Jurassic
30/9-7	1988	3565.0	Early Jurassic
30/9-8 R	1989	3200.0	Early Jurassic
30/9-10	1990	3649.0	Middle Jurassic
30/9-13 S	1991	4027.0	Early Jurassic
30/9-14	1993	3680.0	Early Jurassic
30/9-25	2013	3220.0	Middle Jurassic

Table 2: Table displaying general well information of the wells used in this survey.

All of the wells have a full set of petrophysical well logs and time depth relationships.

The faulted terraces of Oseberg have cases that allow for both cross-fault sealing and leaking. Because of the potential uniqueness of each segment, there have been drilled wells in the majority of the fault blocks to assess reservoir connectivity. The location of the wells and their target fault-block segment can be seen in Figure 12.

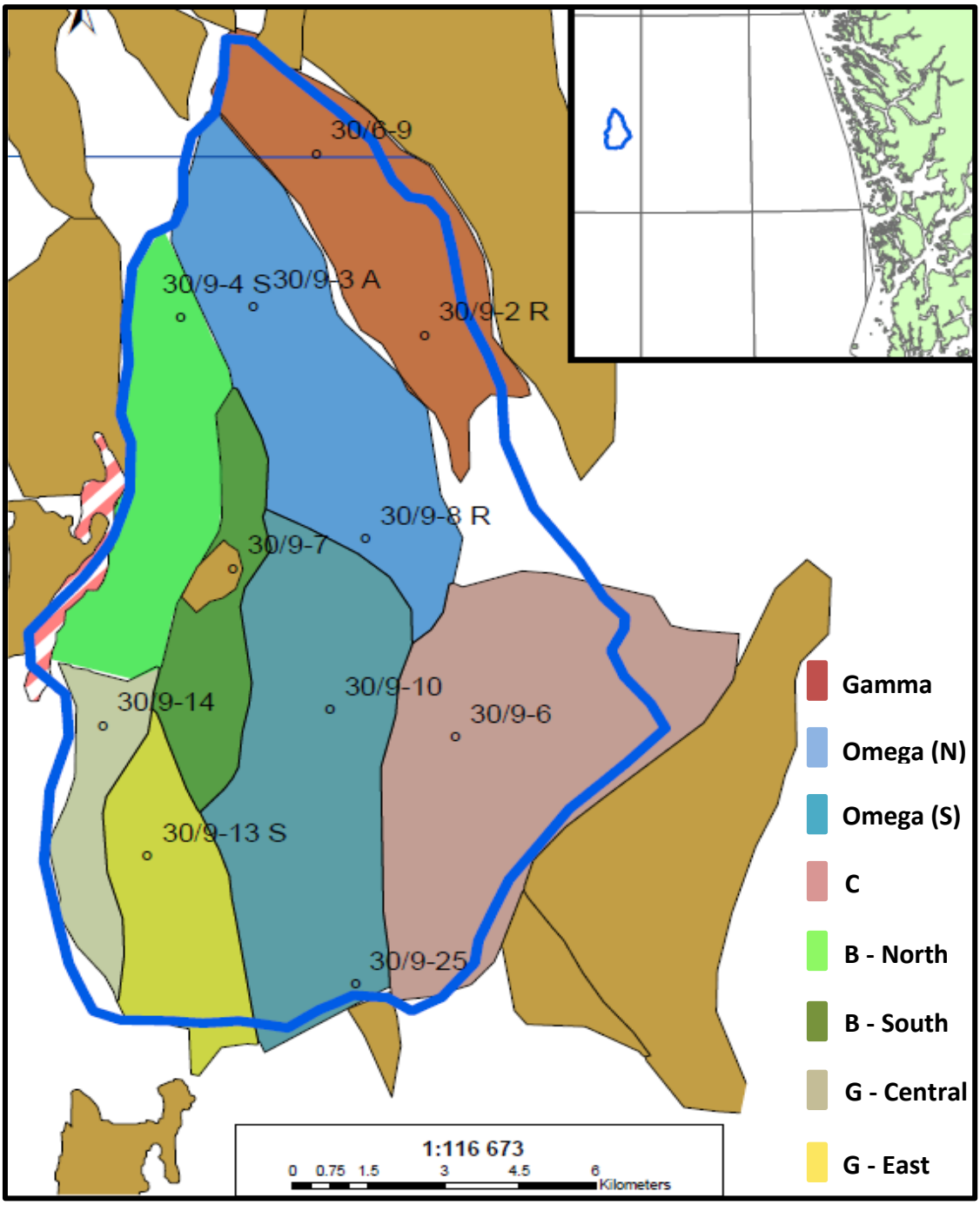

Figure 12: Map showing the location of each well and the name of each structural segment wihtin the area of interest.

3.2 Pressure Data

Formation pressure surveys were provided by Norske Shell (Table 3), to test specific reservoir intervals and determine fluid contacts:

Formation Pressure Survey

Well	Year	Formation Pressure Interval TVDSS [m]	Formation(s) tested
30/6-9 R	1990	2434.5 – 3411.0	Ness, Etive, Oseberg, Drake
30/9-2 R	1986	2562.8 – 2737.3	Oseberg
30/9-3A	1984	2715.8 – 3888.6	Ness, Etive, Oseberg, Drake
30/9-4 S	1985	2751.4 – 3507.4	Tarbert, Ness, Etive, Oseberg, Drake
30/9-7	1988	2786.5 – 3142.5	Heather, Tarbert, Ness, Etive, Oseberg
30/9-8 R	1989	2802.2 – 3109.4	Tarbert, Ness, Etive
30/9-10	1990	2730.7 – 3076.1	Heather, Tarbert, Ness
30/9-13 S	1991	2880.7 – 3924.8	Heather, Tarbert, Ness
30/9-14	1993	2975.8 – 3482.0	Heather, Tarbert, Ness

Table 3: Table displaying the range of the pressure tested intervals and the formations tested in the surveys.

3.3 Seismic Data

Norske Shell provided the following seismic data to be used in interpretation of the Oseberg area (Table 4).

Seismic survey information (3D)

NH05M01		NH8502		NH0402	
CRS	ED50 UTM 31 N	*CRS*	ED50 UTM 31 N	*CRS*	ED50 UTM 31 N
Inlines	4889	*Inlines*	1092	*Inlines*	2399
X-lines	6695	*X-lines*	850	*X-lines*	3035
Inline interval	12.5	*Inline interval*	25	*Inline interval*	18.75
X-line interval	12.5	*X-line interval*	25	*X-line interval*	12.5
Inline rotation	0.0	*Inline rotation*	90.0	*Inline rotation*	90.0
Sample interval	4	*Sample interval*	4	*Sample interval*	4
Volume format	Float pt. 32	*Volume format*	Float pt. 32	*Volume format*	Float pt. 32
Bytes consumed	106.7 GB	*Bytes consumed*	2.66 GB	*Bytes consumed*	20.4 GB

Table 4: General information about the seismic surveys used in this thesis.

Survey NH0402 was subject for the main interpretation, substituted by other surveys where a comparative qualitative control was deemed necessary. Although other surveys were used for comparative analysis, no interpretation was conducted on surveys NH05M01 and NH8502, as NH0402 covered the area in sufficient detail.

3.4 Seismic Well-tie

3.4.1 Wavelet

The construction of a statistic seismic wavelet was conducted based on the Brent level intervals. This wavelet was then used for the seismic well tie for all wells. The wavelet is zero phased and is calculated to have a wavelength of 128 m and a sample interval of 2 ms (Figure 13). From the power spectrum it is possible to observe that the highest frequencies can be located in the range of 20-30 Hz (**Error! Reference source not found.**). The Shell company standard applied to the wavelet after construction is displayed in Appendix 1.1.

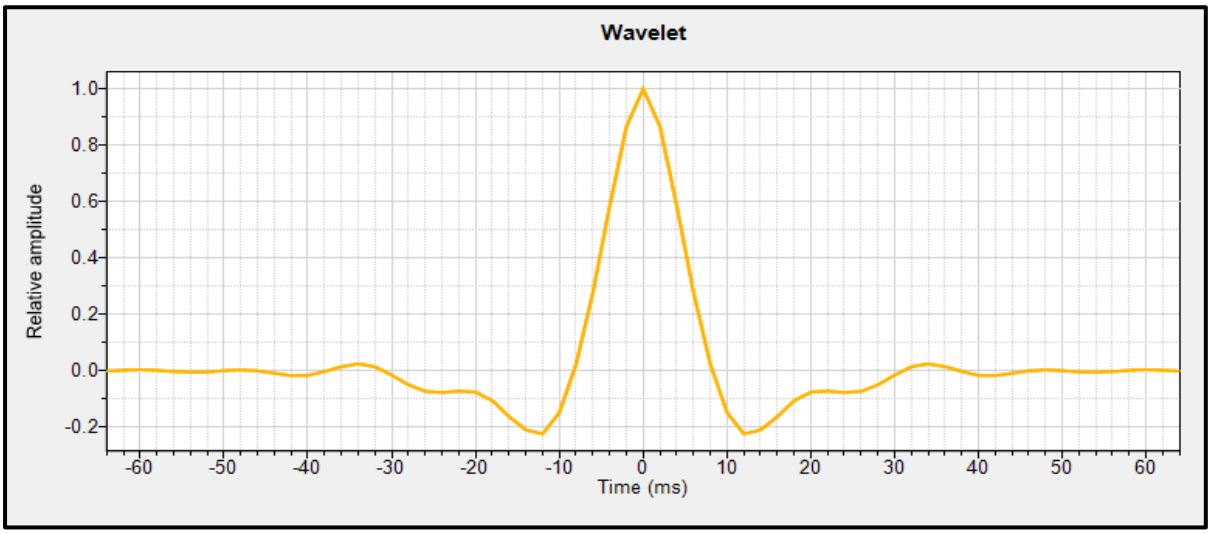

Figure 13: Seismic wavelet used to develop a seismic well-tie.

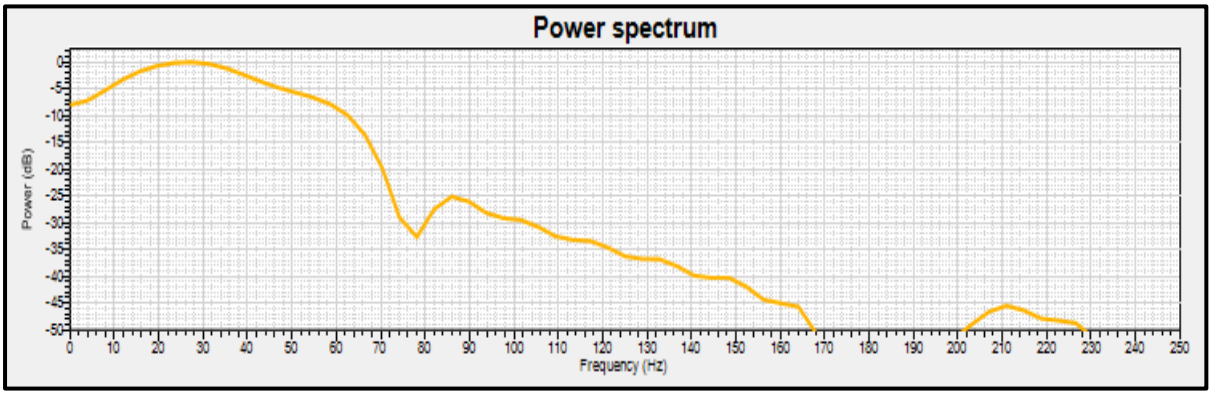

Figure 14: Power spectrum of the statistic seismic wavelet

3.4.2 Well-Tie

A seismic well tie was produced by the constructed wavelet with the sonic and density well-logs (Figure 15). A series of check-shots was provided to establish a time depth relationship between seismic survey NH0402 and the well data.

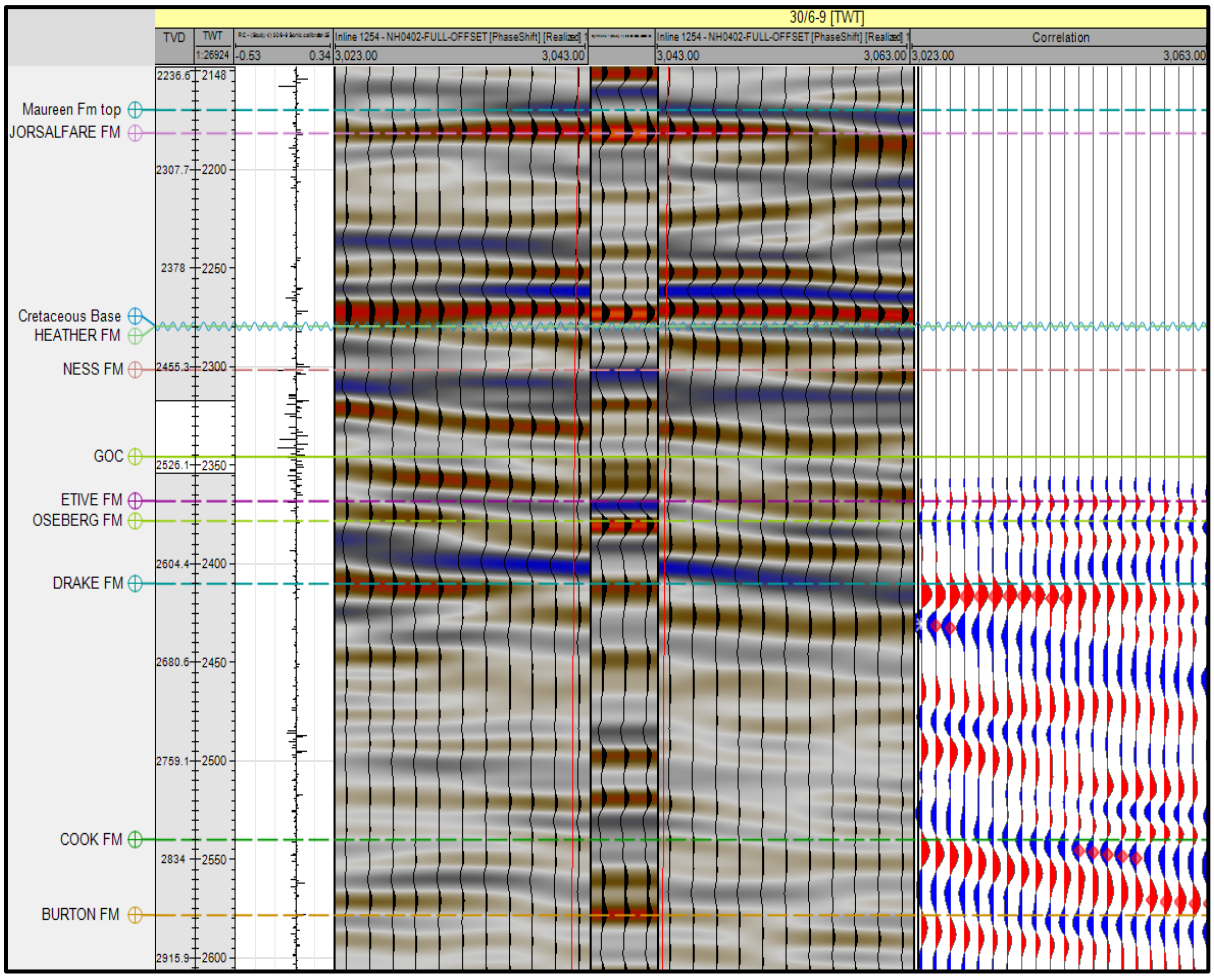

Figure 15: Seismic well tie exemplified by synthetic seismogram generated for well 30/6-9.

3.5 Software

Petrel 2014 was used for seismic interpretation, well analysis, structural modeling, property modelling, fault seal analysis, SGR calculations, column height predictions and volumetrics.

Excel was used for petrophysical calculations for parameters such as Vsh and the construction of formation pressure plots and subsequent analysis.

Adobe Illustrator and Corel DRAW were used to create original or modify existing figures for this thesis.

ArcGIS were mainly used to construct maps, data locations or property distributions.

4. Methodology

4.1 Data Preparation

Because of the input-sensitive nature of the fault seal analysis process, it is important to properly analyze the data in order to make sure that there are no irregularities or inconsistencies. In order to reduce uncertainty in the model, a consistent methodology followed by a qualitative analysis was performed on the data.

Well tops were compared to available litho-stratigraphic markers from NPD, OpenWorks and FMB. These markers were then further controlled by a comparison with the well logs. In some cases, NPD provided a more satisfactory match with the listed litho-stratigraphic markers than OpenWorks or FMB. Based on this comparative analysis and discussion with exploration data management team at Shell Risavika, it was decided to use NPD tops as the primary litho-stratigraphic and chrono-stratigraphic well markers in the Oseberg area. Seismic data was QC'd for parameters such as phase and polarity throughout the surveys to make sure that all possible future interpretations were consistent. Since the project is to be available for future analysis in Norske Shell, the company-specific setup was applied to the dataset (Appendix 1.1).

4.2 Well Data - Analysis and Correlation

The wells were analyzed in a well section window and by examining the well reports for any discrepancies which would undermine the credibility of the log data (wash outs, cave-ins etc.). When no significant indications of bad boreholes could be found, it was decided to proceed with the assumption that the logs were trustworthy.

Before initiating any interpretational studies on the seismic data, it was decided to perform a quick well correlation analysis in order to determine the trends in changing thickness of the focus intervals. These observed trends **(**Figure 16**)** were then used as guide when later conducting seismic interpretations.

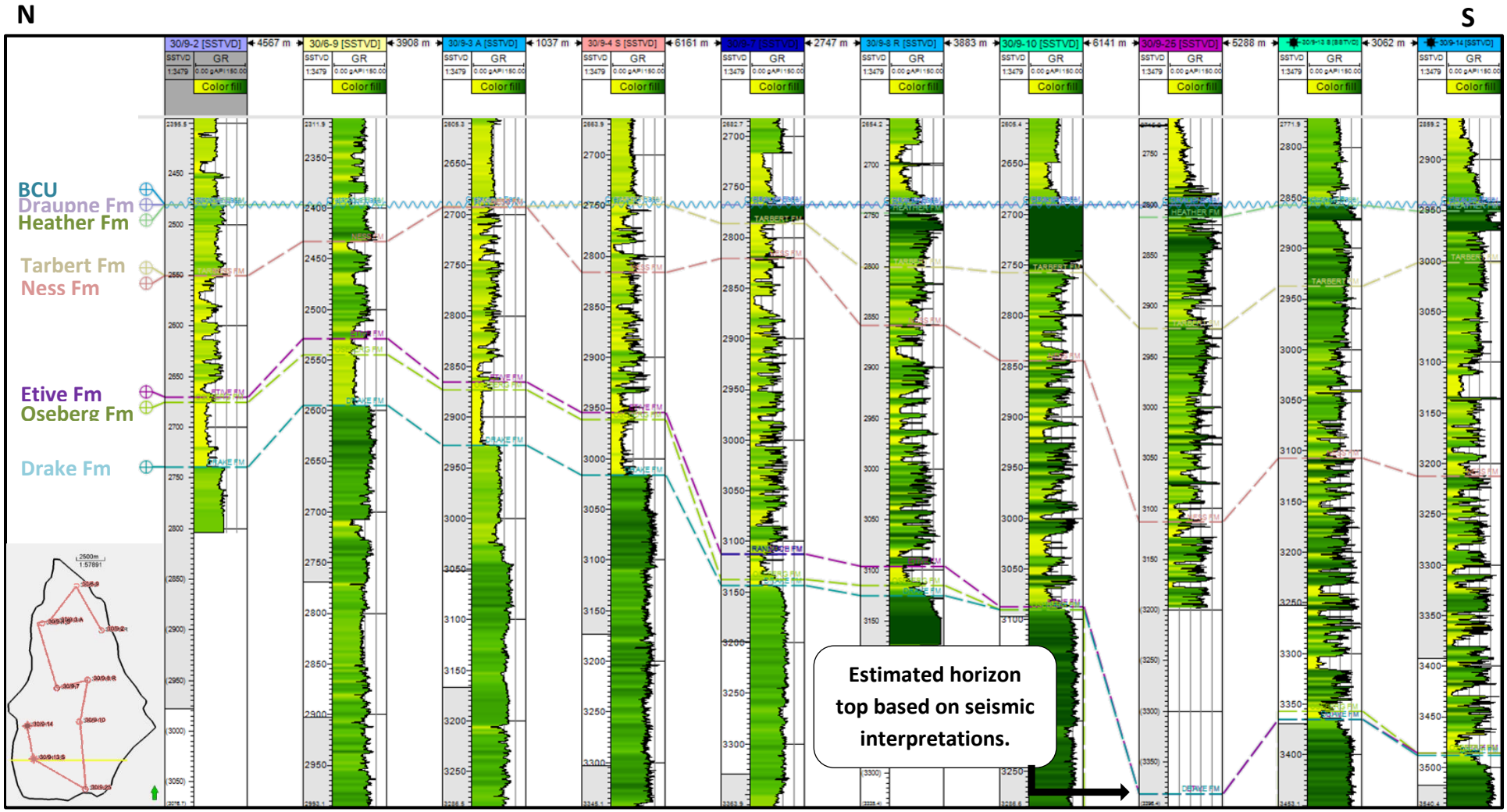

Figure 16: Well correlation pane with all wells, in a general North (left) – South (right) direction. The map displaying the well location can be seen in the bottom left corner.

4.3 Petrophysical Calculations

As explained in chapter 2.4, Vsh is a critical parameter in the calculation of fault related properties such as SGR and consequently the associated column height. Vsh can be calculated by a variety of methods, each with its own merits. Often a project will be conducted using a particular method due to data availability only, where possible best practice would link well log data to actual measured data from core for proper calibration. Due to the time constraints imposed on this project, core calibration has not been completed.

4.3.1 Vsh Calculation from Gamma-Ray

Calculating the Vsh from Gamma-ray logs is relatively simple operation, but it is important to regulate which input-parameters to use. The base equation used for calculating the Vsh from GR-logs can be formulated as such:

$$Vshg = \frac{GR - "Clean"}{"Shale" - "Clean"} \qquad \textbf{E.q. 1}$$

Where Vshg is the volume of shale (0-1), GR is the reading from the Gamma-ray log at a given depth, "Clean" is the GR-value indicating clean sand and "Shale" is the GR-value indicating shale matrix. With this equation as a foundation, a conditional equation could be formulated:

$$Vsh = If(GR < "Clean";0;\text{If}(GR > "Shale";1;\frac{GR - "Clean"}{"Shale" - "Clean"})) \qquad \textbf{E.q. 2}$$

The conditional equation utilize the listed "Clean" and "Shale" parameters to force the maximum range the GR input by leveling at 0 and 1. These values vary across wells and formations, and can be impacted by the presence of radioactive trace elements. This holds especially true for the GR logs which can be affected by increased levels of micaceous trace elements in the matrix. It is therefore important to conditionally pick the "clean" and "shale" values based on where the lithology is the most certain. Core data from the key intervals of the Brent Group is available for most of the wells, and allow for confident lithological picks for certain GR-values.

An example of how to pick these values can be seen in Figure 17. This is a section of the base of the Brent Group displaying cored intervals which provide good control over the lithological components and therefore a more certain pick of Clean and Shale GPI values. It is however important to keep in mind that even subtle variations in the sand/shale line selection has a significant impact on the Vsh output.

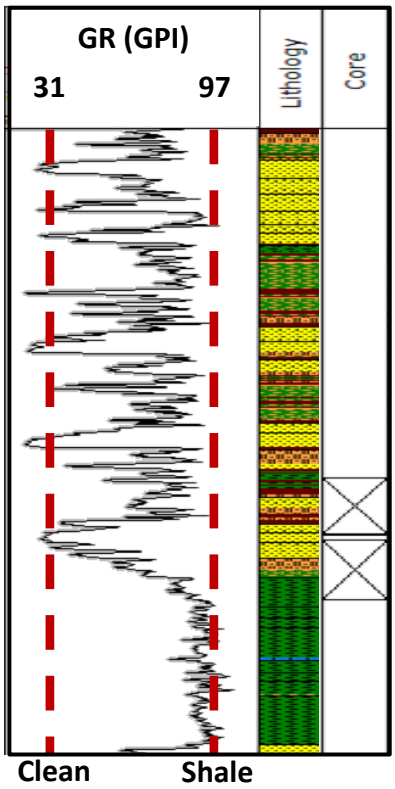

Figure 17: Log of well 30/9-14 from FMB's well panel plug-in displaying interpreted facies and cored sections with clean and shale lines.

Using these values as input parameters for the conditional Vsh equation (E.q. 2) along with the extracted Gamma-ray curves against depth in a simple Excel spreadsheet provide a Vsh versus depth output. This Vsh curve can then be imported as a separate log into Petrel and used in further analysis.

4.3.2 Vsh Calculation from Neutron-Density

Calculating the Vsh from Neutron Density curves is more complex and requires more input parameters than when calculating Vsh from GR logs. It is however based on the same principle, where the simplified equation can be written like this:

$$Vsh = \frac{X1 - X0}{X2 - X0} \qquad \textbf{E.q. 3}$$

Where: $X1 = Neu + M1 * (Rho_{matrix} - Den)$

$$X2 = NPHI_{shale} + M1 * (Rho_{matrix} - Rho_{shale})$$

$$X0 = NPHI_{matrix}$$

$$M1 = \frac{NPHI_{fluid} - NPHI_{matrix}}{RHO_{fluid} - RHO_{matrix}}$$

Combining these, the complete equation which will be used for calculations can be written like this:

$$Vsh = \frac{(Neu + \frac{NPHI_{fluid} - NPHI_{matrix}}{Rho_{fluid} - Rho_{matrix}} * (Rho_{matrix} - Den)) - NPHI_{matrix}}{\left(\left(NPHI_{shale} + \frac{NPHI_{fluid} - NPHI_{matrix}}{Rho_{fluid} - Rho_{matrix}}\right) * Rho_{matrix} - Rho_{shale}\right) - NPHI_{matrix}} \qquad \textbf{E.q. 4}$$

Where:

Den: Log reading for density at specific depth.	(g/cm^3)
RHO_{fluid}*:* Density at 100% fluid.	(g/cm^3)
RHO_{matrix}*:* Log reading for density at 100% matrix.	(g/cm^3)
RHO_{shale}*:* Log reading for density at 100% shale.	(g/cm^3)
Neu: Log reading for neutron at specific depth.	(Neutron porosity, 0-1)
$NPHI_{fluid}$*:* Neutron at 100% fluid.	(Neutron porosity, 0-1)
$NPHI_{matrix}$*:* Log reading for neutron at 100% matrix.	(Neutron porosity, 0-1)
$NPHI_{shale}$*:* Log reading for neutron at 100% shale.	(Neutron porosity, 0-1)

By applying the same conditional Vsh parameter-range operation as when calculating Vsh from GR, the following conditional equation can be formulated:

$$Vsh_{capped} = If(VSH < 0; 0 ; If(VSH > 1; 1; VSH)) \qquad \textbf{E.q. 5}$$

Depending on which values are used for the parameters in ***E.q. 4,*** the results may vary. It is therefore important to keep in mind that just like the GR-log, the Neu-Den curves area also affected by other minerals such as micas, siderite, ankerite, and volcanic rock fragments etc. (Crain, 2000).

The methodology for acquiring these parameters is therefore essentially the same as with GR-based Vsh calculations. The numbers of the 100% shale and matrix parameters is based on analysis of well logs along with the control of core data (Figure 18). These readings had to be conducted for each well restricted to the area of interest (Brent Group) as the values differ across intervals and wells. Clean matrix and shale bodies were selected, and an average over five readings from different clean matrix bodies (core data based) were used.

An example of a comparison between the results from the two methods can be seen in Figure 19. This impact of this is discussed in further detail later in chapters 5.2 and 6.2.1.

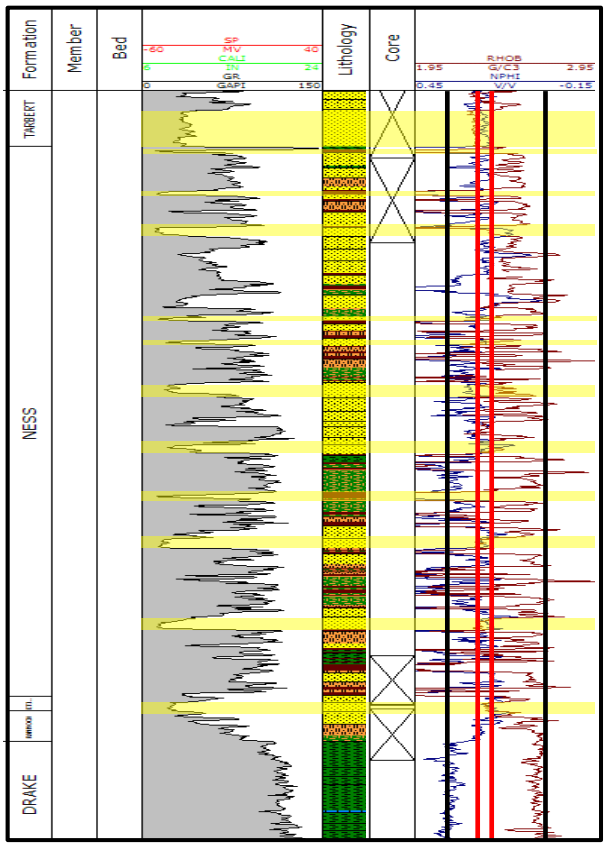

Figure 18: Well section from well 30/9-14 displaying Neu-Den values for 100% shale (black lines) and 100% matrix (red lines).

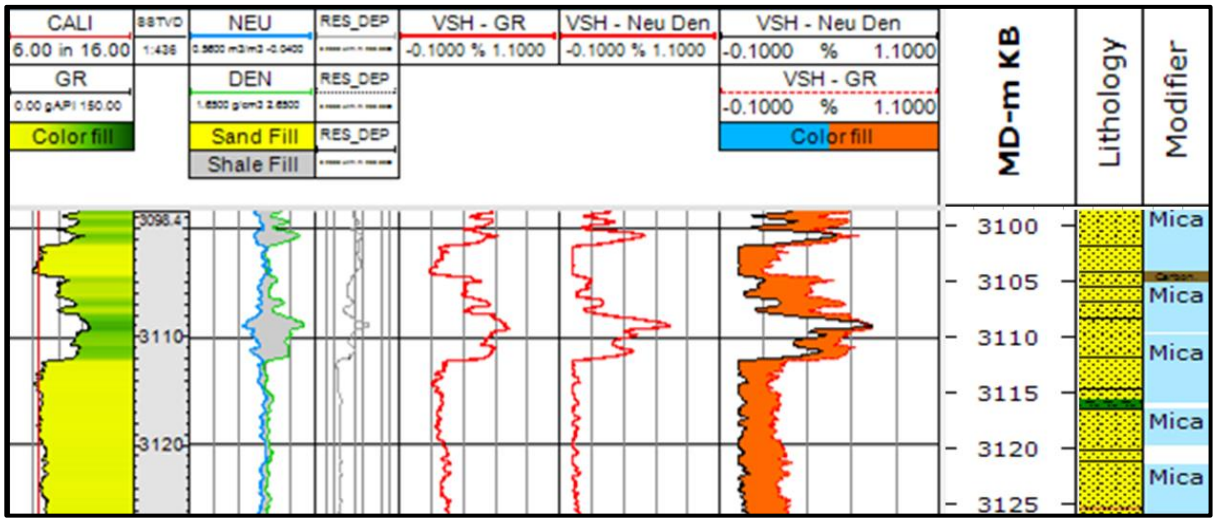

Figure 19: Example of a comparison between the calculated Vsh logs. Complete figure can be seen in chapter 5.2.

4.4 Seismic Interpretation & Surface Construction

The seismic interpretation was conducted on 3D seismic survey NH0402 with lithostratigraphic control from NPD and Shell Open Works well tops. Since this thesis will produce a direct comparison to the paper published by Fristad et al. (1997), the boundary for interpretation was set to the main fault blocks interpreted in that study).

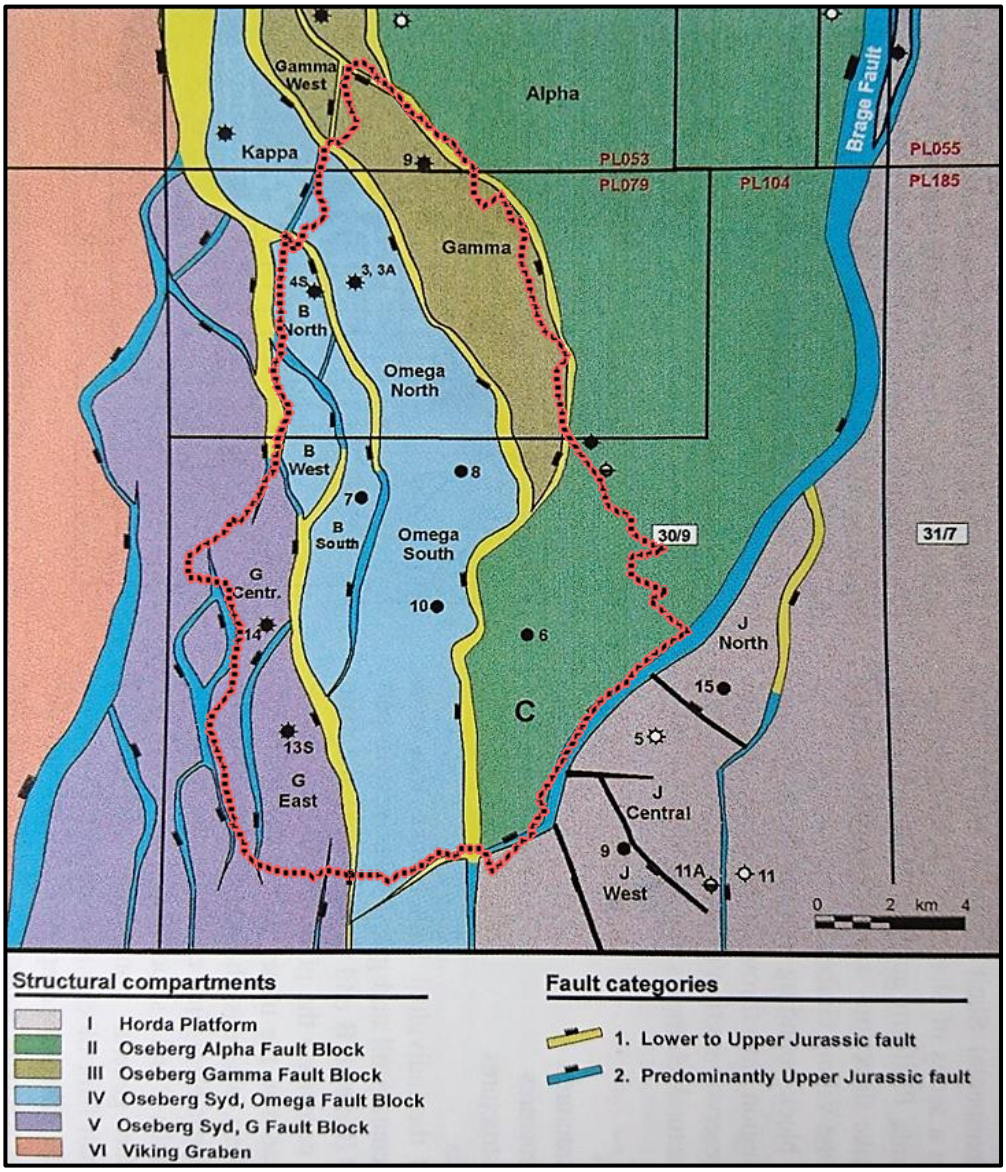

Figure 20: Structural elements defined within Block 30/9 with area of interest outlined in red. Modified from Fristad et al. (1997)

Seismic interpretation was initiated by mapping the Base Cretaceous Unconformity (referred to as the "BCU") as this marks the top of the zone of interest. The BCU usually display a very characteristic change on well logs such as gamma ray. Here the Draupne and Heather Formations have a hot shale response (>120 gAPI) compared to the overlying strata (< 90 gAPI) of the lower Jorsalfare Formation Figure 21. Due to the fact that the BCU was mainly formed after the main rift event in the Late Jurassic, it is continuous and relatively un-faulted. The BCU is a high quality regionally interpretable event, with a clearly recognizable seismic character due to strong reflectivity coefficients and an often angular relationship with the underlying strata (Figure 22).

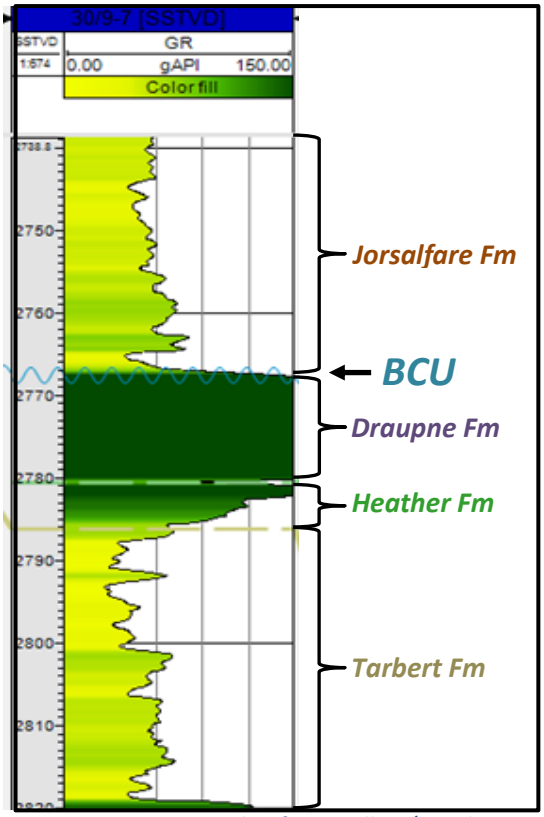

Figure 21: Gamma ray log from well 30/9-7 showing the clear boundary between Cretaceous and Jurassic.

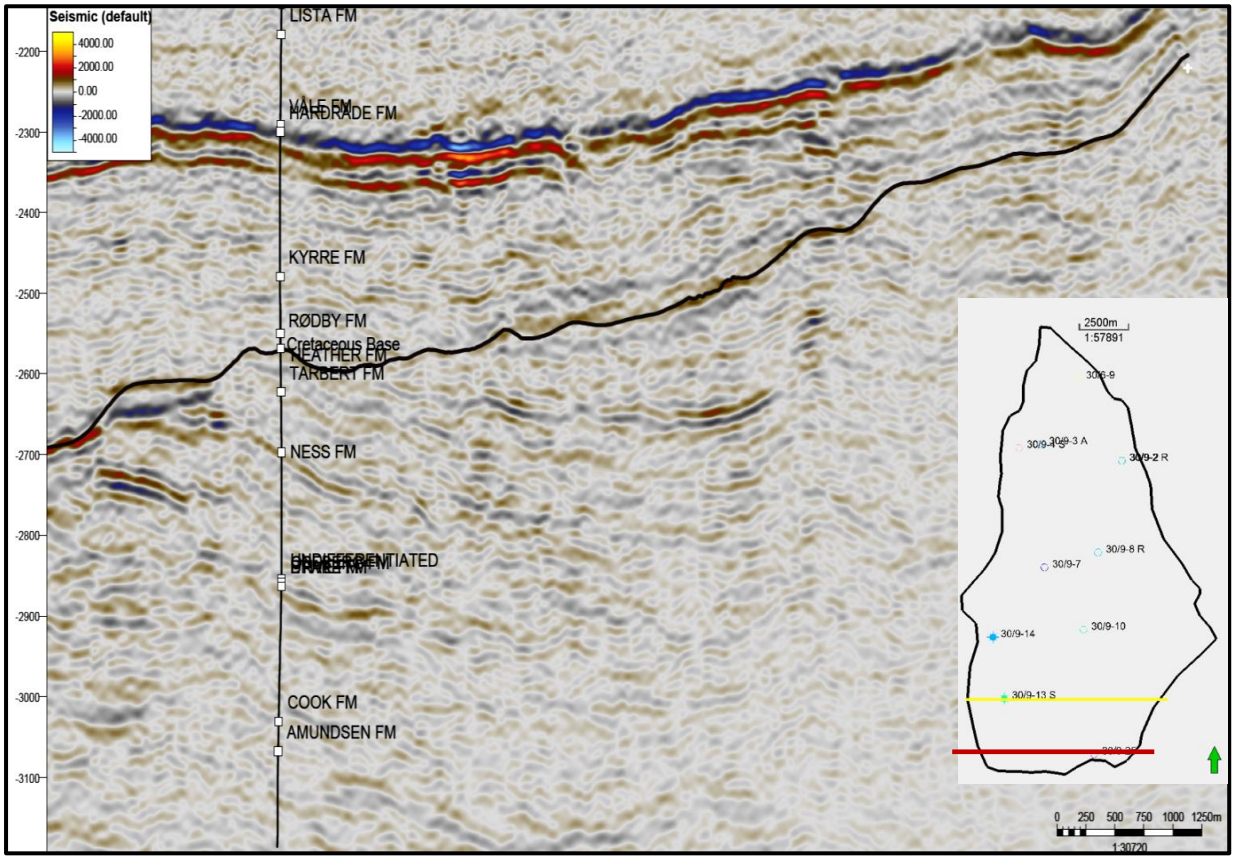

Figure 22: TWT seismic Inline 412 showing well 30/9-13 S with well tops and interpreted Base Cretaceous Unconformity (Black line). Map section (bottom right), show area of interest outline from figure x and seismic section in red.

A 10x10 seed grid was interpreted which given the inline and crossline spacing translates to a seed grid spacing of 125 x 187 m. This grid spacing should provide a high enough resolution to be able to cover the main horizons and faults in the Oseberg area in sufficient detail. The BCU was fairly easy to trace, and it was interpreted throughout the seismic area Figure 23.

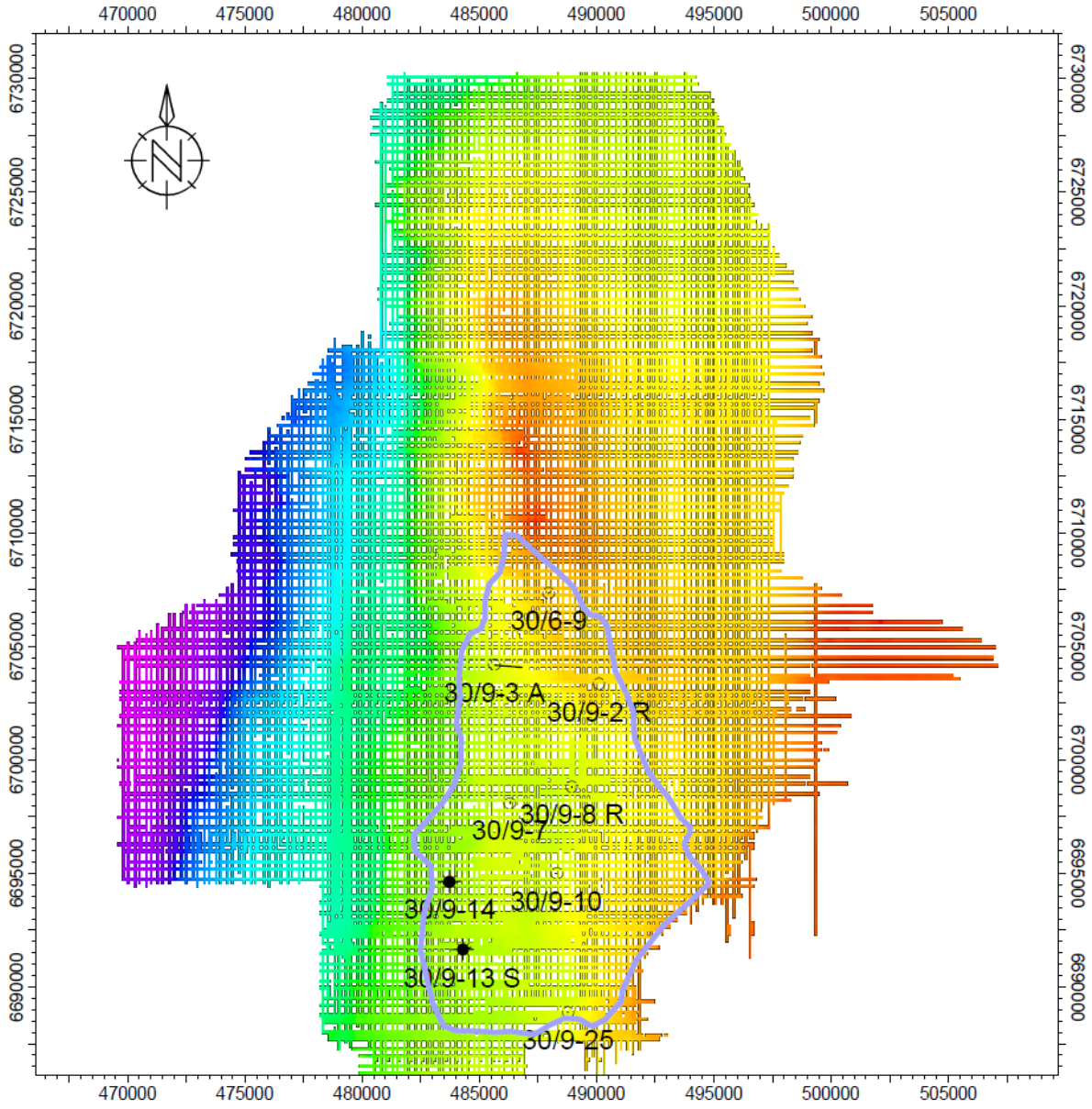

Figure 23: Interpretation grid of BCU from petrel with outlined area of interest

After interpreting the BCU, the faults and remaining key horizons were interpreted by following the same methodology, only this time the interpretations were restricted to the area of interest. Due to the relatively complex structural setting of the area, it was deemed practical to conduct fault interpretation simultaneously with the horizon interpretation. The decision on which horizons to interpret was based on the continuity of the seismic to well-tie, thickness and the availability of well data from that interval. On this basis it was decided to interpret the Tarbert, Ness and Drake Formations, and leave out the Draupne and Heather Formations. Since most of the wells are drilled on the structural highs of the rotated fault blocks, the youngest strata encountered below the BCU is of Kimmeridgian age in the Draupne Formation. Top of the Draupne Formation is only encountered by wells in an eroded state, and is therefore difficult to trace. Similarly, the Heather Formation suffers from the same erosional features. The uncertainty of the location of the horizon tops made it so that these were left out of the primary seismic interpretation, the construction of these intervals is further discussed in chapter 5.2. The strata of Oseberg and Etive formation display sub-seismic characteristics in major parts of the area, meaning that they are not resolvable on the seismic.

The main faults interpreted can be seen in Figure 24 along with the interpretational grid of the Drake Formation. The same grid was used for the Ness and Tarbert Formation. When interpreting the seismic, a mix of manual and guided auto-tracking was utilized with special focus to detail in the near fault areas. Given the objective of the project, it was imperative to accurately interpret the stratigraphic juxtaposition at the segment bounding faults.

.

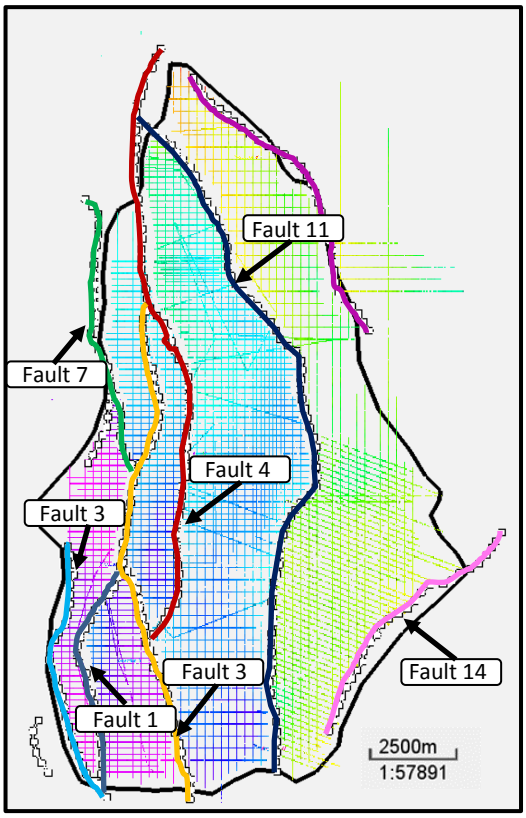

Figure 24: Seicmic interpreation in-lines and x-lines witn interpreted faults.

To create surfaces for the seismic interpretation, it is required a set of fault polygons encompassing the gap created in between the hanging wall and footwall of the horizons. The fault polygons were extended to also include the partial erosion seen the Tarbert and Ness formations. The eroded nature and spatial limitation of the Tarbert Formation complicate the surface creation process. Since the extent of the interpreted top of Tarbert Formation is limited to where Base Cretaceous unconformity has eroded the uppermost strata of the formation, the resulting surface behaves unexpectedly due to the lack of input data in these areas. In addition to this, the northwards thinning trend of the Tarbert Formation posed an issue for the creation of a consistent structural model.

A workaround was employed to model the Tarbert (Figure 25). To tackle the issue of the partial erosion by the Base Cretaceous Unconformity, the interpretations were initially extended above the erosional surface. The second issue of missing Tarbert strata in the north was handled by extending interpretations below the top of the underlying Ness Formation (Figure 25 A). While both of these interpretational work-arounds result in geological impossibilities, it is possible to apply specific operations on the resulting surface to rectify this and end in a structurally and stratigraphically consistent model. In this case, both the surfaces of the Base Cretaceous Unconformity and Ness Formation were used for this purpose. It was made so that when the surface of the Tarbert Formation is situated above the erosional surface of the Base Cretaceous Unconformity it is made equal to the erosional surface. The inverse of this operation was used for the missing strata issue; if the surface of the Tarbert Formation is situated below the surface of the top of Ness Formation, make it equal to Ness Formation.

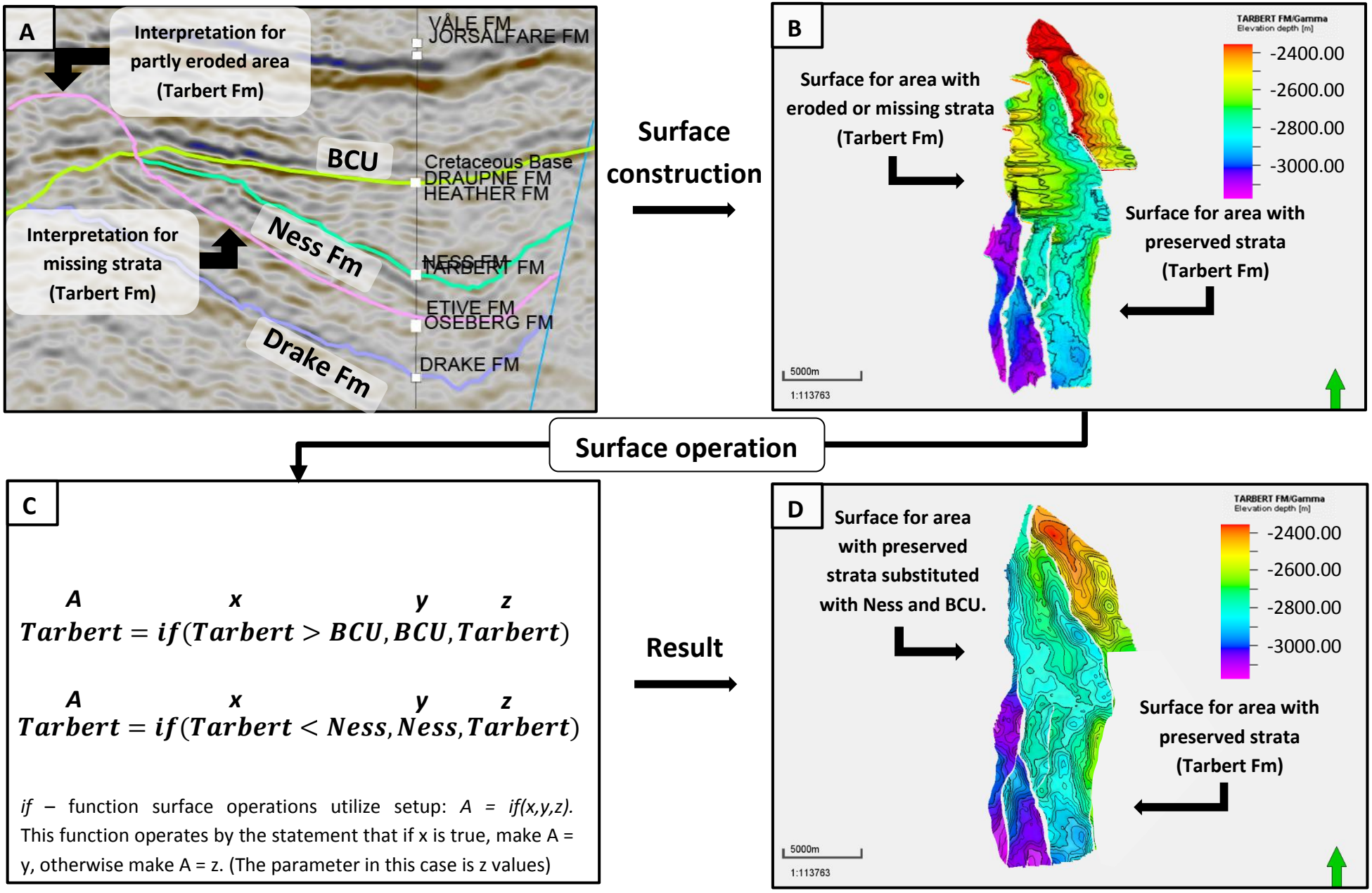

Figure 25: Workflow depicting the process applied to the Tarbert Formation interpretations. A) display the raw interpretation data with the workaround discussed previously. B) show the resulting surface from the initial interpretations. C) describe the surface operation and formula that were used to create the resulting surface visible in D).

4.5 Depth Conversion

To be able to use the interpreted horizons to forma structural model, the interpretations have to be converted from time domain to the depth domain. For this purpose, velocity cube NS1215T was utilized, an average velocity cube provided by Norske Shell.

After conducting a depth conversion of the time domain data, the results were compared to the well data to control if the operation were successful.

4.6 Structural Modelling

Once interpretation and depth conversion is completed, it is possible to initiate the construction of a structural model. At this stage there are some qualitative steps that need to be completed before any work on the model can be done.

4.6.1 Fault Modelling & Pillar Gridding

The faults interpreted earlier have to be converted to faults in the active fault model in order to be used in the construction of a 3D grid. When converting the faults, Petrel allows for a variety of fault types. In this case the fault model honored the semi-listric nature observed in the fault interpretations. The fault pillars were then limited to the area of interest. A series of fault operations was conducted across the fault model, where the top of the fault pillars were limited to the BCU-surface and the base limited to a specific z-value outside the data range. The setup of this operation can be seen in the Appendix (2.1)**.**

Where the individual faults had been interpreted as intersecting, they must be manually linked in the structural model. When this is completed, the fault model can then be used in the pillar gridding process. Before creating a pillar grid it is however, necessary to restrict the area which should generated. For this purpose, the area of interest polygon used for limiting seismic interpretations was applied.

The resulting structural grid contained no irregularities such as peaks or discontinuous grid cells (Figure 26), and could therefore have horizons added.

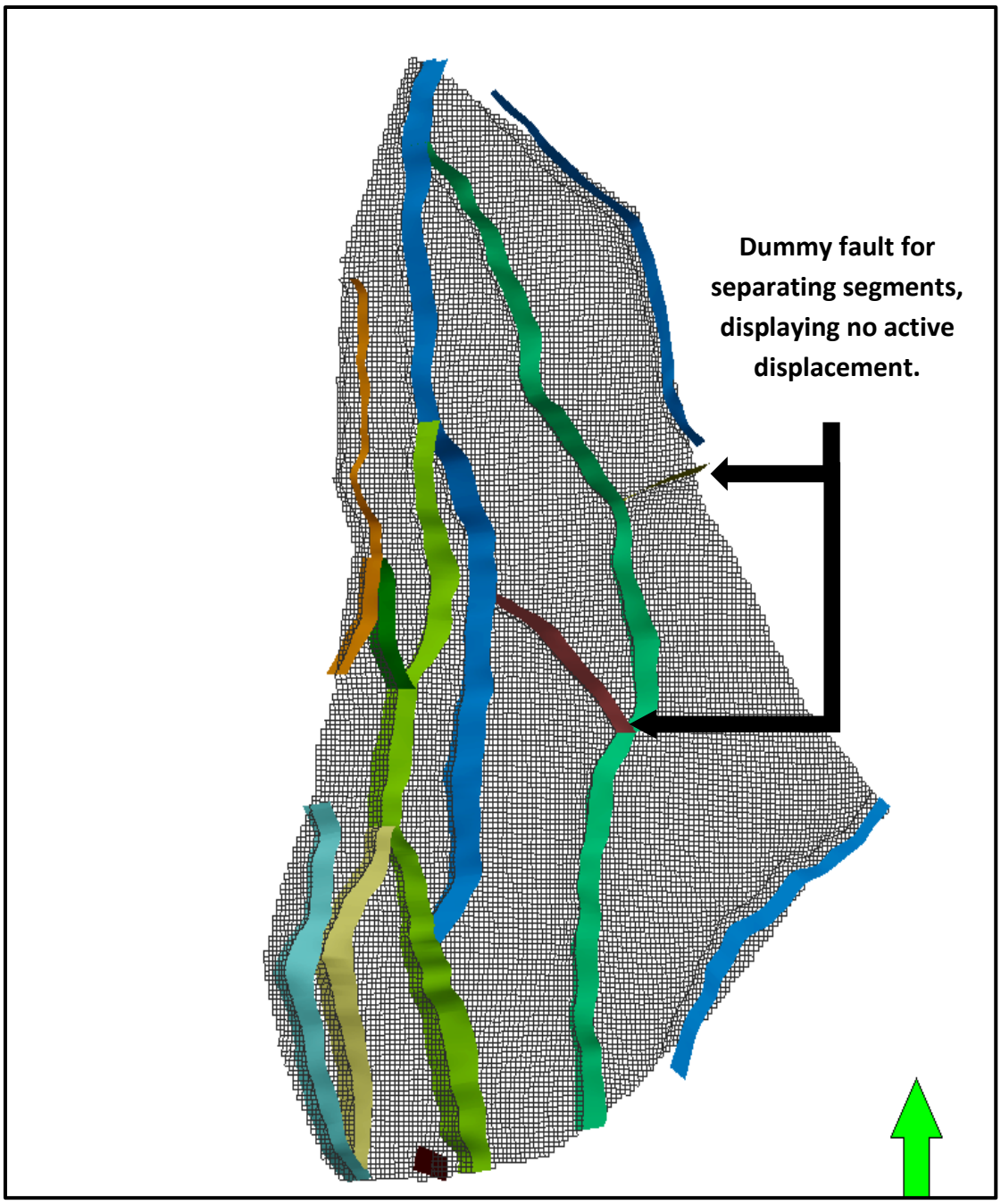

Figure 26: 3D structural grid for area of interest with fault aligned and connected fault-planes.

4.6.2 Horizons & Horizon-fault Lines

All interpreted horizons are modelled as conformable with the exception of the Base Cretaceous Unconformity; which had to be specified as an erosional horizon type. The full setup in Petrel can be seen in the Appendix (2.2).

After generating the horizons in the structural model, the horizons should be subject to quality control by analyzing various aspects such as isopachs and horizon-fault lines. During seismic interpretation, careful mapping was conducted close to the fault planes. Combined with the detailed plotting of the boundary polygons from the surface construction, the resulting horizons displayed minimal amounts of drag effects and. Local minor drag effects occurring in the fault intersection zones, were edited by manipulating the horizon fault lines for proximal surface anomalies and peak removal was applied for more distal surface-anomalies. Manipulating the horizon-fault lines requires a re-sampling of the 3D grid for the changes to take effect.

4.6.3 Zones & Layers

During the make zones process, the horizons that were not interpreted and the seismic were incorporated. This was done by the use of well-tops and simple rest-calculations to produce the missing horizons as conformable surfaces with well-tops as input. This method was used to create Draupne, Heather, Etive, and Oseberg horizons. The full setup of the zone construction can be seen in the Appendix (2.3). A cross-section displaying the product of the zone creation can be seen in Figure 27.

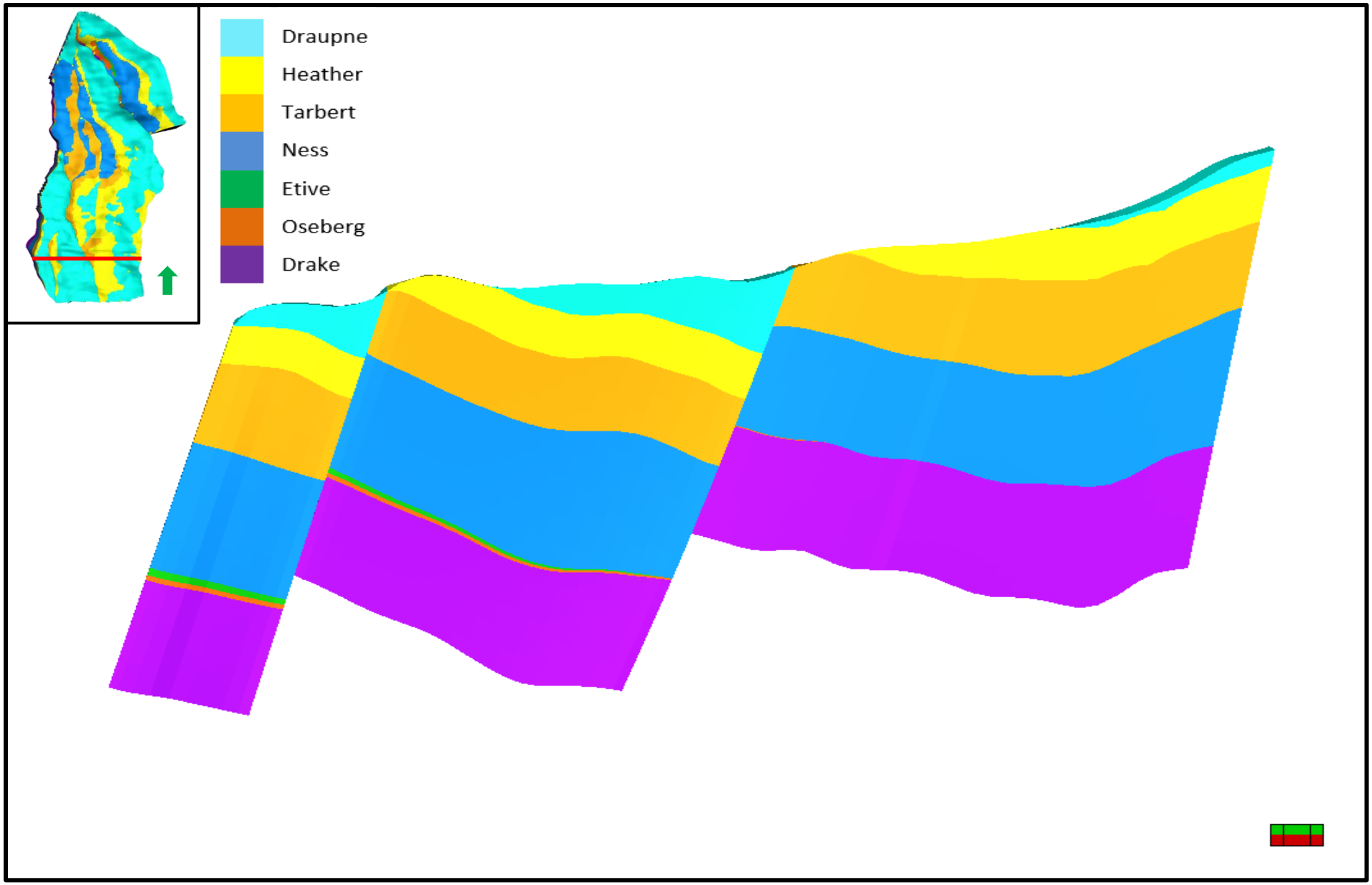

Figure 27: Intersection displaying the constructed zones based on well tops and rest calculations.

After making the zones, each individual zone is divided into layers. The layers will ultimately linked to the vertical resolution of the model and the methodology used for layer construction and subsequent number of layers created will therefore have a significant impact on the quality of up-scaled well logs. This especially holds true for sections such as the Ness Formation, which display interchanging intervals of channel-fills and floodplain deposits manifesting in the well logs as heterogeneous sub-sections (Figure 28**)**. In heterogeneous formations such as Ness, it is necessary to create a layering scheme that best represent the vertical heterogeneity observed at the well.

For the zones that are un-affected by the erosional surface of the Base Cretaceous Unconformity, a proportional zone division was used with a reasonable amount of layers reflecting the nature of the formation it is based on. For the formations that are more affected by the BCU, the zone division had to be modelled to reflect the eroded nature of these formations. In order to accomplish this, the layering was built from the base and up with a layer thickness small enough to capture any significant heterogeneity. The setup of the layer division and methodology applied can be seen in the Appendix (2.3). The result of the layer division of the zones can be seen in Figure 29.

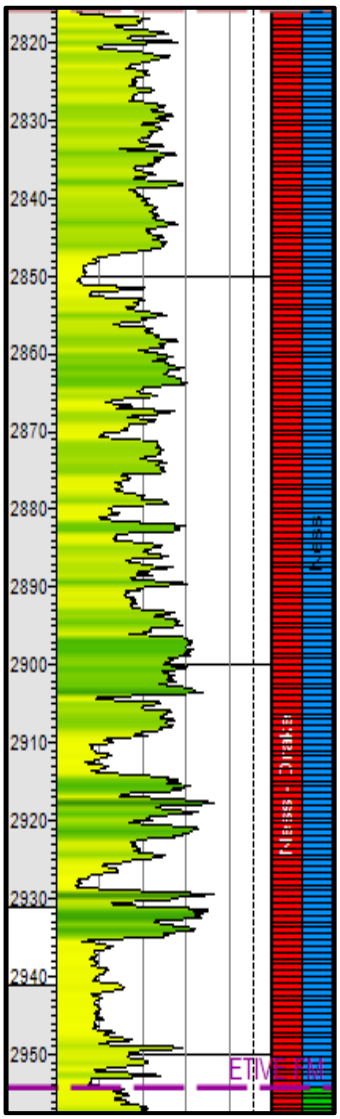

Figure 28: Example of the heterogeneity of the Ness Formation illustrated by the GR-log from well 30/9-4S. Right column display the layers.

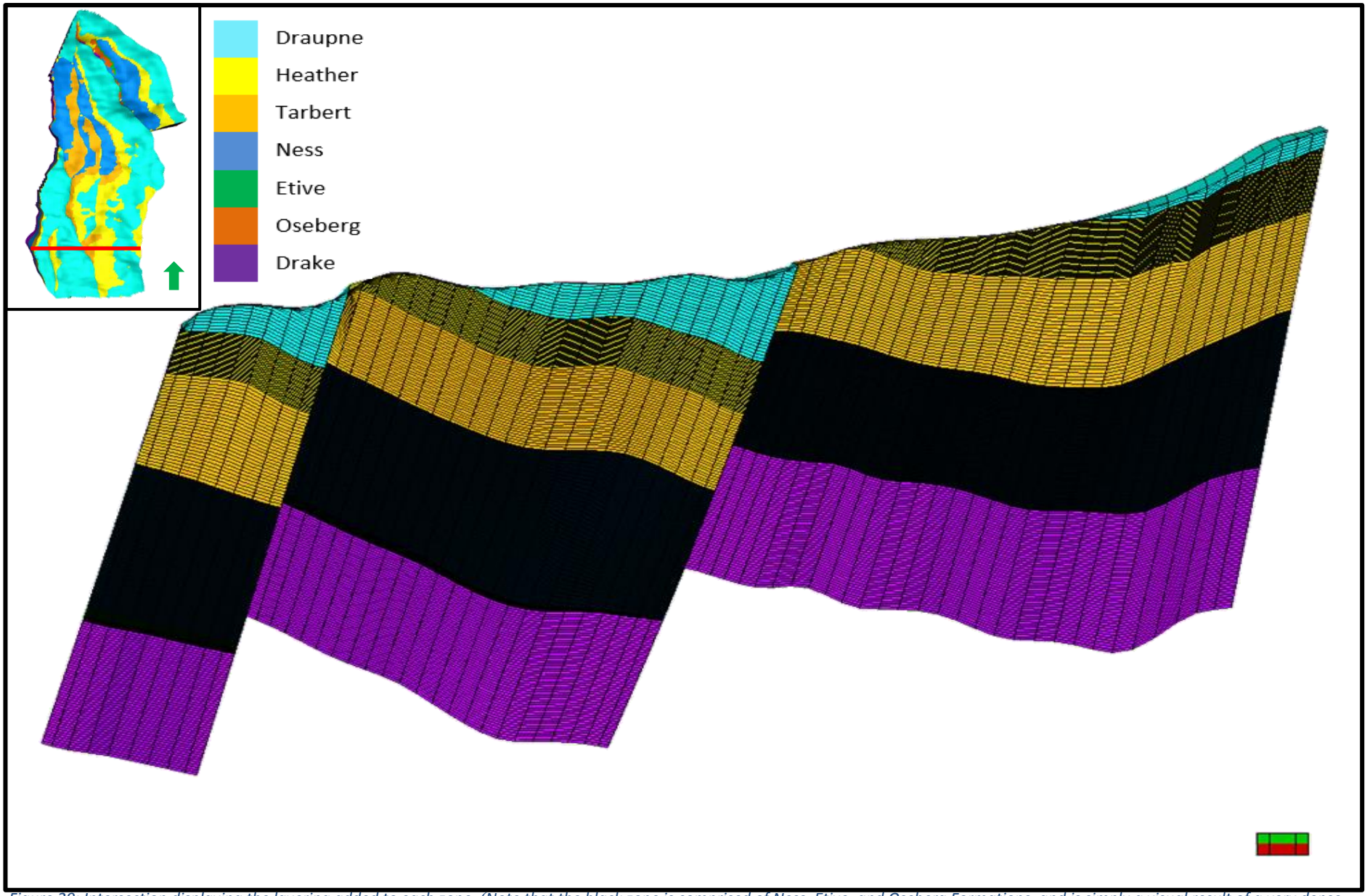

Figure 29: Intersection displaying the layering added to each zone. (Note that the black zone is comprised of Ness, Etive, and Oseberg Formations, and is simply a visual result of a very dense layer interval)

4.7 Facies Modelling

Facies modelling is based on the depositional system of each formation and was conducted in order to successfully capture the spatial distributions observed from the well-data. Trends were used to capture specific depositional environments unique to each formation of the Brent Group.

No digital facies-logs were available for the wells used in this thesis, and while the production of such facies logs could potentially increase the overall quality of the facies model, it was decided to use a simpler approach than a complete facies interpretation. With this in mind, it was decided to utilize the Vsh well-log curves for this purpose.

4.7.1 Scaling Up Well Logs

Before the Vsh log-curves could be used for operations applicable to the structural model, they had to be up-scaled. This was done in Petrel by using the calculated Vsh-logs from both Gamma-ray and Neutron/Density curve logs. The setup for this upscaling of the Vsh logs can be seen in the Appendix (2.3).

4.7.2 Facies Log – Vsh Based

A 4-facies subdivision was created; High perm/porosity, Low perm/porosity, No perm/porosity and Coal. This was intended to aid in the distribution and visual inspection of the properties. The sandy intervals are represented by High perm/porosity indications, sand-shale transition zone represented by Low perm/porosity, and shale represented by No perm/porosity. Some boundary parameters for the different facies were picked to get results best matching the listed facies logs used for comparison. The conditional equation using the up-scaled Vsh log and boundary parameters to produce a simple three-part facies log can be formulated as such:

$$Facies = If(Vsh \leq 30, 0, If\big(Vsh \leq 60, 1, If(Vsh \leq 100, 2, Facies)\big)) \qquad \textbf{E.q. 6}$$

Where facies codes 0 = High perm/porosity, 1 = Low perm/porosity, and 2 = No perm/porosity.

The values of Vsh % used to define facies separation were picked to reflect the listed facies logs for the wells. In addition to the 0, 1, and 2 facies zones, there is also 3, supposed to signify coal seams. Since coal often is characterized by a significant drop in the density curve, a new parameter was added to capture this:

$$Facies = If(Den < 1.7, 3, If\left(Vsh \leq 30, 0, If\left(Vsh \leq 60, 1, If(Vsh \leq 100, 2, Facies)\right)\right)) \quad \textbf{E.q. 7}$$

Based on available core data and well logs a density value of less than 1.7 was used to indicate a coal bearing interval.

4.7.2 Facies Modelling Methods

Different methods with trends and parameters were used for extrapolating well data, depending on the nature of the depositional environment of each formation. The depositional systems and environments for each formation have been previously discussed in detail in chapter 2.3.

4.7.2.1 Drake Formation

The Drake Formation is a generally homogenous marine shale interval in this part of the North Sea, and it is therefore not displaying any noteworthy major trends or changes in the cells or seismic data. For this interval, a standard Truncated Gaussian Simulation method was applied with the pre-defined facies. The setup can be seen in the Appendix (2.4).

4.7.2.2 Oseberg Formation & Etive Formation

The wells capture a northward progradation by displaying a general coarsening upwards shoreface facies trend towards the north in the Oseberg and Etive Formations. This, combined with the relatively thin combined interval thickness observed, meant that by simply using a default Sequential Indicator Simulation it was possible to satisfactory recreate a progradational trend. The setup of this operation can be seen in the Appendix (2.5).

4.7.2.3 Ness Formation

The Ness Formation can be characterized as a heterolithic interval of delta-plain deposits with sandy distributary channels and fine-grained over-bank deposits. It was modeled in Petrel by utilizing object modeling for the fluvial distributary channels for the high perm channel sands, and no perm for the background over-bank deposits. Additionally, ellipse objects were added to simulate the coal-seams observed in the wells. It is possible to modify the shape, size, and orientation of the modelled fluvial channels in order to make them more representative. Since the Brent Delta was building northwards from the North Sea Dome in the southern North Sea, the distributary channels modelled were given a north-south orientation with slight westwards offset (~10^{o}). The width, thickness, sinuosity, and general orientation of the channels were based on estimations, ratios and calculations from Ryseth (2000). The complete setup of the Ness Formation can be seen in the Appendix (2.6).

4.7.2.4 Tarbert Formation & Heather Formation

Tarbert and Heather Formations mark the initial stages of a drowning Brent Delta, characterized by retrograding shoreline sandstones in the Tarbert Formation and marine mudstones in the Heather Formation. These two formations combined complete the sequence from terrestrial to marine deposits, and can be modelled with a general transgressive trend line by Truncated Gaussian with trends. The setup of these trends can be seen in the Appendix (2.7).

4.7.2.5 Draupne Fm

The Draupne Formation has limited well-coverage in the Oseberg Area due to the extensive erosion at the crest of the target structures. It is predominantly composed of marine mudstones, supported by the models from R. Færseth and Ravnås (1998) and observations from the well logs. Because of this, it was decided to simply apply a continuous Vsh-value equal to that of marine shales (Vsh > 90%) throughout this section of the model.

4.8 Property Modelling

By using the scaled up Vsh well logs and the established facies model, it is possible to extrapolate petrophysical data from the well logs to the model by utilizing the facies model as a trend modifier.

4.8.1 Data Analysis

Data analysis was conducted for the Vsh-based well logs before they were used to model the trend of the petrophysical properties. Since the property of the Vsh is split across multiple zones and defined trough different facies sub-classes, multiple operations had to be conducted separately based on the specific data range in that zone or facies sub-class. In general, the data analysis was conducted in a three-step transformation operation. The first step was to filter out any outliers in the data by applying an *Input Truncation* transformation operation (Figure 30).

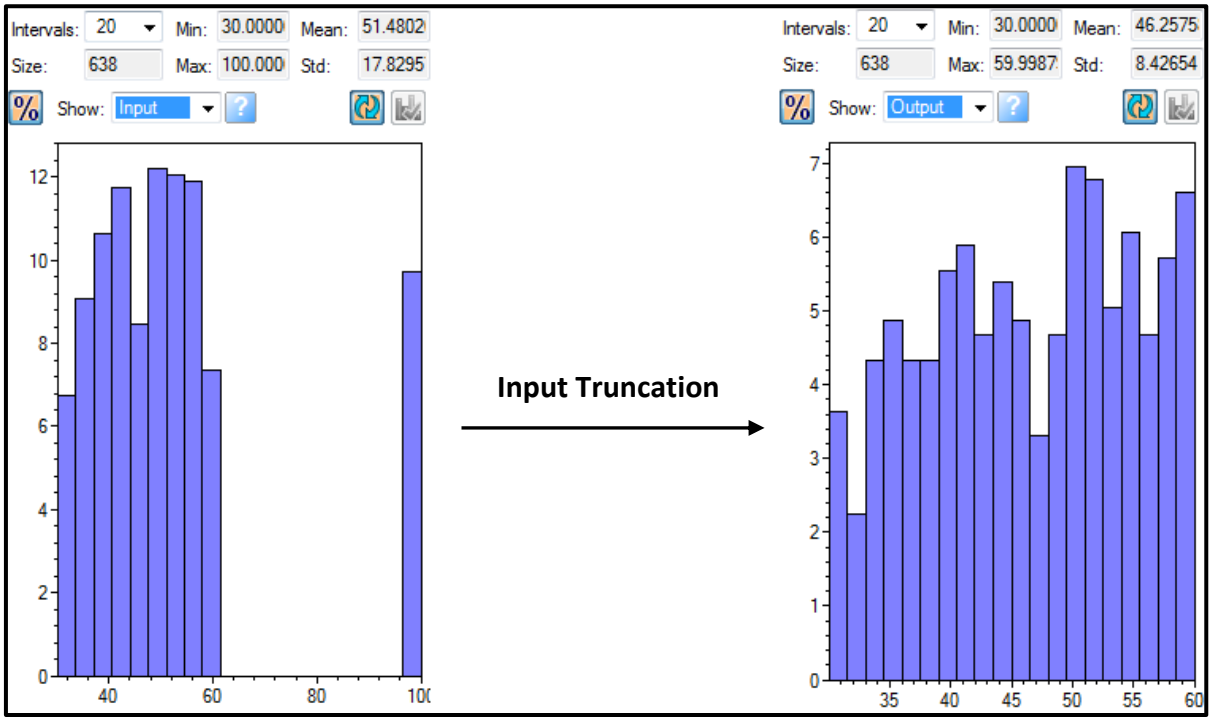

Figure 30: Example of where input truncation has been applied (Right image) to the original input data (left image).

The second step of the transformation operation process was to apply a *directional data trend* to the intervals that indicate the existence of trends in the petrophysical data such as Vsh. Intervals like the Etive Formation displaying a clear trend with depth due to the changing depositional system, benefit from this directional data trend transformation operation. For heterogeneous intervals like the Ness Formation displaying interchanging channel fills and over-bank deposits with no significant trend, the directional data trend was not weighted as heavily. Figure 31 show the example of a directional data trend line for the Low Perm/Porosity facies sub-class for both the Etive and Ness Formations.

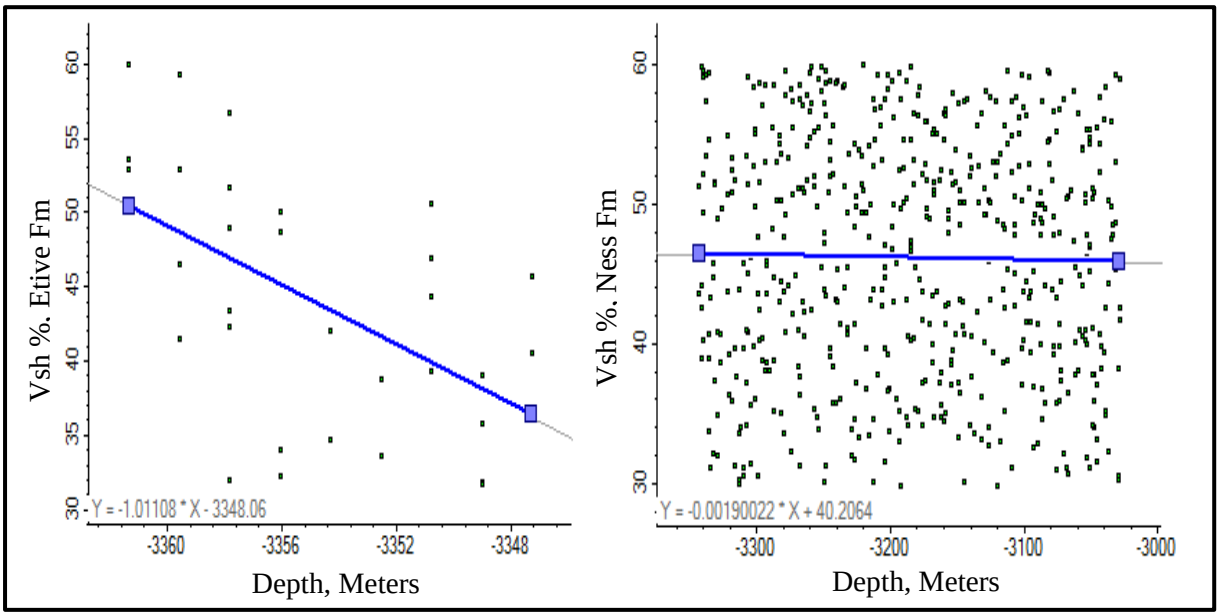

Figure 31: Directional Data Trend lines for Etive Fm (Left) and Ness Formation (Right) (Petrel, 2014).

The third and last step of the transformation operation process was to apply a *Normal Score* operation to the data, by utilizing a spline-curve to match the data (Figure 32). The result of this operation can be seen in Figure 33.

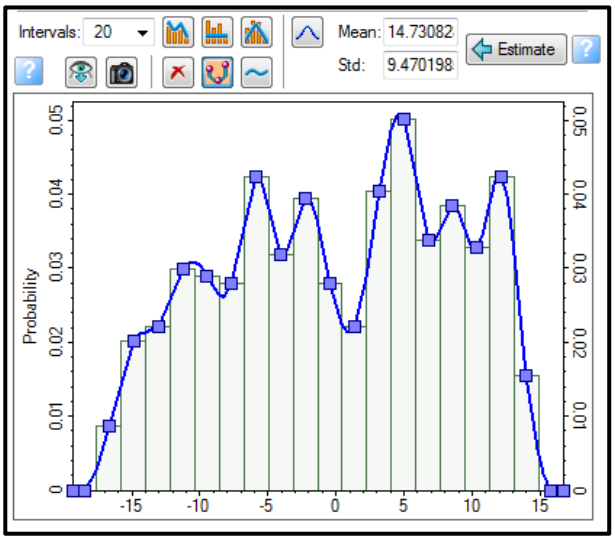

Figure 32: Example of a Normal Score operation on Ness Formation (Petrel, 2014).

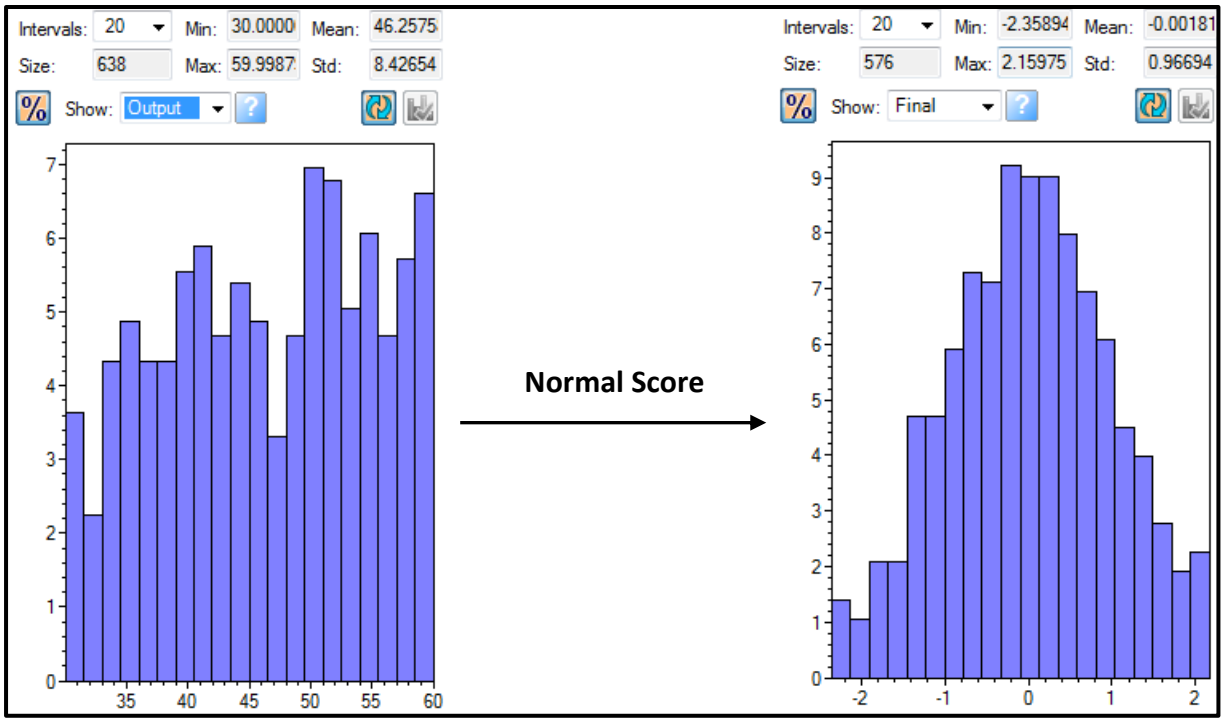

Figure 33: Example of a Normal Score operation with the input (left figure) and output (right figure). (Petrel, 2014)

4.8.2 Petrophysical Modelling

Data from the previously constructed and now analyzed Vsh well-logs, a Gaussian Random Function Simulation method with transformations from the data analysis was used. This operation had to be similarly conducted for all zones and facies-subclasses. The complete setup of this operation can be seen in the Appendix (2.8).

4.9 Fault Seal Analysis

4.9.1 Shale Gauge Ratio Calculations

Shale Gouge Ratio (SGR) was calculated for all faults by using the Shell developed proprietary Stochastic Trap Analysis and Risking (STAR) plug in Petrel tool. The concept of the SGR calculations in STAR is point based, where parameters such as Vsh and fault-throw are utilized. The STAR plugin operates by using the each grid-cell as a SGR point similar to what is shown in Figure 34. By doing this, the SGR variation across each fault plane is calculated for the hanging-wall side, the foot-wall side, and an average between the footwall and the hanging-wall.

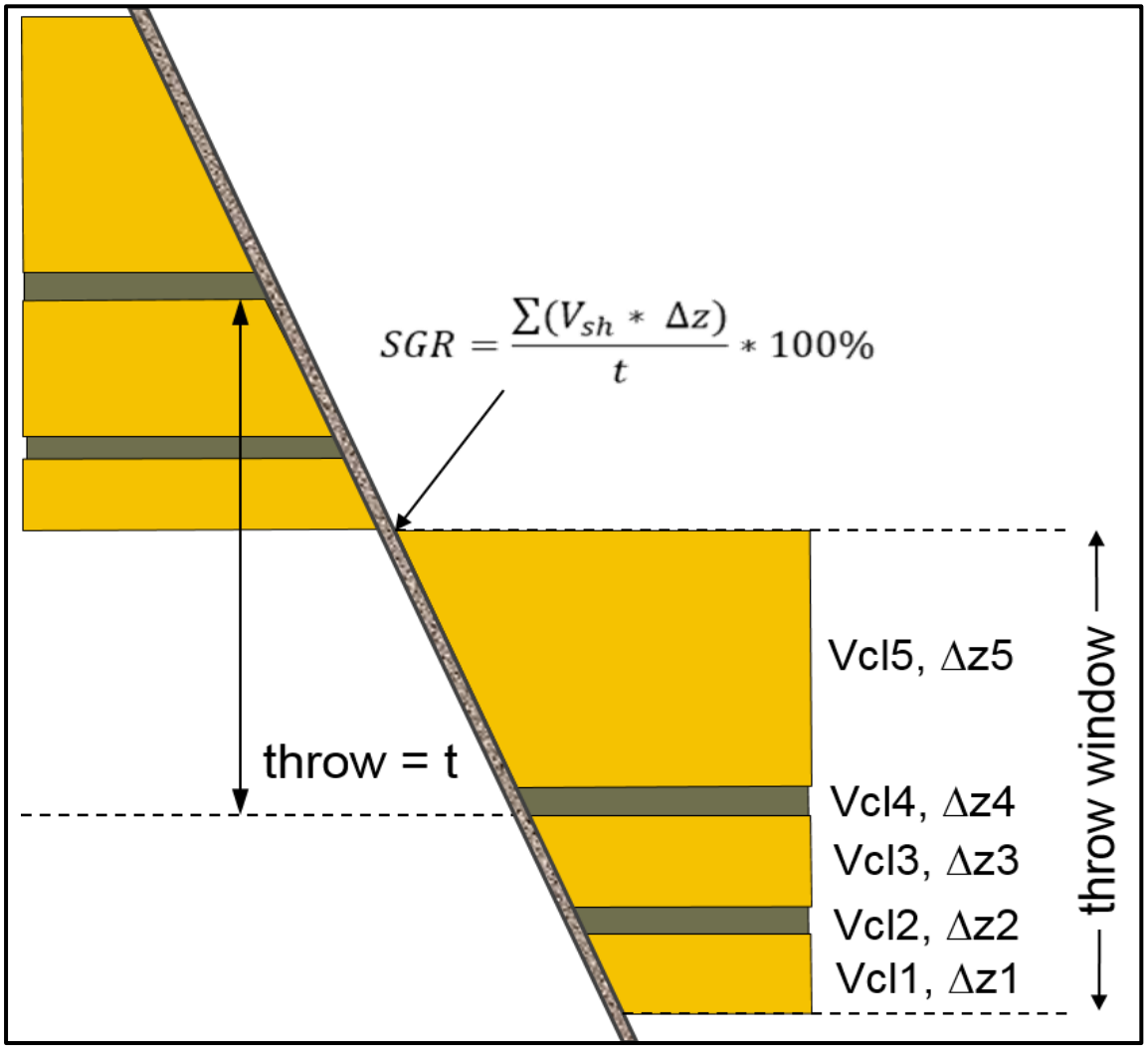

Figure 34: Conceptual figure on how to calculate SGR with formula and parameters. Redrawn from Fristad et al. (1997)

4.9.2 Column Height Predictions

The STAR plugin can, based on the previous SGR calculations, give stochastic predictions on hydrocarbon column heights for each structural segment with control on structural and fault spill points. The structural spill points are based on the horizons from the structural model while the fault spill points are based on fault seal weaknesses. In Figure 35 it is possible to see the main concept the STAR plugin operates with; the maximum HC column height is in principle always limited to the first spill point. The maximum spill point will at any given time be equal to or less than the structural spill point unless elements like stratigraphic pinch-outs or heterogenic compartmentalized reservoirs are present. If the critical fault seal zone is located below the structural spill-point, the retained hydrocarbon column is unaffected by this leakage point other than allowing for fluid communication in the water zone across the fault. If the critical fault seal zone is located above the structural spill-point, the retained hydrocarbon column will be limited to the fault leakage zone. STAR takes all of these factors into consideration, and provides P10, P50 and P90 cases of the hydrocarbon column heights in the entire fault bounded zones.

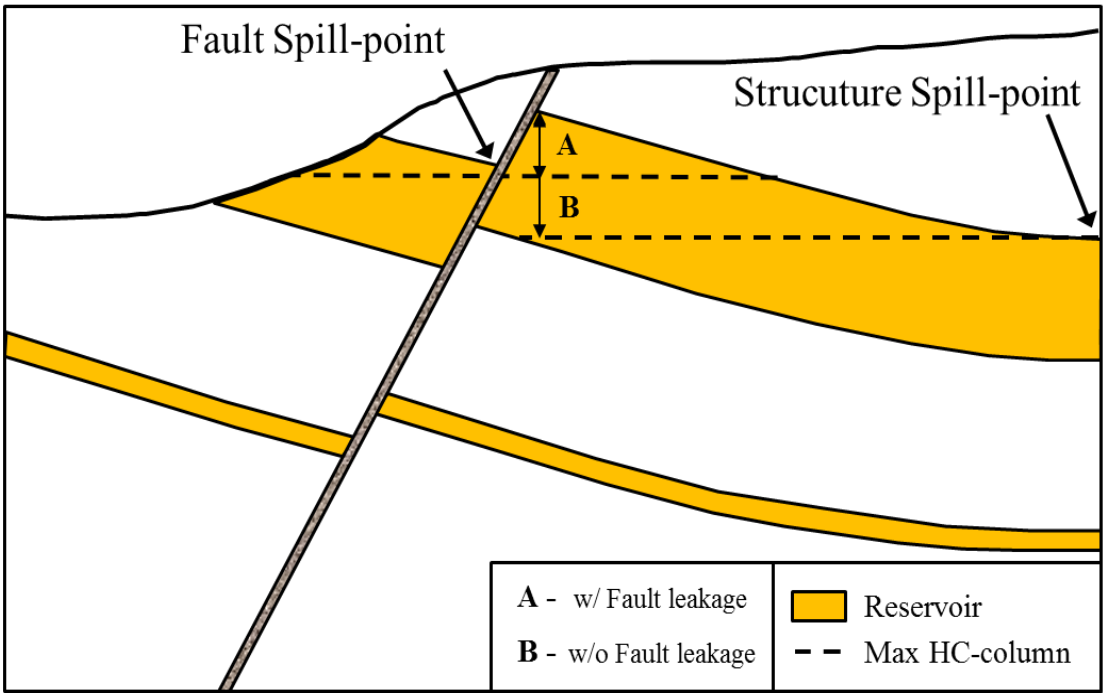

Figure 35: Conceptual figure showing the principle behind calculating the column height from the spill point.

The predictive output from the STAR calculations will be subject for comparison to published field data in order to evaluate the applicability of the analogue dataset used as basis to the area of study. To evaluate the applicability of STAR calculations to this area, the results were compared to the findings from previous studies. One way of doing is this is to compare the hydrocarbon column heights from the previous studies in an area with the proposed column heights from the STAR calculations. The column heights are not listed directly in the publicly available data or previous studies, but can rather be defined by analyzing fluid contacts listed in well reports and formation pressure surveys provided by Norske Shell. The formation pressure change along depth was plotted against the listed fluid contacts for each well. It is possible to use established fluid gradients along with the pressure plots to estimate fluid contacts where the fluid gradients intersect. By doing this it is possible to examine if the suggested contacts from the pressure plots corresponds with the actual listed contacts.

Following the creation of the formation pressure plots and fluid contacts, it is possible do cross-fault comparisons. This was done from segment to segment, across all faults in order to evaluate the differences in pressures and fluid contacts and possibly decide if there is cross-fault fluid communication. This information could then be used to evaluate the success of the predicted fault seal and leak zones of the STAR plugin. Additionally, the calculated column heights from STAR were evaluated by comparison with column heights from the actual observed fluid contacts. This was done by measuring the depth between the top of reservoir and the fluid contact in the reservoir zone (Figure 36).

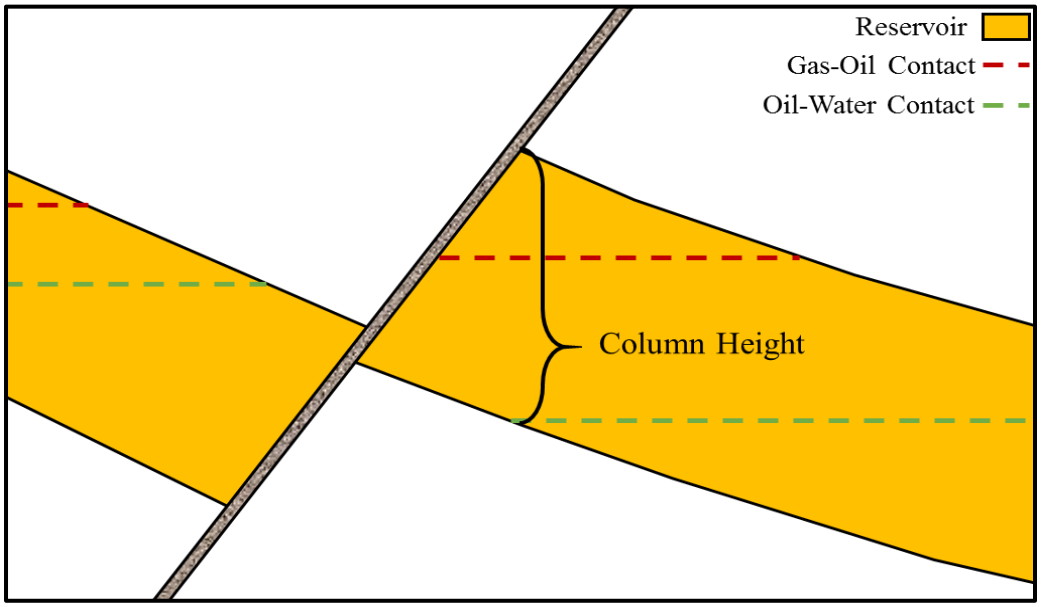

Figure 36: Conceptual figure showing the column height from determined fluid contact.

The STAR plugin provide a column height distribution throughout the entirety of the model based on the distance from top reservoir to proposed OWC. To compare this with the actual column height based on the observed OWC from well logs, a thickness map displaying the same thickness interval for the top of reservoir to the observed OWC was made for each segment (Figure 37).

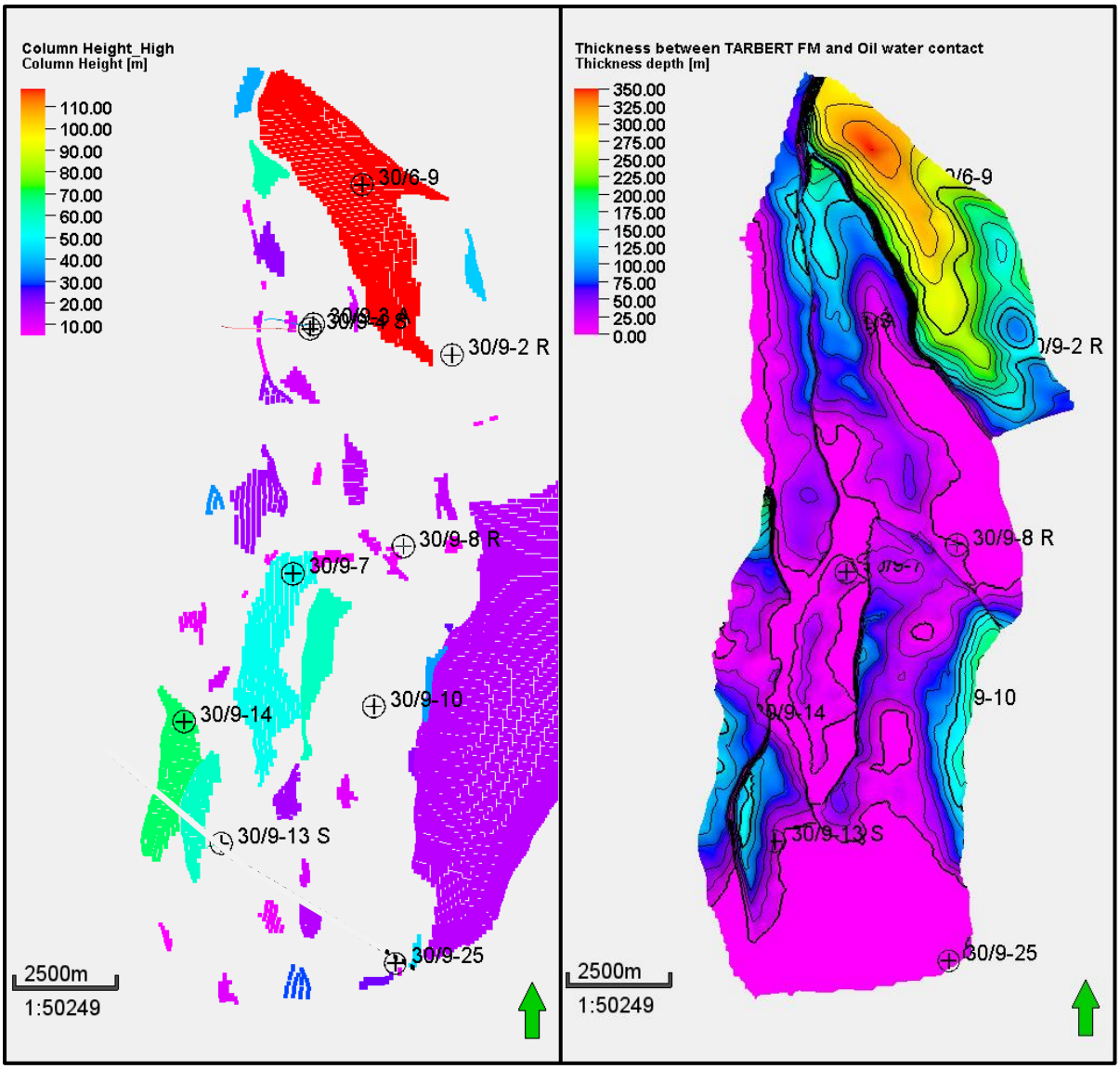

Figure 37: Column heights predicted by STAR (left) and column heights calculated with fluid contacts.

5. Observations

5.1 Well Correlation

A notable upwards coarsening trend in the Etive and Oseberg Formations is demonstrated in Figure 38 and can be linked with the proposed transition from marine muds to an upper shoreface setting as discussed in the geological settings chapter. Similarly, it is possible to observe the backstepping shorefront of the Tarbert and Heather Formations. In general all formations display an overall fining trend that supports the proposed retro-gradation of the Brent Delta during this period.

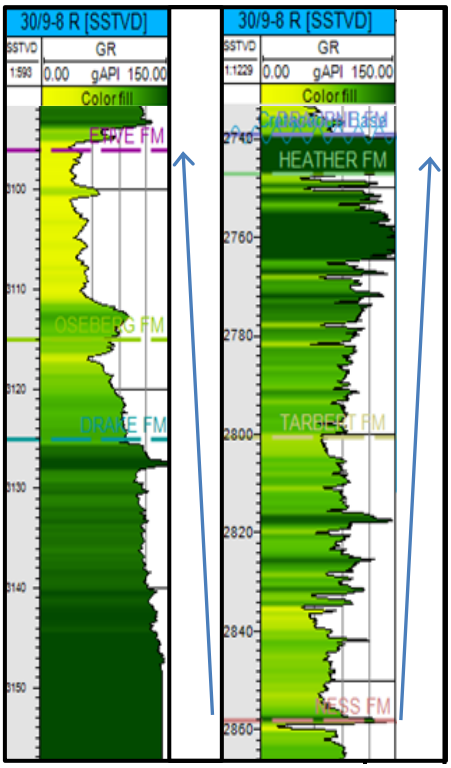

Figure 38: Well logs, displaying the upwards coarsening trends of the Etive and Oseberg formations and fining upwards trend of the

Wells 30/9-3A, 30/9-8 R. 30/9-10 and 30/9-25 were used to create a continuous un-faulted cross-section view of the northward-prograding thickness change of the Brent Group. In the area of interest, the combined terraces of the Omega North and Omega South segments provide a relatively continuous interval of Brent Group stratigraphy unobstructed by major fault-displacement.

The provenance of the Brent Group can be sourced back to the North Sea Dome which is consistent with the northwards thinning observed in a field-scale well-correlation in Figure 39.

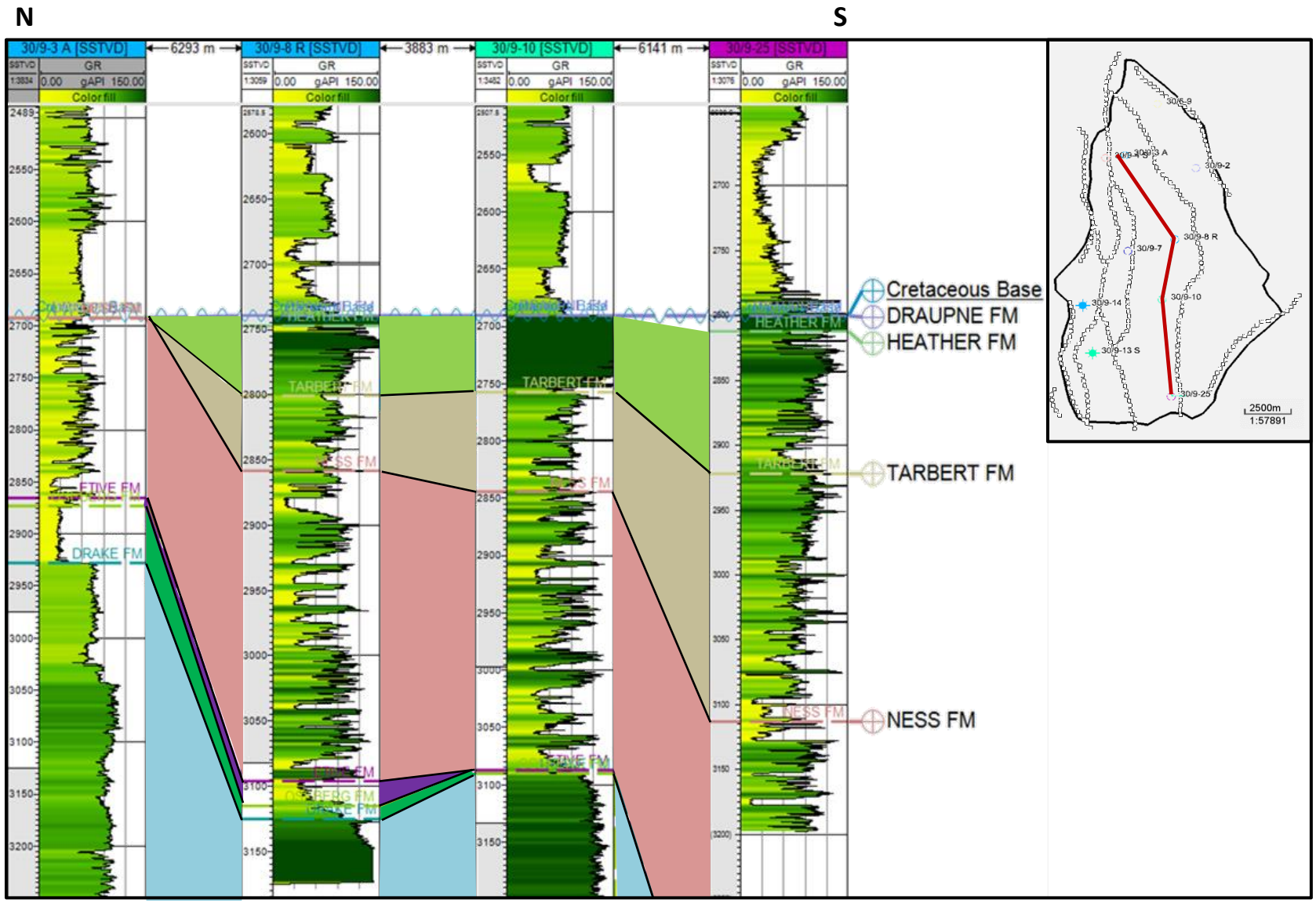

Figure 39: Northwest – southeast well correlation for wells 30/9-3 A, 30/9-8 R, 30/9-10 and 30/9-25 flattened on the Base Cretaceous Unconformity.

5.2 Petrophysical Operations

As expected the Vsh log calculated from the GR follows the same trend as the GR log, meaning that any issues or inconsistencies with the GR curve will be transmitted to the Vsh curve. Core data is available for the target interval in most of the wells, making it possible to determine any discrepancies between the suggested amount of shale from the logs and the shale measured in the core analysis. The Jurassic deposits in this part of the North Sea are known to be especially rich in mica, a radioactive mineral that is known to result in elevated GR readings. The presence of the mica in a sandstone interval will therefore depending on the amount, occasionally give exaggerated GR-readings similar to what would be expected from a more shaly interval. Basing Vsh calculations on these GR-logs affected by micaceous intervals will therefore result an overestimation of the real Vsh. The Neu/Den logs are also affected by increased levels of mica, but when comparing Neu/Den- and GR-based Vsh logs **(**Figure 40**),** it is apparent that the overestimation is less significant than in the GR-based Vsh log. As a result, it was decided to use the Neu/Den based Vsh logs in the continued petrophysical operations.

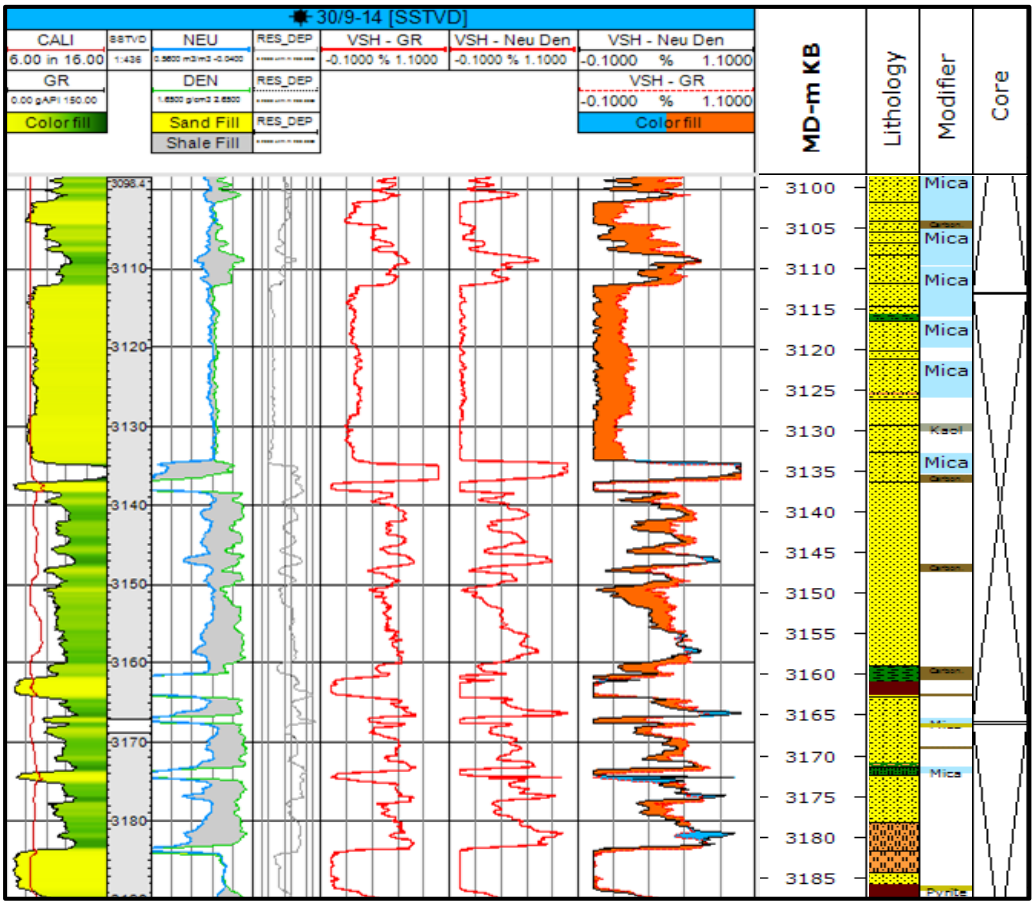

Figure 40: Well logs displaying the GR curve, Neu/Den curve, Vsh curves from both methods, difference between GR-based and Neu/Den-based Vsh curves (Orange fill: GR-based Vsh is higher than Neu/Den - ased Vsh)(Blue fill: Neu/De- based Vsh is higher than GR-based Vsh) and Core interpretations.

5.3 Seismic Interpretation

NH0402 is of sufficient resolution to interpret most key horizons, with increased local complexity in areas of erosion and fault displacement. The majority of structural segments have one or more exploration wells. These wells are however usually proximal to the crest of the structure. Consequently, complications arise due to predominant well-sampling in the eroded footwall crest. This erosion is caused by the regional erosive Base Cretaceous Unconformity, and affects Middle to Late Jurassic deposits. This leads to associated uncertainty near the crest of structures where the strata have undergone the most erosion. Consequently, interpretations made for these intervals have a significant associated uncertainty when moving away from the crest of the structures where well-sampling is absent.

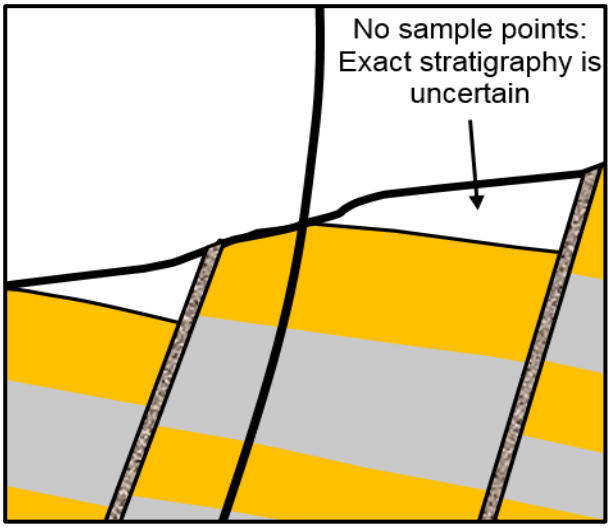

Figure 41: Conceptual sketch displaying uncertainty related to well-sampling and erosional features.

The Brent Group interpreted displays increasing interval-thickness towards the Viking Graben in the west, typically exhibited in the Ness and Tarbert Formations. Inline 412 (figures 42 & 43) display a typical seismic cross-section of the area, crossing structural segments C, Omega South, G-East and G-Central. Figure 43 illustrates a 50% thickness increase in the Ness Formation from Omega to G-East. The observed thickness change across segments supports the concept of influence by the existence of an early Viking Graben postulated by Fristad et al. (1997).

By superimposing the fault-interpretation from this study and that from previous evaluations, a clear correlation is observed (Figure 44). A difference is however observed in the interpretation of the B-North segment. The fault interpreted in this survey defines the boundary segment between the B-North and B-West structural segments. This boundary has not been defined in the structural segment map used for correlation, possibly due to the fact that B-west has no well coverage at the time of this study.

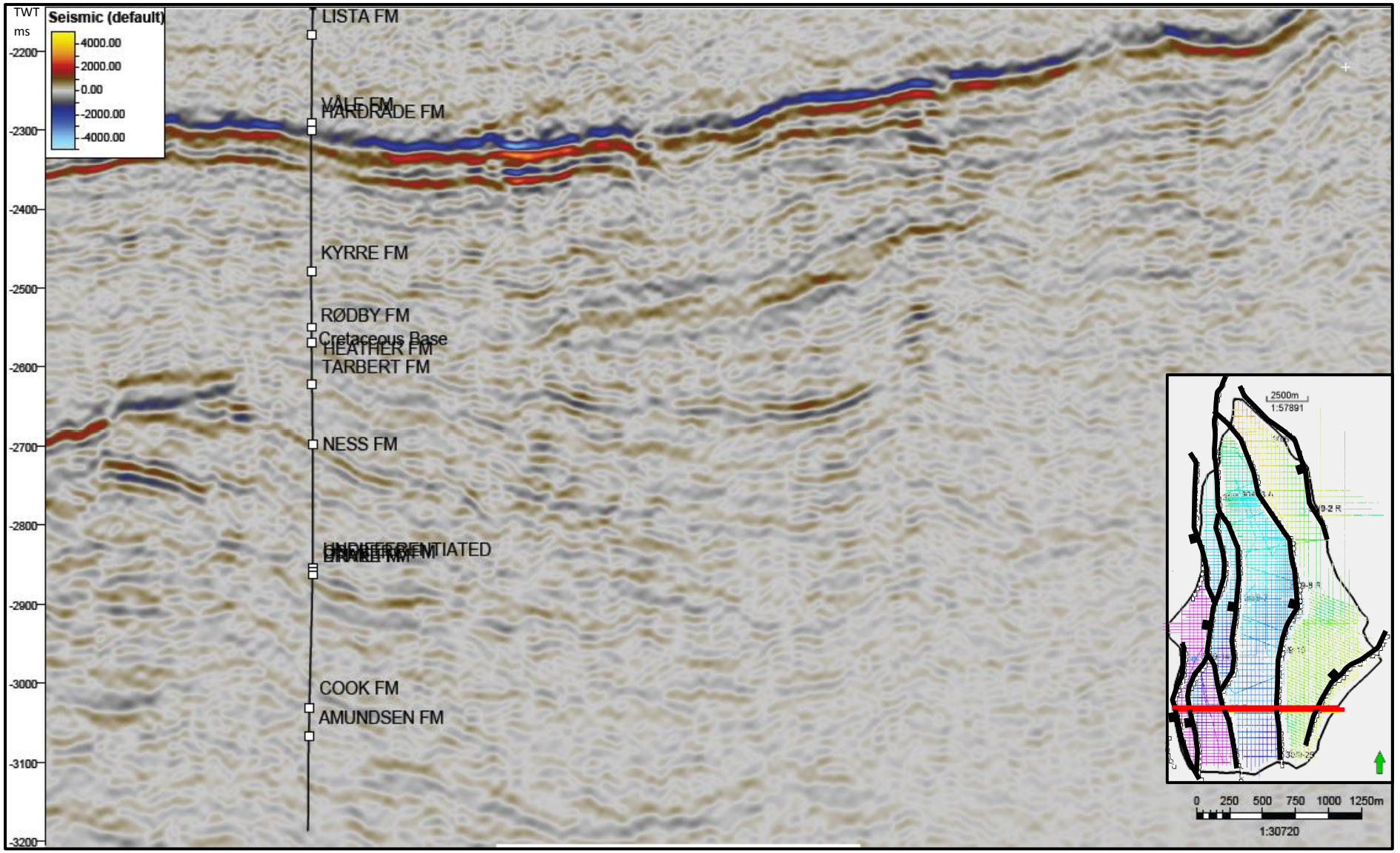

Figure 42: Inline 412 displaying uninterpreted seismic with well 30/9-13S and corresponding well tops.

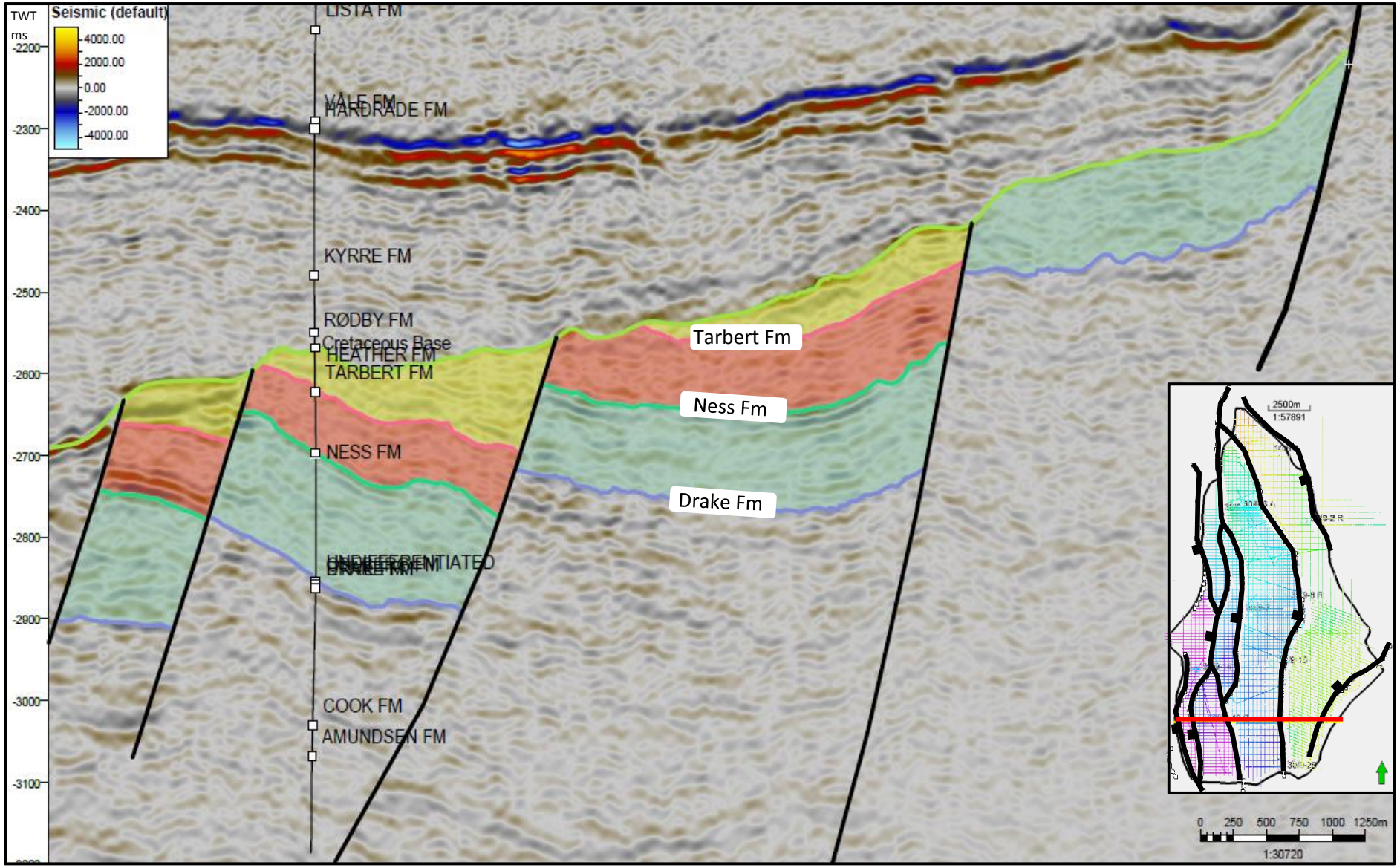

Figure 43: Inline 412 displaying the interpreted seismic with well 30/9-13 S and corresponding well tops. Horizons and faults are intrepreted across the model.

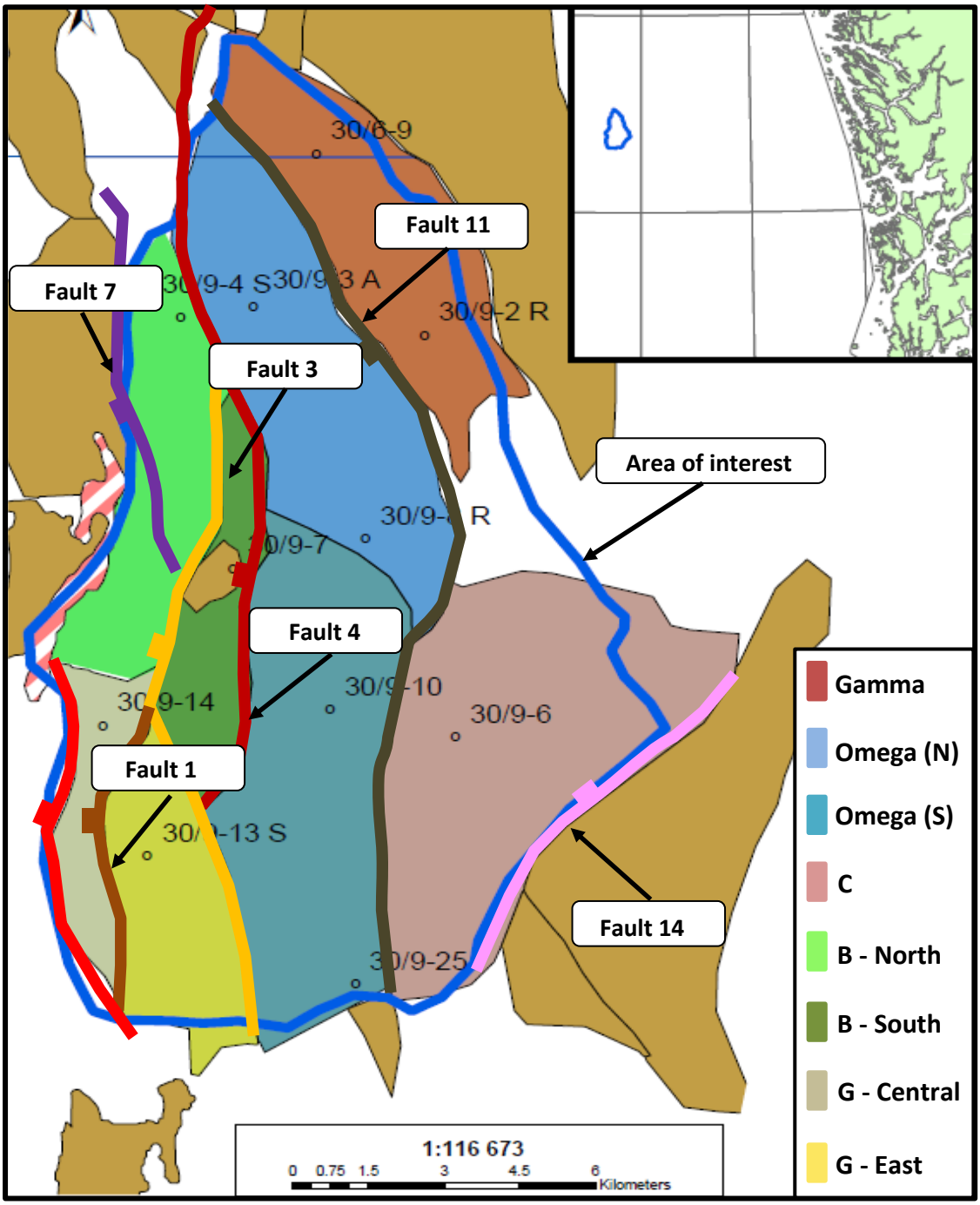

Figure 44: Map displaying the defined strucutral segments of the Oseberg area compared to the intreptredet faults .

5.4 Horizons and Interval-Thicknesses

Isochore maps were created to review the structural model and assess any anomalies, such as “bulls eyes”, that could indicate any artifacts of the modelling process (figures 45-50**)**.

The Draupne Formation is defined as the interval between the Base Cretaceous unconformity and the top of Heather Formation. The isochore map between these two horizons (Figure 45), clearly demonstrates that the Draupne Formation has undergone significant erosion in most of the Oseberg area with strata preserved only in parts of the hanging wall basins.

By analyzing the isochore map of the Heather Formation (Figure 46), a clear trend of thinning is observed from south to north. The Heather Formation was as previously discussed in chapter 2.3.2, sourced from the south and deposited in a marine setting with paleo-waters of more than 60m (Ravnas et al., 1997). After taking the erosion of the Heather Formation into account, it is clear that accommodation space has played a big role in the deposition of this Formation. Any significant stratigraphic thickness is restricted to the established hanging wall depocenters.

The Tarbert Formation display the same thickening towards the south (Figure 47), fitting the proposed southern sourced shorefront depositional model. The thinning can also be attributed to the differential erosion by the Base Cretaceous Unconformity, which is generally higher in the northern parts of Oseberg. It is furthermore possible to observe a significant increase in thickness towards the west likely controlled by the increased accommodation space created by these syndepositional active western half-graben fault blocks.

The Ness Formation also displays the same thinning towards the north (Figure 48), but to a less degree than that observed in the Heather and Tarbert formations. The main thickness-increase across fault blocks can be seen from the Omega structural segment to B-South, compared to Tarbert Formation which has the main thickness increase from B-South to G-Central. This indicates that the faults were active in the B structural segment during the deposition of Ness and in the G-block for the deposition of Tarbert.

The Etive-Rannoch formations thicken towards the center of the Oseberg area, with limited presence in the north (Figure 49). A similar observation can be made in the stratigraphic thickness of the Oseberg Formation (Figure 50) where the thickness is greatest towards the north with limited deposits in the south.

Interpreting the thickness of each formation up to the Base Cretaceous unconformity (oldest to youngest), a broadly transgressive trend can be observed with the thickest sections progressively migrating south with time. This is especially visible in the transition from the Oseberg Formation to the Heather Formation. Is it known that in the Northern North Sea, there was already established noteworthy submergence during the Middle Jurassic (I. B. Ramberg et al., 2008). This can be used to explain how the deposcentre is situated in a more northerly location during deposition of the Oseberg Formation, before migrating south during Etive-Rannoch times.

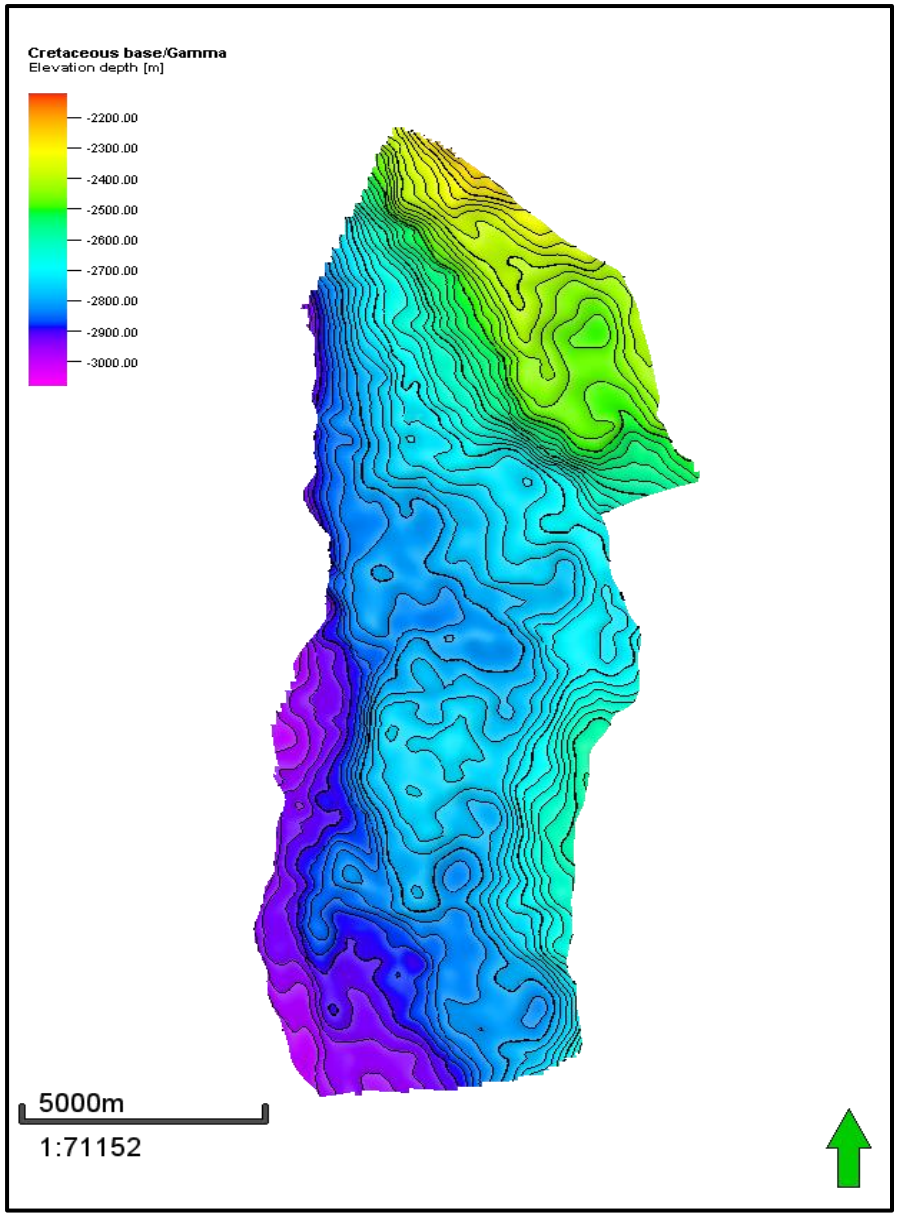

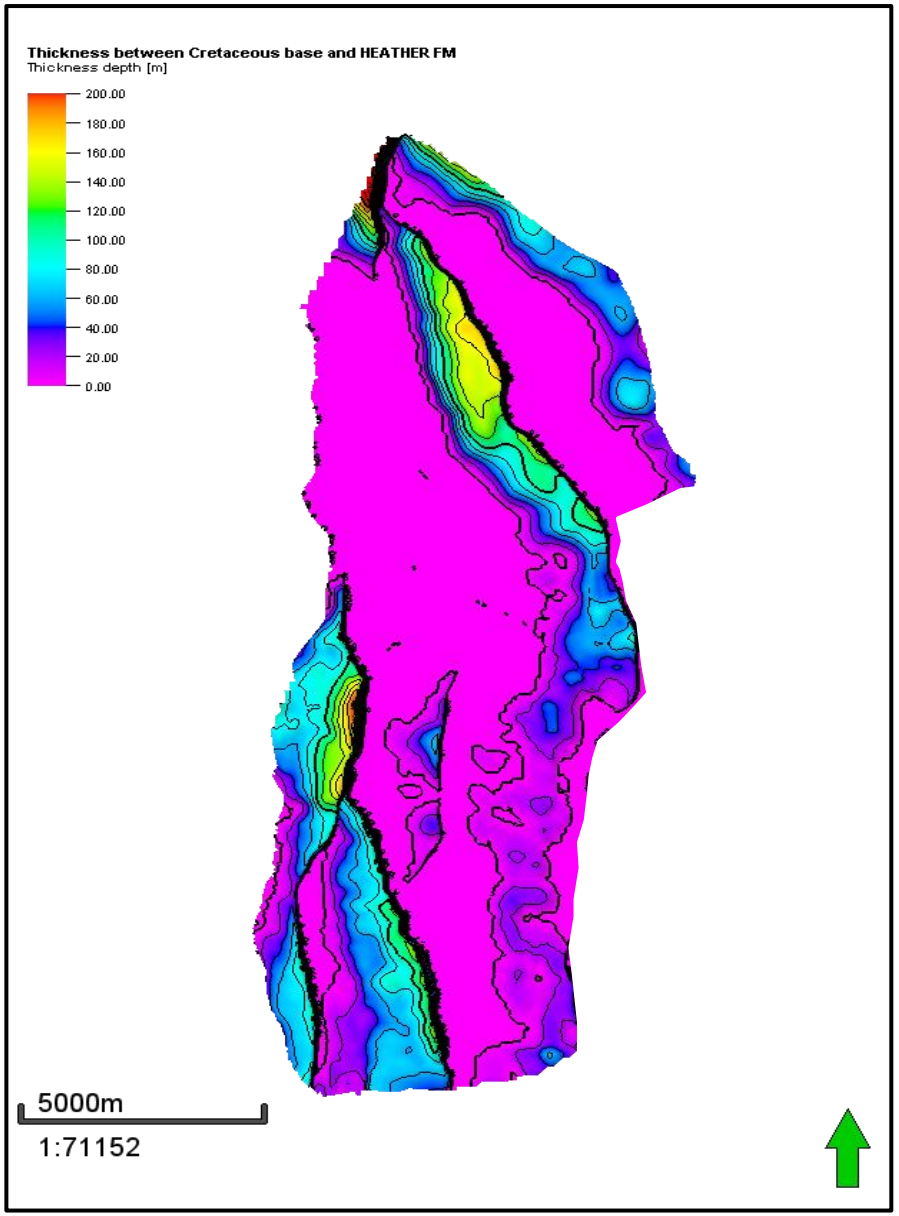

Figure 45: Depth surface for Base Cretaceous Unconformity (left) and thickness map between the Base Cretaceous unconformity and the underlying Heather Formation (right).

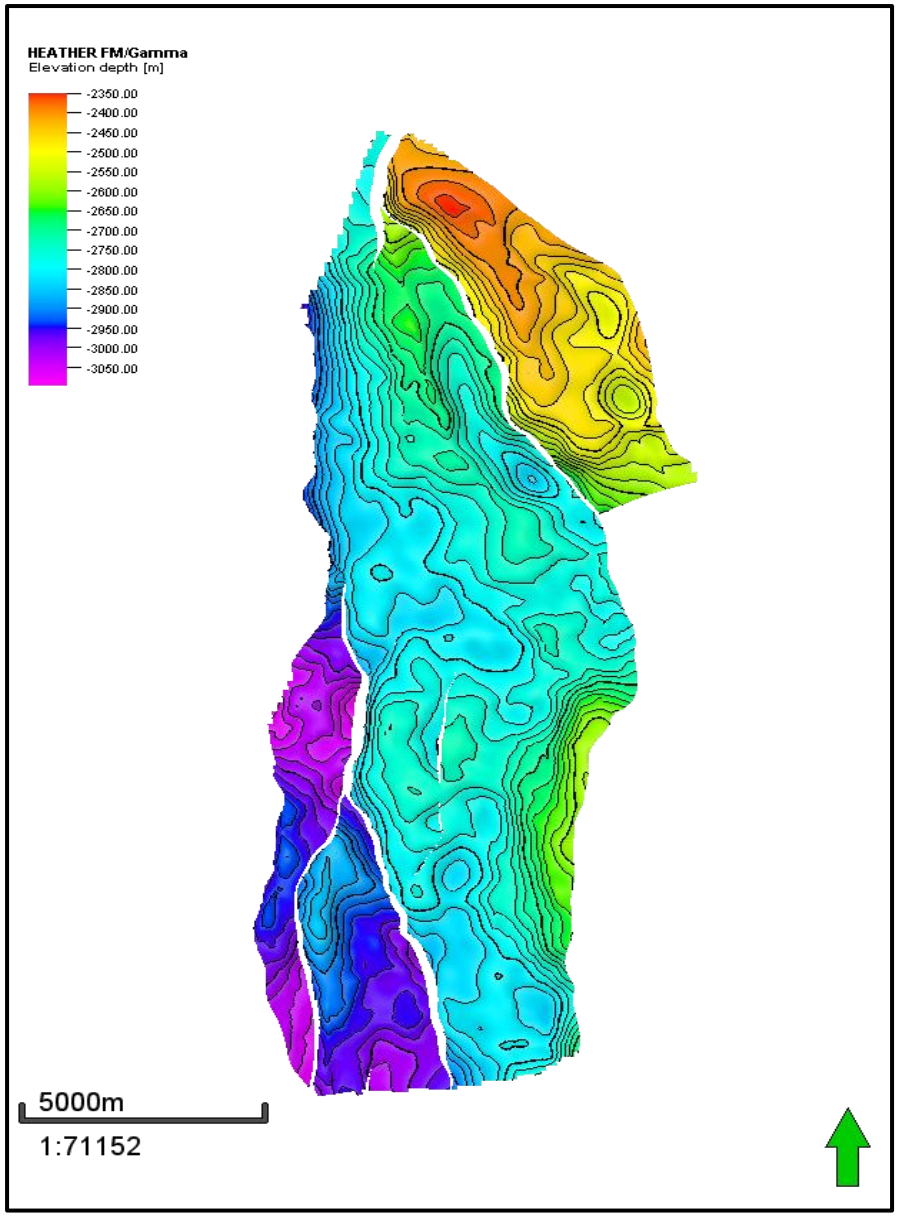

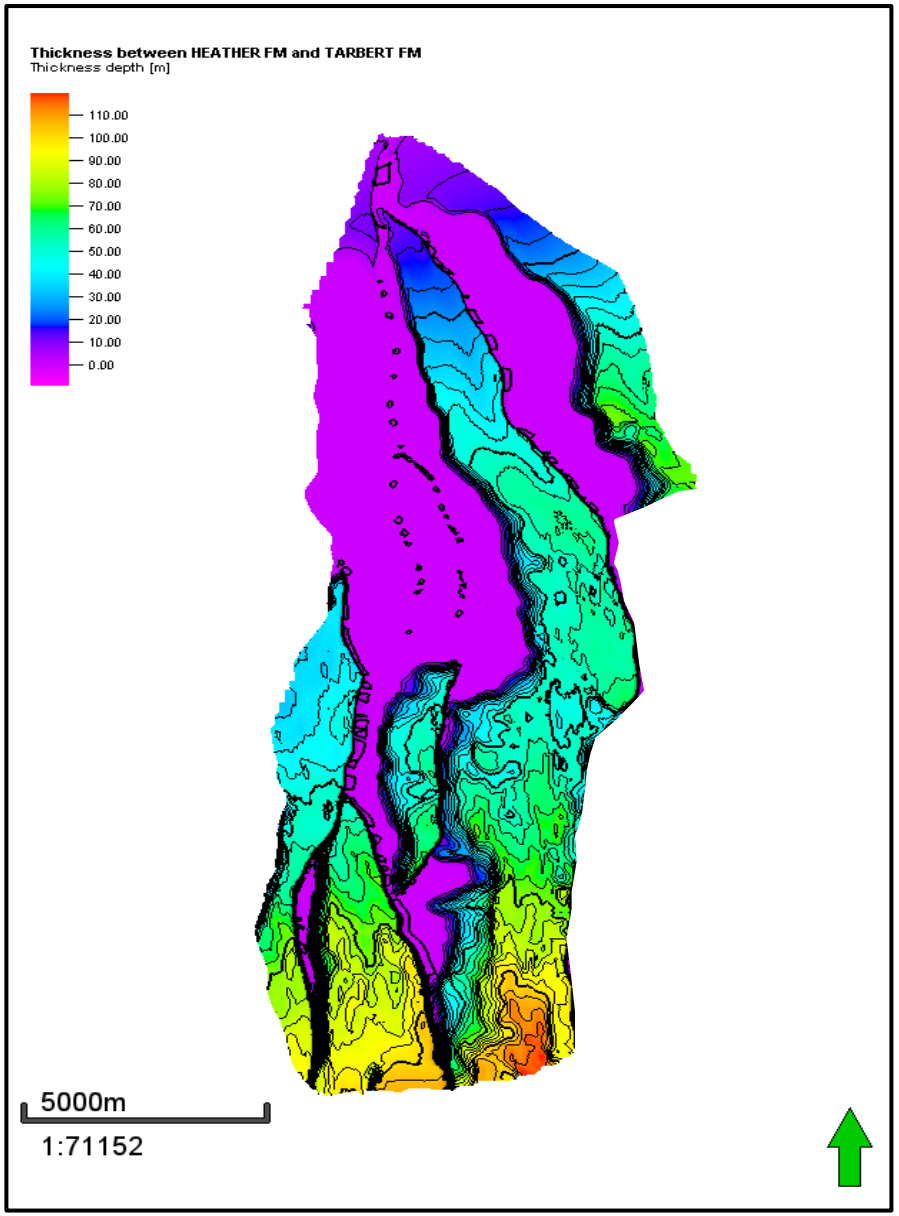

Figure 46: Depth surface for Heather Formation (left) and thickness map between Heather Formation and the underlying Tarbert Formation (right).

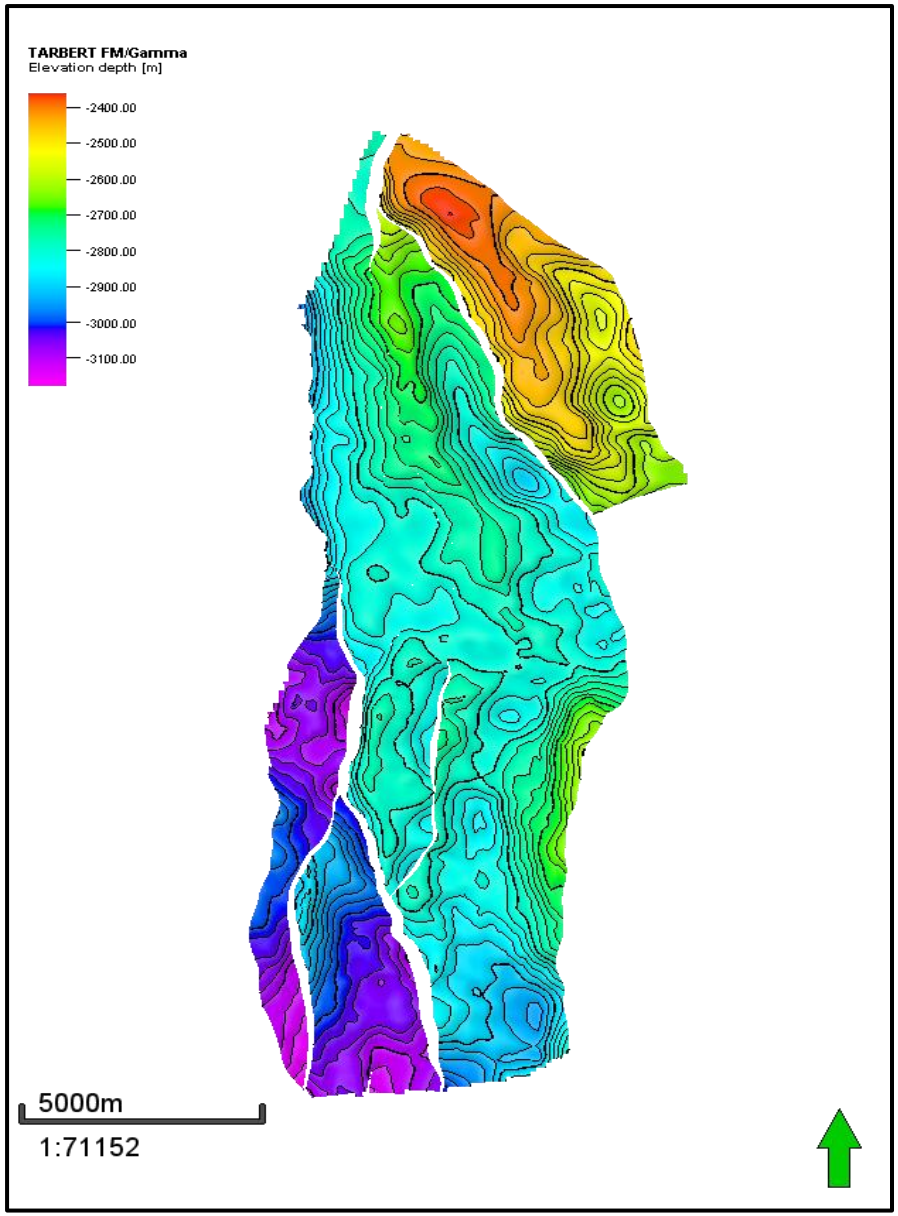

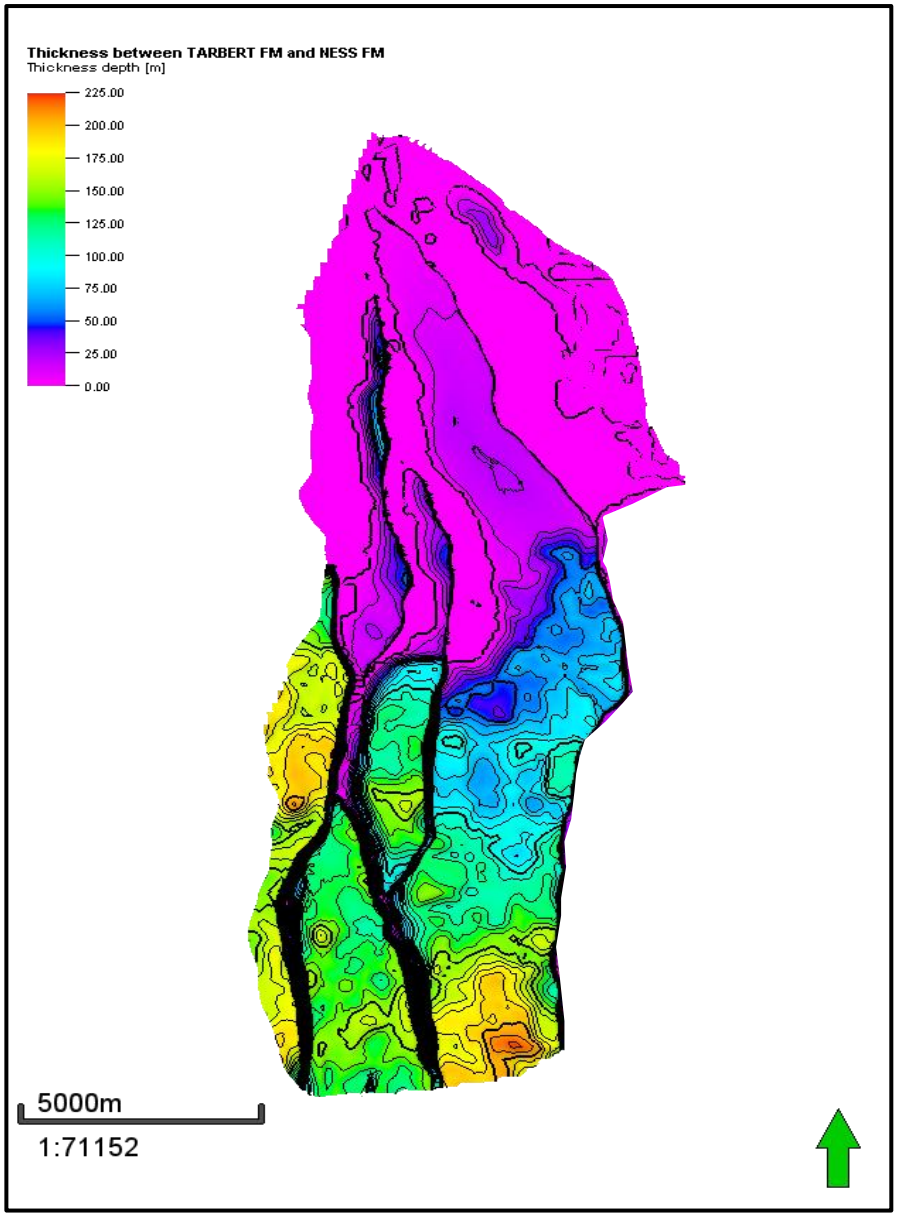

Figure 47: Depth surface for Tarbert Formation (left) and thickness map between Tarbert Formation and the underlying Ness Formation (right).

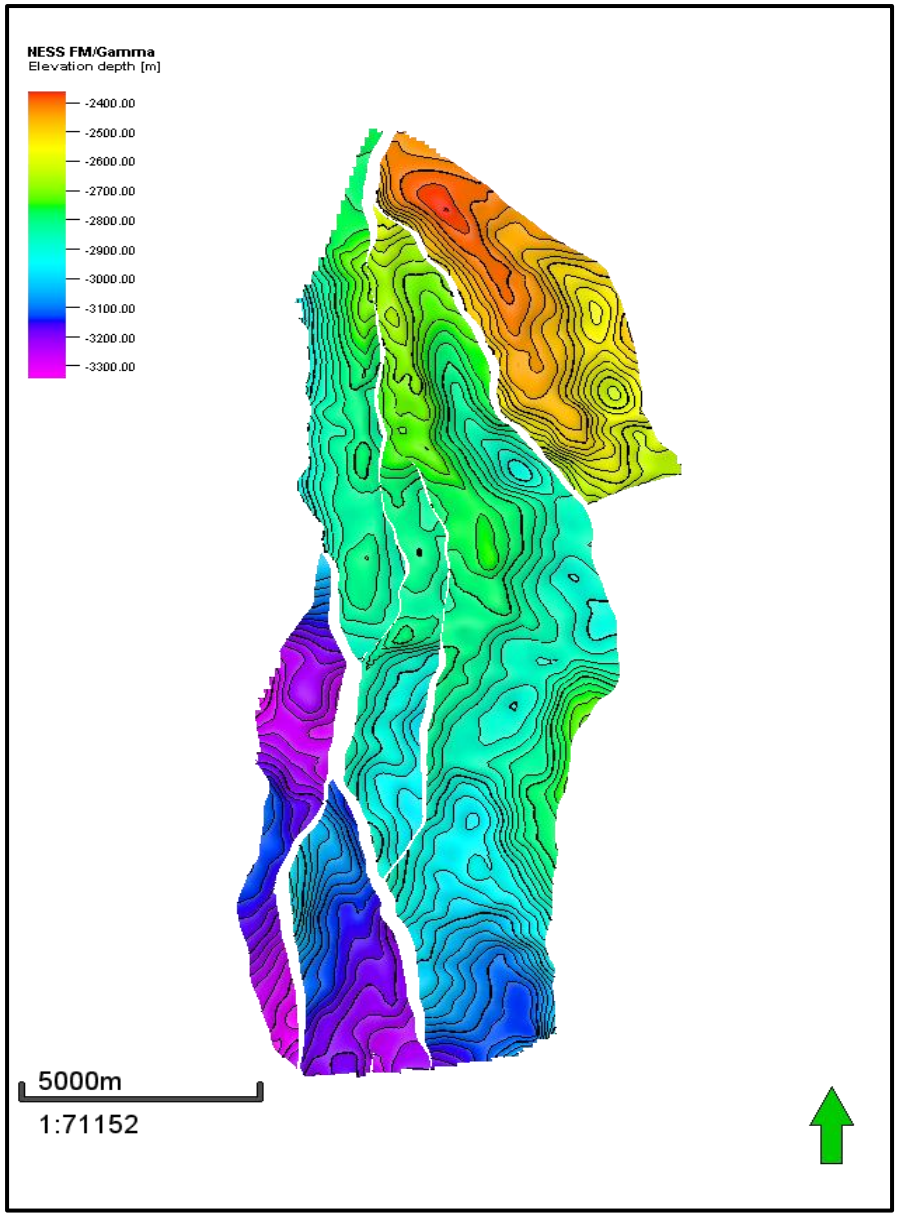

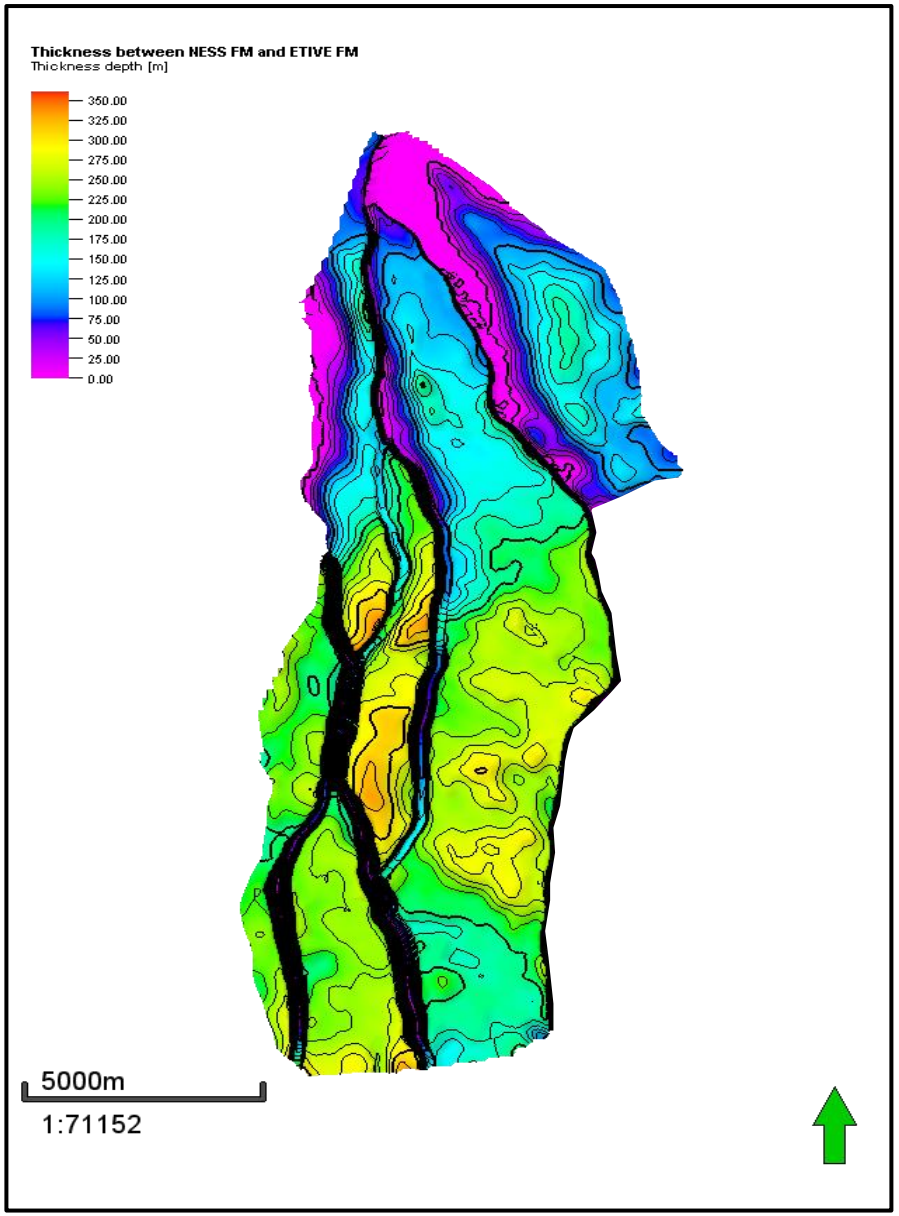

Figure 48: Depth surface for Ness Formation (left) and thickness map between Ness Formation and the underlying Etive Formation (right).

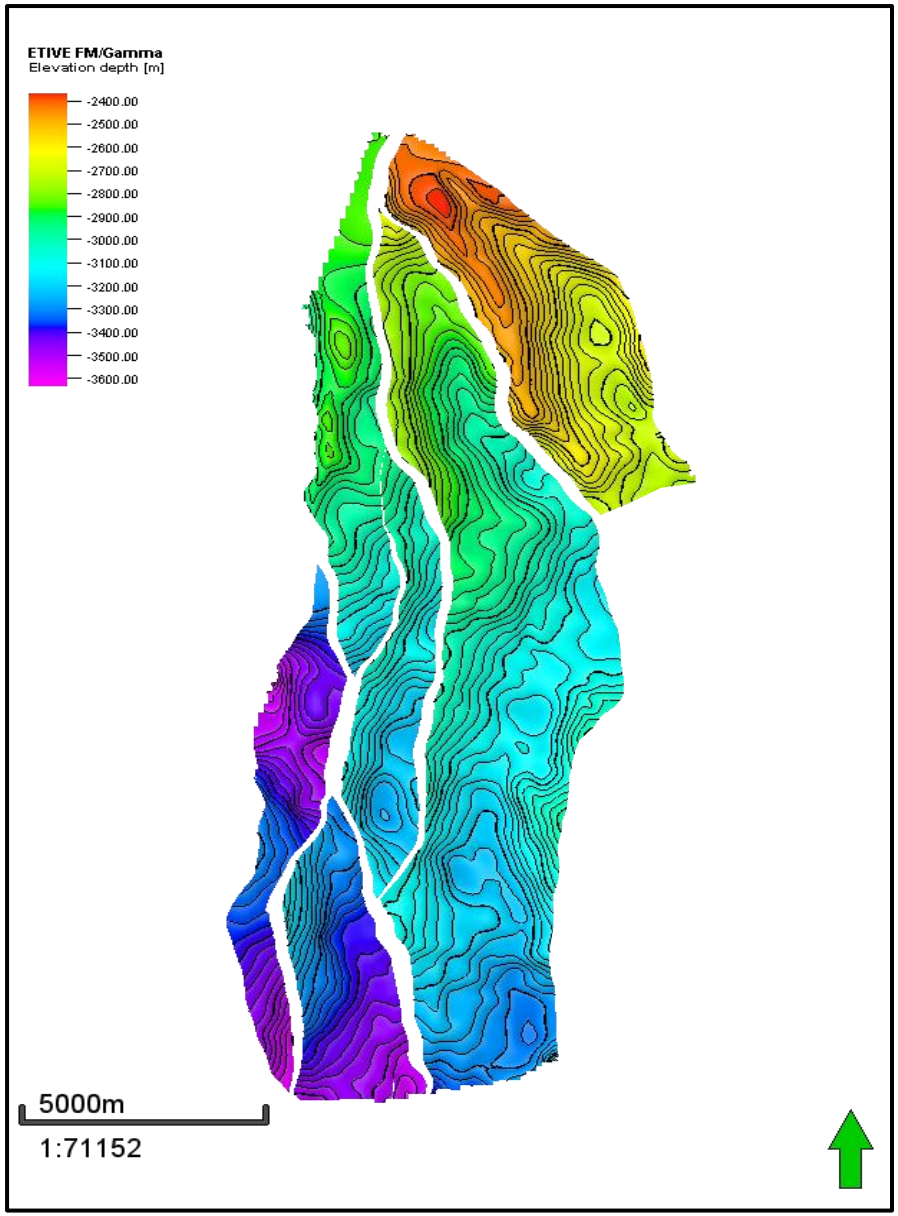

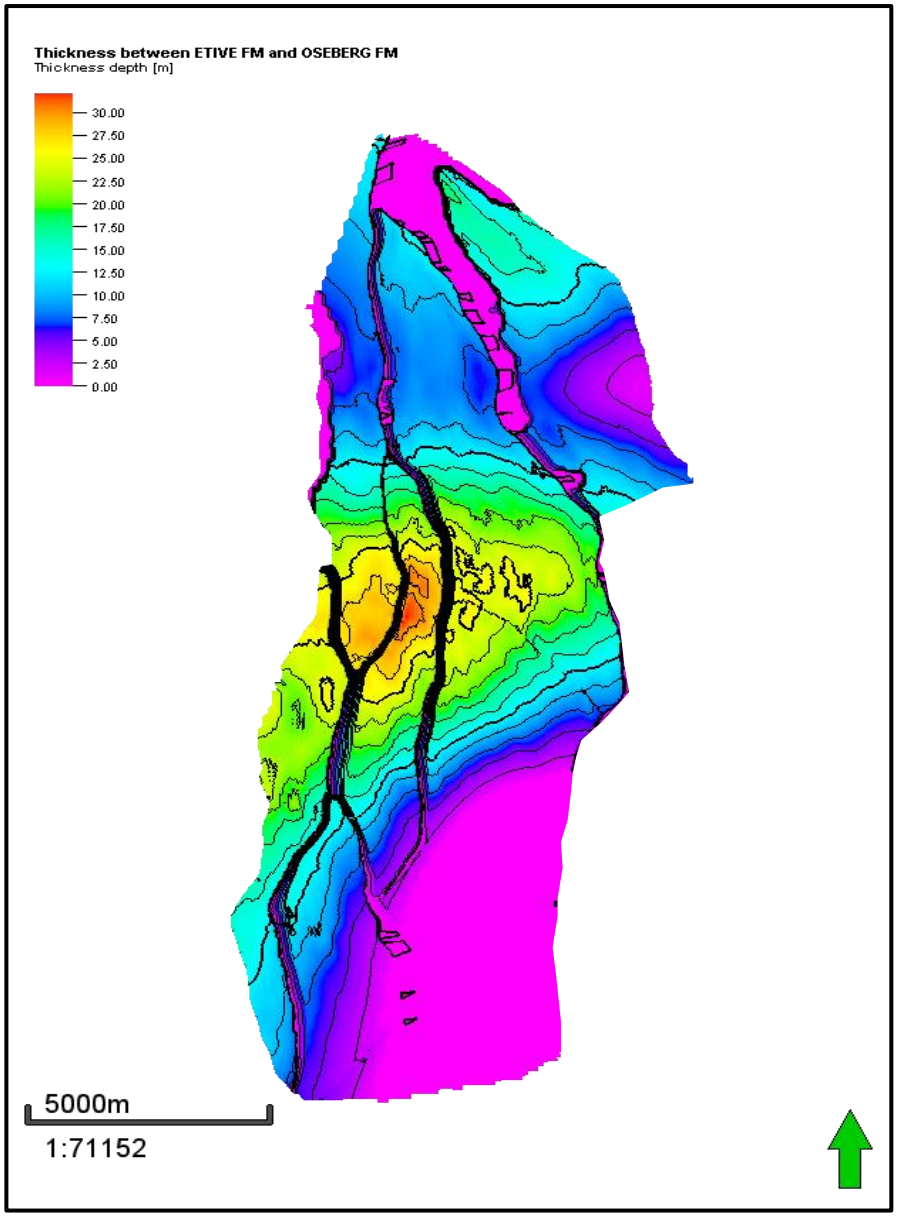

Figure 49: Depth surface for Etive Formation (left) and thickness map between Etive Formation and the underlying Oseberg Formation (right).

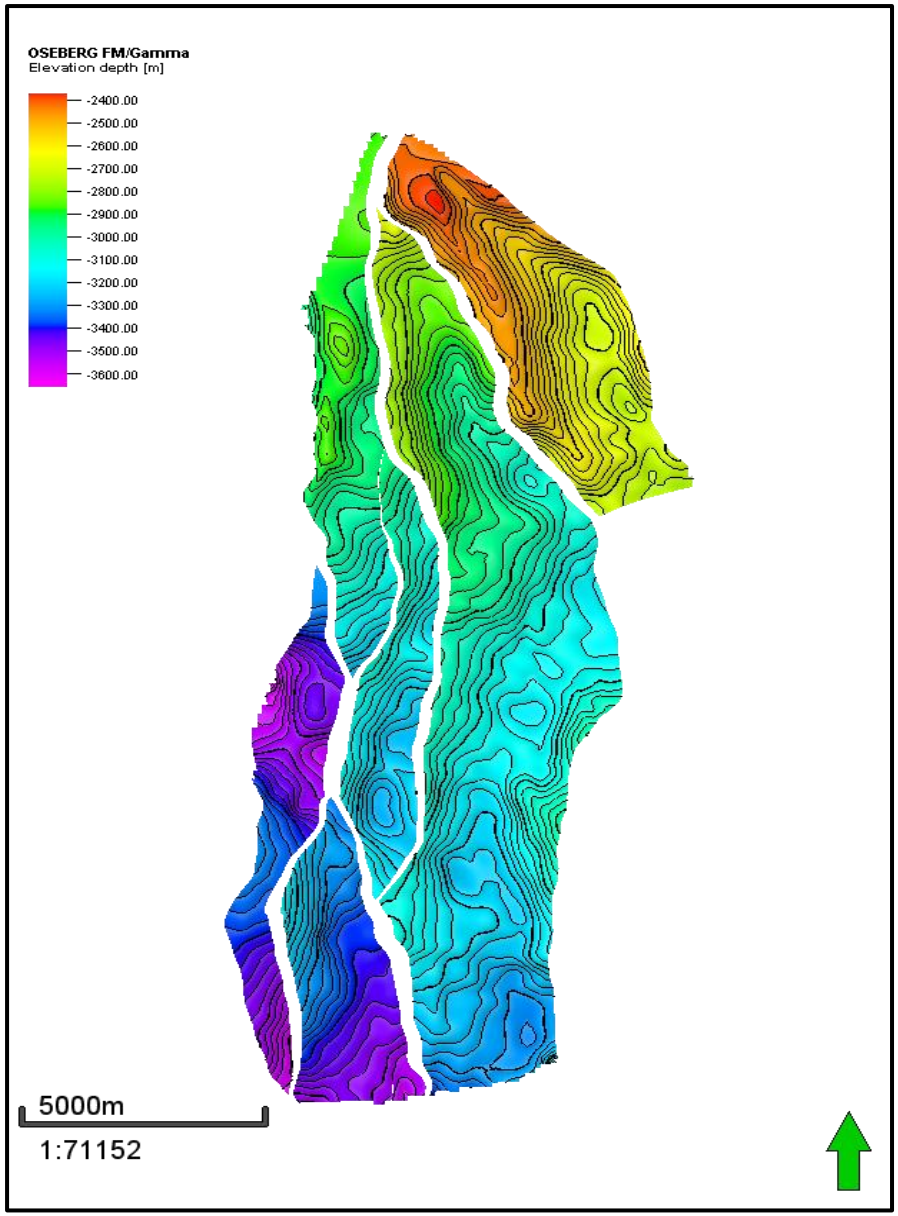

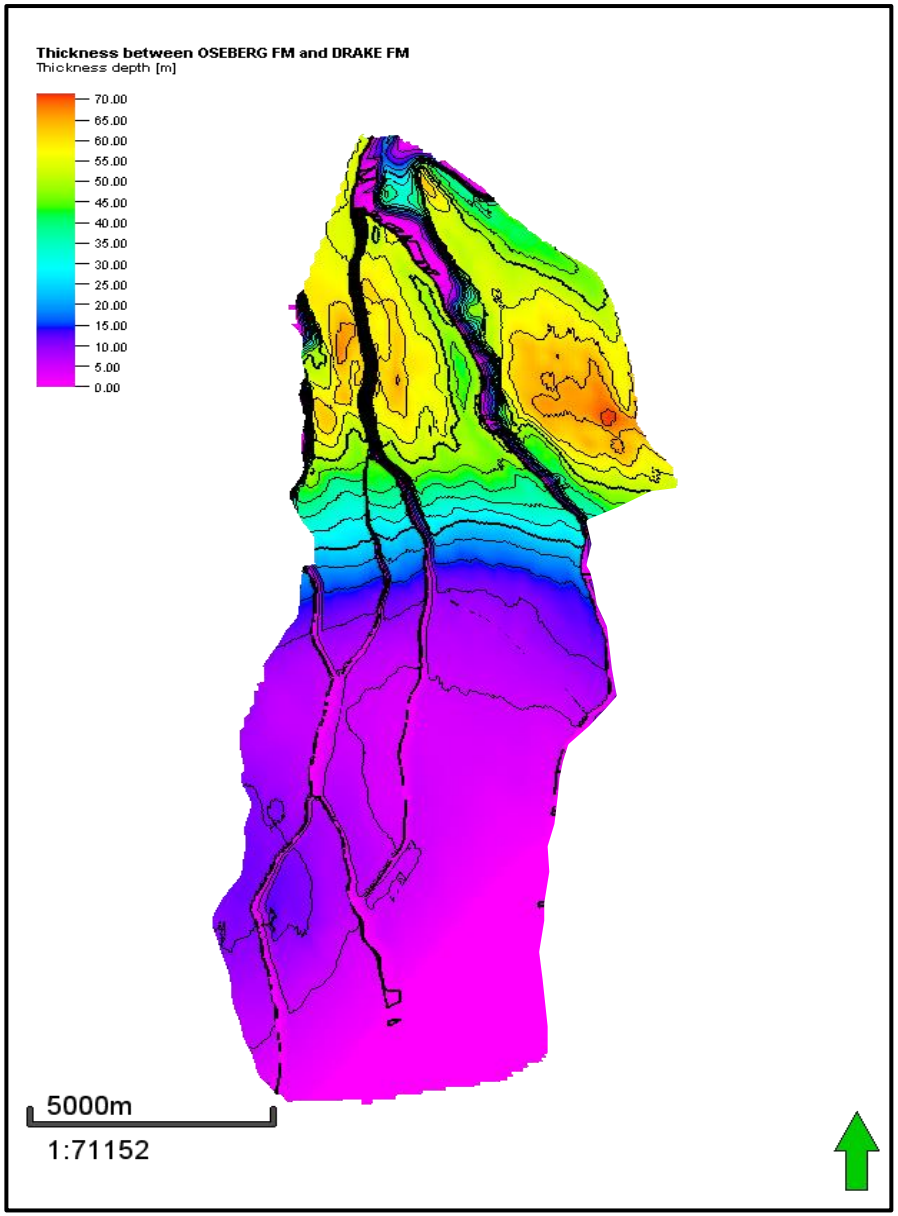

Figure 50: Depth surface for Oseberg Formation (left) and thickness map between Oseberg Formation and the underlying Drake Formation (right).

5.5 Fault Analysis - Displacement

As a part of the qualitative analysis of the interpreted and modelled faults, the displacement distribution of each separate fault was examined. The STAR plugin in Petrel calculates the fault displacement along the fault planes in addition to SGR and column heights, and was therefore used for this purpose.

By analyzing the fault displacement of the different fault planes (Figures 51 – 55), some key observations can be made. The fault interpretations are bound by the area of interest meaning that the faults are not necessarily expected to show less displacement towards the end of the interpreted fault plane. Where faults do tip out within the AOI, this has been modelled. Faults 4 and 3 (Figure 52 & Figure 53), display sections of the faults where the active displacement is approaching zero.

Sudden variations in the displacement on multiple faults can be observed (Figure 52 & Figure 53). This occurs where faults with different displacement converge on or split from the same fault plane and is recognized as an infliction point on the fault throw profile. Along Fault 3 this is visible where faults 1 & 7 are intersected. In this case, Fault 3 transfers the displacement seen in faults 1 and 7, causing a locally increased in displacement of around 200 meters. The combined displacement across faults 7 and 3 (100 + 300 meters) is roughly equivalent to the maximum displacement seen in Fault 3 (400 meters). In the displacement calculations of Fault 11 (Figure 51), local areas of high displacement not caused by intersecting faults are observed. This high displacement is an artifact from the modelling due to lacking seismic interpretation in Segment C, and should therefore be disregarded. The fault interpretations in the rest of the model are however displaying reasonable fault displacement profiles.

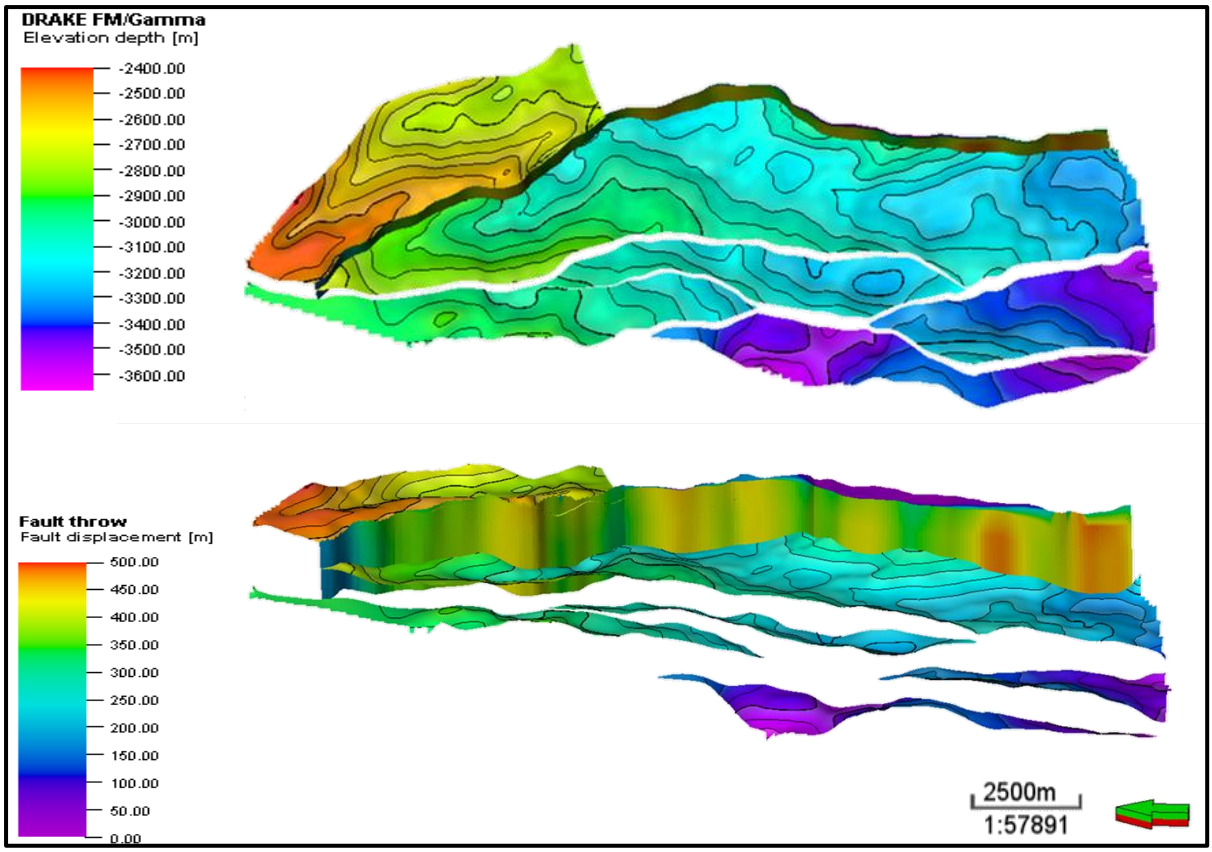

Figure 51: Fault 11 with displacement along the fault plane and the topographic map of the interpreted Drake Formation. Note the increased throw along the southern part of the fault plane due to the lack of interpretations on the foot-wall side.

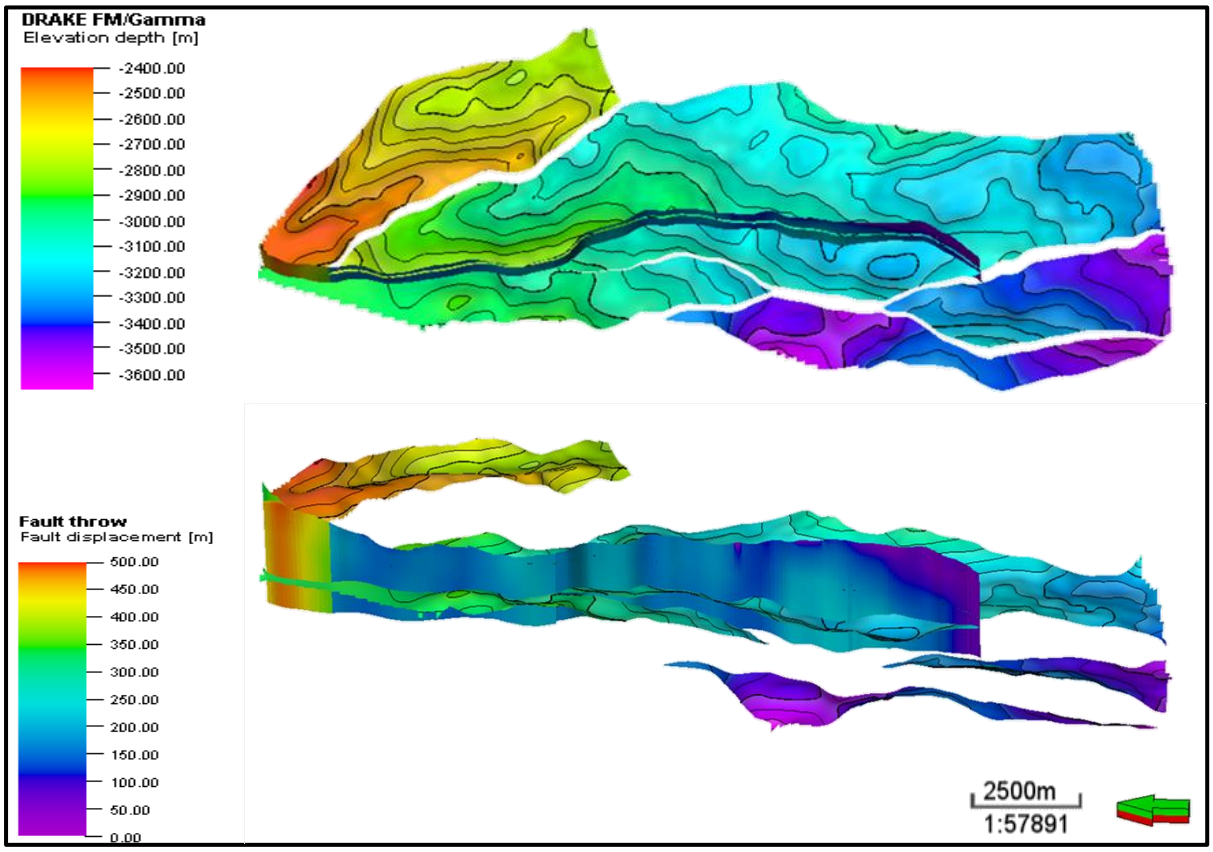

Figure 52: Fault 4 with displacement along the fault plane and the topographic map of the interpreted Drake Formation. Note the abrupt change in throw in the northern part where the fault takes over the displacement of fault 11.

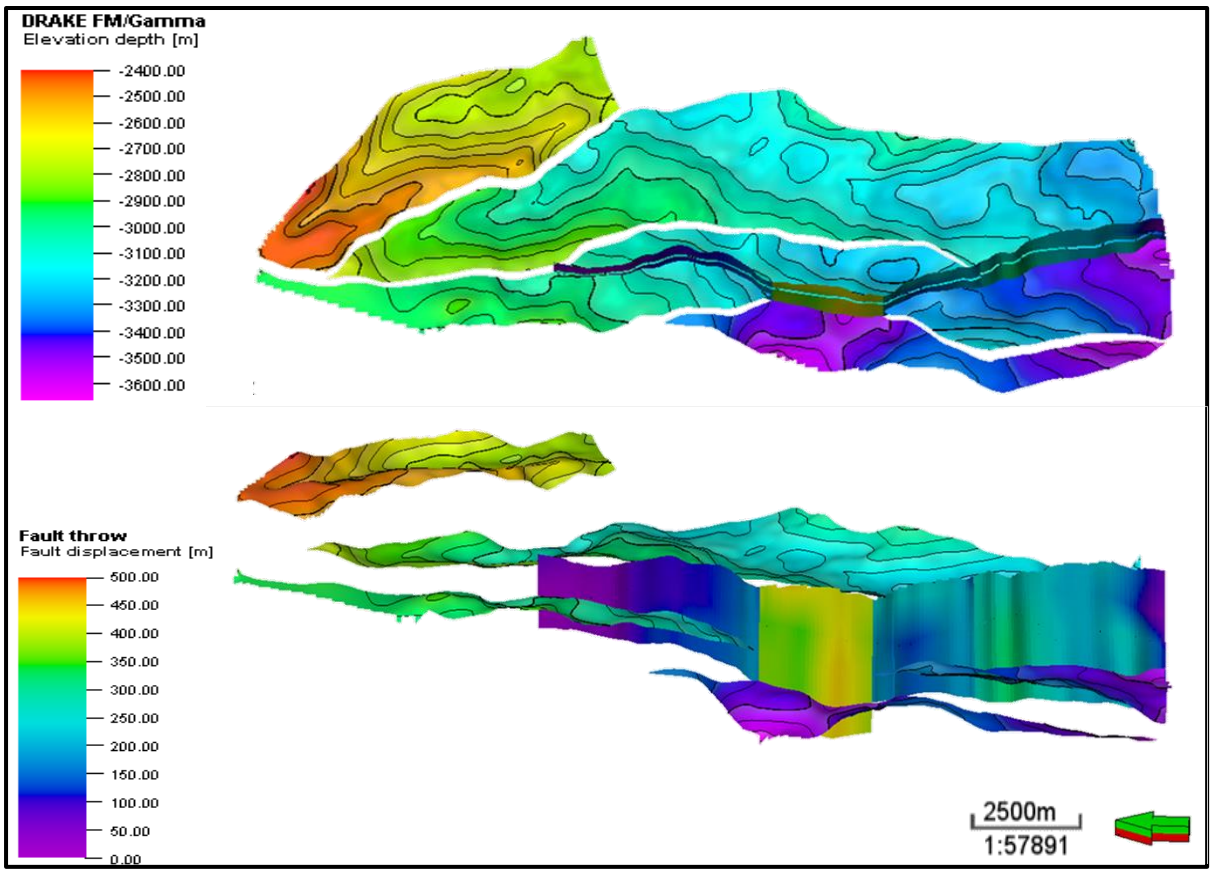

Figure 53: Fault 3 with displacement along the fault plane and the topographic map of the interpreted Drake Formation. Note the abrupt change in throw in the central part where the fault takes over the displacement of faults 1 and 7.

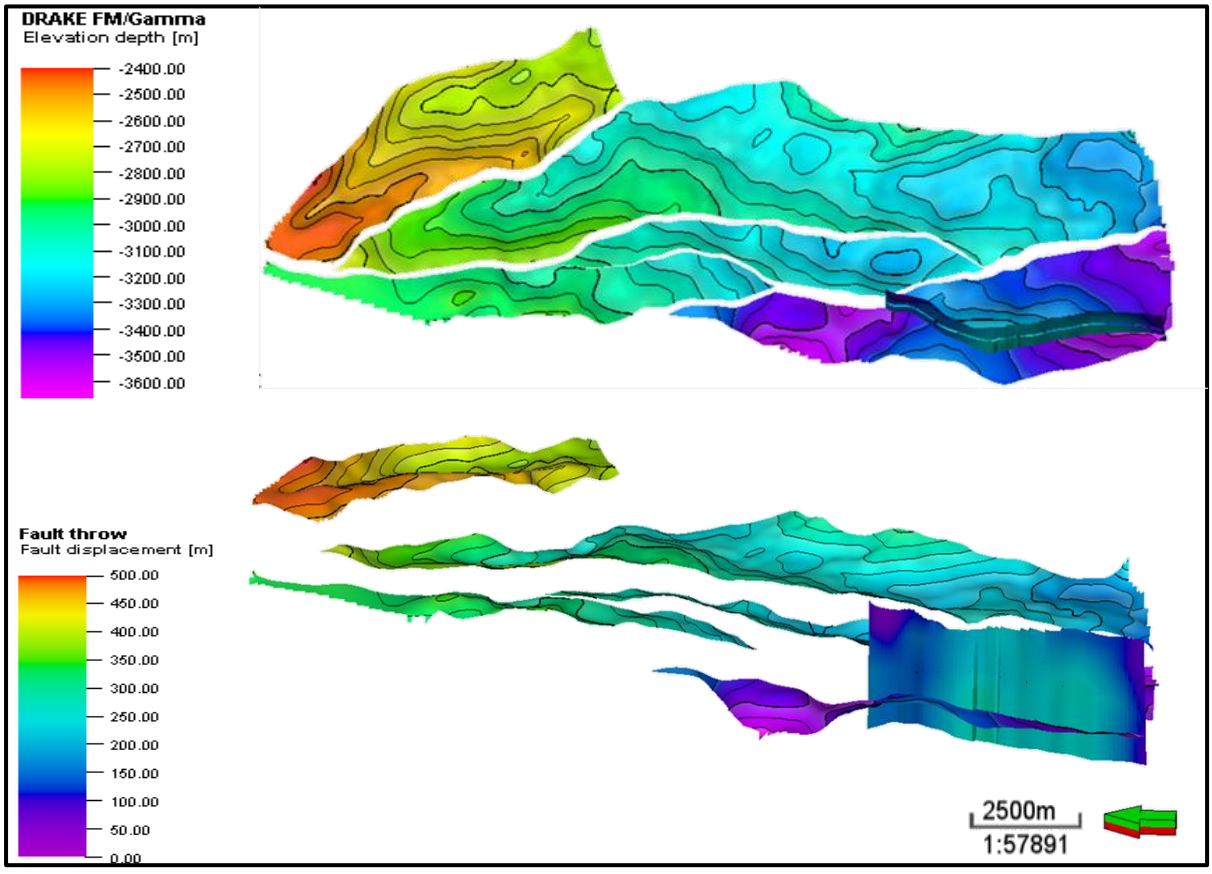

Figure 54: Fault 1 with displacement along the fault plane and the topographic map of the interpreted Drake Formation.

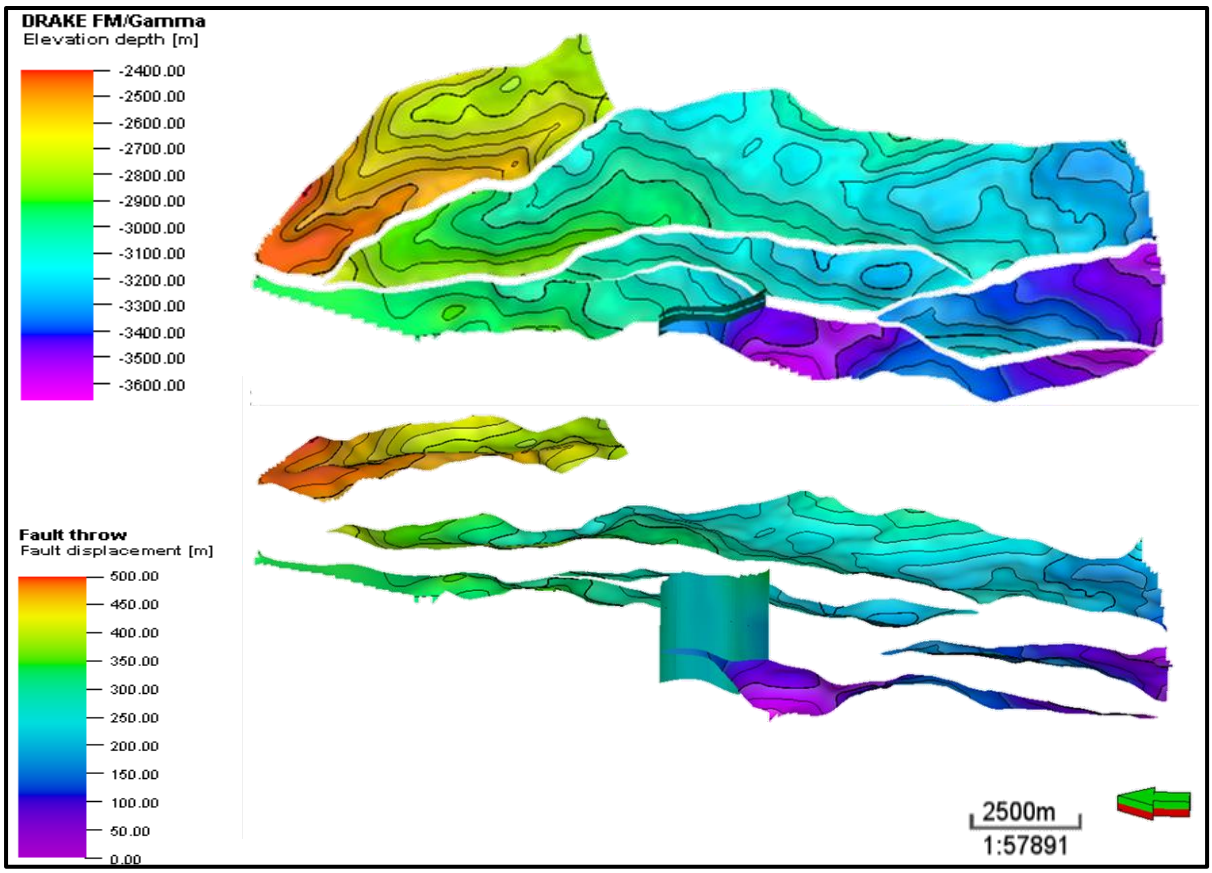

Figure 55: Fault 7 with displacement along the fault plane and the topographic map of the interpreted Drake Formation.

5.6 Property Modeling

The result of the facies and petrophysical modelling can be seen in figures 56-62. "Simbox-view" was used to better display facies variations. The intersections do not display true cell thickness as modelled, but rather the result of leveling at a base interval with a constant cell thickness. This allows true distribution to be presented without interfering elements such as fluctuating interval thickness and fault displacement.

The Draupne Formation has limited presence in the modelled area due to extensive erosion this (Figure 56). Due to the lack of well coverage for this formation, Vsh values that represent the marine shales characteristic of the Draupne Formation were used.

The overall trend observed across Heather and Tarbert formations match the proposed backstepping depositional shore-line environment (Figure 57 & Figure 58). Even though the formations are modelled separately, the trend is continuous and can be traced across both

formations. The figures both show the same intersection where the combined Heather Formation and Tarbert Formation are stacked to better display this backstepping nature.

The conceptual model used for the construction of the facies distribution of the Ness Formation was based on examples from (I. B. Ramberg et al., 2008) and conceptual facies models from Martinius et al. (2014). Specific parameters and orientations for the distributary channels was based on the work done by Ryseth (2000). When comparing the result from the Ness Formation property model with the proposed conceptual model (Figure 59), it is evident that the resulting property model is a fair depiction that arguably honors the conceptual setting.

Etive and Oseberg formations appear to have a patchy distribution of facies classes when looking at the modelled distribution from the top of the formations (Figure 60 and Figure 61). This is because a default "sequential indicator simulation" method was used for calculating the probable distribution of facies across the model. This method has by default no specified trends, and calculates the facies distribution by the well data alone, honoring the input data by forcing the same percentage observed in the well logs across the model. Since the Etive and Oseberg formations are both part of a single progressive shorefront system, it could be argued that using a truncated Gaussian with trends like the Heather and Tarbert Formations would yield a better result. It is however difficult to create such a model while still honoring the well data for such a thin and irregular stratigraphic interval. When analyzing the result of the sequential indicator simulation in the intersections of the two formations, it is clear that a progradational trend can be recognized. The trend can be established by the general progradation of sands in the south and the upwards decrease in marine shales in the north of the model.

The Drake Formation is predominantly composed of homogenous marine shales punctuated with sporadic intervals of coarser marine sands. Due to the lack of any significant trends a simple truncated Gaussian simulation facies calculation method was used to keep the high Vsh percentage observed in the up-scaled well logs. By analyzing the result from this operation (Figure 62), it is clear that the calculated facies model depict a predominantly marine shale interval with small clusters of marine sands or silts originating from the anomalies in the well data. This is however apparently not affecting fault sealing as these are not in contact with the fault plains and are vertically limited (couple of meters).

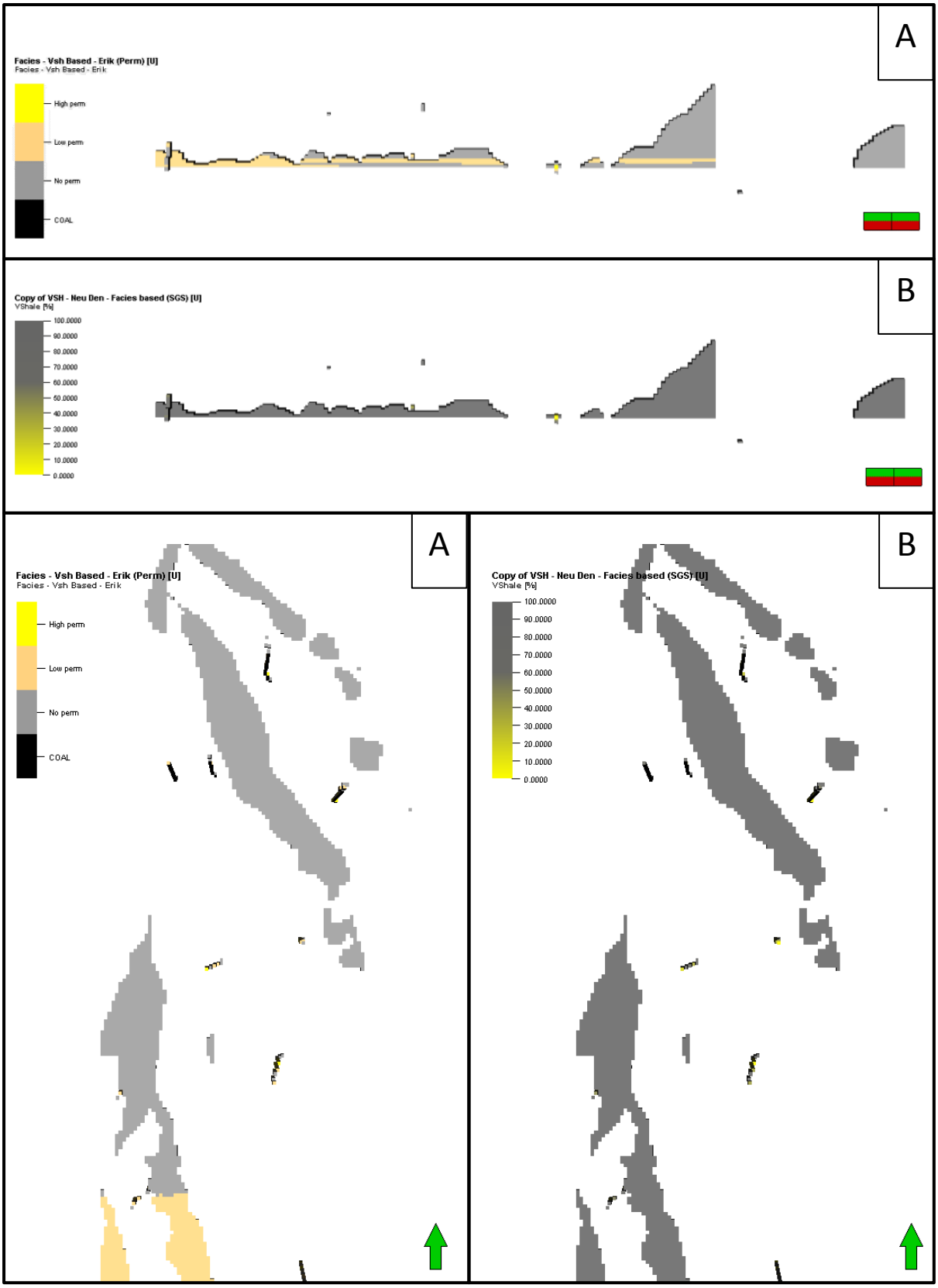

Figure 56: Figure displaying a "sim-box" view of the Draupne Formation with north-south intersection and top view. Sections A display the constructed facies model for this interval, and sections B display the resulting petrophysical model by applying the up-scaled Vsh parameters to the facies model.

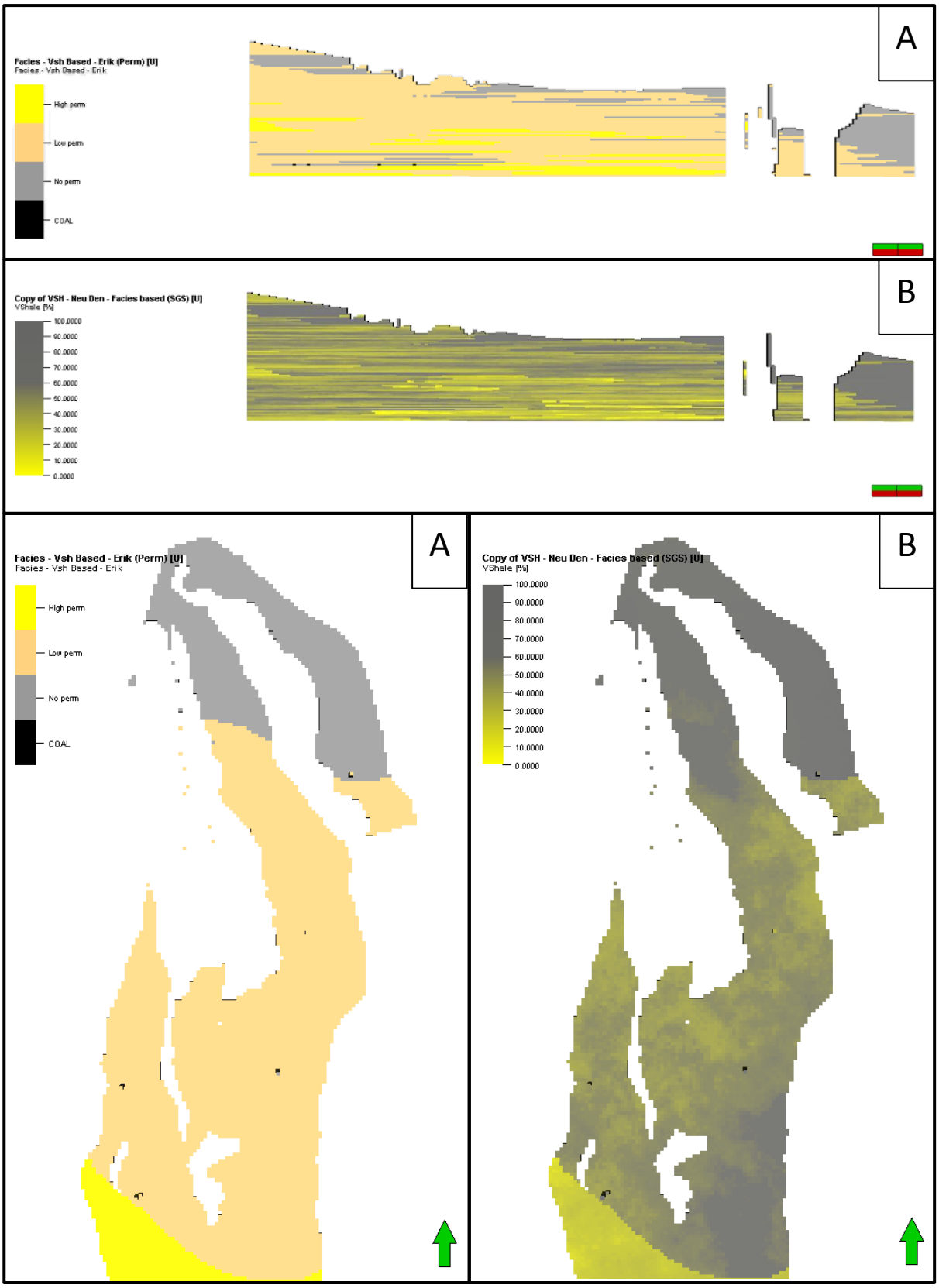

Figure 57: Figure displaying a "sim-box" view of the Heather Formation with top view and north-south intersection displaying the joint interval of the Heather and Tarbert Formations. Sections A display the constructed facies model for this interval, and sections B display the resulting petrophysical model by applying the up-scaled Vsh parameters to the facies model.

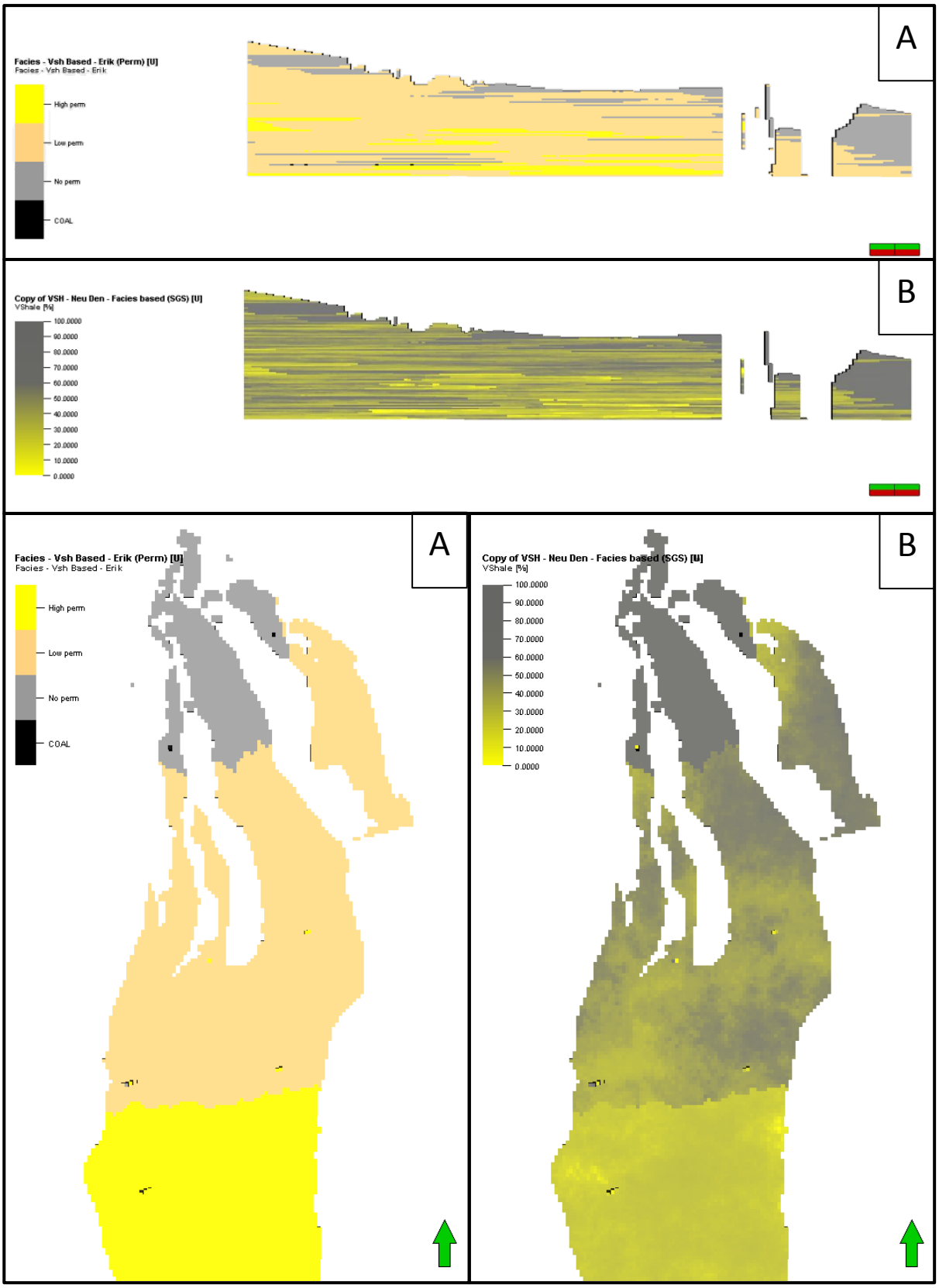

Figure 58: Figure displaying a "sim-box" view of the Tarbert Formation with top view and north-south intersection displaying the joint interval of the Heather and Tarbert Formations. Sections A display the constructed facies model for this interval, and sections B display the resulting petrophysical model by applying the up-scaled Vsh parameters to the facies model.

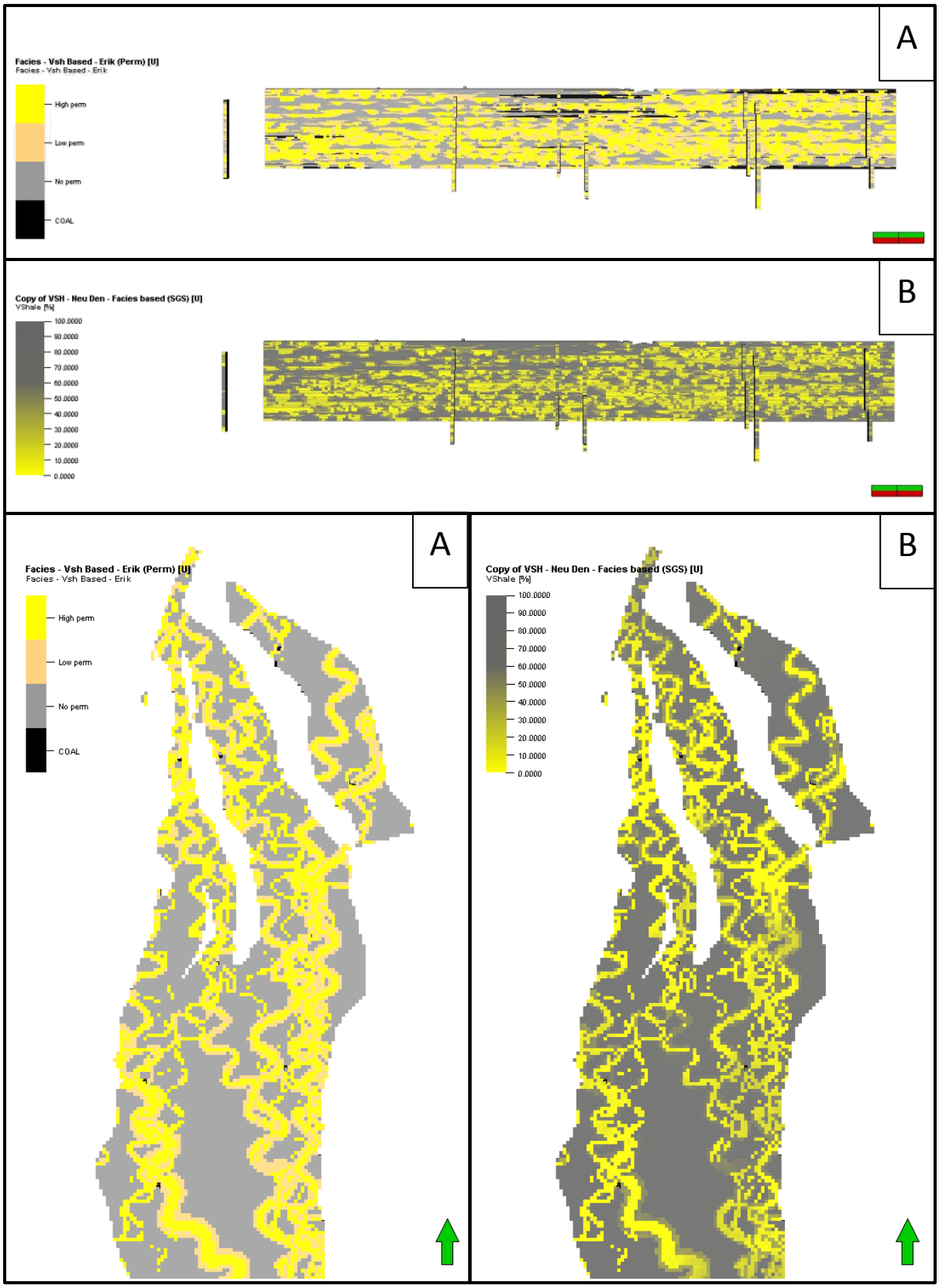

Figure 59: Figure displaying a "sim-box" view of the Ness Formation with north-south intersection and top view. Sections A display the constructed facies model for this interval, and sections B display the resulting petrophysical model by applying the up-scaled Vsh parameters to the facies model.

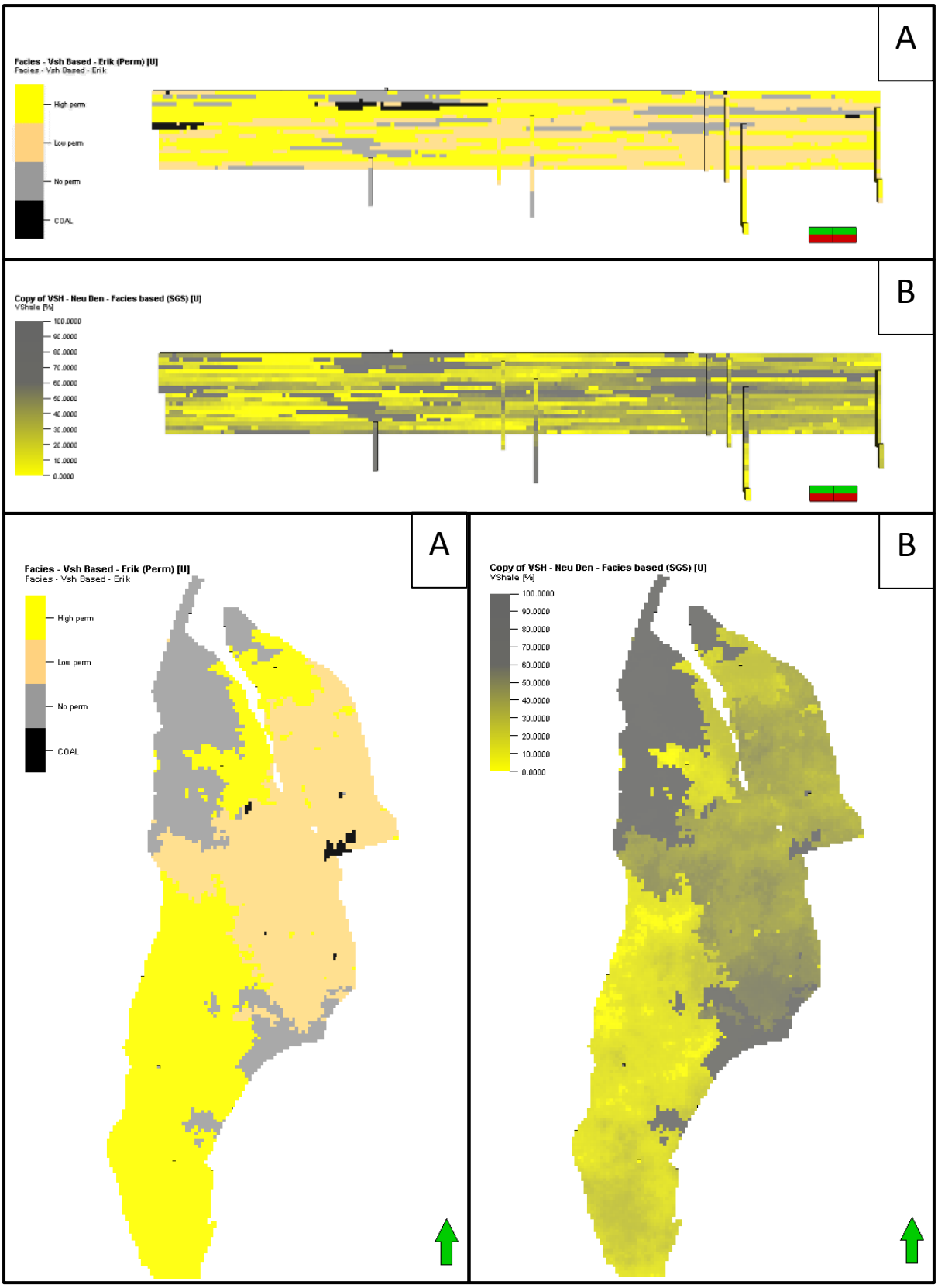

Figure 60: Figure displaying a "sim-box" view of the Etive Formation with top view and north-south intersection displaying the joint interval of the Etive and Oseberg Formations. Sections A display the constructed facies model for this interval, and sections B display the resulting petrophysical model by applying the up-scaled Vsh parameters to the facies model.

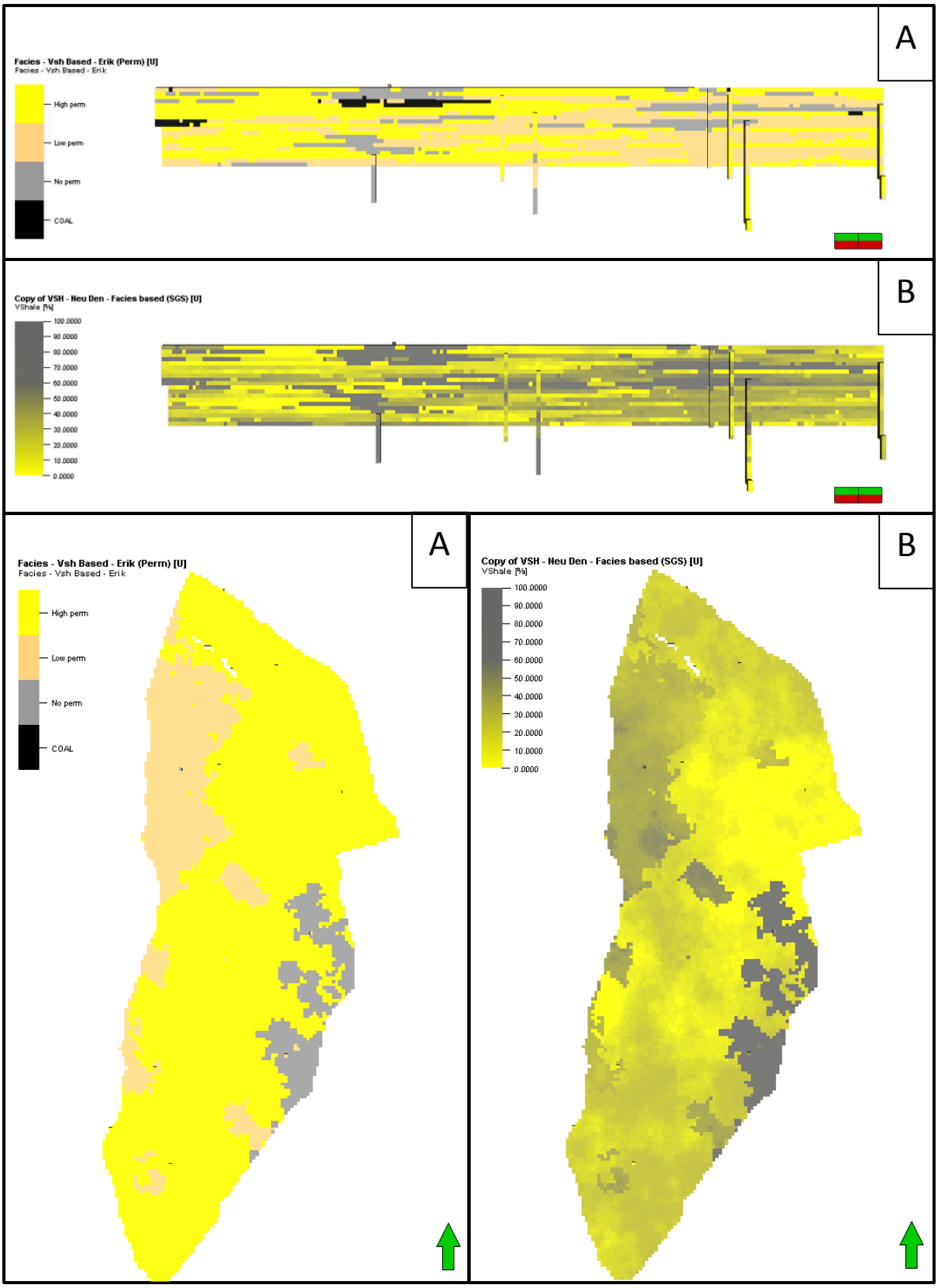

Figure 61: Figure displaying a "sim-box" view of the Oseberg Formation with top view and north-south intersection displaying the joint interval of the Etive and Oseberg Formations. Sections A display the constructed facies model for this interval, and sections B display the resulting petrophysical model by applying the up-scaled Vsh parameters to the facies model.

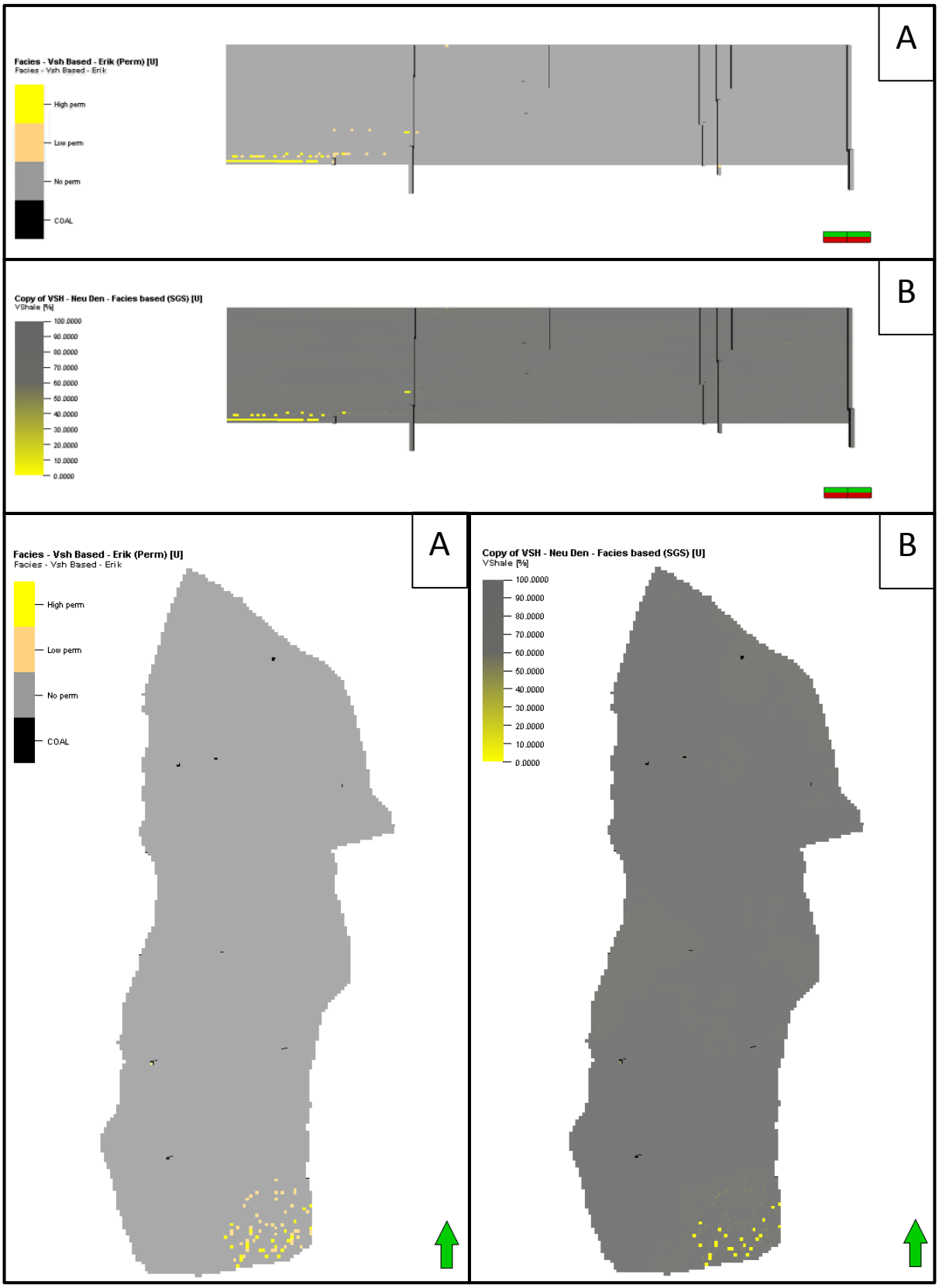

Figure 62: Figure displaying a "sim-box" view of the Drake Formation with north-south intersection and top view. Sections A display the constructed facies model for this interval, and sections B display the resulting petrophysical model by applying the up-scaled Vsh parameters to the facies model.

To analyze how accurately the property model match the up-scaled well logs, a histogram can be produced (Figure 63). By analyzing this histogram it is evident that although some variation is present between the two, the overall match is good.

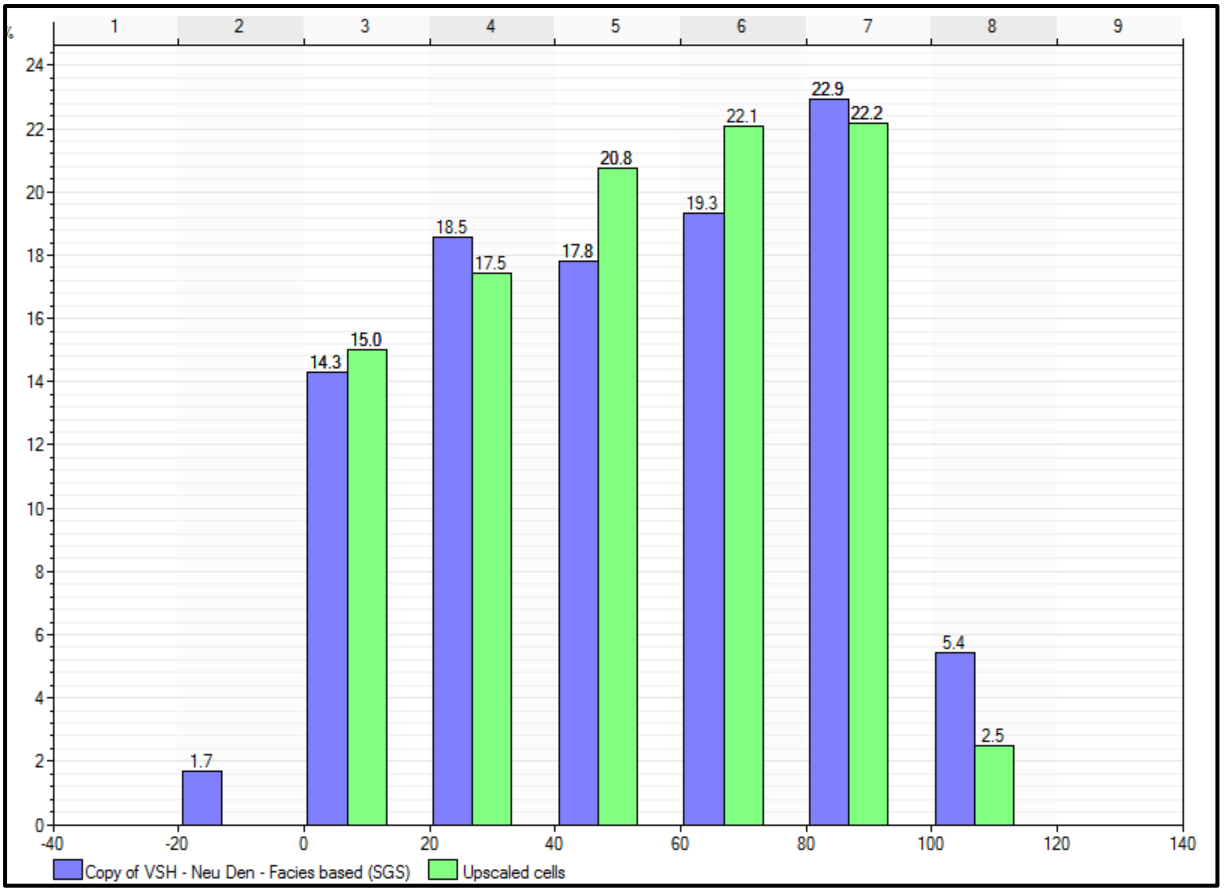

Figure 63: Histogram displaying the differences in the percentage of Vsh distributed across the model from the up-scaled well logs and the property model.

5.7 Pressure Survey Analysis

5.7.1 Gamma

The formation pressure survey from 30/6-9 (Figure 64) has identified gas in the Ness Formation with a GOC at 2495 meters. Formation pressure data from 30/9-2 R continues along the established oil-leg from 30/6-9 with an encountered OWC in the Oseberg Formation at 2709 meters. Based on the formation pressure plots it is apparent that there is cross-stratigraphic fluid communication in Ness, Etive and Oseberg formations in the Gamma structure indicating no internal compartments.

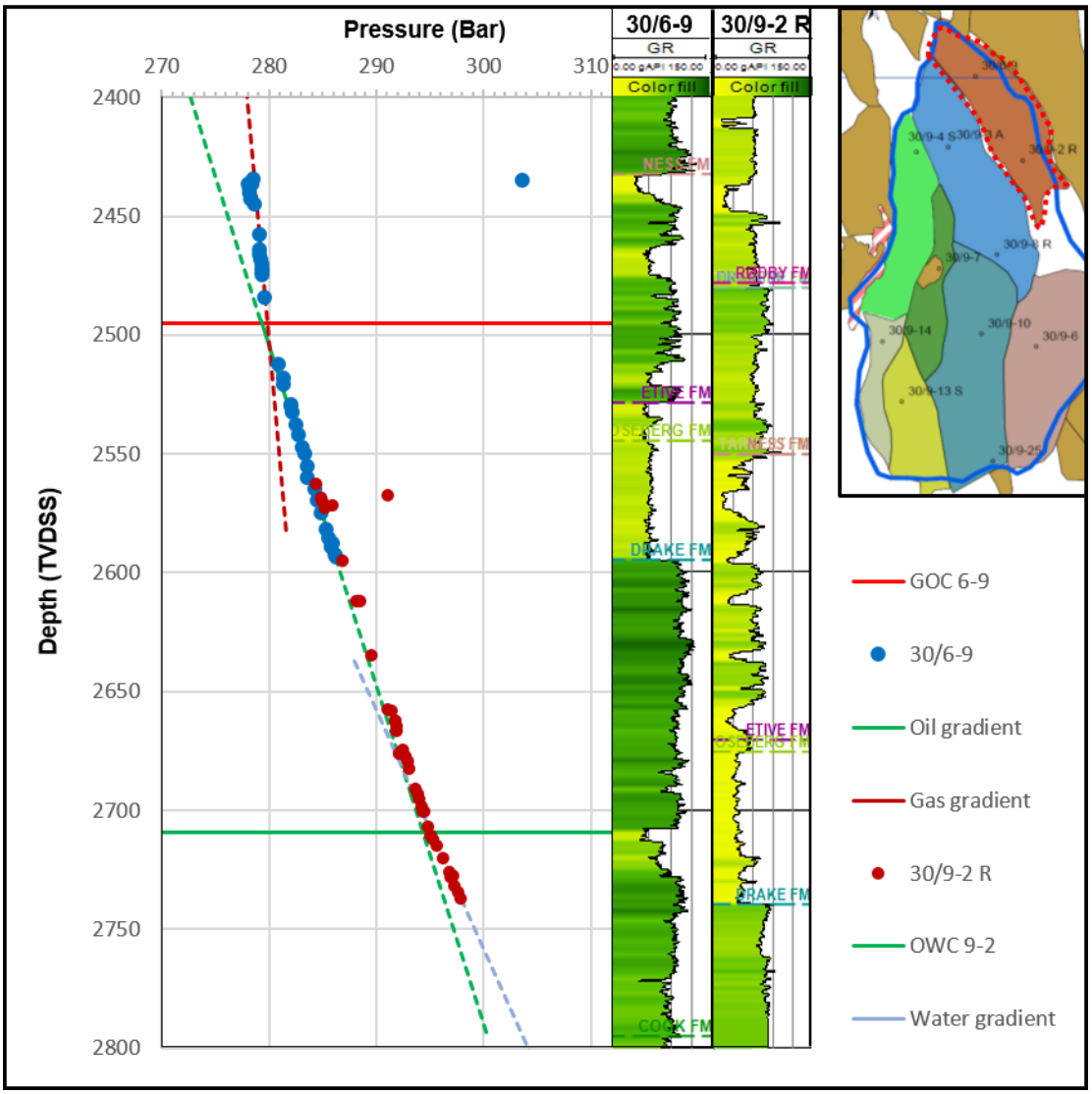

Figure 64: Formation pressure plots of 30/6-9 and 30/9-2 R in Gamma displaying fluid contacts and gradients.

5.7.2 Omega

30/9-3 A encountered a GOC in the upper Ness Formation at 2726 meters and an OWC at 2801 meters with an isolated water leg in the lower Ness Formation (Figure 65). This well has suggested hydrostatic isolation in the water leg at Brent level reservoirs, displaying an over-pressure of 10 bars compared to the other wells in the Omega structure. Wells 30/9-10 and 30/9-8 plot along the same pressure gradient as in the upper Ness Formation suggesting the presence of cross-stratigraphic fluid connection in the Omega structure with the exception of the water leg in 30/9-3 A. Conclusively, this indicates that a vertical stratigraphic compartmentalization is present between the upper and lower Ness Formation in the northernmost section of the Omega structure.

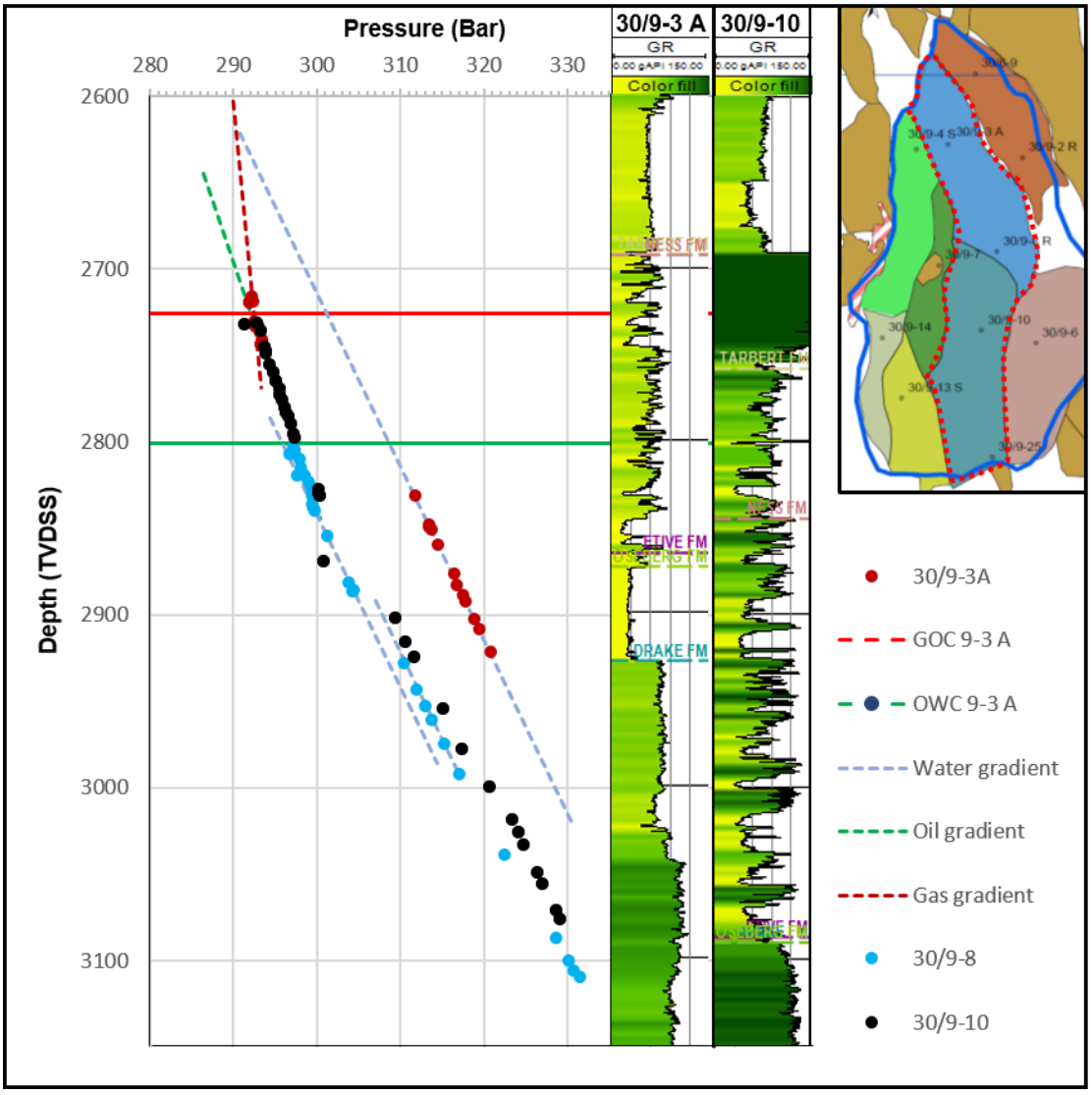

Figure 65: Formation pressure plots of 30/9-3 A and 30/9-8 30/9-10 in Omega displaying fluid contacts and gradients.

5.7.3 B-North

Well 30/9-4S in B-North encountered no direct fluid contacts, but determined gas in the Tarbert Formation and a leg from the lower Ness Formation and down indicating the existence of a GOC/OWC between 2800 and 2850 meters (Figure 66). The pressure difference between the gas zone and water leg is indicating stratigraphic compartmentalization between the pressure tested interval in the Tarbert Formation and the Ness Formation.

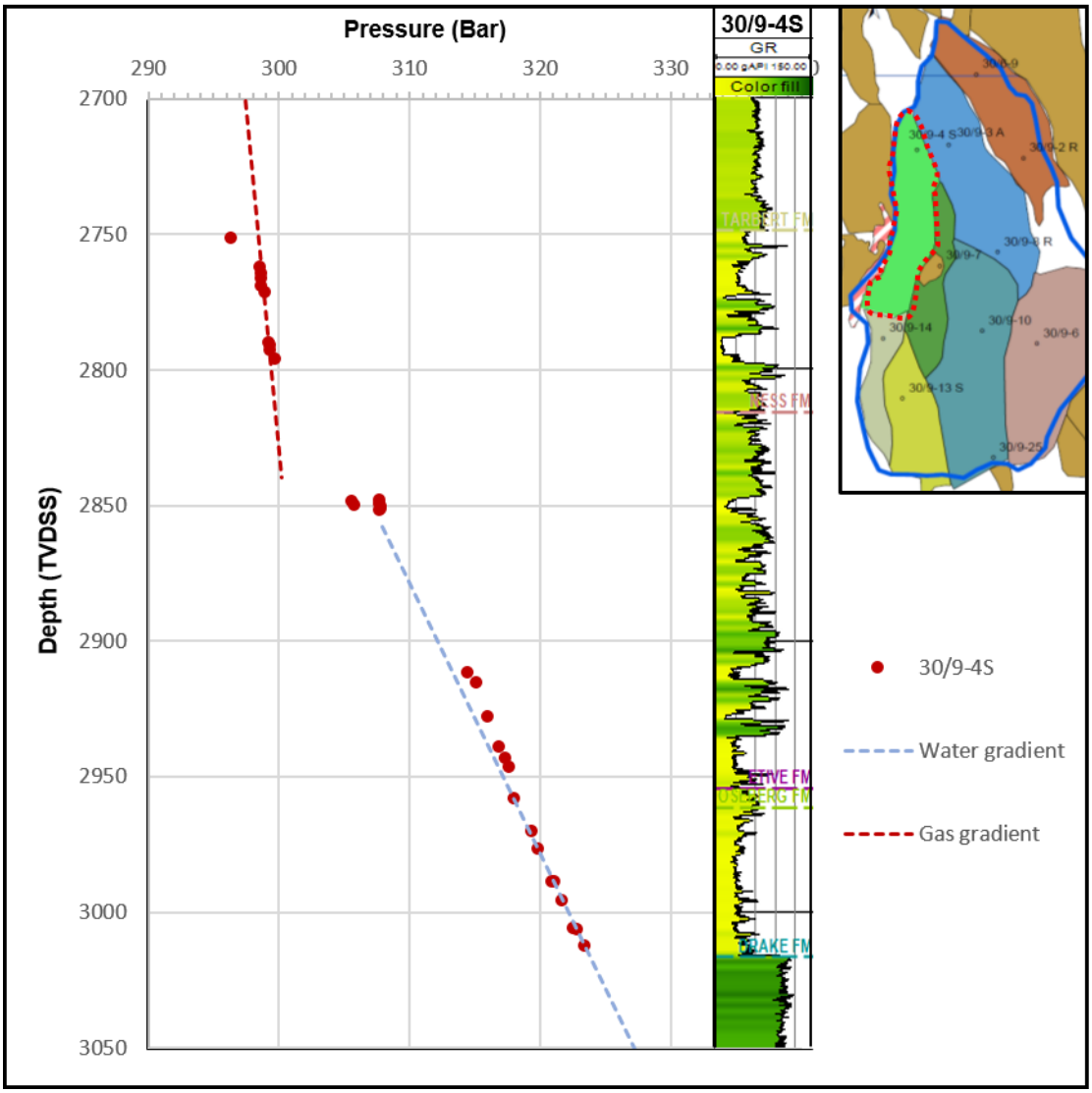

Figure 66: Formation pressure plots of 30/9-4 S in B-North displaying fluid contacts and gradients.

5.7.4 B-South

B-South is covered by well 30/9-7 which encountered oil and a GOC at 2808 meters in the Tarbert Formation with a continuous water-leg in the Ness, Etive, and Oseberg formations (Figure 67). No indications of stratigraphic compartmentalization that can be seen from this formation pressure plot, signifying that B-South support cross-formation pressure differences at least in the area drilled by 30/9-7.

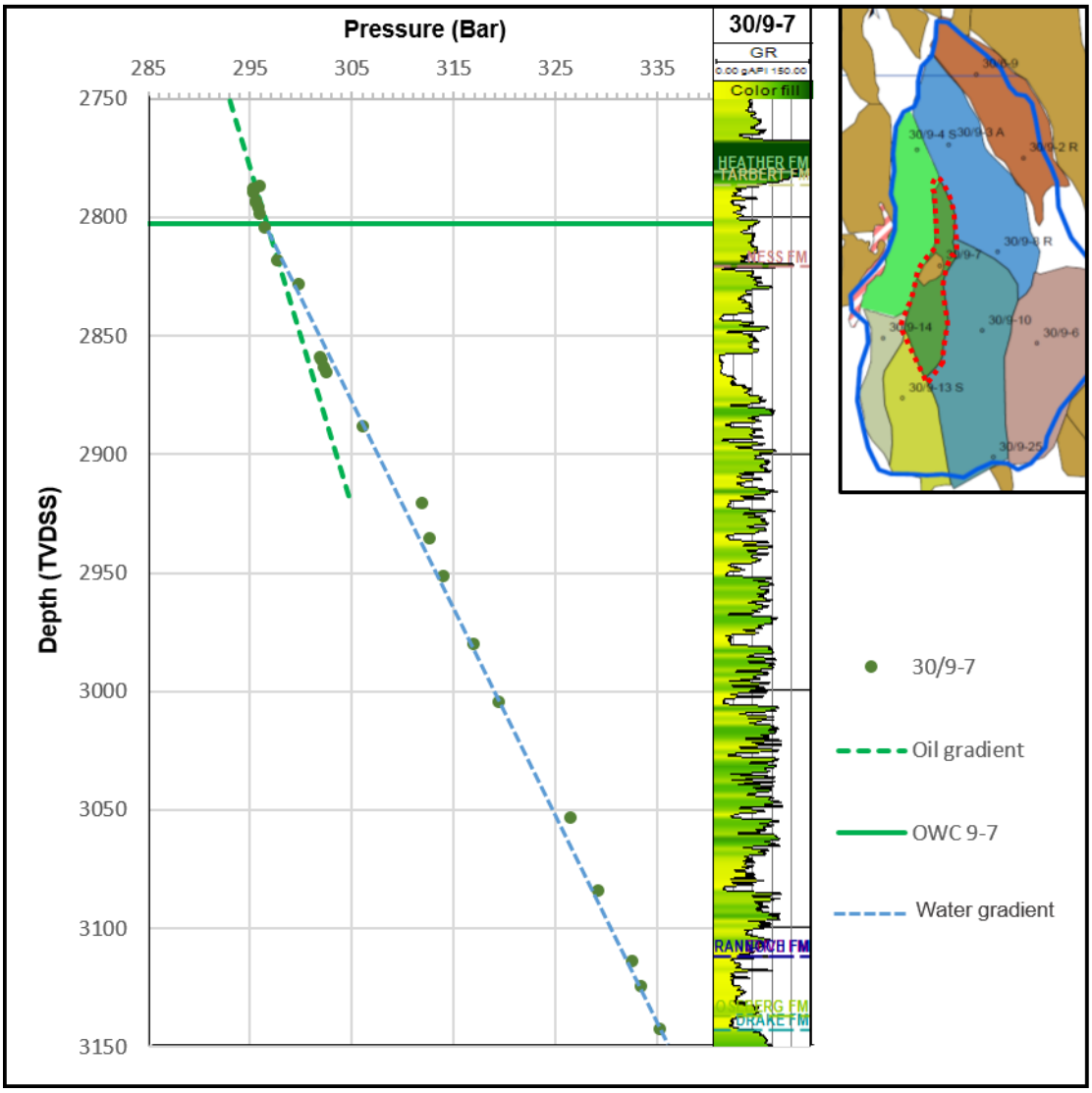

Figure 67: Formation pressure plots of 30/9-7 in B-South displaying fluid contacts and gradients.

5.7.5 G-Central

30/9-14 encountered a GOC at 3032 meters and an OWC at 3094 meters, both in the Tarbert Formation (Figure 68). The oil leg in 30/9-14 appears to be over-pressured compared to the water leg, indicating that the hydrocarbons are in a different pressure regime than the water leg. This signifies that the oil and gas encountered in the shales of the upper Tarbert Formation are stratigraphically isolated from the water leg, and thus limiting the fluid communication.

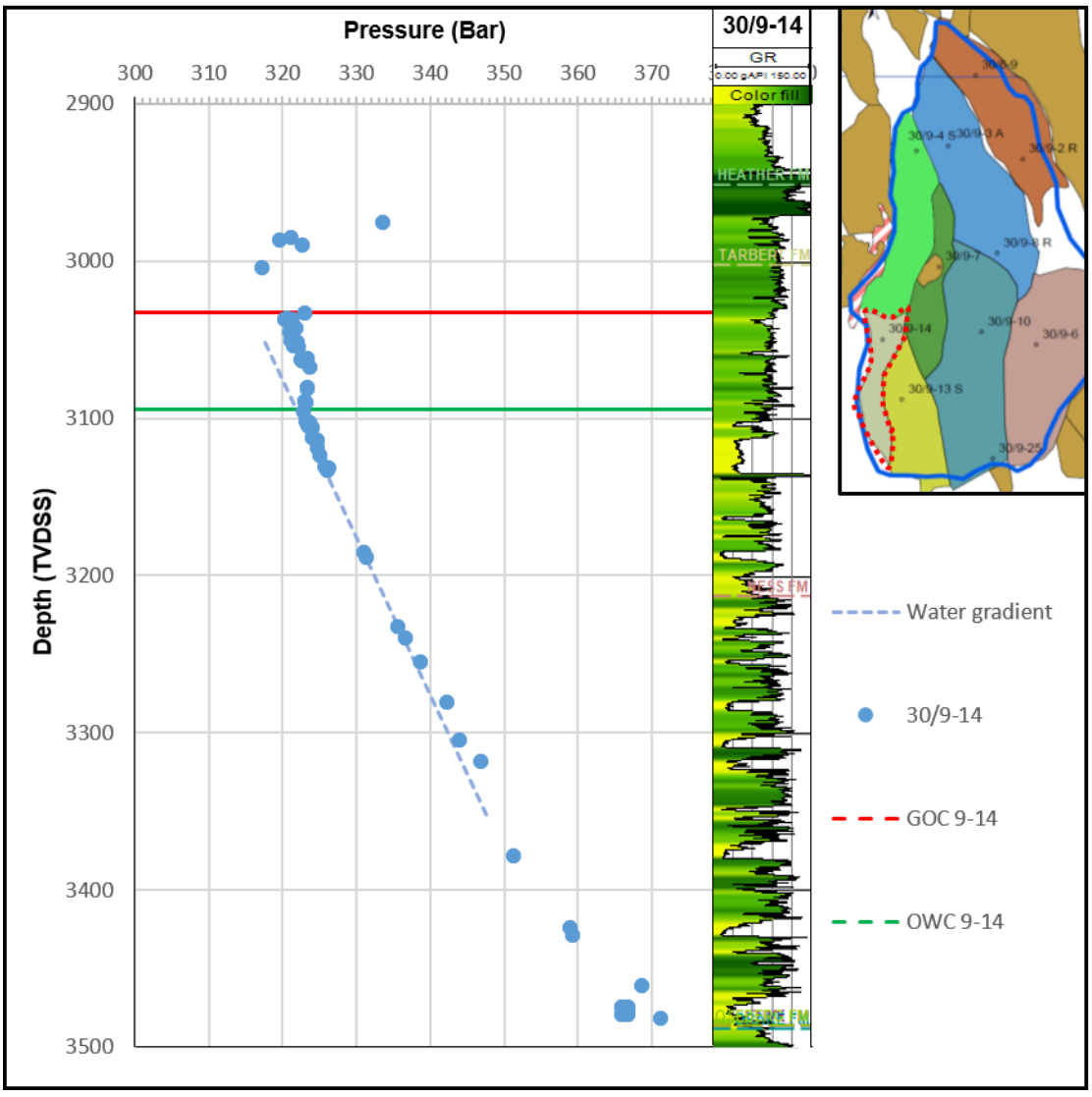

Figure 68: Formation pressure plots of 30/9-14 in G-Central displaying fluid contacts and gradients.

5.7.6 G-East

The formation pressure survey from 30/9-13 S in B-South has established a GOC at 2915 meters and an OWC at 3014 meters depth in the Tarbert Formation (Figure 69). By analyzing the pressure plot, it is apparent that there is established cross-stratigraphic fluid communication. There are some outliers along the water leg in the Ness Formation, which might indicate the presence of isolated over-pressured channel sands.

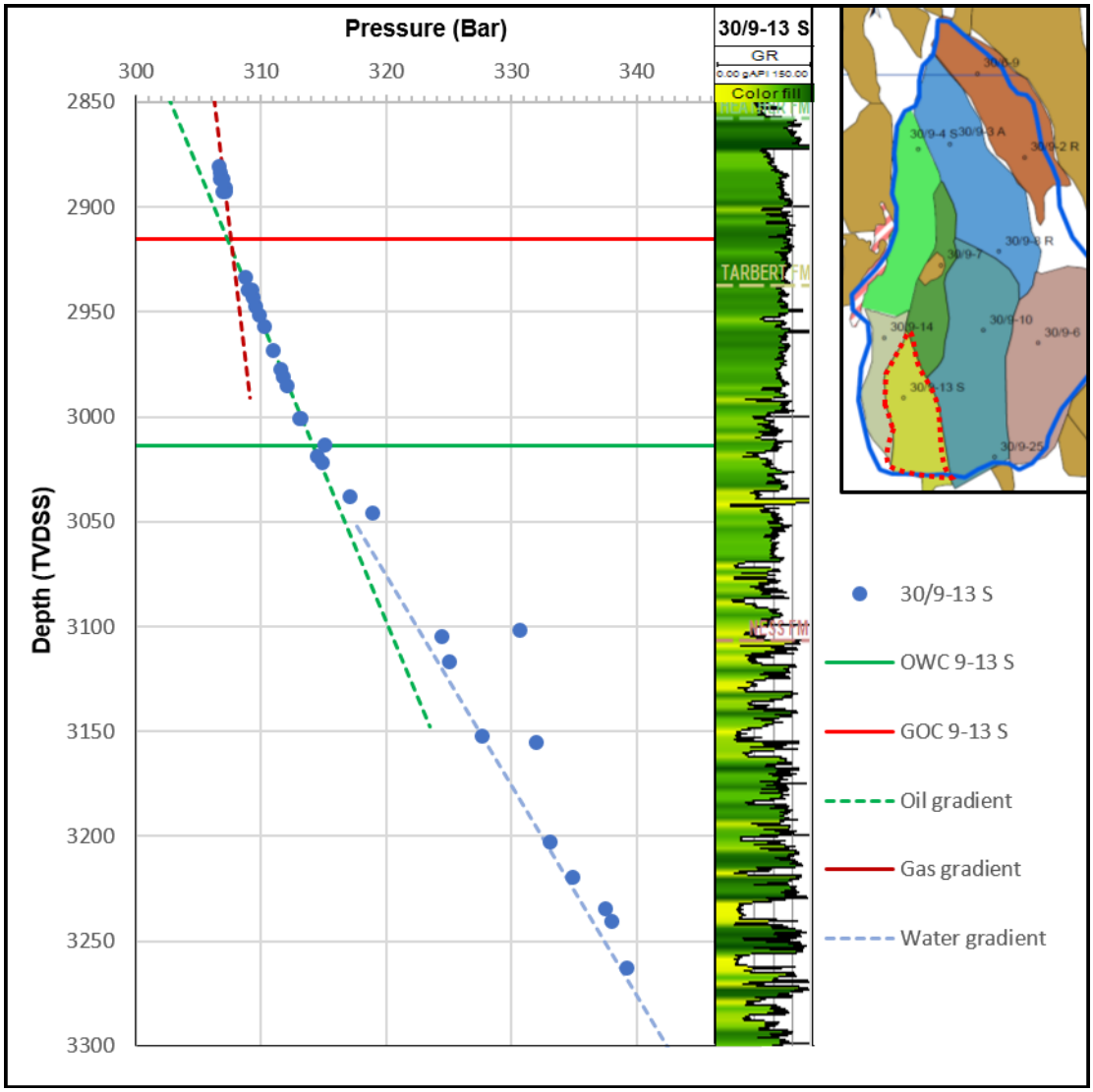

Figure 69: Formation pressure plots of 30/9-13 S in G-East displaying fluid contacts and gradients.

5.8 Fault Seal Analysis

5.8.1 Cross-fault Pressure analysis

The pressure differences and varying fluid contacts across the different faults is illustrated in the formation pressure plots in figures 70 – 76. When comparing the formation pressure plots across the Gamma and Omega structural segments, it is clear that the hanging wall and the footwall have different pressure regimes (Figure 70**).** Comparing across Fault 11 between Gamma and Omega structures, a substantial difference in the fluid contacts is observed. Additionally, the gas zone in the Omega structure displays an 8 bar pressure difference compared the Gamma structure, and a -4 bar pressure difference in the oil leg. These observations support the interpretation and hydrostatic isolation between the Gamma and Omega structures above the OWC, with fault seal as a possible interpretation.

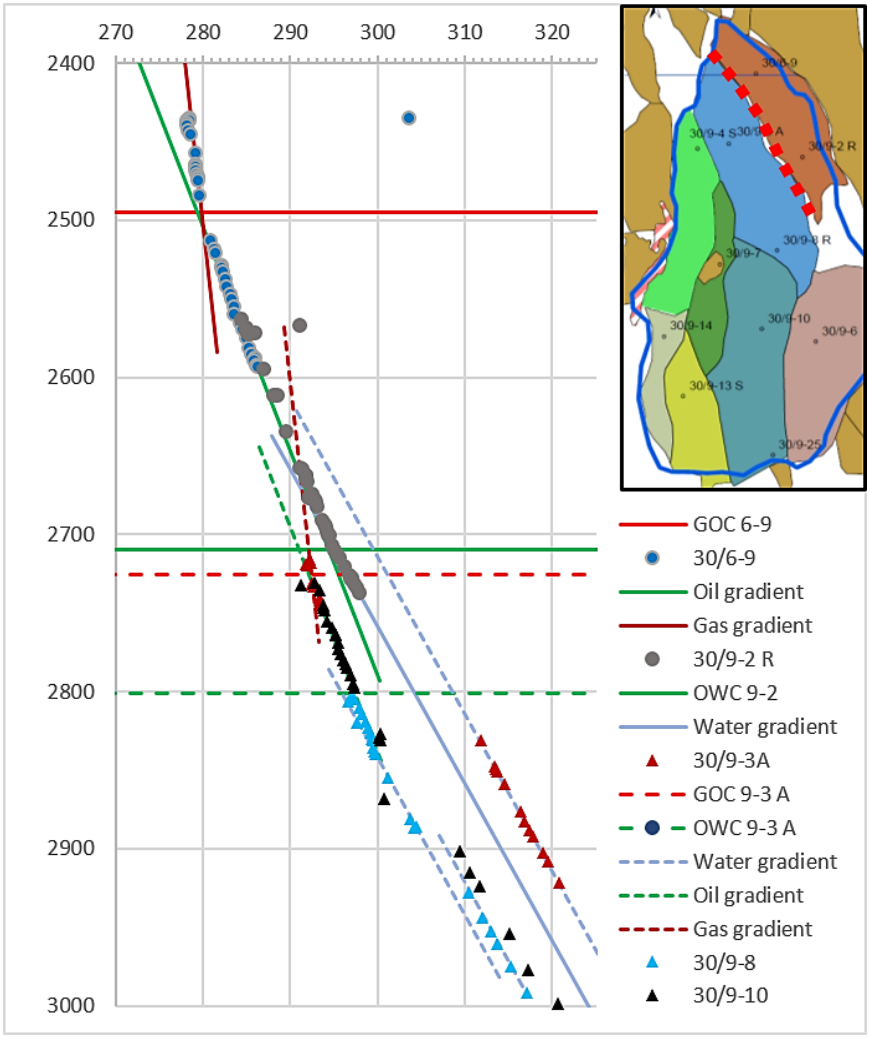

Figure 70: Chart displaying the formation pressure points for the Gamma and Omega structures (outlined in red) across fault 11. The hanging wall is represented by triangle pressure points and dashed fluid contacts and gradients. The footwall is represented by circle pressure points and solid fluid contacts and gradients

Similarly, when comparing the formation pressure plots between the Omega and B-North structures across fault 4 (Figure 71), differences in formation pressures can be observed. No direct fluid contacts were encountered in the B-North structure (well 30/9-4 S) and fluid contacts were based on upon analysis of the available pressure data. Based on the formation pressure plots of the gas and water zones of the B-North structure, it can be argued that a notional GOC should be located somewhere in the range of 2800 meters to 2850 meters. This means that a GOC contact would be 75 to 125 meters deeper in the B-North structure than in the Omega structure. This information along with a pressure difference of 4 bar in the gas zone indicate that fault 3 should be displaying sealing qualities between the Omega and B-North structures.

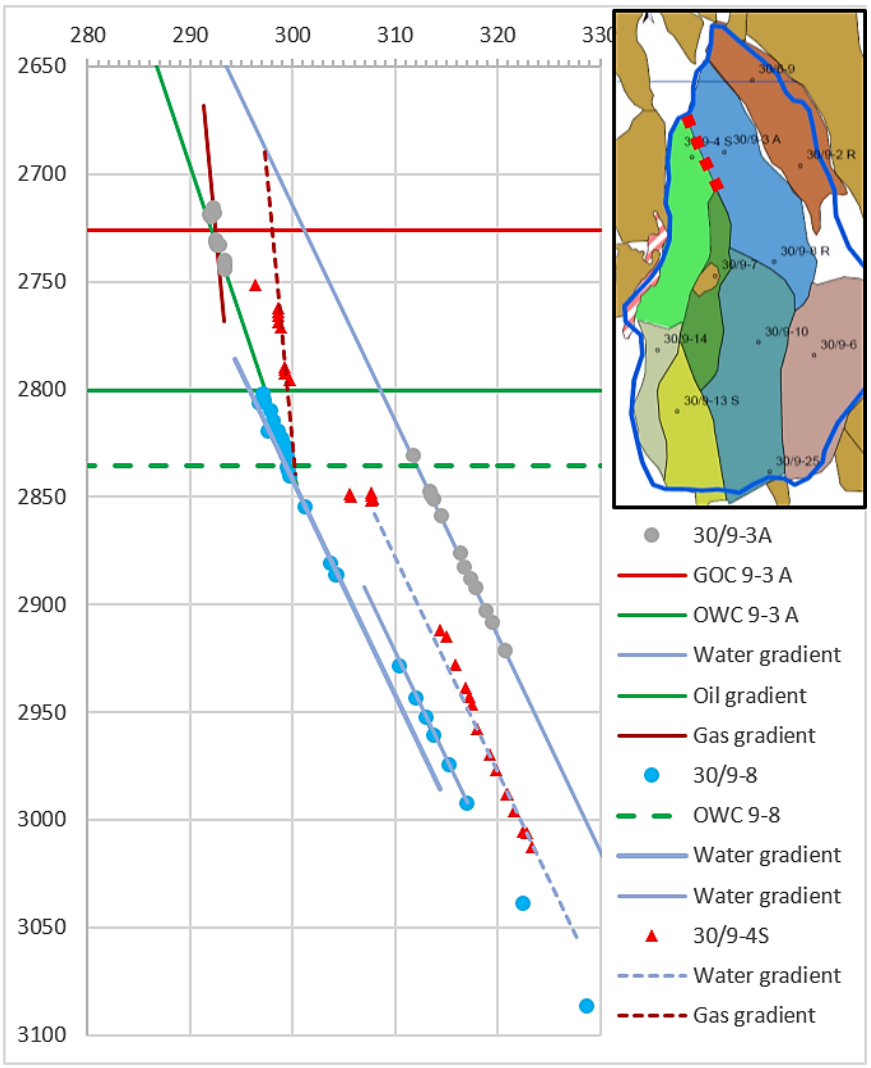

Figure 71: Chart displaying the formation pressure points for the Omega and B-North structures (outlined in red) across fault 4. The hanging wall is represented by triangle pressure points and dashed fluid contacts and gradients. The footwall is represented by circle pressure points and solid fluid contacts and gradients.

A comparison of the formation pressure plots and fluid contacts between the Omega and B-South structures segmented by fault 4 can be seen in Figure 72. Although no GOC was encountered in the B-South segment, formation pressure points from an established oil and water leg with OWC is available. The OWC in the B-South structure coincides with the established OWC in the Omega structure. The pressure difference in the oil zone is 1 bar, and the pressure difference in the water zone is also comparable to what is observable from the water zones in wells 30/9-8 and 30/9-10 in the Omega structure. This information indicate that fault 4 between Omega and B-South structures is not hydraulically isolating the structures.

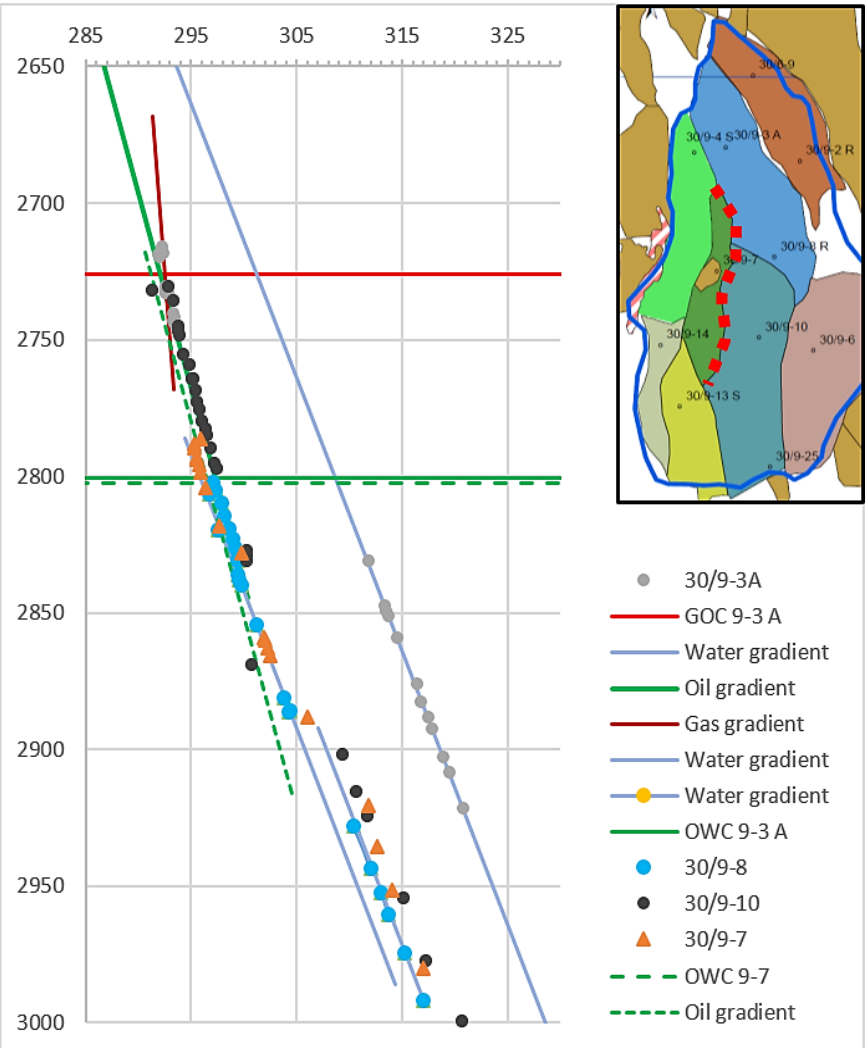

Figure 72: Chart displaying the formation pressure points for the Omega and B-South structures (outlined in red) across fault 4. The hanging wall is represented by triangle pressure points and dashed fluid contacts and gradients. The footwall is represented by circle pressure points and solid fluid contacts and gradients.

The formation pressure plots between B-North and B-South (Figure 73), show that the B-North gas interval is at the same depth and therefore overlapping with the B-South oil interval. Based on this observation, an interpretation can be made that the two structures are hydraulically isolated. It is however important to note that there is suggested internal compartmentalization in the B-North structure from the formation pressure plot in 30/9-4 S, and the observed pressure difference could be a mix between fault-sealing and stratigraphic compartmentalization.

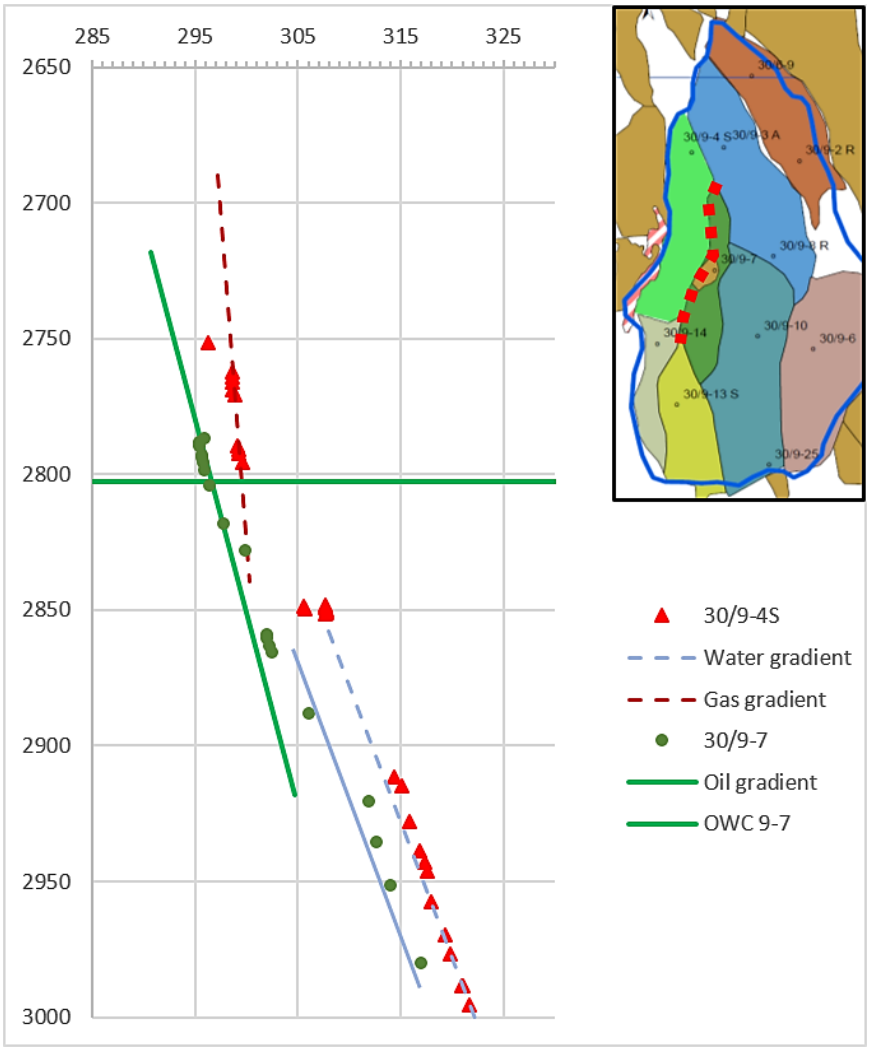

Figure 73: Chart displaying the formation pressure points for the B-North and B-South structures (outlined in red) across fault 3. The hanging wall is represented by triangle pressure points and dashed fluid contacts and gradients. The footwall is represented by circle pressure points and solid fluid contacts and gradients.

The formation pressure difference and fluid contacts across fault 1 between G-Central and G-East (Figure 74), show a significant difference in depth. The fluid contacts in the G-Central structure show a GOC 117 meters deeper than in the G-East structure, and an OWC 80 meters deeper than the G-East structure. The few pressure points in the gas zone of the G-Central structure signify a pressure difference between the two structures of 10-13 bars. The pressure difference in the oil zone is 4 bar, assuming the same fluid gradient as in G-East. The water leg between the two structures show pressure plots indicating fluid communication at water levels below the OWC in the G-Central structure.

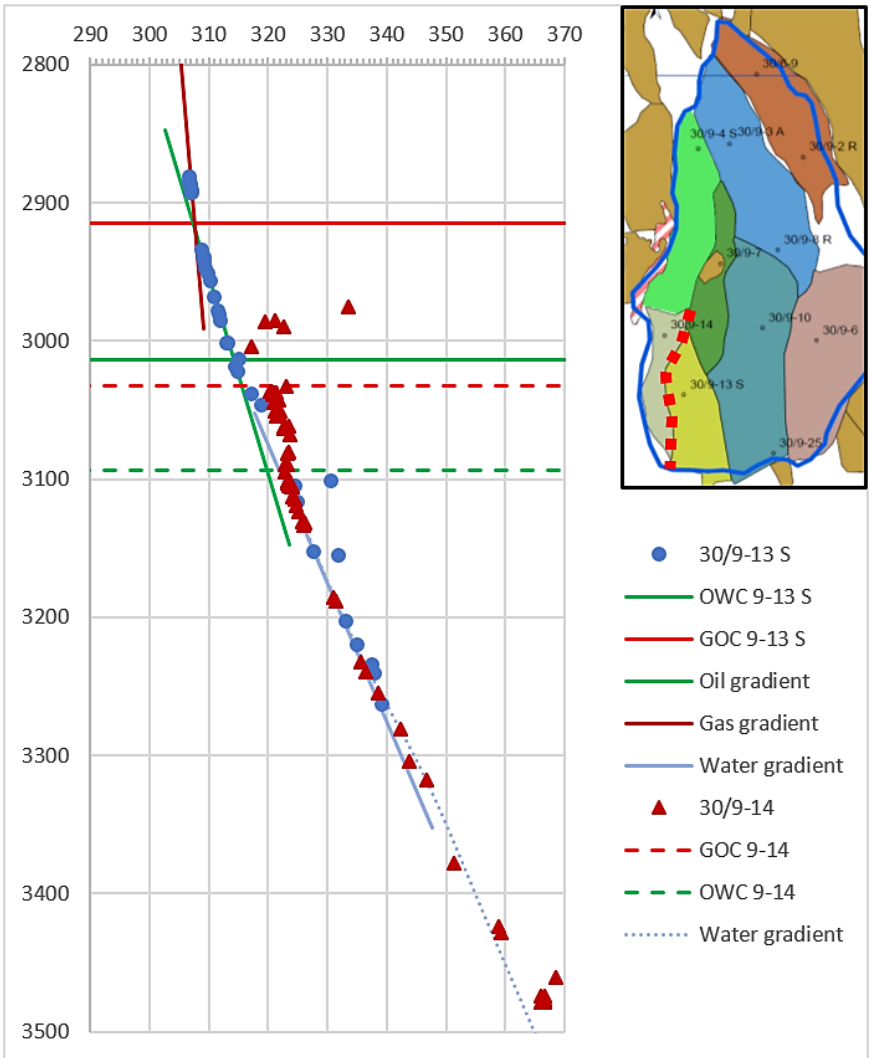

Figure 74: Chart displaying the formation pressure points for the G-Central and G-East structures (outlined in red) across fault 1. The hanging wall is represented by triangle pressure points and dashed fluid contacts and gradients. The footwall is represented by circle pressure points and solid fluid contacts and gradients.

The formation pressure data in the G-East and G-Central structures is compared with the formation pressure in the B-South structure across fault 3 (Figure 75). With differences in OWC of more than 200 meters and formation pressure differences in the oil zone of 3 bar and 9 bar in the water zone, everything indicates the presence of significant fault sealing between B-South and the G-structures.

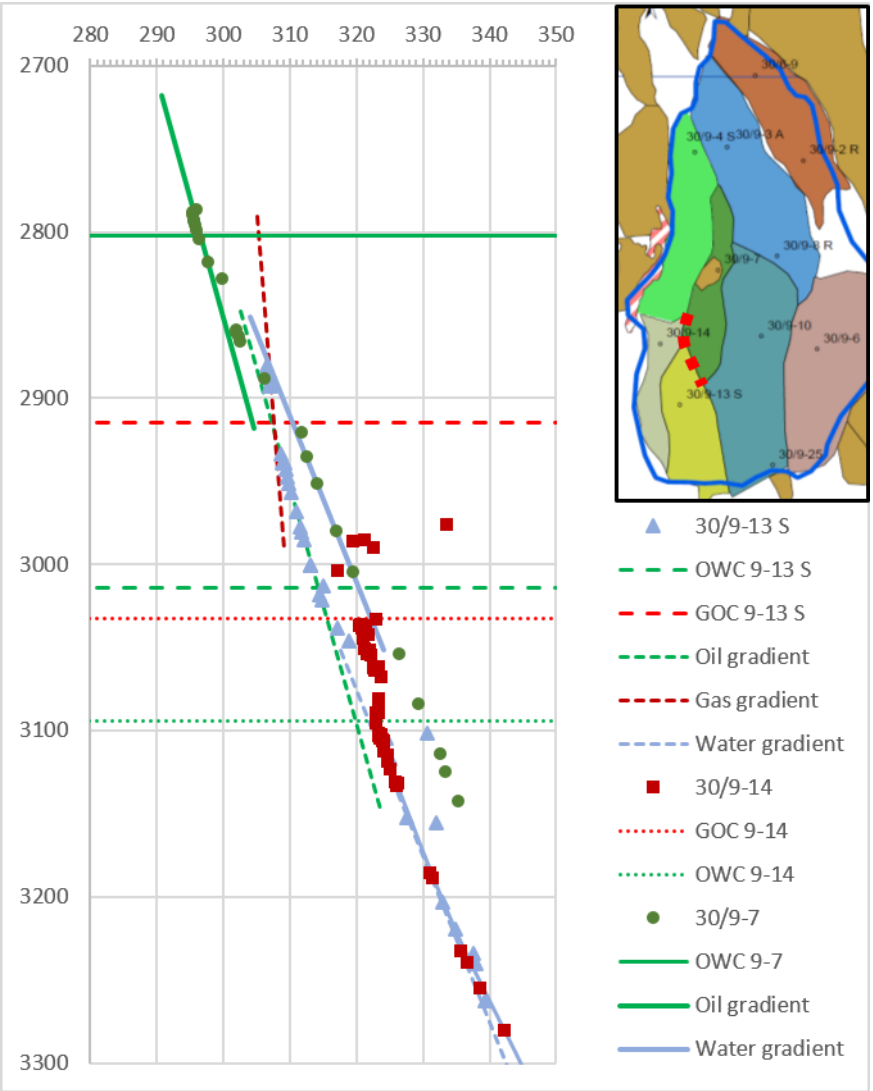

Figure 75: Chart displaying the formation pressure points for the G-Central, G-East and B-south structures (outlined in red) across faults 1 and 3. The hanging wall is represented by triangle pressure points and dashed fluid contacts and gradients. The footwall is represented by circle pressure points and solid fluid contacts and gradients

Comparing between the Omega and G-East structures across fault 3 (Figure 76), the OWC in the G-East structure is located 208 meters deeper than in the Omega structure, and the pressure difference in the oil zone is around 2 bar. For the water zone, the pressure difference is close to 10 bar. There are no indications of established fluid communication between the two structures, signifying that static fault seal is in place.

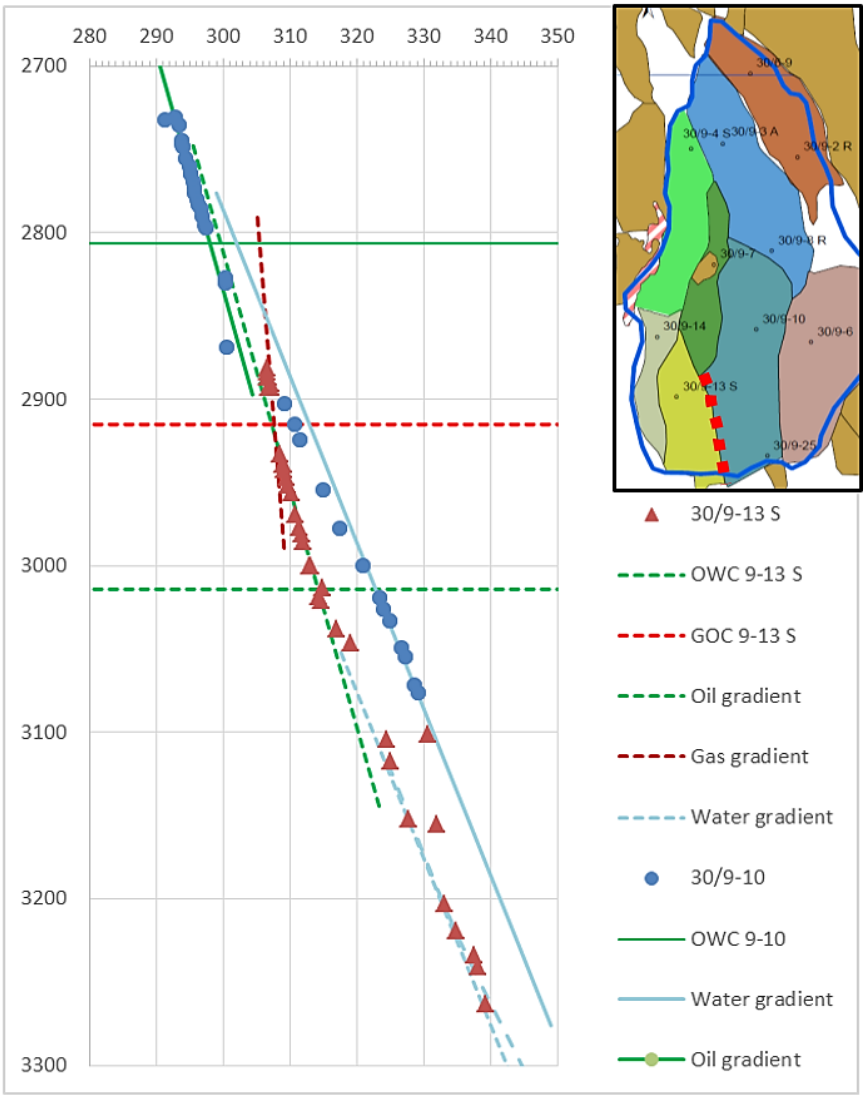

Figure 76: Chart displaying the formation pressure points for the G-East and Omega structures (outlined in red) across fault 3. The hanging wall is represented by triangle pressure points and dashed fluid contacts and gradients. The footwall is represented by circle pressure points and solid fluid contacts and gradients.

The complete list of fluid contacts gathered from the formation pressure plot analysis and corresponding formation for each well can be seen in Table 5.

Wells	Structure	GOC (depth)	Interval	OWC (depth)	Interval
30/6-9	Gamma	2495 m	Ness	N/A	N/A
30/9-2 R	Gamma	N/A	N/A	2709 m	Oseberg
30/9-3 A	Omega(N)	2726 m	Ness	2801 m	Ness
30/9-8	Omega(N)	N/A	N/A	2835 m	Tarbert
30/9-10	Omega(S)	N/A	N/A	2806 m	Tarbert
30/9-4 S	B-North	N/A	N/A	2825 m	Ness
30/9-7	B-South	N/A	N/A	2808 m	Tarbert
30/9-13S	G-East	2915 m	Heather	3014 m	Tarbert
30/9-14	G-Central	3032 m	Tarbert	3094 m	Tarbert

Table 5: Table displaying the known fluid contacts based on formation pressure plots and well reports.

5.8.2 SGR Calculations from STAR

By inputting the Vsh property model data into the STAR plugin, Petrel is able to calculate SGR over all of the fault planes covered by the property model (Figures 77 – 84). From analyzing the resulting SGR plots along with fault displacement and fluid contacts from the formation pressure survey, it is possible to determine critical spill-spots in the SGR defining fault seal chances.

The average SGR value for the entire fault plane of fault 11 is relatively high, with no apparent critical spill-points (Figure 77). The high SGR values may be attributed to the significant throw interpreted in this fault, and the juxtaposition of the Ness Formation in the footwall to the Drake Formation in the hanging wall. From the formation pressure analysis, there are significant differences in the fluid contacts and pressure (up to 12 bar in the water zone), displaying no indications of established fluid communication across Fault 11. SGR calculations for fault 4 between B-North and Omega structures display relatively high values across the entire fault plane (Figure 78). The high SGR values across the fault plane and differences in fluid contacts and formation pressure (4 bar in the gas zone and 5-6 bar in the water zone), is in consensus with the previous observations for fault 11.

When analyzing the results across fault 4 between the B-South and Omega structures (Figure 79), local zones with low SGR (20-30 %) can be found in the areas where the Ness Formation from the footwall and hanging wall overlap. The OWC can be found at the same depth in both fault blocks, and the pressure is at equilibrium in the water leg with only small pressure differences in the oil leg of around 1 bar. The information from the pressure plot points at existing fluid communication in the water-leg with limited fault sealing in the oil-leg. Comparing this information with the SGR plot, it is clear that the areas with low SGR values overlap with the intervals indicating cross-fault fluid communication. This is most prominent in the water leg and less so in the oil leg where the SGR is generally higher (30-50 %). It is however already determined that the OWC is at the same depth across both these fault blocks, indicating that only a small critical point with low SGR values would be able to accommodate for the cross-fault fluid communication. Such a critical point can be seen in the Northern region of this SGR plot in the oil zone, and could therefore potentially justify the lesser pressure difference and partial cross-fault fluid communication observed in the oil zone.

Fault 3 between structures B-North and B-South have an interpreted fault throw decreasing towards the North, and therefore present significant stratigraphic overlap. In the SGR plot for this fault (Figure 80), this minimal displacement leads to locally low SGR zones. This is especially visible in the lower Ness Formation, where overlapping modelled distributary channel deposits generate local SGR as low as 20 %. However, when analyzing the formation pressure plots it is apparent that there are a 3 bar pressure difference in the water zone between these two wells (30/9-4 S & 30/9-7) and no fluid communication in the oil zone. While the SGR plot indicates fluid-communication between the structural segments should be possible, based on the formation pressure plots this is not the case. Several theories can be made as for why this discrepancy between the model and measured data can be observed, and will be addressed in detail later in subsection 6.2.2 of the discussion chapter.

Fault 7 separating B-North and G-Central generally display high SGR values (Figure 81) with the formation pressure plots indicating no established cross-fault fluid communication. Similar observations can be made for fault 3 separating G-East from Omega and B-North. The SGR plot for these segments of fault 3 (Figure 82) display high SGR values, indicating the presence of fault sealing. This is supported by the formation pressure analysis, which shows substantial differences in the fluid contacts and pressures between G-East, Omega and B-North. The oil legs have a pressure difference of 2 bar while the water legs have a pressure difference of more than 10 bar. Continuing along fault 3 (Figure 83), the fault displacement between B-North and G-Central is greatly increasing. As a result, a high SGR, supported by the formation pressure survey that display large differences in fluid contacts and differential hydrostatic pressures indicate that static fault sealing is present between the segments.

The SGR plot of fault 1 between G-Central and G-East (Figure 84) is displaying zones where the SGR values drop to 25 %. The lowest values are located just below the OWC in the hanging wall with the pressure surveys indicating hydraulic communication in the water zone.

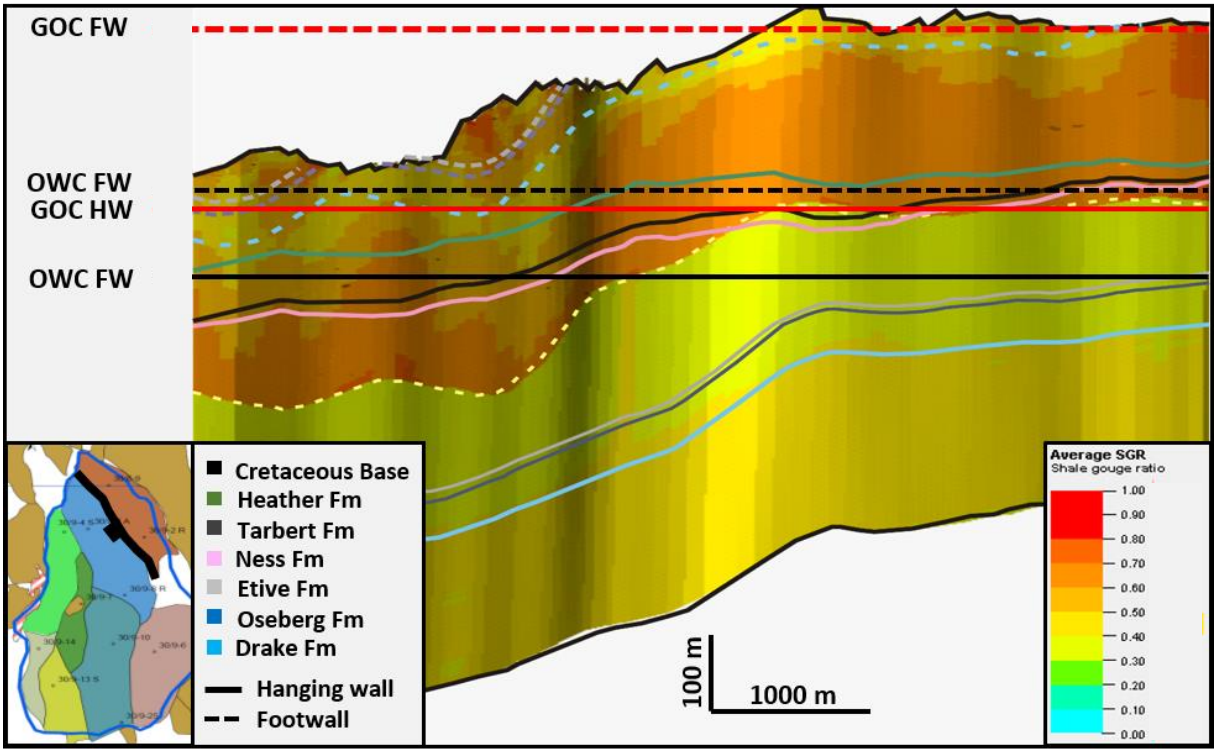

Figure 77: Fault profile window displaying Fault 11 and the calculated average SGR with Horizon lines from the footwall and the hanging wall of Gamma and Omega structures. The fluid contacts derived from the formation pressure plots and well reports are also presented for the footwall and hanging wall.

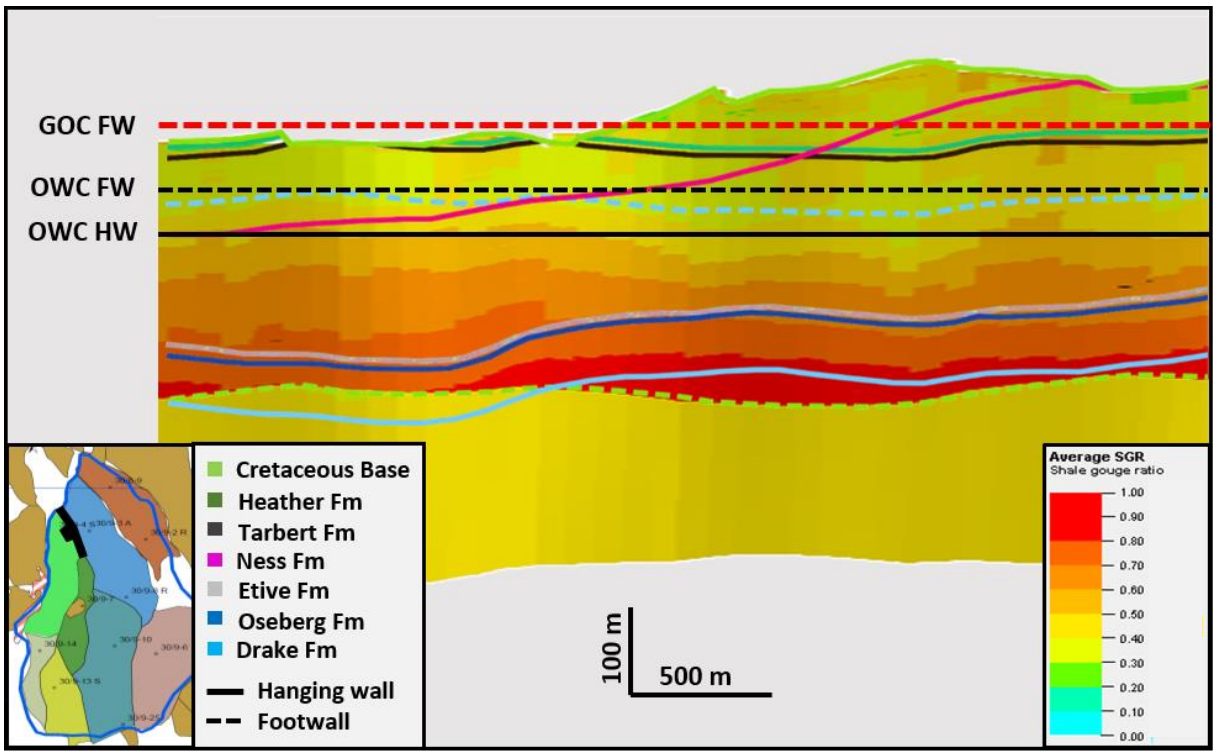

Figure 78: Fault profile window displaying Fault 4 and the calculated average SGR with Horizon lines from the footwall and the hanging wall of Omega and B-north structures. The fluid contacts derived from the formation pressure plots and well reports are also presented for the footwall and hanging wall.

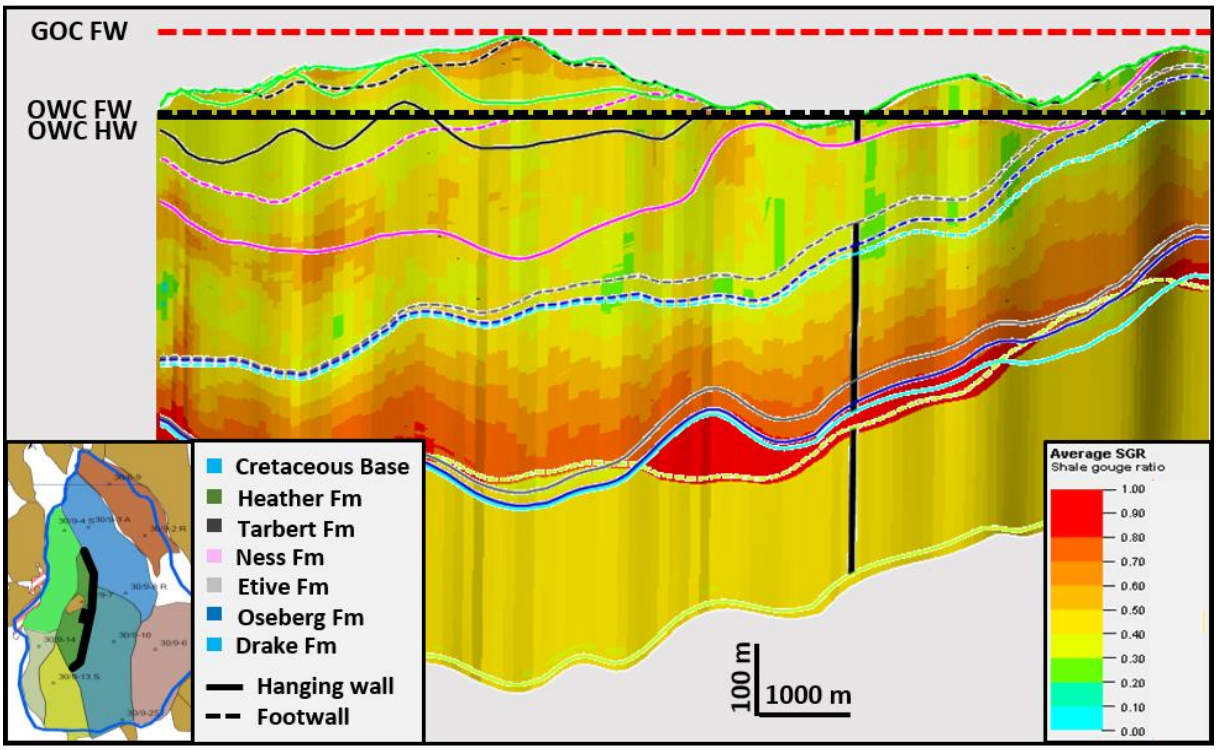

Figure 79: Fault profile window displaying Fault 4 and the calculated average SGR with Horizon lines from the footwall and the hanging wall of Omega and B-north structures. The fluid contacts derived from the formation pressure plots and well reports are also presented for the footwall and hanging wall.

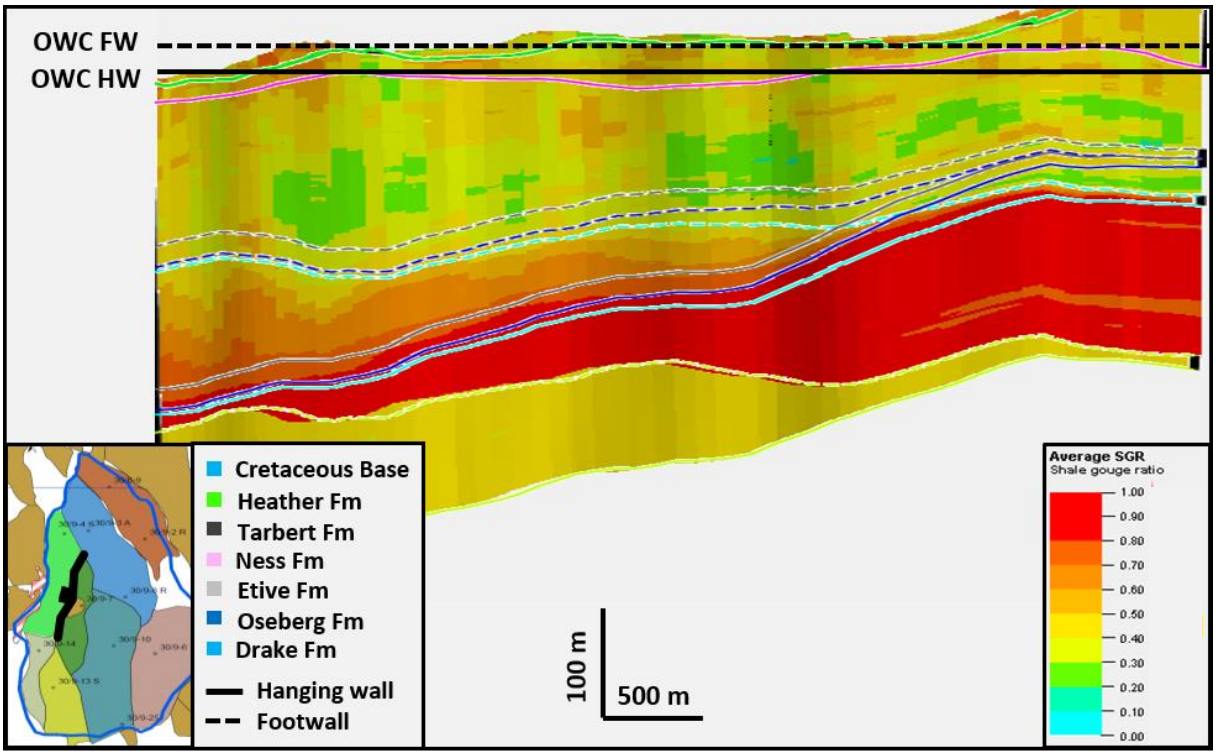

Figure 80: Fault profile window displaying Fault 3 and the calculated average SGR with Horizon lines from the footwall and the hanging wall of B-north and B-south structures. The fluid contacts derived from the formation pressure plots and well reports are also presented for the footwall and hanging wall.

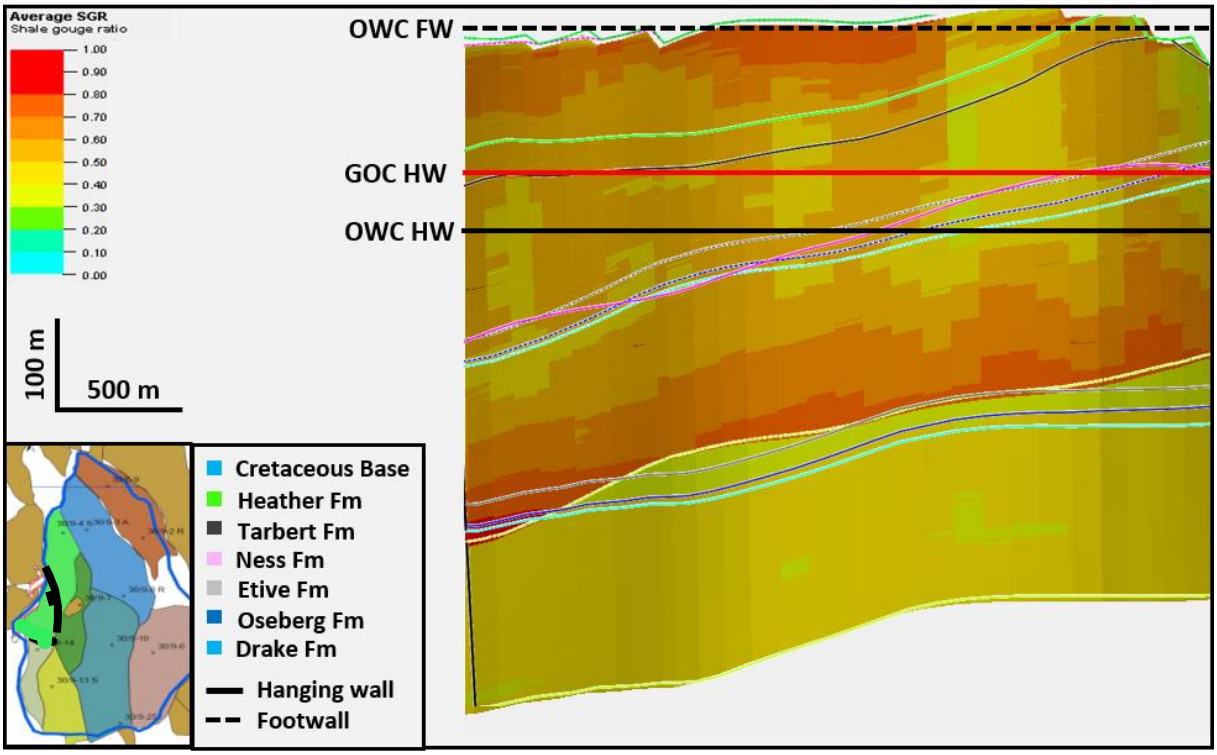

Figure 81: Fault profile window displaying Fault 7 and the calculated average SGR with Horizon lines from the footwall and the hanging wall of B-north and G-central structures. The fluid contacts derived from the formation pressure plots and well reports are also presented for the footwall and hanging wall.

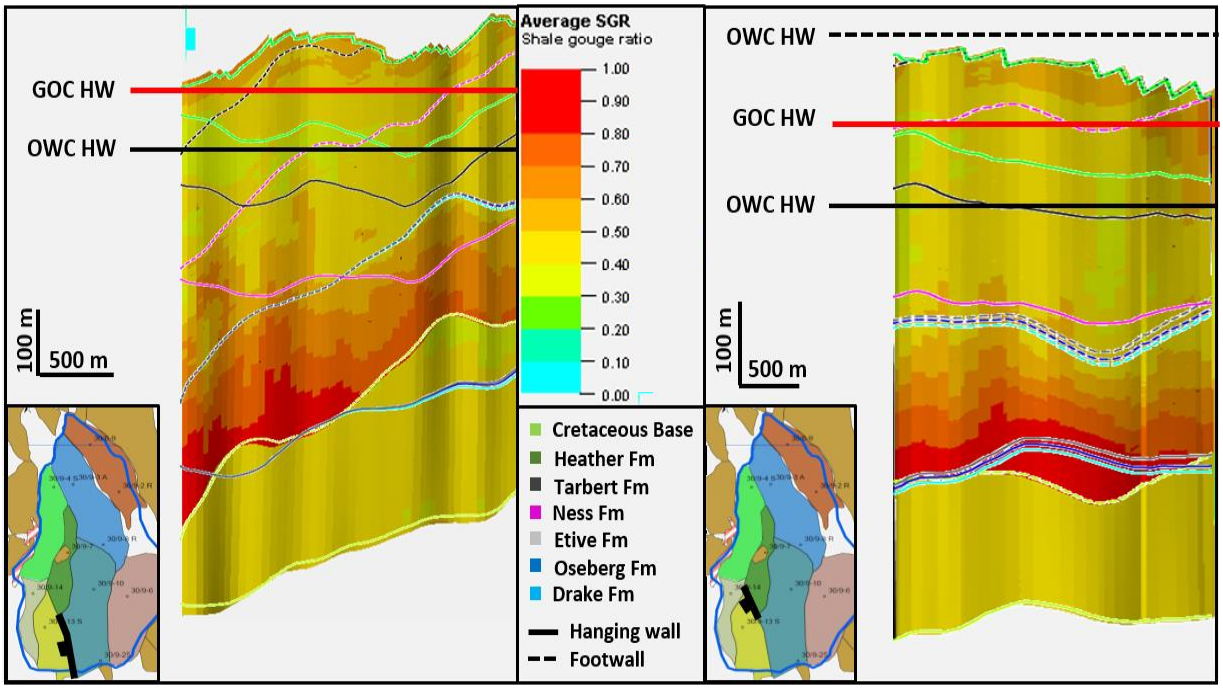

Figure 82: Fault profile window displaying two sections of Fault 3 and the calculated average SGR with Horizon lines from the footwall and the hanging wall of Omega and G-east structures. The fluid contacts derived from the formation pressure plots and well reports are also presented for the footwall and hanging wall.

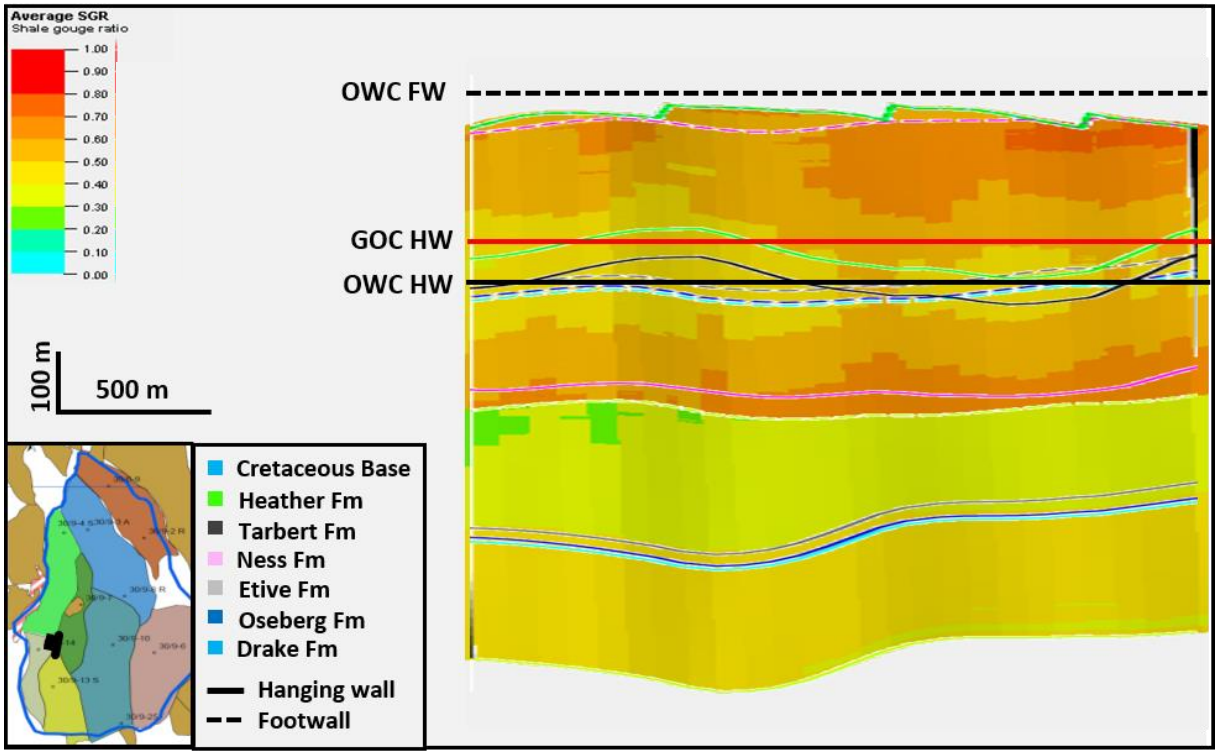

Figure 83: Fault profile window displaying Fault 3 and the calculated average SGR with Horizon lines from the footwall and the hanging wall of B-south and G-central structures. The fluid contacts derived from the formation pressure plots and well reports are also presented for the footwall and hanging wall.

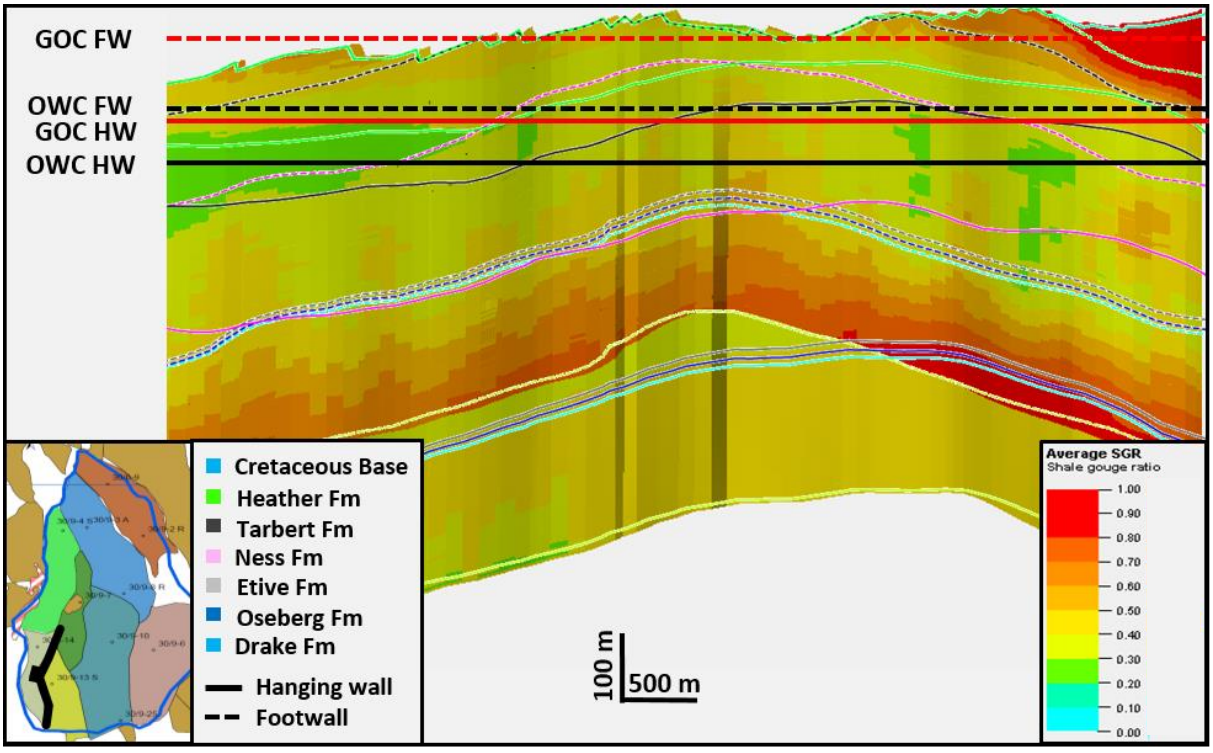

Figure 84: Fault profile window displaying Fault 1 and the calculated average SGR with Horizon lines from the footwall and the hanging wall of G-east and G-central structures. The fluid contacts derived from the formation pressure plots and well reports are also presented for the footwall and hanging wall.

5.8.3 Column Height Predictions & Volumetric

The end product of the STAR plugin is a P(10), P(50), and P(90) case of the total hydrocarbon column height for the Brent Group in each structural segment. The column height is ultimately controlled by elements such as fault seal and structural spill based on the structural interpretation and property model used as input to the STAR plugin.

By comparing the results from STAR with the known column height based on the fluid contacts gathered from the formation pressure surveys and well reports, it is possible to determine the applicability of STAR in this evaluation to the Brent Group. To assess the column heights throughout the model, the differences between the P(10) case scenario from STAR and the observations from well data were documented in all the defined structural segments (figures 85 – 88). The P(10) case was used for comparison as this provided most similar values to what is seen in the actual field observations. Column heights are calculated from the crest of the reservoir structure to the OWC and volumetrics are done by calculating the total capacity in the Brent Group from the top of the Tarbert Formation to the top of the Drake Formation and OWC.

In the Gamma segment, it is possible to observe that the P(10) case from STAR is underestimating the true capacity of the Gamma structure. The actual column height in the Gamma segment is over 330 meters compared to the 118 meters suggested by STAR. This has a significant impact on the total volume, where STAR leads to an underestimation of 2235 x 10^6 m^3. Similar observations can be made for the Omega North segment, where the column height estimated from STAR is approximately one third of the real column height.

It is clear that the general observations made from Gamma and Omega North segments are similarly applicable to Omega South, G- Central and G-east. The STAR plugin consistently underestimate the column height and volumes in each of these structures. The outliers from this general trend are the B-North and B-South segments. STAR suggests that fluid communication should be present across fault 3 between the two fault blocks, leading to an underestimation of column height and volumes in the B-North segment and consequently an overestimation of the same attributes in the B-South segment. This can be tied back to the observed inconsistency between the model and the formation pressure plots between B-North and B-South.

A

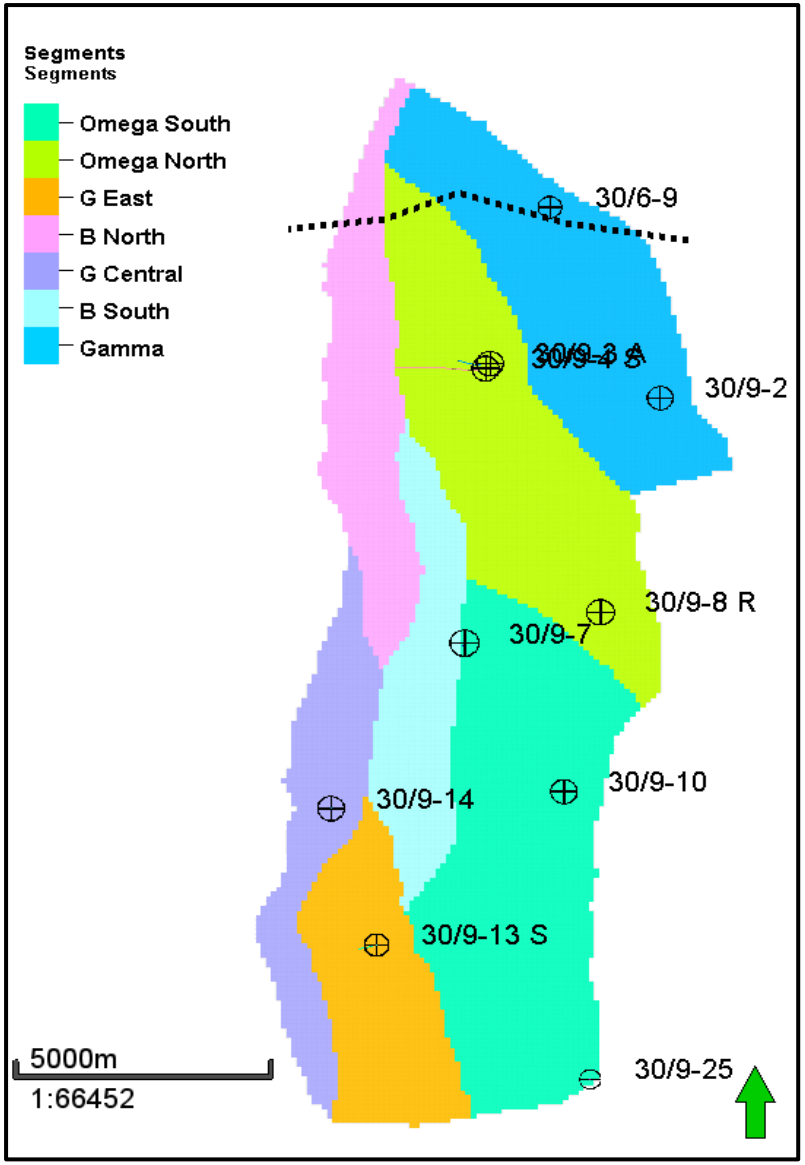

B

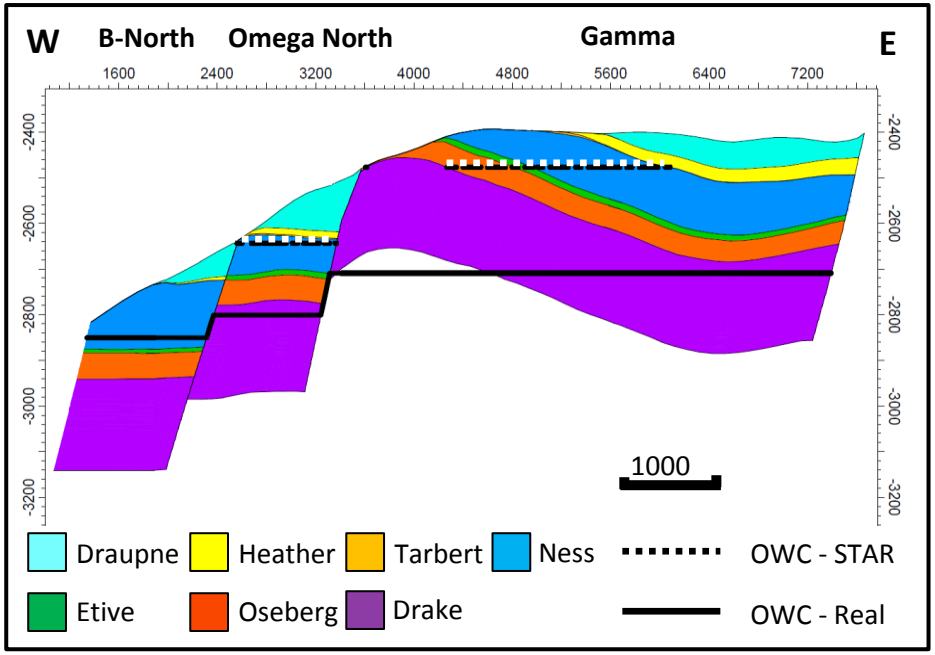

C

Total Column Height & Bulk-Volumetrics

Segment	Observed (Tarbert - OWC)		STAR based (Tarbert - OWC)		Difference (Real – STAR)	
	Height	10^6 m^3	Height	10^6 m^3	Height	10^6 m^3
Gamma	331 m	2706	118 m	471	213 m	2235
Omega N	188 m	962	62 m	13	126 m	949
B-North	129 m	581	18 m	37	121 m	544

Figure 85: A) Map view of the structural segment, wells locations and intersection line. B) Intersection line displaying the modelled zones and fluid contacts from the well data and STAR predicted fluid contacts. C) Table displaying the observed differences between STAR and the real fluid contacts.

A

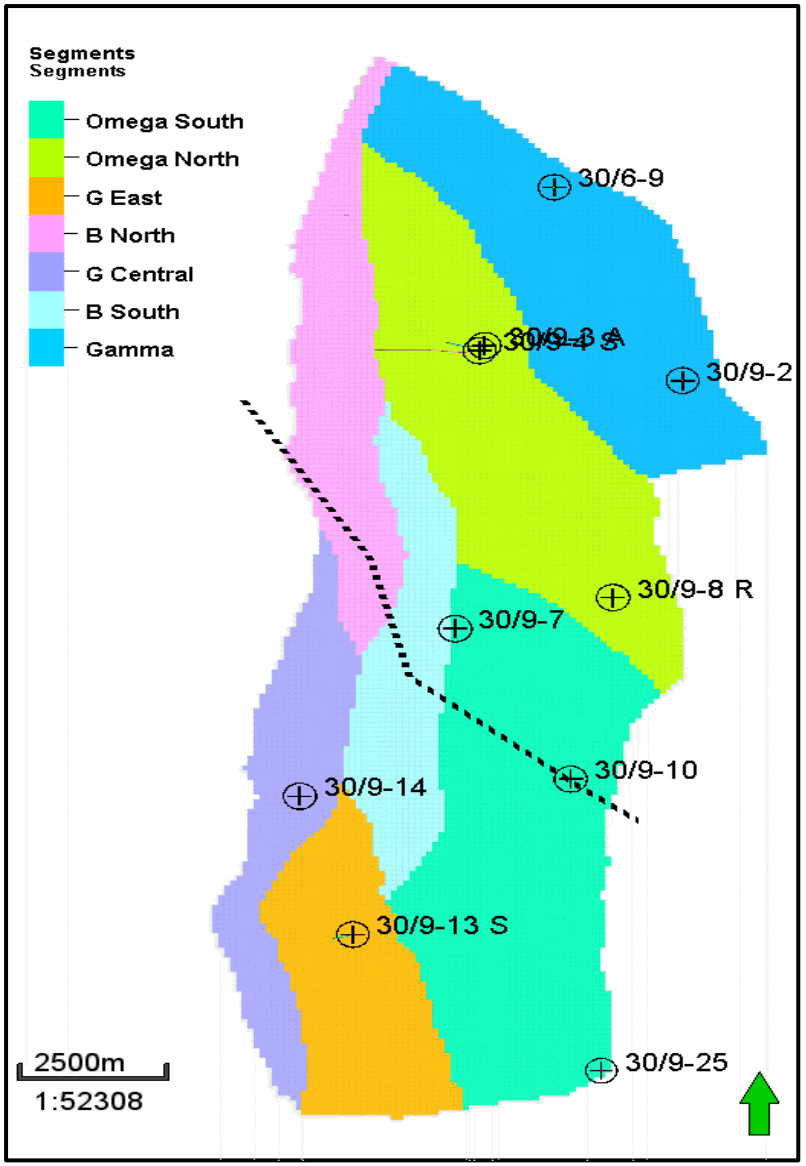

B

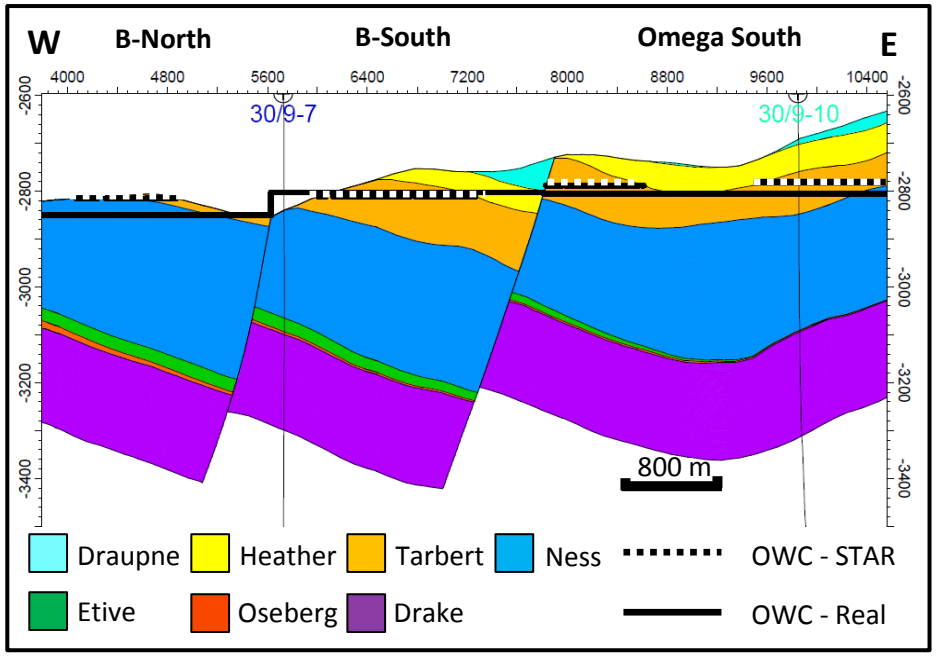

C

Total Column Height & Bulk-Volumetrics

Segment	Observed (Tarbert - OWC)		STAR based (Tarbert - OWC)		Difference (Real – STAR)	
	Height	10^6 m^3	Height	10^6 m^3	Height	10^6 m^3
Omega South	192 m	619	60 m	448	132 m	171
B-South	43 m	79	53 m	136	-10 m	57
B-North	129 m	581	18 m	37	121 m	544

Figure 86: A) Map view of the structural segment, wells locations and intersection line. B) Intersection line displaying the modelled zones and fluid contacts from the well data and STAR predicted fluid contacts. C) Table displaying the observed differences between STAR and the real column height.

A

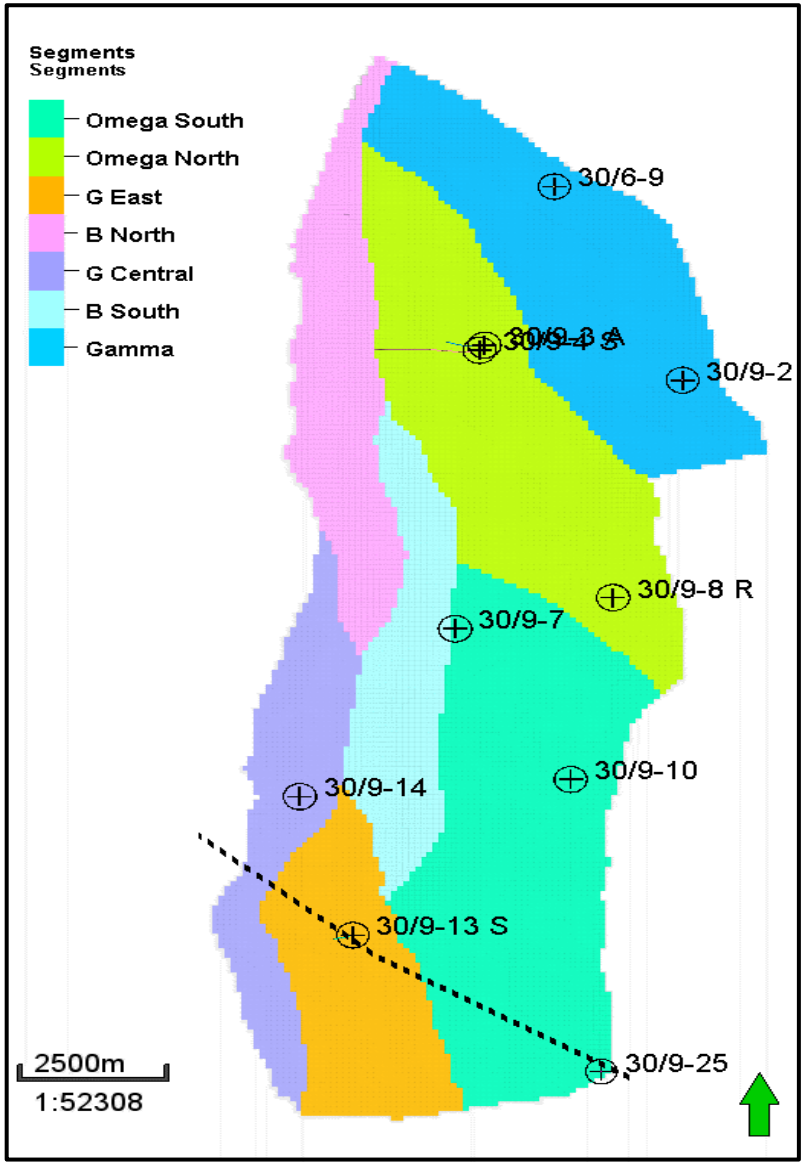

B

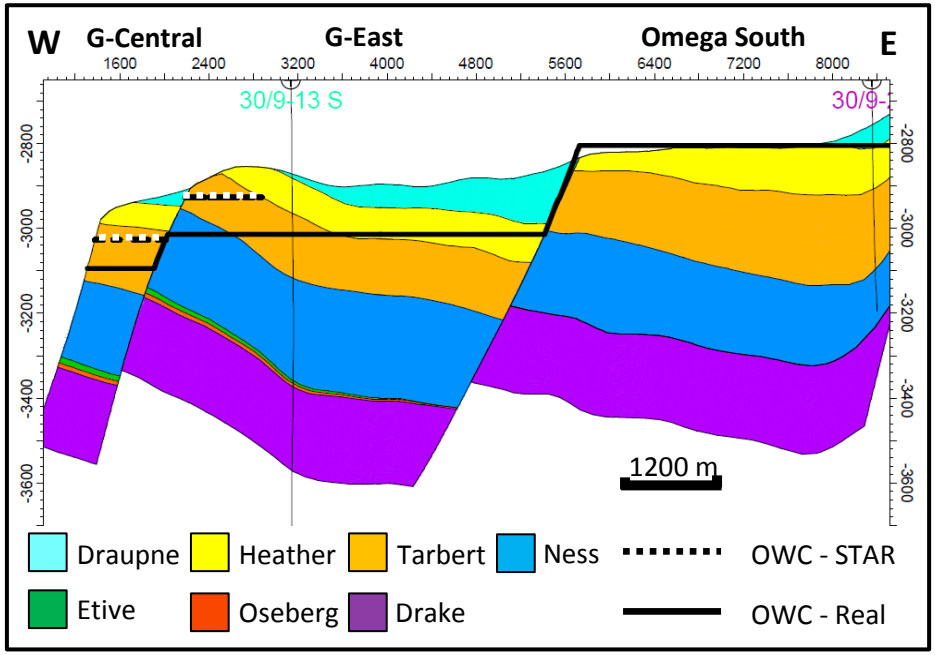

C

Total Column Height & Bulk-Volumetrics

Segment	Observed (Tarbert - OWC)		STAR based (Tarbert - OWC)		Difference (Real – STAR)	
	Height	10^6 m^3	Height	10^6 m^3	Height	10^6 m^3
G-Central	128 m	484	69 m	110	59 m	415
G-East	139 m	309	59 m	32	80 m	277
Omega South	192 m	619	60 m	448	132 m	171

Figure 87: A) Map view of the structural segment, wells locations and intersection line. B) Intersection line displaying the modelled zones and fluid contacts from the well data and STAR predicted fluid contacts. C) Table displaying the observed differences between STAR and the real column height.

6. Discussion

6.1 Quality of Interpretations and Property Models

6.1.1 Interpretation of Horizons

The seismic interpretation can be verified by a number of wells with lithostratigraphic control covering the different structural elements found in the Oseberg area. Although the interpretation of the Base Cretaceous Unconformity and Drake, Ness, Tarbert formations proved to be matching the established lithostratigraphic well tops, there is a degree of uncertainty tied to the interpretation of Draupne, Heather, Etive and Oseberg formations.

Most of the wells are drilled on the structural highs of the rotated fault blocks, where significant erosion has taken place meaning wells encounter a significant hiatus. The youngest formation encountered in this area below the BCU is the Kimmeridgian Draupne Formation. This formation is only encountered by wells in a fully or partially eroded state, and therefore difficult to trace to less eroded parts of the half graben structures where younger stratigraphy may be expected. Similarly, the underlying Heather Formation is also often encountered in a semi-eroded state at most well-locations. Oseberg and Etive formations display varying thickness in the Oseberg area and sub-seismic characteristics as intervals of limited stratigraphic thickness making them difficult to trace. To define these formations, the well tops and interpreted horizons of Ness and Drake were used to construct conformable horizons with estimated thickness variations. It is therefore a measure of uncertainty linked with the construction of Draupne, Heather, Oseberg, and Etive horizons, but based on the analysis of the interval thickness and distribution (see chapter 5.4), the results appears to correspond with the proposed depositional model.

6.1.2 Facies distribution and Property model

The facies distributions of the different intervals were based on a number of previous studies covering distributions, trends, lithological components and petrophysical properties of each interval in the Brent Group (see chapter 2.3.2).

Most of the interpreted intervals exhibit depositional systems that are relatively simple to model, with prograding (Etive, Oseberg) and back-stepping (Tarbert, Heather) shorefront systems and marine shale deposits (Drake, Draupne). For the heterogeneous delta plain of the Ness Formation, parameters such as channel width, sinuosity, orientation, curvature etc. have a significant impact on the modelled facies distribution. Small changes in either of these parameters will greatly impact the resulting facies model of the Ness Formation and consequently the distribution of petrophysical parameters such as Vsh. Due to time restrictions on this project, it was decided to model the interval with information from previous studies such as Mackey and Bridge (1995), Johannessen et al. (1995), Johnsen et al. (1995),R. Færseth and Ravnås (1998), Ryseth (2000), and Vrolijk (2005). The distribution of channel bodies is therefore a noteworthy uncertainty in this project, and important to keep in mind when assessing the observations, especially in areas with significant Brent juxtaposition.

6.2 Fault Seal Analysis with Comparison to Previous Work

6.2.1 Vsh Comparison

Fristad et al. (1997) used petrophysical analysis of the well data to define the shale fraction in each stratigraphic unit. The calculation of the SGR was done by CPI logs to derive Vsh and then compiled geographically to estimate likely Vsh compositions between the wells. Fristad et al. (1997) defines the intervals by sequential internal layering to capture the vertical heterogeneity found in the stratigraphy (Figure 88).

In this thesis, the constructed Vsh property model covers the vertical heterogeneity on a layer based scale, meaning that the modelled vertical variation and resolution in the up-scaled well data is directly transferred to the property model with the aim of maximizing vertical resolution of the model. The lateral distribution of the Vsh throughout the model has been defined by the application of a facies based property distribution. This means that the Vsh model captures the vertical variations in the well data and estimates lateral distribution based on the facies trends settings.

To compare the calculated Vsh from Fristad et al. (1997) with this thesis, a schematic illustration displaying the fractional shale-values used for each interval was compared to the sum average Vsh values for the corresponding intervals from this thesis. By calculating a mean value for each interval, the captured vertical variation and resolution is sacrificed. This mean average is therefore only used to provide a comparative analysis between the Vsh values used in this thesis and Fristad et al. (1997)'s paper.

Comparing the two shale fraction diagrams from the G-structures, it becomes clear that the Vsh calculated in this model have a higher overall average. The most significant difference can be seen in the Ness formation, which has a difference in Vsh of almost 30 %. Reasons for this could be the specific sand and shale values used for calculating Vsh. Fristad et al. (1997) does not cover the methodology used to calculate Vsh in detail, but it is safe to assume that it was done with slightly different parameters for sand and shale than what's used in this thesis. This notable difference makes a quantitative comparison impossible. As discussed earlier, the sands in these intervals often exhibit concentrations of micaceous trace elements, which impact the petrophysical logs by causing an overestimation of shale content. A similar problem can be observed in coal layers where coal often display a "sandy" response on the GR-log, although the effect of coal minerals in the fault-plane has similar fault-sealing

characteristics as shale (Løseth et al., 2009). It is therefore important to calculate and model the Vsh accordingly. Since the Ness Formation exhibits a number of coal beds throughout the interval, the existence of coal will have a decreasing effect on the average Vsh if not accounted for. Coal was therefore modelled with the same facies parameters as shale in the Vsh calculations and could therefore explain some of the increased average Vsh.

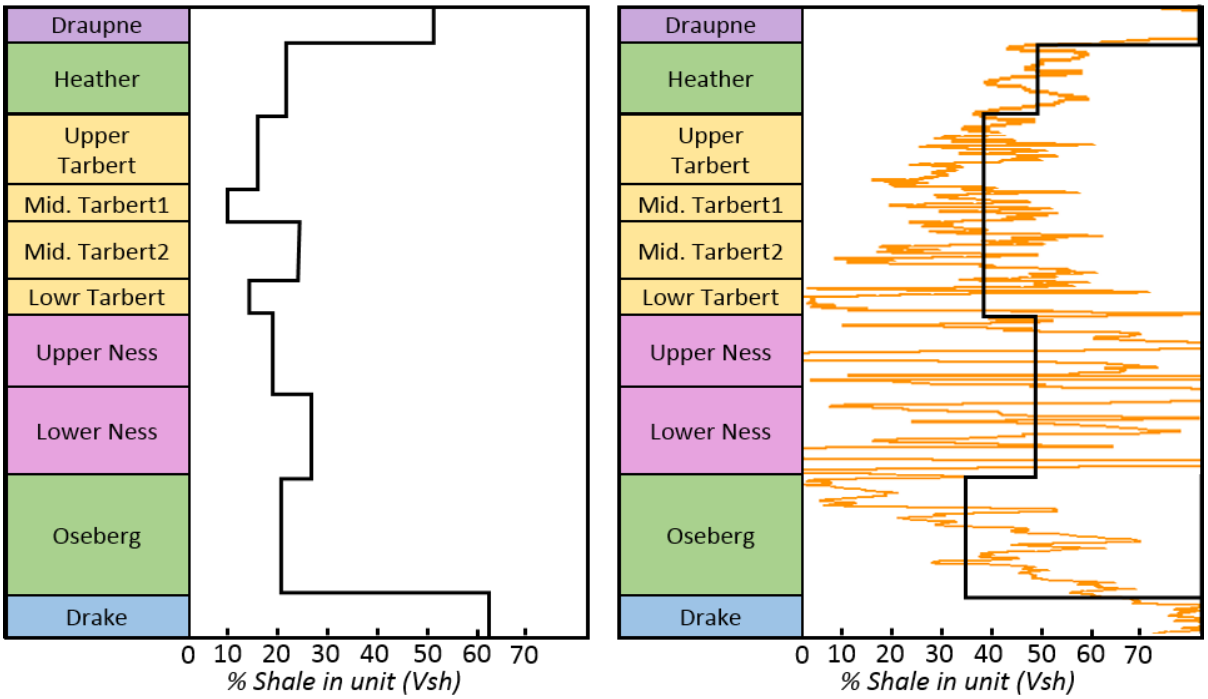

Figure 88: Schematic illustration of the shale-fractions for the G-structure, redrawn from Fristad et al. (1997) (left) and corresponding average shale-fraction from the constructed property model in the G-structure (right) with modelled variation.

6.2.2 SGR Calculations & Fluid Contacts

As discussed previously, Fristad et al. (1997) have proposed classification of specific SGR values that are based on the likelihood and strength of fault seal. The paper suggests that SGR values of above 18 % should display significant fault seal capacity, where the static fault-seal is able to support pressure differences of 8 bar and up. Faults displaying SGR values between 15 – 18 %, should only be able to support minor pressure differentials from 2 bars or less. Finally, zones with SGR values lower than 15 % indicate that the fault seal is incomplete and therefore have critical spill points in these zones permitting cross-fault fluid communication.

With this as a foundation, it is possible to compare the findings from STAR with what is established in previous studies. The fault spill point is defined by the topmost low SGR value along a fault. To exemplify this, the difference between the estimated OWC from STAR and the OWC observed in 30/9-14, along with the SGR plot for fault 1 separating G-East and G-Central can be seen in Figure 89**.** In this case, the OWC from STAR underestimates the true capacity of the G-Central structure by almost 70 meters. STAR has defined a fault-spill point and consequently a fluid contact close to a SGR value of 29 %, which according to Fristad et al. (1997) should be well above the low-end 18 % sealing limit. This observed difference further highlights how the SGR values between Fristad et al. (1997) and STAR cannot be quantitatively compared. The OWC observed in the well data overlap with a local SGR zone of 24 %, indicating that STAR might operate with slightly elevated critical SGR fault spill parameters. Similar observations were also made between Omega and B-South (see Figure 79). It is however rare that the modelled low-SGR zones align perfectly with the observed OWC from the well data like the case in fault 4, further emphasizing the impact the facies distribution can have on the SGR calculations.

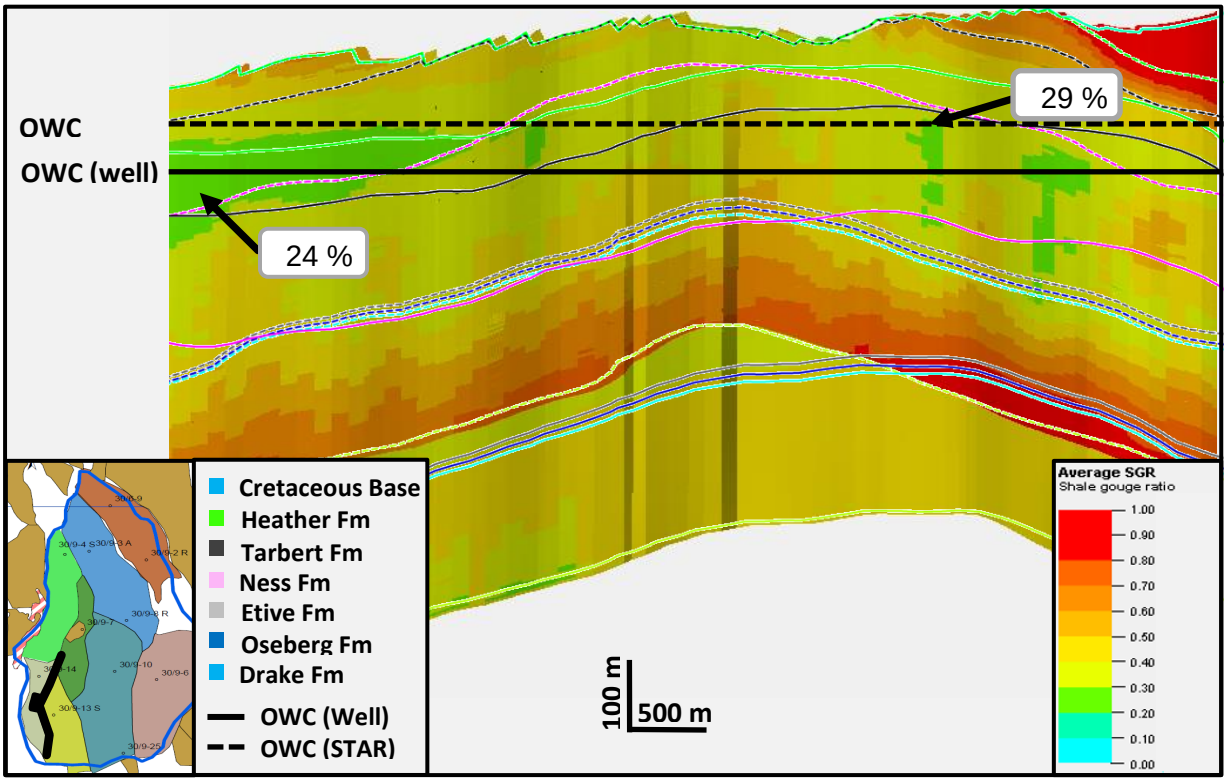

Figure 89: SGR plot for the fault 3 separating G-Central and G-East. Not the OWC estimated from STAR overlap with the 29% SGR zone in hanging wall and that the observed OWC from well data overlap with the 24% SGR in the hanging wall.

Comparing the SGR plots with facies distribution and fault displacement, it is evident that the lowest SGR values linked with cross-fault communication is usually found in the Ness Formation, where significant Brent overlap is present. Specifically, the critical fault seal zones can be assigned to areas where distributary channels in the Ness Formation overlap. This can be seen in the fault between B-North and B-South (see Figure 80), where the Brent overlap result in areas with SGR down to 20 %. This causes STAR to estimate that fluid communication is present across the fault trough the critical SGR zones. Even though STAR estimates fluid communication to be present, there has been observed no pressure communication between the wells in the oil or gas zone. A pressure difference of 4 bar in the water zone does however indicate that limited fluid communication could be present. Out of the nine SGR plots created, this is the only case where the SGR plot contradicts the well observations. It is therefore important to understand why this difference is present, due to the implications it has for the estimated column heights and consequently calculated volumes in the B-structures.

Since Brent overlap seemingly is causing low SGR values, the seismic interpretation was analyzed for any discrepancies. The seismic interpretation and the vertical displacement across fault 3 between B-North and B-south was evaluated as satisfactory with support from wells 30/9-7 and 30/-9 4 S. Since the seismic and well data indicate that the interpreted Brent juxtaposition is correct, the focus was shifted towards the distribution of channelized sand bodies in the Ness Formation. Overlapping distributary channel bodies in the footwall and hanging wall have been linked with the presence of low SGR zones. The modelled distribution of these distributary channel bodies could prove to have a significant impact on whether a fault is sealing or not. Combining the observations from the modelled facies distributions and the formation pressure surveys from wells 30/9-7 and 30/9-4 S, two theories were constructed to explain the discrepancies between the model and observed field data.

The first theory addresses the accuracy of the modelled distribution of channel bodies. By analyzing the modelled distribution of channel bodies in the boundary between B-South and B-North (Figure 90), it is apparent the distribution is unaffected by the fault boundary. This would be accurate in a pre-rift depositional setting, but as discussed in horizon and interval thickness analysis (chapter 5.4), the B-structure display significant thickness change in the Ness Formation compared to the other structures. Based on this, it can be argued that the Ness Formation should display syn-depositional characteristics in the B-structures. If Ness was deposited in a syn-rift setting, the channels would naturally accumulate in the lowest part of the fault block (Figure 91). While the formation thickness maps of the Ness Formation indicate lateral variations in subsidence rates across other segments as well, the variation is most prominent in the B-North and B-South blocks. This was also confirmed by Ryseth (2000), by mapping the formation thickness of the Ness Formation across the Oseberg – Brage area.

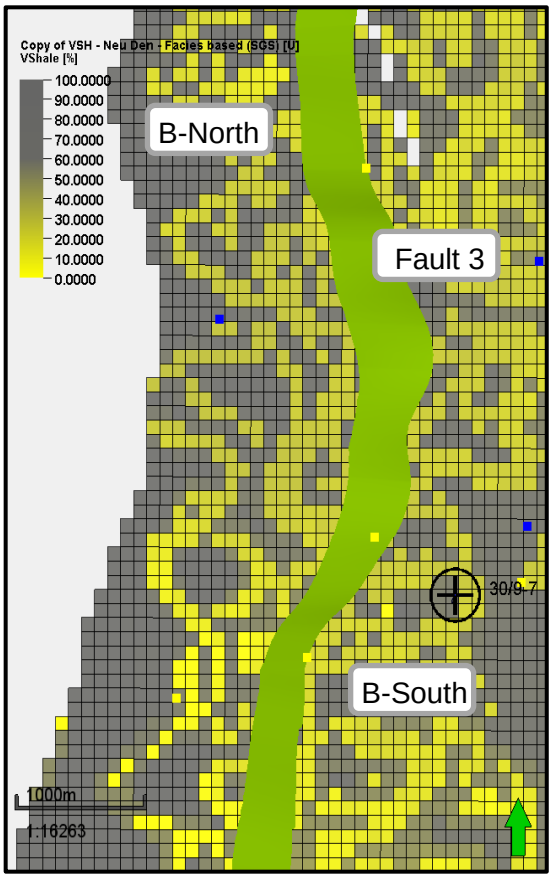

Figure 90: Close-up of the channel distribution in the Ness Formation over fault 3, between B-North and B-South.

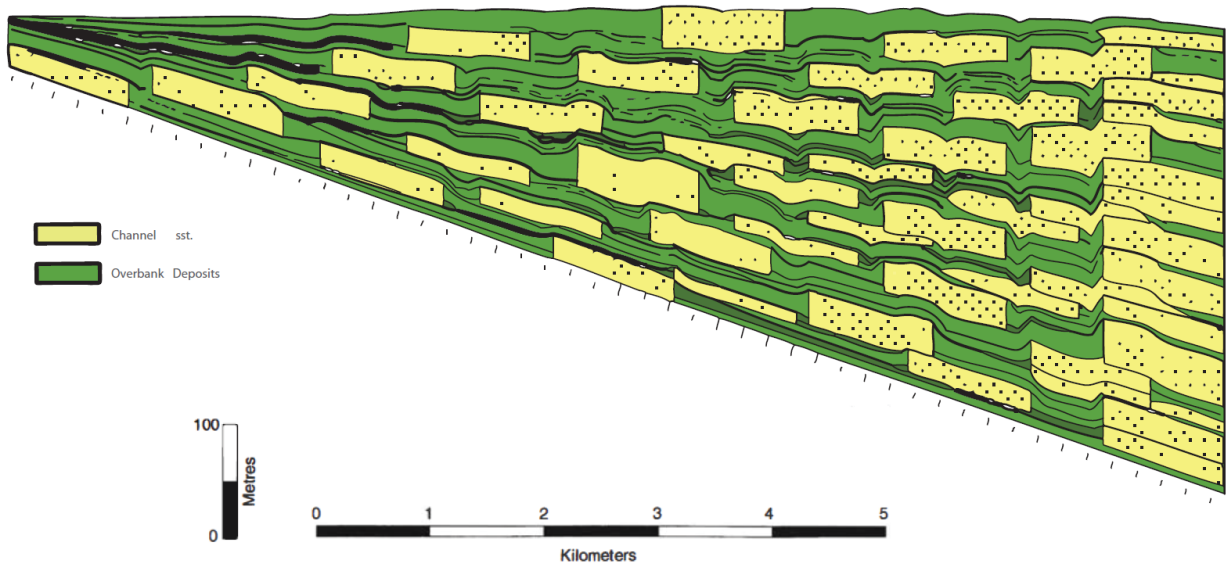

Figure 91: Theoretical model of alluvial architecture predicting higher frequency and greater thickness proportion of fluvial sandstones in areas of stronger subsidence. Modified from Ryseth (2000).

Mackey and Bridge (1995) have concluded that lateral variations in subsidence rates across an alluvial plain, may lead to preferential stacking of the channel sandstones in the areas undergoing maximum subsidence. Ryseth (2000) successfully linked this with the observations in the Oseberg area, supporting the observations made in this thesis. In addition to the influence that preferential stacking can have in a reservoir connectivity assessment, Vrolijk (2005) recognized the impact elements like 'breakover' spill relations and capillary leak has in channelized and fault compartmentalized reservoirs, proving that even simple reservoir geometries may lead to complex fluid contact relationships. With this in mind, it is safe to assume that a facies model not honoring the theorized syndepositional characteristics would produce an unrealistic distribution of the channel deposits of the Ness Formation and therefore present a significant uncertainty in the reservoir connectivity analysis. In the B-North and B-South case, applying a syndepositional trend to the modelled distribution of the channel sands would likely reduce the cross-fault channel overlap, and consequently increase SGR in the fault-plane.

The second theory questions whether or not well 30/9-4 S has drilled through isolated distributary channels isolated from an interconnected multistory successions such as in 30/9-7. As discussed earlier in the formation pressure analysis subchapter (5.7), the formation pressure survey from well 30/9-4 S (Figure 92) show that pressure data from the gas zone and water zone is from two separate pressure regimes.

This stratigraphic compartmentalization between the gas and water zone is important to keep in mind when extrapolating well information from well 30/9-4 S. The heterogeneous Ness Formation could also display lateral compartmentalization in the form of isolated channel bodies (Figure 93). Pressure data gathered from an isolated channel body would not be representative of interconnected channels in the rest of the formation. Utilizing pressure data from these isolated sand bodies to determine fault seal could therefore prove to be misleading. Combined with the fact that wells 30/9-4 S and 30/9-7 are located a considerable distance from are another along the fault plane (7 km), the applicability of the formation pressure survey from 30/9-4 S in the areas closer to 30/9-7 is questionable.

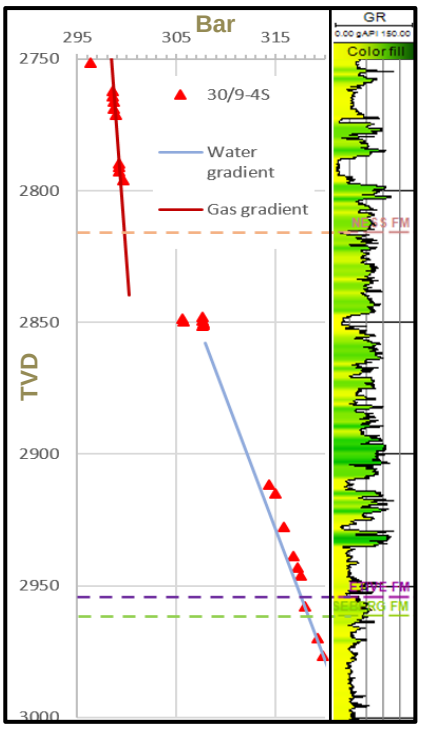

Figure 92: Formation pressure plots for 30/9-4 S with GR-log formation tops.

On the 25th of February 2016, well 30/9-28 S was drilled in the B-North structure, just west from 30/9-7 to test the reservoir quality of the Tarbert Formation. No fluid contact was encountered, but based on the pressure data, a GWC is calculated to be present at 2870 meters depth. This GWC is different than the estimated contact in 30/9-4 S by 20 – 70 meters, indicating that fluid communication is also limited restricted internally in the B-North structural segment. Unfortunately, the pressure data is not yet made public and can therefore not be used for formation pressure survey comparison.

While both these theories might explain the observations made between B-North and B-South, the reality it is most likely a combination of the two. Lateral variations in subsidence rates across the Ness Formation, may lead to preferential stacking of the channel sandstones in the areas undergoing maximum subsidence. This is further contributing to forming lateral and vertical compartmentalization that both restrict the fluid communication internally in structural segments and across fault planes.

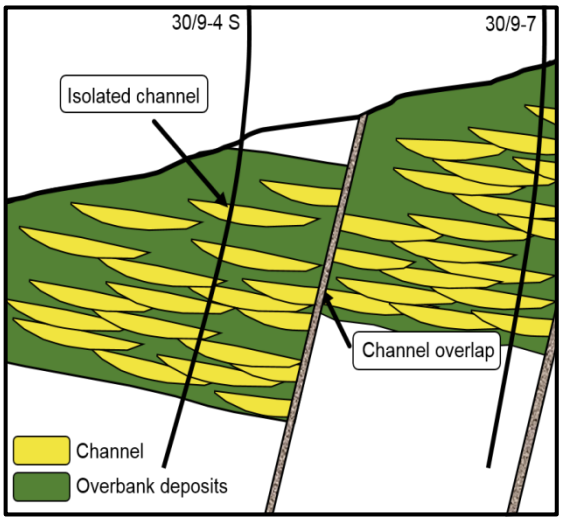

Figure 93: Conceptual model illustrating isolated and interconnected sand bodies in a Ness type environment.

6.3 STAR Troubleshooting

To understand why STAR is consistently underestimating the true column height retention potential, it is important to analyze the local spill points suggested by STAR in the different structural segments. STAR provides a data-point classification at the limiting cell, either as a structural spill or fault spill. By comparing this cell with the constructed model, it is possible to evaluate the STAR plugin.

In the Gamma structure, STAR estimates the column height to 118 meters, compared to the 331 meters from the well data. Since the gamma structure is dipping towards the south and retained by high SGR fault planes to the east, west, and to the north, there are no immediate candidates that should allow spilling at the depth of the OWC proposed from STAR. Upon closer inspection, it is however clear that STAR has estimated a fault spill point in a high SGR zone with SGR values up to 80 % (Figure 94.A). This is most likely caused by a mistake during the calculation process, and should therefore not be used to estimate the column height. Instead, it was attempted do define a new secondary spill point. Since the Alpha structure to the east of Gamma has not been modelled, no SGR plots have been made for the fault between them and the lack of interpretation in the Gamma South and C segments makes it difficult to accurately determine a new spill point.

Similar to the Gamma structure, the Omega structure have the estimated column height limited by what appears to be miscalculated spill points in high SGR zones (Figure 94.B). The Omega structure is bounded by faults on all sides, so by visually inspecting the SGR plots it is possible to determine the presence of secondary fault spill-points. From the SGR plot analysis (Chapter 5.8.2), it is evident that no such fault spill points can be located along the Omega Structure. However, a structural spill point has been determined to the South by STAR (Figure 94.C). By assigning a fluid contact down to this spill point, the resulting column height is only a couple of meters smaller than what has been observed in the well data. By adding this visual control, it was possible to determine a column height similar to what has been observed from the well data.

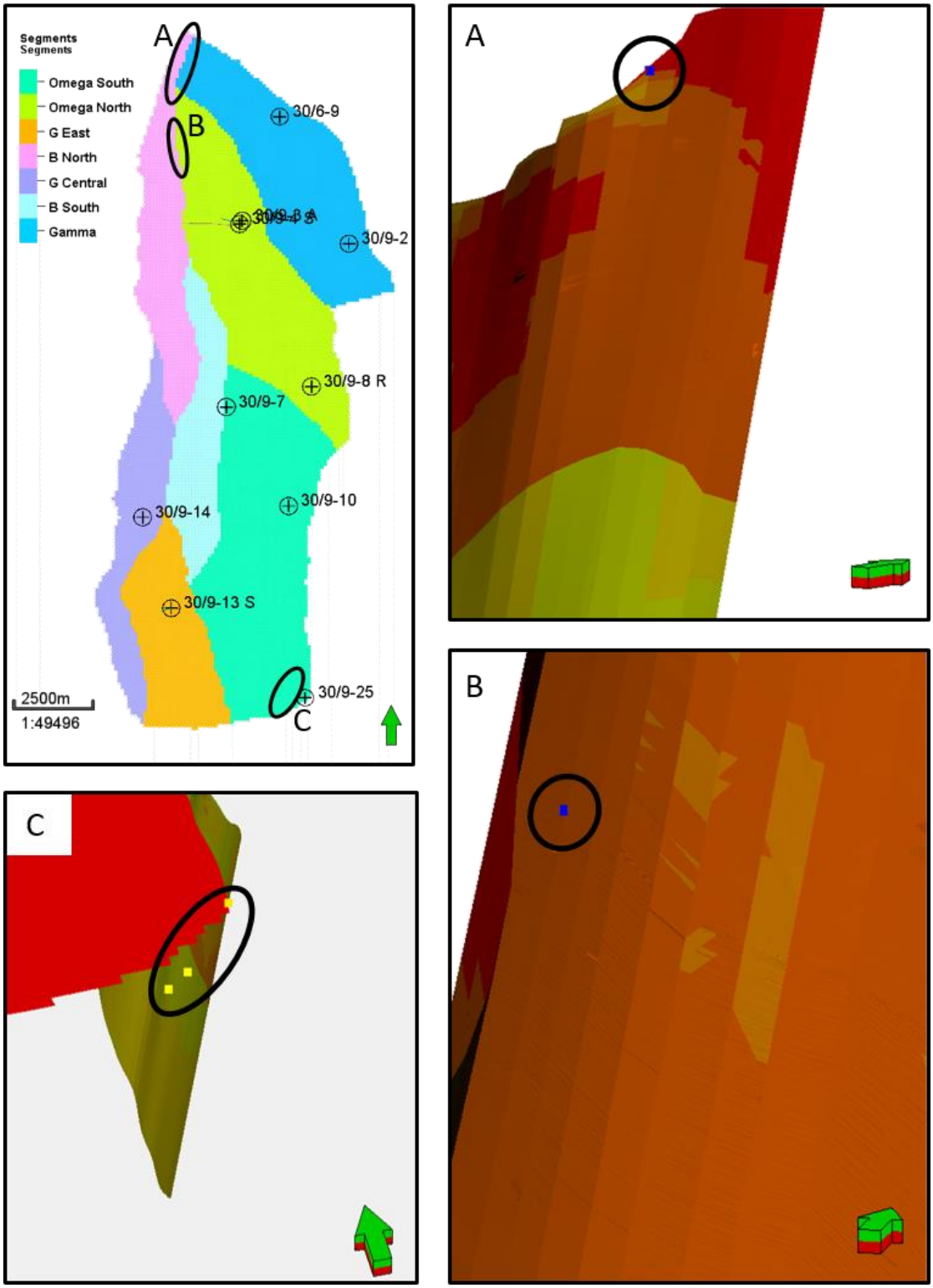

Figure 94: Figure displaying the interpreted structural elements of the Oseberg Area with problem areas in the SGR plots (A & B) and interpreted structural spill points from STAR (C).

6.4 Column Height Retention and Controlling Factors

Since the Upper Jurassic and Lower Cretaceous top seal is qualified as regionally present (Doligez et al., 1987), fluid contacts in the Oseberg field are interpreted to be limited to either fault or structural spill.

An example of both these elements being in effect can be seen in the relationship between the fluid contacts in the B-South and the Omega structures (Figure 95 and Figure 96). The B-South structure is limited to Fault 3 in the west and Fault 4 in the east. From the examination of SGR in fault 4 and formation pressure plots between the B-South and Omega South (Chapter 5), hydraulic communication has been identified between the two structures. The column height in B-South is effectively limited to a defined fault spill point, while the column height in Omega is limited to a structural spill point to the south. Similarly, this is also the case for G-Central and G-East, where the column height in G-Central is limited a fault spill window as in B-South, spilling into G-East which is limited to a southern structural spill point.

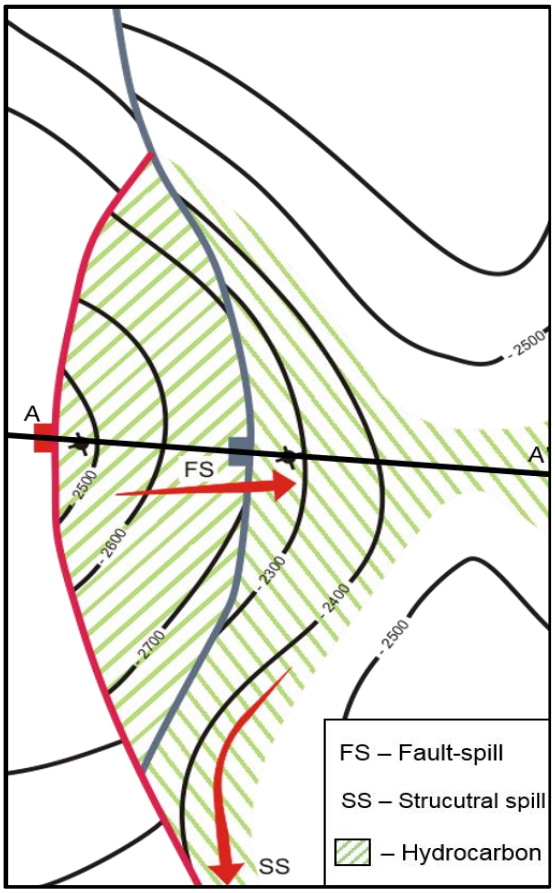

Figure 95: Conceptual sketch displaying the relationship between B-South and Omega-South. A similar relationship has been defined for G-Central and G-East. Cross-section A-A' can be seen in Figure 96.

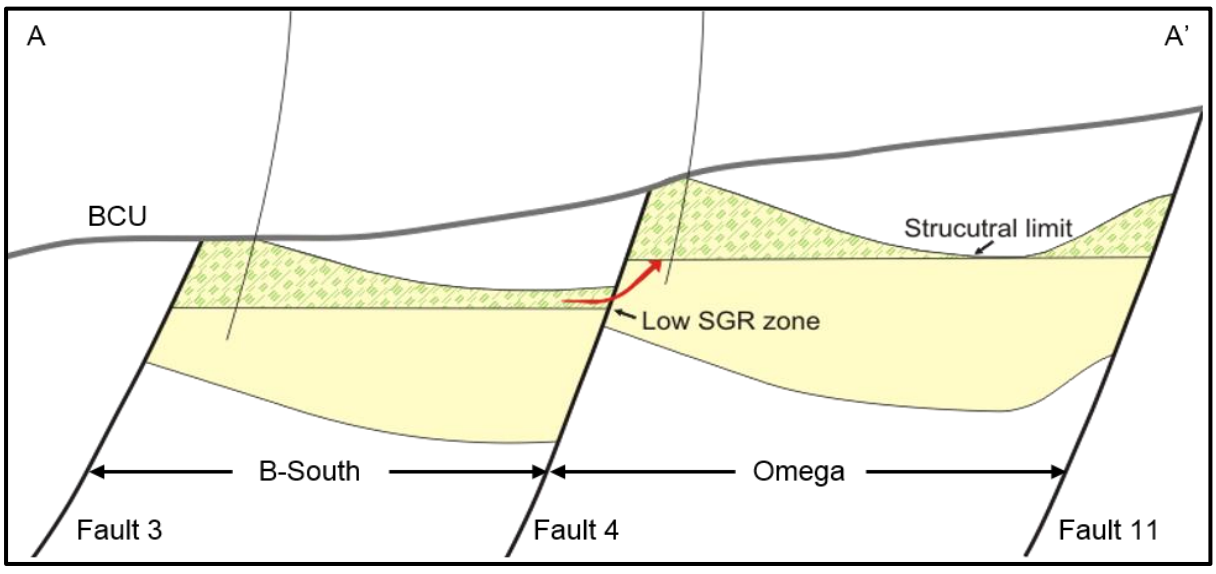

Figure 96: Conceptual cross-section from Figure 95, displaying cross-fault leakage from B-South to Omega-South. A similar relationship is has also been established in between G-Central and G-East.

By combining the results from this project with a conceptual regional structural model of the Troll-Brage-Oseberg area (Figure 97), it is possible to define the limiting factors for hydrocarbon column height in each of the structural segments.

As discussed, the maximum column height in G-Central appears to be controlled by a spill to G-East trough low SGR zones in the fault between the two structures. G-East is not displaying any spill-points in the encompassing faults, but is instead limited to a structural spill point just south of the structure. This structural spill-point is defined by a shared plateau between the G-Central, Omega South and J-structures (Figure 97), and is effectively limiting the column height of G-Central to the southern tip of fault 3. B-South's fluid contact similarly overlaps with critical SGR spots along fault 4 and has a pressure regime similar to Omega-South. Combined with the fact that this is a fault bounded structure, it is reasonable to assume that the fault spill point is limiting the total column retention observed in B-South

The limits of Omega and Gamma structures are difficult to define, as no data has been interpreted in the C or Gamma South structures in this thesis. This makes it difficult to positively determine SGR between these structures. It is however possible to assume that high SGR values exist in the faults defining the Gamma and Omega structures as well, based on the observations made from SGR plots over structures displaying similar throw distances (i.e. Gamma - Omega North, Omega – G-Central). By analyzing the available SGR plots and assuming the structural boundary as sealing, it was determined that the limiting factor is likely of a structural nature. This notion is supported by the fact that the observed fluid contact in the interpreted Omega structure appear close to the structural spill point defining the column height in the G-Central structure. Similarly, the observed column height of the Gamma structure overlaps with an interpreted structural spill point close to the segment boundary to Gamma South. This suggested structural spill point between Gamma and Gamma South agrees with the conceptual structural model defined by Johnsen et al. (1995), displaying a structural link between the Gamma, Gamma South and C-structures.

The SGR plot between B-North and Omega North display no critical low SGR zones that can be directly linked with fault spill. As no structural spill points have been determined in B-North, this shifts the focus towards the fault between B-North and B-South. Since the exact nature of the fluid communication between B-North and B-South is debatable, the exact nature of it what is truly controlling the column retention between these two structures is still uncertain.

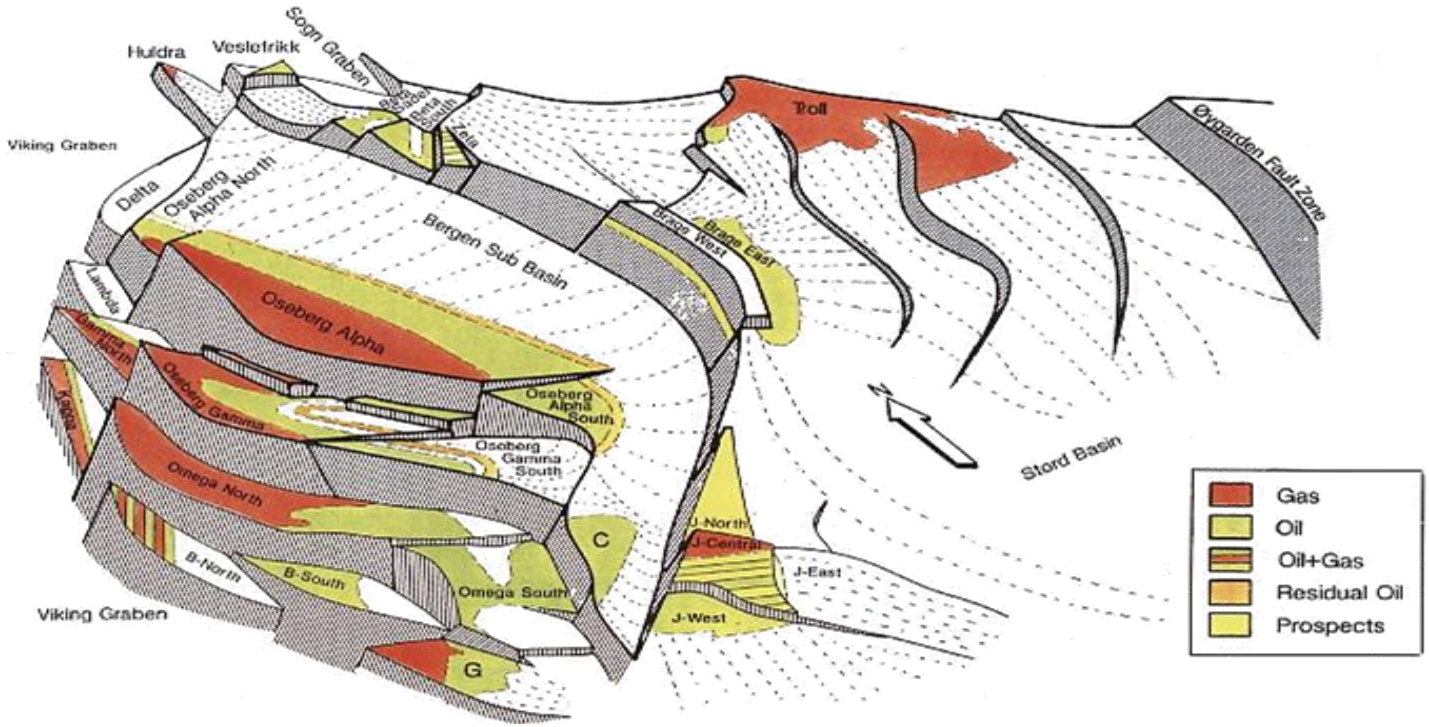

Figure 97: Structural model displaying the main fault blocks in the Oseberg-Brage-Troll area (Johnsen et al., 1995).

7. Conclusions

This thesis has served as a local calibrated case study of the application of STAR and column height prediction within the Brent Group of the North Sea. Consequently, this study demonstrates that further local calibration should be undertaken in order to avoid underestimation of possible column heights in Brent Group prospect when using STAR.

To summarize the results of this thesis, each of the main objectives has been addressed with the correspondent findings.

1) Identify and study fault-structures and key lithostratigraphic intervals in the Oseberg area.

This case study has defined the following fault-structures based on the data quality and previous studies in the area: Gamma, Omega North, Omega South, B-North, B-South, G-Central and G-East structures. Additionally, key stratigraphic horizons were defined based on predetermined lithostratigraphic and chronostratigraphic well markers along with previous studies about the development of the Brent Group in the Oseberg area. The following horizons were defined throughout the designated study area: The Base Cretaceous Unconformity and Drake, Oseberg, Etive, Ness, Tarbert, Heather, and Draupne Formations. The interpreted structures and lithostratigraphic intervals have been compared to compiled results from previous studies and deemed consistent to what has been previously observed in the Oseberg area. The internal trends and facies distributions of the different formations was based on and ultimately compared to well-documented and established conceptual facies models from a number of previous studies in the northern North Sea. Modelled intervals were evaluated to match well-data and previous studies with low associated uncertainty. The Ness Formation is however displaying vertical and lateral heterogeneity with complex channel distribution, meaning there is a significant uncertainty tied to any accumulations based on the facies distribution of this interval.

2) Investigate the fault seal capacity in the Oseberg structures with resulting retained hydrocarbon column heights.

Based on the findings in this thesis, certain SGR values can be directly linked to fault sealing potential in the Brent Group. Even though some faults are classified as not sealing, it is not necessarily the column defining factor, sometimes there is a structural spill point limiting the maximum seal potential. A complete spill-study of all the defined structural segments was undertaken to determine the individual retaining factor. Faults which are classified as sealing show that higher SGR values (>40 %) can support hydrostatic pressure differences of >8 bar (Gamma - Omega, Omega – Bnorth, Omega – Geast). Faults displaying SGR values between 24 % and 30 % can be linked with minor cross fault pressure differences of around <1 - 4 bars (Gamma - Bsouth, Bnorth – Bsouth). SGR zones displaying values < 24 % are found to be acting as conduits for cross-fault fluid communication (Gamma-Bnorth, Gcentral-Geast). These conclusions are based on the observed well fluid contacts, and how they in some cases are limited to critical SGR zones in the faults between structures. These low SGR zones proved to be linked to the distribution of sandy channel bodies in the Ness Formation. It is therefore important to note the impact this channel distribution ultimately presents on the fluid contacts in some structures and ultimately the maximum retained column height.

3) Examine the applicability of Shell developed proprietary Stochastic Trap Analysis and Risking (STAR) -module as a reliable tool for predicting fault seal-dependent hanging-wall traps and discuss possible recommendations for local calibration.

After correlating SGR calculations and cross-fault formation pressure surveys in this thesis, it was found that the P(10) column heights proposed from STAR is underestimating the potential of structures where fault sealing is the retaining factor. In structures limited by structural spill points, STAR produced values comparable to that which is observed in the well data. As a result, is can be argued that STAR needs to be recalibrated to the specific components and parameters that we see in the Brent Group to be better suited in fault seal evaluation in the northern North Sea. However, it is important to note that preliminary STAR underestimation can be attributed to miscalculations in SGR plots, where STAR occasionally define fault spill points in continuous high SGR zones. This is seemingly a reoccurring event where the cell density is high, making it necessary to perform a visual inspection of the suggested fault spill points and manually filter out any miscalculations.

8. Future work

Although this thesis has highlighted strengths and weaknesses in the STAR plugin applied to fault seal evaluation of the Brent Group, there are still areas that could be improved but were left out due to time limitations.

Significant uncertainty has been acknowledged in the distribution of Ness Formation channels, proven to impact the SGR calculations in intervals displaying Brent overlap. To better assess this, it could be beneficial to conduct a sensitivity analysis of the channel distribution and evaluate the impact it has on fault sealing in the Brent Group. This could for example be done by the uncertainty and optimization tool in Petrel.

A geochemical analysis could be conducted in order to further analyze whether the formation pressure data is indicative of stratigraphic compartmentalization in the cases where isolated reservoirs are proposed. This would provide valuable data about the individual composition in each penetrated hydrocarbon bearing interval, and could consequently provide important information about the segment fill history and compartmentalization between reservoirs.

To further broaden the comparative database, it could prove beneficial to expand the study area to C, Gamma South & North, J-, and Kappa-structures, hopefully making it possible to further support the conclusions made regarding the applicability of STAR to the Brent Group.

The limiting values gathered from the analogues defining the STAR dataset are underestimating the sealing capacity of the faults in the Brent Group. This can partly be attributed to miscalculations in some of the fault-planes. When filtering out these outliers, it is however clear that even the P(10) case in STAR underestimate the true potential of the column heights retained in the Oseberg fault blocks. It would therefore be beneficial to assess whether a recalibration of the STAR tool should be performed before applying STAR to column height prediction in the Northern North Sea.

References

Brekke, H., Sjulstad, H. I., Magnus, C., & Williams, R. W. (2001). Sedimentary environments offshore Norway—an overview. *Norwegian Petroleum Society Special Publications, 10*, 7-37.

Crain, E. (2000). Crain's petrophysical handbook. *Spectrum*.

Doligez, B., Ungerer, P., Chenet, P., Burrus, J., Bessis, F., & Bessereau, G. (1987). Numerical modelling of sedimentation, heat transfer, hydrocarbon formation and fluid migration in the Viking Graben, North Sea. *Petroleum Geology of Northwest Europe. Heyden, London*, 1039-1048.

Farseth, R. B., Johnsen, E., & Sperrevik, S. (2007). Methodology for risking fault seal capacity: Implications of fault zone architecture. *AAPG bulletin, 91*(9), 1231-1246.

Fraser, S., Robinson, A., Johnson, H., Underhill, J., Kadolsky, D., Connell, R., . . . Ravnås, R. (2003). *The millennium atlas: Petroleum geology of the central and northern North Sea*.

Fristad, T., Groth, A., Yielding, G., & Freeman, B. (1997). Quantitative fault seal prediction: a case study from Oseberg Syd. *Norwegian Petroleum Society Special Publications, 7*, 107-124.

Færseth, R., & Ravnås, R. (1998). Evolution of the Oseberg fault-block in context of the northern North Sea structural framework. *Marine and Petroleum Geology, 15*(5), 467-490.

Færseth, R. B. (2006). Shale smear along large faults: continuity of smear and the fault seal capacity. *Journal of the Geological Society, 163*(5), 741-751.

Goldsmith, P., Hudson, G., Van Veen, P., Triassic, D. E., Graham, C., Armour, A., & Bathurst, P. (2003). *The millennium atlas: Petroleum geology of the central and northern North Sea.* Paper presented at the Geological Society London.

Helland-Hansen, W., Ashton, M., Lømo, L., & Steel, R. (1992). Advance and retreat of the Brent delta: recent contributions to the depositional model. *Geological Society, London, Special Publications, 61*(1), 109-127.

Johannessen, E. R., Mjøs, R., Renshaw, D., Dalland, A., & Jacobsen, T. (1995). Northern limit of the “Brent delta” at the Tampen spur—a sequence stratigraphic approach for sandstone prediction. *Norwegian Petroleum Society Special Publications, 5*, 213-256.

Johnsen, J. R., Rutledal, H., & Nilsen, D. E. (1995). Jurassic reservoirs; field examples from the Oseberg and Troll fields: Horda Platform area. *Norwegian Petroleum Society Special Publications, 4*, 199-234.

Løseth, T. M., Ryseth, A. E., & Young, M. (2009). Sedimentology and sequence stratigraphy of the middle Jurassic Tarbert Formation, Oseberg South area (northern North Sea). *Basin Research, 21*(5), 597-619.

Mackey, S. D., & Bridge, J. S. (1995). Three-dimensional model of alluvial stratigraphy: theory and application. *Journal of Sedimentary Research, 65*(1).

Martinius, A. W., Ravnås, R., Howell, J., Steel, R., & Wonham, J. (2014). *From Depositional Systems to Sedimentary Successions on the Norwegian Continental Margin (Special Publication 46 of the IAS)*: John Wiley & Sons.

NPD. (2014). *Lithostratigraphic chart - North Sea*. http://www.npd.no/Global/Engelsk/2-Topics/Geology/Lithostratigraphy/NS-OD1409001.pdf.

Ramberg, I. B., Bryhni, I., Nøttvedt, A., & Rangnes, K. (2008). *The making of a land: geology of Norway*.

Ramberg, I. B. B., Inge, Nøttvedt, A., & Rangnes, K. (2008). *The making of a land: geology of Norway*.

Ravnas, R., Bondevik, K., Helland-Hansen, W., Lømo, L., Ryseth, A., & Steel, R. (1997). Sedimentation history as an indicator of rift initiation and development: the late Bajocian-Bathonian evolution of the Oseberg-Brage area, northern North Sea. *Norsk Geologisk Tidsskrift, 77*(4), 205-232.

Ravnås, R., Nøttvedt, A., Steel, R., & Windelstad, J. (2000). Syn-rift sedimentary architectures in the Northern North Sea. *Geological Society, London, Special Publications, 167*(1), 133-177.

Ryseth, A. (2000). Differential subsidence in the Ness Formation (Bajocian), Oseberg area, northern North Sea: facies variation, accommodation space development and sequence stratigraphy in a deltaic distributary system. *Norsk Geologisk Tidsskrift, 80*(1), 9-26.

Vollset, J., & Doré, A. G. (1984). *A revised Triassic and Jurassic lithostratigraphic nomenclature for the Norwegian North Sea*: Oljedirektoratet.

Vrolijk, P. (2005). *Reservoir Connectivity Analysis-Defining Reservoir Connections & Plumbing.* Paper presented at the SPE Middle East Oil and Gas Show and Conference.

Watts, N. (1987). Theoretical aspects of cap-rock and fault seals for single-and two-phase hydrocarbon columns. *Marine and Petroleum Geology, 4*(4), 274-307.

Yielding, G., Freeman, B., & Needham, D. T. (1997). Quantitative fault seal prediction. *AAPG bulletin, 81*(6), 897-917.

Appendix

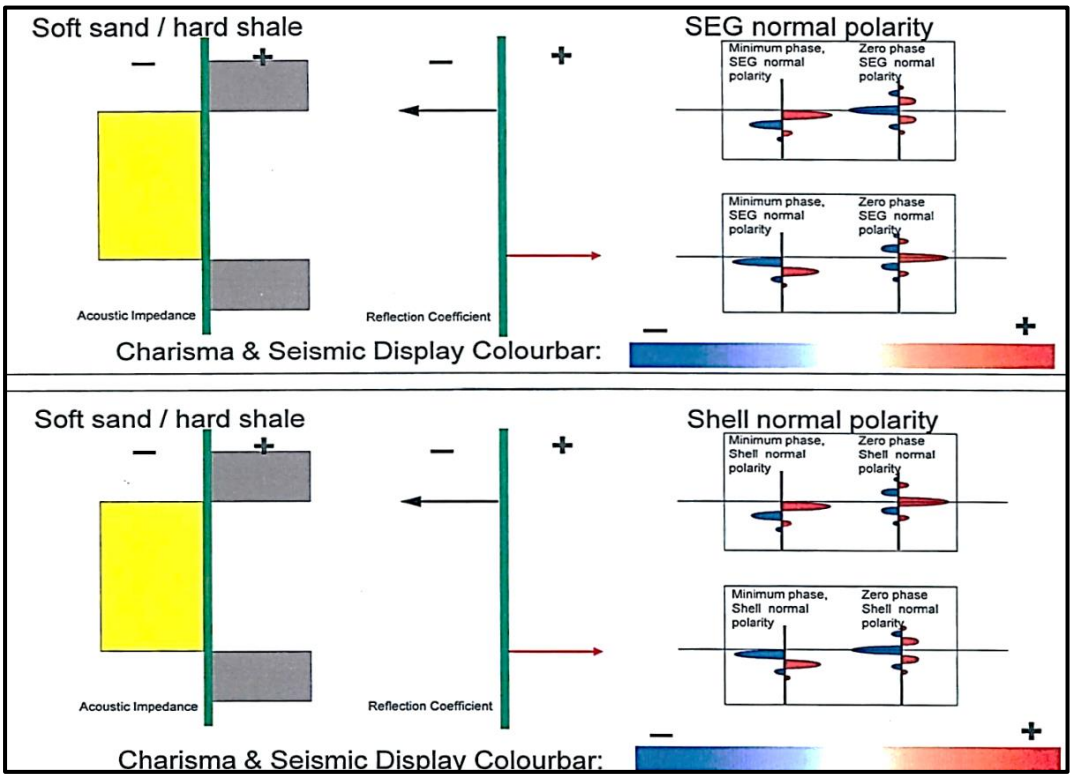

Appendix 1.1: Shell seismic wavelet setup.

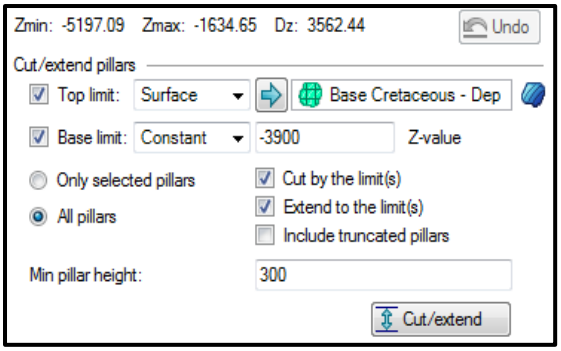

Appendix 2. 1: Operation conducted on fault pillars.

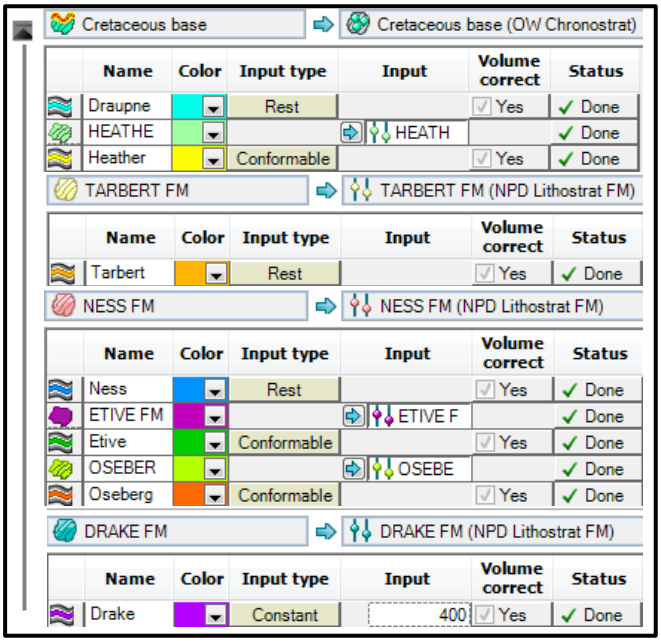

Appendix 2. 3: Zone construction-setup menu from Petrel 2014.

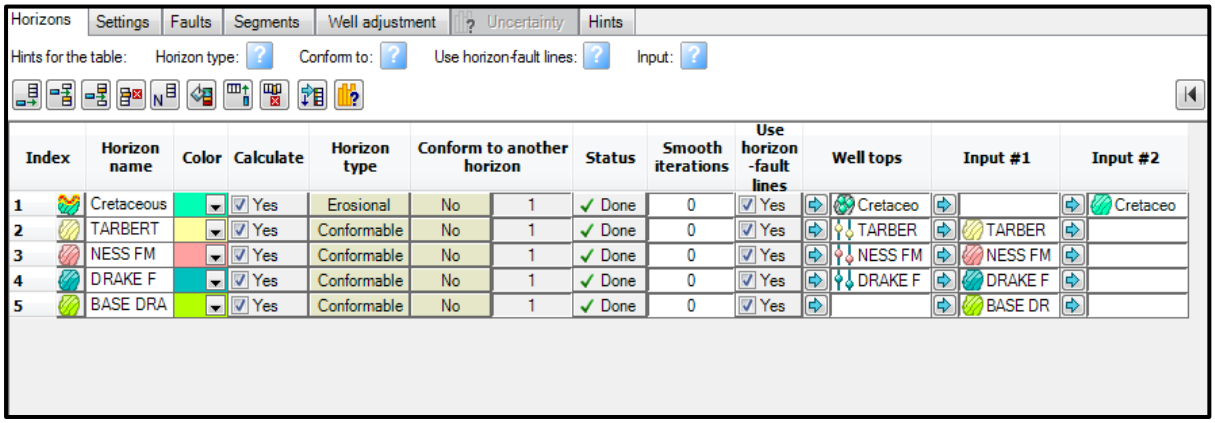

Appendix 2. 2: Setup and input data for constructing horizons in the structural model. Petrel 2014.

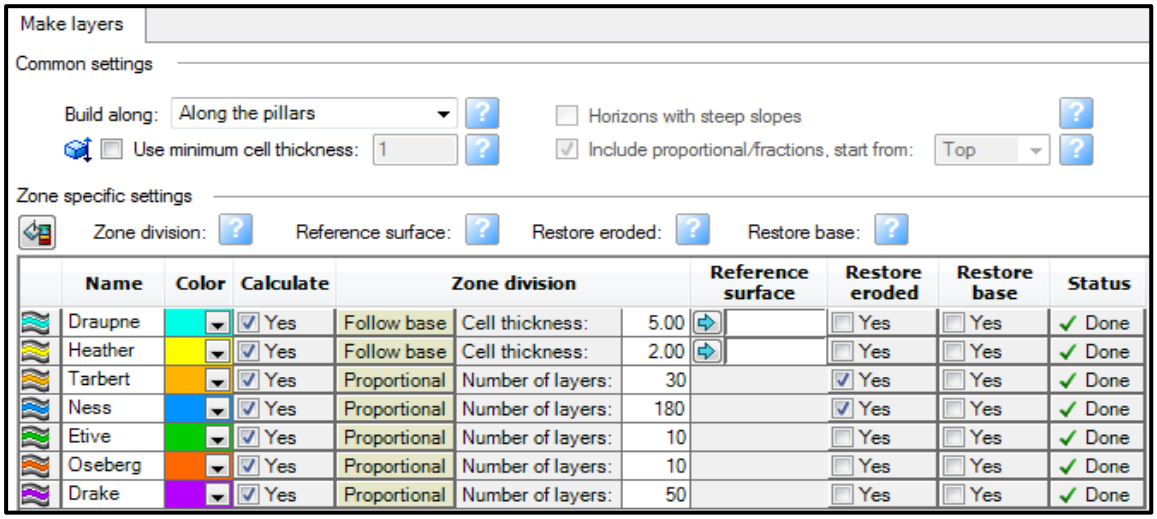

Appendix 2. 4: Methodology applied for layer division. (Petrel 2014).

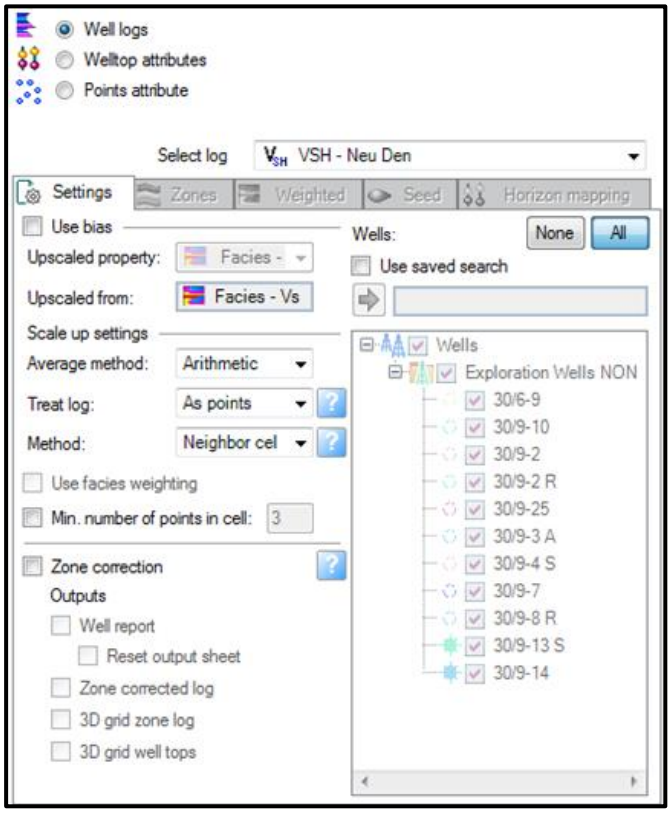

Appendix 2. 5: Setup for up-scaling of Vsh well logs (Petrel, 2014)

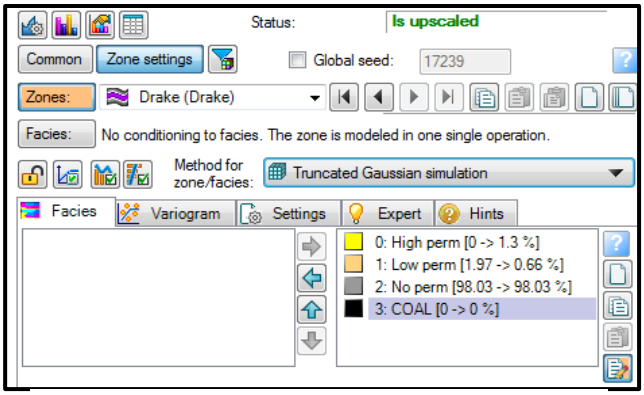

Appendix 2. 7: Method for facies – Drake Fm (Petrel, 2014).

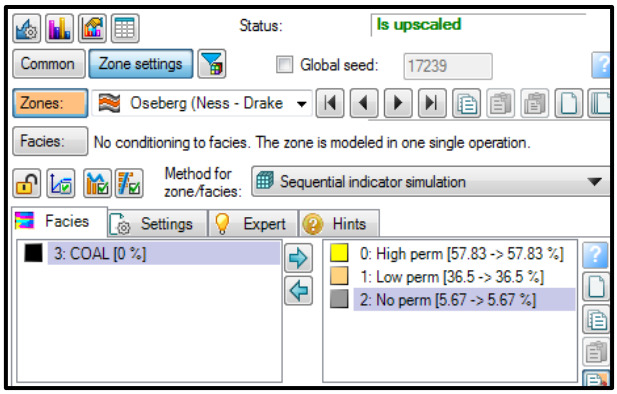

Appendix 2. 6: Method for facies – Oseberg & Etive Fm (Petrel, 2014)

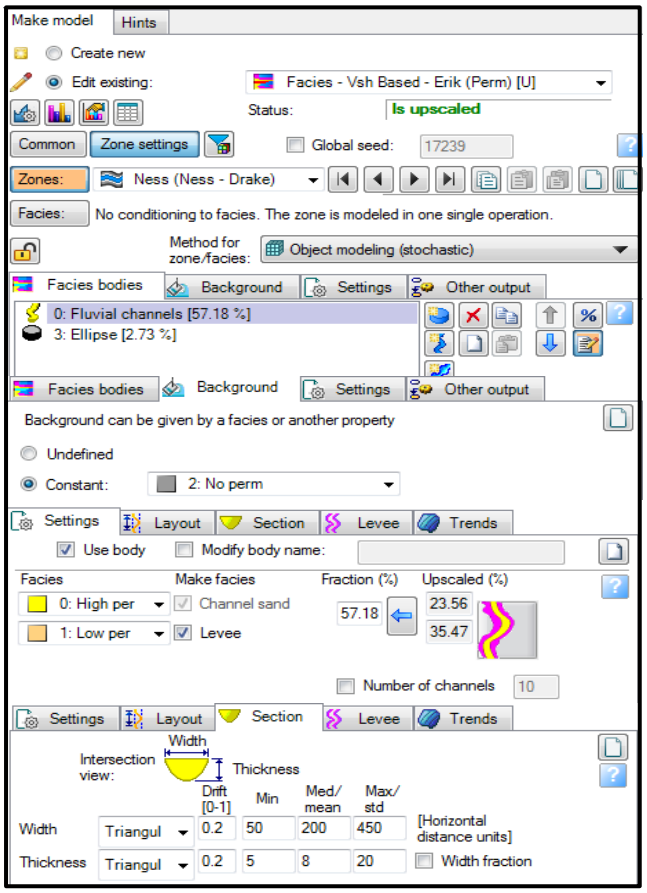

Appendix 2. 8: Method for facies – Ness Fm (Petrel, 2014)

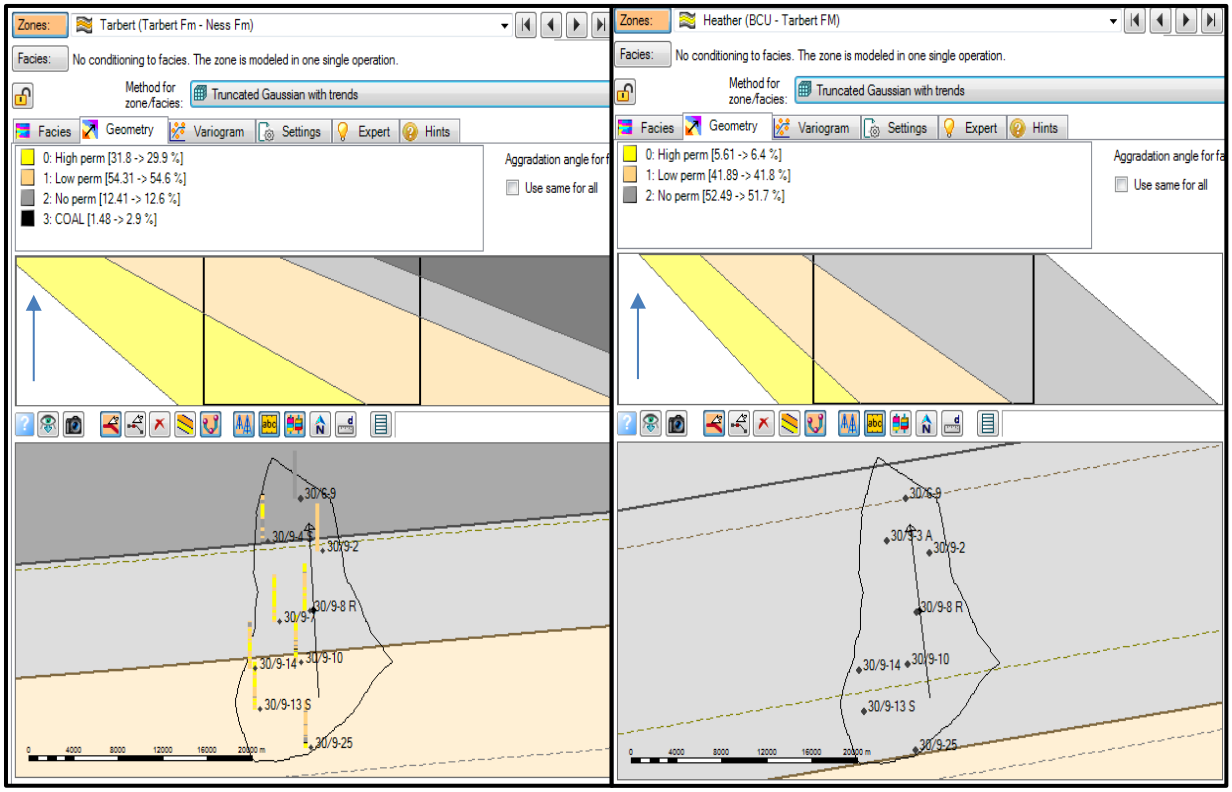

Appendix 2. 9: Method used for facies calculation – Tarbert and Heather Formation (Petrel, 2014).

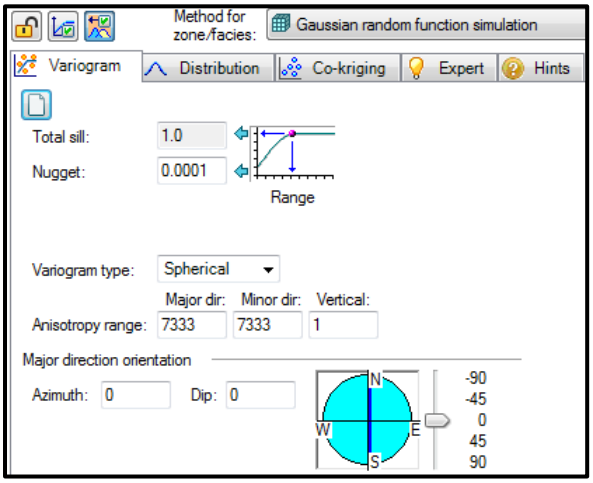

Appendix 2. 10: Method applied for Petrophysical modelling for all zones and facies-subclasses